DEVELOPMENT OF RICE STRAW-BASED NANOCELLULOSE COMPOSITE FILM INCORPORATED WITH MUCILAGE

Thesis Submitted for the Award of the Degree of

DOCTOR OF PHILOSOPHY

in

Food Science and Technology

By

Renu Kamboj

Registration Number: 11919229

Supervised By

Dr. Prince Chawla (25073)

Department of Food Technology and Nutrition

(Assistant Professor)

Lovely professional university

LOVELY PROFESSIONAL UNIVERSITY, PUNJAB

2025

Dedicated

to

My Beloved Parents, My in-laws, My Husband Dr. Aman Kamboj And My Beloved Son Ivaan Kamboj

DECLARATION

I, hereby declare that the presented work in the Project entitled **"Development of rice straw-based nanocellulose composite film incorporated with mucilage"** in fulfilment of degree of **Doctor of Philosophy (Ph.D.)** is outcome of research work carried out by me under the supervision of **Dr. Prince Chawla**, Assistant Professor (Food Technology and Nutrition) of School of Agriculture, Lovely Professional University, for the award of degree Ph.D. Food Science and Technology.

Renu Kamboj

(Reg. No. 11919229)

I certify the above statement made by the student is correct to the best of my knowledge and belief**.**

Date: 07/02/2025 **(Supervisor - Dr. Prince Chawla**)

Place: Phagwara, Punjab (India) Food Technology and Nutrition

The Ph.D. Viva-Voce examination of research scholar Renu Kamboj has been held on 07/02/2025 and accepted for the award of Ph.D. Degree

Supervisor **External Examiner**

Head of Department **Dean**

CERTIFICATE

This is to certify that the work reported in the Ph. D. thesis entitled **"Development of rice straw-based nanocellulose composite film incorporated with mucilage"** submitted in fulfillment of the requirement for the award of the degree of **Doctor of Philosophy (Ph.D.)** in the **Department of Food Technology and Nutrition/ School of Agriculture,** is a research work carried out by **Renu Kamboj**, **11919229**, is bonafide record of his/her original work carried out under my supervision and that no part of thesis has been submitted for any other degree, diploma or equivalent course.

(Signature of Supervisor)

Name of supervisor: Dr. Prince Chawla

Designation: Assistant Professor

Department/School: Food Technology and Nutrition/School of Agriculture

University: Lovely Professional University, Phagwara, Punjab

TABLE OF CONTENT

ACKNOWLEDGMENT

First and foremost, I extend my deepest gratitude to the Almighty, whose blessings have been unfailing and abundant. It is with a profound sense of reverence that I acknowledge His ever-present guidance and strength throughout the course of this research. The peace and perseverance granted to me by the Divine were essential in overcoming the numerous challenges faced during my studies. I am forever grateful for the grace bestowed upon me, providing the opportunity, courage, and wisdom to complete this work. Every step of this journey has been guided by His unseen hand, and I am eternally thankful for this.

This journey of academic and personal growth would not have been possible without the guidance, encouragement, and wisdom of several key individuals to whom I owe a great deal of gratitude. First and foremost, I extend my deepest appreciation to my respected advisor, Dr. Prince Chawla for his wisdom, vision, expertise, guidance, enthusiastic involvement, and persistent encouragement during the planning and development of this research work. His profound expertise and unwavering dedication to the pursuit of knowledge have profoundly influenced my professional development. The ability of Dr. Chawla to nurture curiosity and inspire innovative thinking has been crucial in the progression and success of my research. Without his inspiration, untiring efforts, enthusiastic attitude, and personal care, the accomplishment of this research work would have been impossible. I am exceptionally fortunate to have had the opportunity to work under his guidance and to benefit from his visionary academic and scientific insights.

With the same spirit and respect, I would like to express my deep sense of gratitude to members of my research advisory committee, Dr. Sawinder Kaur, Dr. Prasad Rasane, Dr. Mukul Kumar, Dr. Prerna Gupta from the Department of Food Technology and Nutrition, Lovely Professional University, Phagwara, Punjab, India for their remarkable guidance and valuable feedback and comments that helped me to raise the standard of this research work. Each committee member has generously contributed their time and expertise to guide my research with invaluable insights and suggestions. Their diverse perspectives and expert advice have been pivotal in enhancing the quality and integrity of my work. I also extend my special thanks to all the cited authors in my thesis whose research findings provide me a battleground to choose upon the research directions. I express my deep sense of gratitude towards you for inculcating a scientific temperament and caliber in me and for your valuable suggestions in my work.

I extend my special thanks to all the faculty members administration and staff of the university for their valuable and timely help throughout my research work. Special thanks are due to the laboratory technician—Mr. Devender, Mr. Vishal, Mr. Mukesh, Miss Rubal, Miss Suman, Mr. Bansilal Mr. Praveen, Mr. Rajkumar, Mr. Tilakraj whose technical support and dedication have been indispensable. Their willingness to assist at any time and their meticulous attention to detail have greatly facilitated my experimental work.

Some friends are never too busy to give us a hand whenever they are needed. I express my sincere love and affection towards all those benevolent souls and true friends who have provided both moral support and academic collaboration. Sweezee Thakur, Vaishali Singh, Akriti Thakur, Samriti Guleria, Jashanveer Kaur, Tosif Mansuri, Ashwathi, Madhu Sharma and Nikhil Patil. Your friendship and readiness to help have been a source of joy and comfort throughout this journey and your presence and support have enriched my experience immeasurably.

Words cannot fully convey my gratitude to my dear husband, Dr. Aman Kamboj, for his unwavering support. He consistently provided me with encouragement and confidence, enabling me to complete my thesis. I am thankful for his cooperation, affection, motivation, understanding, patience, and sincere advice. His support and care helped me overcome setbacks and remain focused on my work. I deeply value his friendship and greatly appreciate his belief in me. Further most profound gratitude goes to my beloved son Ivaan Kamboj my father, Sh. Jai Prakash Singh, my father in-law Sh. Parveen Kumar and my mother, Smt. Geeta Devi, my mother in-law kushalya Rani, for their endless love, sacrifices, and belief in my abilities even when I doubted myself. To my sister Neeta Negi my brother Mr. Vivek Prakash and my brother in-law, Mr. Sourav Kamboj for his constant encouragement and support. Your faith in me has been the foundation of my strength and resilience. Above all, I thank God for His grace and guiding light, which has shone on me throughout this journey.

Renu Kamboj

LIST OF TABLES

LIST OF FIGURES

LIST OF ABBREVIATIONS AND SYMBOLS

-	Negative
+	Positive
%	Percentage
µg	Micro gram
µM	Micro molar
ANOVA	Analysis of variance
VM	Volatile matter
DSC	Differential scanning calorimetry
FTIR	Fourier transform infrared spectroscopy
g	Gram
IR	Infrared
NDF	Neutral detergent fiber
ADF	Acid detergent fiber
ADL	Acid detergent lignin
SDS	Sodium dodecyl sulfate
EDTA	Ethylene Diamine Tetra Acetate acid
mg	Milli-gram
$MgSO_4$	Magnesium sulphate
ml	Millilitre
NaOH	Sodium hydroxide
nm	Nanometre
XRD	X-Ray diffraction analysis
TGA	Thermogravimetric Analysis
℃	Degree Celsius
EDX	Energy Dispersive X-ray Analysis
PRS	Parmal rice straw
BRS	Basmati rice straw
PTPRS	Pretreated Parmal rice straw
PTBRS	Pretreated Basmati rice straw
PRSC	Parmal rice straw cellulose
BRSC	Basmati rice straw cellulose
PRSNC	Parmal rice straw nanocellulose
BRSNC	Basmati rice straw nanocellulose
SEM	Standard error mean
UV	Ultraviolet
UV-VIS	Ultraviolet Visible
FFA	Free Fatty Acid
TBA	Thiobarbituric Acid
Br	Bread
Bi	Biscuits
Nd	Noodles

Abstract

Rice straw burning is a major environmental concern, especially worldwide. Farmers burn rice straw after harvesting paddy to clear fields early to grow the next crop. Which releases smoke and pollutants that cause air pollution, greenhouse gas emissions, and respiratory health issues. The recent studies focus on sustainable alternatives to conventional agricultural practices of burning rice straw and their impact on the environment. Rice straw waste, a form of lignocellulosic biomass, can be utilized and transformed into value-added products. This thesis work aimed to develop an energy-efficient approach i.e. using low alkali concentrations to optimize the process of cellulose extraction from rice straw. The low-alkali method uses lower concentrations of sodium hydroxide to break down lignin and hemicellulose. This eco-friendly approach reduces chemical usage, enhances safety, conserves energy, and preserves the quality of the cellulose, offering a sustainable alternative to traditional extraction methods

In this study, two different varieties of rice straw Basmati (BRS) and Parmal (PRS) were utilized to evaluate the work. The pure cellulose was efficiently extracted using an alkali pretreatment method with varied concentrations of 3, 4, and 5% of NaOH. The method was optimized using Box Behnken design with varying temperatures of 90, 120, and 150℃ and a time duration of 90, 120, and 150 min. The method resulted in cellulose yields of 89.23 % from BRS (BRSC) and 89.37 % from PRS (PRSC). The cellulose was further processed and transformed into nanocellulose (BRSNC and PRSNC) through a combined approach of citric acid and ferric chloride-derived hydrolysis.

The quality of rice straw, pretreated rice straw, cellulose, and nanocellulose was analyzed by different characterization techniques such as Fourier-transform infrared spectroscopy (FTIR), Scanning electron microscopy (SEM), Energy dispersive X-ray (EDX), Thermogravimetric analysis (TGA), Differential Scanning Calorimetry (DSC) and X-ray diffraction analysis (XRD). The FTIR and chemical composition revealed that the optimized method developed for pure cellulose extraction has eliminated hemicellulose and lignin content from pretreated samples. TGA and DSC have shown the thermal stability of samples. The surface morphology was analyzed using scanning electron microscopy.

Further, the nanocellulose-based film was prepared by a casting method with different concentrations of nanocellulose (1, 1.5, 2, 2.5, 3, 3.5, 4, 4.5, 5, 5.5, 6 %) and mucilage (1, 2, 3, 4 %) as reinforcement content. Film F33, containing 5% nanocellulose and 4% mucilage, exhibited a good mechanical strength of 23.06 ± 0.78 MPa among 37 films, in comparison to control films CN-38 and CM-39. Additionally, 12 films with the best mechanical strength were selected for further analysis to assess their physical properties. According to experimental findings, film F8 demonstrated the best physical properties compared to the control films (CN-13 and CM-14), and was selected as the final choice for packaging. The selected composite film underwent further examination by sealing the bakery products (Bread, Biscuits, and Noodles), as a packaging material. The physicochemical and microbial properties of the products were evaluated every 2 days over 8 days for bread, and every 15 days over 120 days for biscuits and noodles. It was found that the quality was preserved for up to 6 days for bread, 90 days for biscuits, and 105 days for noodles, compared to the control films. In addition to this, the degradability of the film also was measured at every 2-day intervals and found that the film was 98% degraded after 23 days.

Furthermore, the impact of packaging material on the physical properties of bakery products was examined during storage duration. According to experimental findings, the ash and crude fat contents remained stable, suggesting minimal changes in protein, crude fiber, and carbohydrate contents showed significant declines. The standard film has shown the smallest increase in moisture content with 33.37± 0.05, 4.93 ± 0.23, 12.04 ± 1.45, water activity with 0.905 ± 0.002, 0.611 ± 0.08, 0.567 ± 0.005, pH with 5.80 ± 0.021, 6.51 ± 0.360, 6.80 ± 0.02 and hardness with 4.47 ± 0.34, 34.76 ± 1.09, 365 ± 1.45 values for bread (Br) biscuits (Bi) and noodles (Nd) respectively and displayed the most stable performance. However, the results implied that nanocellulose-infused film and mucilage-infused films were significantly often leading to a faster reduction compared to standard film. The impact on free fatty acid (FFA) TBA, and peroxide values of bakery products levels was also assessed on the same products over time. The results signified that mucilage-infused films consistently led to the highest increases in FFA levels across all bakery products, indicating

more rapid fat degradation. Also, the mucilage-infused films consistently showed the highest TBA readings, for instance, over 8 days, TBA values in bread packaged with mucilage-infused films rose from 6.88 to 15.34, significantly higher than those in nano cellulose-infused (up to 13.67) and standard films (up to 12.67) indicating the greatest lipid oxidation. The oxidative stability of products packaged in standard, nanocellulose-infused, and mucilage-infused nanocomposite films over various storage periods was also measured. Similarly, mucilage-infused films reached peroxide values of 4.62 in bread over 8 days, 0.93 in biscuits over 120 days, and 1.64 in noodles over the same period. Results revealed that mucilage-infused films and nanocellulose-infused films consistently showed the highest peroxide values across all products, suggesting they are less effective at preventing oxidation in comparison to standard nanocellulose film.

The antimicrobial efficacy of products sealed in standard film, nanocellulose-infused film, and mucilage-infused nanocomposite films was also examined. Initially, all products exhibited nonsignificant microbial growth over time. however, nanocellulose and mucilage-infused films had higher microbial counts than standard film. These findings suggest that bakery products exhibited good stability when packaged with standard nanocellulose film, particularly evident on day 8 for bread, day 90 for biscuits, and day 105 for noodles. These results emphasize the necessity of selecting the right packaging material based on the moisture sensitivity of the product, as the performance of these films can vary significantly with different types of food products. These results revealed that the proposed bio-nanocomposite film appears to be an excellent replacement for conventional food packaging materials.

Keywords: Rice Straw, cellulose extraction, RSM, nanocellulose, nanocomposite film, characterization

Rice is considered as the staple food grain crop produced globally, and the requirement for rice production is steadily escalating to meet domestic consumption and export demands. (Wang et al. 2023). It is produced in every region worldwide, such as Oceania (.076 million tons), Europe (4.024 million tons), America (35.33 million tons), Africa (38.77 million tons), Asia (677.28 million tons), (FAO. 2019) (world Map). It is the agricultural byproduct of rice production, consisting of the stems and leaves remaining after the grains of rice have been harvested (Danapriatna et al. 2023). It is one of the most abundant agricultural residues globally, especially in regions where rice is a staple crop (Parihar et al. 2023). Composed primarily of lignocellulosic material—cellulose, hemicellulose, and lignin—rice straw has a complex structure that makes it both a challenge and an opportunity for sustainable management and utilization (Singh, Bedi, and Khajuria 2024). Traditionally, rice straw has been used in a variety of ways, including as fodder for livestock, bedding for animals, and as a raw material for making paper, packaging, mats, and ropes. However, due to the massive volumes produced and the labor-intensive process of its collection and transportation, rice straw is often seen as a waste product. In many rice-producing areas, it is one of the primary environmental issues associated with the communal practice of open-field burning. Farmers often resort to burning rice straw to quickly clear fields for the next planting cycle. This practice emits significant quantities of greenhouse gases, such as carbon dioxide, methane, and nitrous oxide, thereby contributing to climate change. (Han et al. 2024).

Moreover, the smoke generated from burning rice straw includes detrimental pollutants like particulate matter, which poses significant health risks to humans, affecting respiratory and cardiovascular health. The ratio of rice grain to rice straw varies from 0.71 to 1.51, which means for every ton of paddy rice produced, 702 to 1502 kg of rice straw, or every 4 tons of harvested rice left approximately 6 tons of rice straw in the field (Röder, Thornley, and Jamieson 2024). Moreover, Asia is rich in rice production and its annual turnover is 677.6 million tons; thus, with this huge production, in this way a large quantity of straw around 1015.92 million tons is generated annually. Approximately 80% of rice straw becomes a source of pollution due to its improper management (Kaur and Singh

2024). Therefore, a lot of atmospheric particulate matter (minute-sized particles) is generated during this process, which is a complex mixture of suspended particle matter, and its potential environmental and health effects depend upon particle size and composition. Besides, to manage the rice straw waste various practices such as in-field and off-field practices are adopted by the farmers and scientists. Although burning of rice straw in the field is a very feasible and reasonable technique of rice straw management for the farmers (Verma, Singh, and Dhanorkar 2024). Nevertheless, the widespread burning of rice straw remains a major global challenge. Consequently, scientists and researchers are actively working on various alternatives to transform rice straw into a valuable resource, which will greatly benefit rural communities.

However, in recent works, researchers have utilized rice straw as an excellent source of cellulose to develop bio-based packaging. Thus researchers have already revealed that the rice straw residues (non-woody material) could be used as an alternative to woody raw material for the production of paper due to its vital properties (Hawanis et al. 2024). (Physical, chemical, thermal, and biological) and its open structure is easily portable and does not require hard pulping and solid chemicals processing therefore, the isolation of cellulose from the rice straw is economically feasible and could be the best alternative to rice straw burning. Moreover, its utilization as a bio-polymer in the form of nano-composites to formulate bio-based films receiving remarkable attention in the food and medical field. However, the extensive use of synthetic polymers contributes to significant environmental challenges caused by the long-term exposure of ecosystems to packaging materials derived from synthetic polymers. The growing global consciousness regarding environmental and human health concerns represents a paramount issue in contemporary times. Therefore, the utilization of rice straw as an economical cellulose source may serve as an optimal strategy for managing the surplus of rice straw while addressing the problems associated with synthetic polymers (Khalil et al., 2018). Currently, the paper industry encounters considerable challenges related to resource scarcity, environmental contamination, and limitations in technical infrastructure.

Additionally, nonwoody fiber resources exhibit outstanding physical and optical characteristics that can enhance their product quality. The management of rice straw in this manner to utilize excess amount of rice straw, to stop rice straw burning, and to fabricate a bio packaging due to the excessive demand for green materials, and awareness of environmental issues could be the best approach towards sustainable agriculture.

Rice straw, a lignocellulosic biomass, is a residual product of rice cultivation. It predominantly consists of three biopolymers: lignin, cellulose, and hemicellulose along with smaller amounts of extractives and ash (Cabrera-Villamizar et al. 2024). Among all available biopolymers, cellulose is the most utilized plant-derived component. Due to its vigorous properties and soft structure, it is effortlessly portable and also does not require any strong chemical processing and hard pulping. It is composed of a linear homopolysaccharide with β-1,4-linked anhydrous-D-glucose units (Berglund et al. 2020). It forms a linear chain that bundles together to create microfibrils which is a repeating unit of cellobiose mainly consisting of three hydroxyl groups (Selvaraj et al. 2024). These cellobiose units form a strong hydrogen bond with the adjacent glucose unit within the same chain and other chains. The cellulose chains are organized into microfibrils, which are small, thread-like structures. Microfibrils are the fundamental structural elements of cellulose and are bundled together in a hierarchical structure to form fibers (Selvaraj et al. 2024). These microfibrils exhibit both crystalline and amorphous regions, contributing to the rigidity and tensile strength of the plant cell walls. The crystalline regions are highly ordered and provide strength and rigidity, while the amorphous regions are less ordered and provide flexibility. The ratio of crystalline to amorphous regions can affect the properties of cellulose, such as its digestibility by enzymes and its mechanical properties (Ghosh et al. 2024).

The internal structure of cellulose is stabilized by both intermolecular (between molecules) and intramolecular (within a molecule) hydrogen bonds. These bonds give cellulose its high tensile strength and resistance to being pulled apart. The unique internal structure of cellulose, with its combination of crystalline and amorphous regions, hydrogen bonding, and hierarchical organization from glucose units to fibers, underlies its physical

properties and versatility as a material. Cellulose is stiff, highly polar, fibrous, and water-insoluble and plays a significant role in keeping plant cell walls aligned. These physicochemical properties, make it excellent in hydrolysis resistance than other plant-derived biopolymers (Parra-Palma et al. 2024). The crystallinity of cellulose further contributes to durability in nature and a good mechanical property. it is widely used in the food industry as a suitable biodegradable and recyclable packaging material.

In recent years, many demanding research works have been investigated to develop a pure cellulose content from biomass. There are most predominant methods are microbial hydrolysis, ammonia treatment mechanical treatment, acid-chlorite treatment, acid hydrolysis, and alkaline hydrolysis. Some of these methods are very long and laborious during processing and require high temperatures and numerous practices to extract cellulose content. Each of these methods aims to remove the non-cellulosic components such as lignin and hemicellulose, which are present in the plant cell walls alongside cellulose (Mahato and Kumar 2024). Mechanical methods, such as grinding and milling, physically break down the biomass to increase the accessibility of cellulose but often require subsequent chemical treatments for complete isolation. Acid hydrolysis, while effective in hydrolyzing the amorphous regions of cellulose and hemicellulose, can lead to a decrease in the degree of polymerization of cellulose, potentially compromising its quality.

Bleaching, involving oxidizing agents, primarily targets the removal of lignin but may not be sufficient on its own for complete cellulose extraction. Among them, the alkaline treatment is one such practice that has many benefits compared to other methods due to its considerable cost and time of processing and effective results of cellulose extraction (Shakeel et al. 2024). Also. emerges as a preferred method for cellulose extraction, especially due to its efficiency in lignin removal and its gentleness on the cellulose structure. It is known as alkaline pretreatment and involves the saponification of intermolecular ester bonds cross-linking hemicellulose and lignin. It also leads to swelling of the cellulose structure, increasing internal surface area, and reducing the degree of polymerization and crystallinity (Li et al. 2024). Alkaline conditions disrupt the lignin

structure by cleaving ether bonds and dissolving lignin fragments, thereby enhancing the accessibility of the polysaccharides. One of the key advantages of alkali hydrolysis is its ability to preserve the integrity and degree of polymerization of cellulose, ensuring high-quality cellulose is obtained. Additionally, the process conditions for alkali hydrolysis are less corrosive and hazardous compared to acid hydrolysis, making it more environmentally friendly. Particularly its effectiveness in lignin removal, preservation of cellulose quality, and environmental considerations considered alkali treatment as the best method for cellulose extraction from plant biomass.

Nanocellulose is a material derived from cellulose, the most abundant organic polymer on earth, commonly found in the cell walls of plants. It represents a category of nanostructured cellulose materials that have been engineered to have dimensions in the nanometer scale, typically less than 100 nanometers in at least one dimension (Lengowski et al. 2023). The transition from cellulose to nanocellulose involves various processes that break down the bulk cellulose structure into nano-sized fibers or crystals, thereby unlocking a suite of remarkable properties that are not evident in its macroscopic form (Ariga 2024). This transformation influences the inherent characteristics of cellulose—such as its biodegradability, mechanical strength, and chemical modifiability—while introducing new functionalities, including increased surface area, transparency, and unique rheological properties (Rajasekar, Kavyashree, Sangamithra, Baskaran, Maria, and Mary 2024). The derivation of nanocellulose from cellulose can be achieved through several methods, including mechanical disintegration, chemical hydrolysis, or a combination of both, which selectively remove the amorphous regions of cellulose, preserving the crystalline structure, or liberate individual fibrils or crystals.

The expedition of nanocellulose from its natural origins to a versatile nanomaterial involves sophisticated extraction methods and modification to isolate cellulose at the nanoscale while preserving its intrinsic properties. The extraction of nanocellulose from cellulose involves various methodologies, with acid hydrolysis being one of the most common approaches (Li et al. 2024). Traditional acid hydrolysis often employs strong inorganic acids, such as sulfuric acid or hydrochloric acid, to remove the amorphous

regions of cellulose, leaving behind the crystalline structure in the form of cellulose nanocrystals (CNCs) (Rajasekar, Kavyashree, Sangamithra, Baskaran, Maria, Mary, et al. 2024). The use of strong acids demands rigorous safety precautions and can lead to significant environmental concerns related to acid disposal and neutralization. Additionally, the process can introduce sulfate groups to the CNC surface, impacting its properties and potentially limiting its application in certain areas (Sun et al. 2024). Whereas, citric acid, an organic acid, offers as another approach for nanocellulose extraction, aligning with the principles of green chemistry for more environmentally friendly processes. It is less corrosive, safer to handle, and more environmentally benign compared to sulfuric or hydrochloric acid. The process aligns with sustainable practices, reducing harmful waste and minimizing environmental impact (Onwuka and Adu 2024). Additionally, citric acid can impart carboxylic groups to the nanocellulose, which may enhance its dispersion in aqueous and organic solvents. Moreover, offering a high degree of control over the nanocellulose characteristics and yield, citric acid presents a greener, enough potentially and, more efficient alternative that may open new possibilities for the sustainable production of nanocellulose (Badr-Eddine, Idrissi, and Essamlali 2024)

Nanocellulose acts as the primary film-forming agent due to its ability to create a strong, flexible matrix. It provides mechanical strength and structure to the film (Aminah et al. 2024). Increasing the concentration of nanocellulose generally enhances the tensile strength and decreases the elongation, making the film more rigid but also potentially more brittle if not balanced by the other components. Nanocellulose plays a pivotal role in bio-packaging films, primarily due to its exceptional strength, lightweight nature, and biodegradability (Jaouahar et al. 2024). As a nanomaterial derivative of cellulose, the plentiful organic polymer, nanocellulose introduces a new dimension of durability and environmental friendliness to packaging solutions. In bio-packaging films, it serves as a critical structural component, providing mechanical strength comparable to some metals and a barrier to gases and moisture that rivals synthetic polymers. This barrier property is especially important for packaging applications, as it significantly extends the shelf life of perishable goods by protecting them from oxygen, carbon dioxide, and moisture (Barik et

al. 2024). Moreover, nanocellulose's ability to form transparent films makes it an attractive option for packaging where product visibility is desired. Its biodegradability also ensures that these packaging films can decompose naturally, reducing environmental pollution and promoting a circular economy. Additionally, the compatibility of nanocellulose with other biodegradable materials, such as proteins and polysaccharides, allows for the creation of composite materials with tailored properties for specific packaging needs. This adaptability further enhances its role in developing sustainable packaging solutions that fulfill the demands of various industries while justifying the environmental impact of traditional packaging materials (Abaku and Odimarha 2024).

Bio-packaging materials, often referred to as biodegradable or compostable packaging, represent an eco-friendly alternative to traditional petroleum-based packaging. Made from various natural materials such as corn starch, sugarcane, plant fibers, and mushrooms, these biodegradable options are designed to reduce the environmental impact of packaging waste (Cheng et al. 2024). Unlike conventional plastics that can take hundreds of years to decompose, bio-packaging materials break down into natural materials like water, carbon dioxide, and biomass under the right conditions, often requiring only a few months to fully decompose. This rapid biodegradation process significantly reduces pollution and conserves landfill space. Moreover, biopackaging often comes from renewable resources, supporting a more sustainable cycle of production and disposal (Cheng et al. 2024). As the global focus shifts towards sustainability, the development and use of bio-packaging materials are increasingly becoming a priority for businesses seeking to minimize their environmental footprint and for consumers looking for greener alternatives.

Mucilage plays a crucial and multifaceted role in the development of bio packaging films, primarily due to its natural adhesive properties, biodegradability, and non-toxicity. Derived from a wide variety of plants, mucilage is a gelatinous substance that contributes significantly to the mechanical properties and performance of bio-packaging materials. When incorporated into bio packaging films, mucilage serves as an excellent natural adhesive, enhancing the cohesion and flexibility of the film (Thivya et al. 2024). This

ensures that the packaging is not only strong enough to protect the contents but also flexible enough to accommodate various shapes and sizes without tearing or breaking. Furthermore, mucilage's inherent water-binding capacity helps in regulating moisture content within the packaging, acting as a barrier that can extend the shelf life of perishable things by maintaining optimal humidity levels (Gupta, Guha, and Srivastav 2024). Its biodegradability is another critical aspect, aligning with the environmental goals of biopackaging by ensuring that the materials break down naturally without contributing to pollution. Thus, mucilage's role in bio packaging films is vital, contributing to their structural integrity, performance, and sustainability.

Nanocomposite films are sophisticated materials crafted by embedding nanoparticles within a polymer matrix, enhancing the film's inherent properties significantly (Taher, Hasan, and Zhu 2024). These films fall under the broader category of nanocomposites, which exploit the unique benefits of nano-scale particles to improve the mechanical strength, thermal stability, and functional qualities of the base material (Eversole et al. 2024). Commonly used nanoparticles include nanocellulose, carbon nanotubes, graphene, and various metal oxides like titanium dioxide and zinc oxide. These particles, due to their tiny size and high surface area, interact closely with the polymer matrix, often a synthetic polymer like polyethylene or a natural polymer such as starch, enhancing the composite's overall performance (Siddiqui et al. 2024).

The production of nanocomposite films can involve several methods including solvent casting, melt mixing, electrospinning, and extrusion, chosen based on the desired film characteristics and the compatibility of components (Ghosh et al. 2024). These production techniques help in achieving a uniform distribution of nanoparticles, which is pivotal for the optimal performance of the films. The inclusion of nanoparticles not only improves the mechanical properties like tensile strength and elasticity but also significantly boosts the barrier properties against gases, moisture, and volatile compounds, making these films exceptionally suitable for packaging applications (Thivya et al. 2024).

Moreover, nanocomposite films exhibit enhanced thermal properties, allowing them to withstand high temperatures and harsh environmental conditions, which is

advantageous for industrial applications requiring robust materials (Suleiman et al. 2024). When constructed with biodegradable polymers and nanoparticles like nanocellulose, these films offer the added benefit of compost ability, aligning with environmental sustainability goals by reducing plastic waste. In addition to packaging, nanocomposite films have diverse applications across various industries. In electronics, they are utilized for flexible electronic components and energy storage devices due to their improved electrical conductivity (Ponnalagar et al. 2024). The medical field benefits from their use in biocompatible wound dressings and drug delivery systems. Furthermore, their unique optical properties find applications in photonics and optics. Agricultural applications also leverage biodegradable versions for mulch films and controlled release systems for fertilizers and pesticides.

The selection of bakery products as an application for rice straw-based nanocellulose composite films incorporated with mucilage is a strategic choice grounded in both sustainability and functionality. Bakery products are highly sensitive to moisture, oxidation, and microbial contamination, all of which can significantly affect their texture, flavor, and shelf life. Packaging plays a critical role in preserving the freshness and quality of bakery items, yet traditional plastic packaging is environmentally harmful, contributing to pollution and waste. The use of rice straw-based nanocellulose films offers a sustainable alternative, as they are biodegradable, renewable, and derived from an agricultural waste product. Nanocellulose itself possesses excellent barrier properties, including resistance to moisture and oxygen, making it ideal for protecting bakery products from drying out or becoming soggy. Moreover, the addition of mucilage—an organic polysaccharide with high water-binding capacity—further enhances these films by improving their moisture retention and flexibility, which helps maintain the freshness of bakery items for longer periods.

From a health and safety perspective, bakery products are consumed directly from their packaging, so any material in contact with food must be non-toxic and safe. Nanocellulose and mucilage are derived from natural sources, making them ideal for food packaging applications where food safety is paramount. Furthermore, incorporating these

materials aligns with the growing consumer demand for sustainable, non-plastic packaging. Nanocellulose-based films, by their biodegradability and natural origin, present a promising solution to the widespread environmental issue of plastic waste. The use of rice straw, an agricultural byproduct, adds another layer of environmental benefit, contributing to a circular economy by turning waste into a valuable product.

The objectives of the present research were

1. To optimize the cellulose isolation process from rice straw
2. To develop a nanocellulose film incorporated with mucilage
3. To characterize physio-chemical and biological properties of the nanocellulose film
4. To evaluate the shelf life of bakery products packaged with film

2.1 Agricultural waste and challenges

Agricultural waste refers to the by-products and residues generated from farming practices and agro-industrial processes (Rațu et al. 2023). This includes various organic materials such as crop residues (stalks, leaves, and husks), animal manure, poultry litter, and the waste produced while processing agricultural products like rice husks, sugarcane bagasse, and fruit peels. While unused can be a valuable source for generating energy, producing bio-based materials, and enriching the soil, managing it poses significant challenges (Voss et al. 2024). One of the primary challenges is the total volume of agricultural waste produced, which can lead to environmental pollution if not managed properly. Improper disposal methods, such as open burning of crop residues, contribute to air pollution, releasing harmful pollutants and greenhouse gases that exacerbate climate change and pose health risks to local communities (Kolawole and Iyiola 2023).

Additionally, the accumulation of waste in water bodies can lead to water pollution, affecting aquatic life and water quality. Another challenge is the logistical and economic aspects of collecting, transporting, and processing agricultural waste, which can be cost-prohibitive for many farmers and industries (Mulvaney, Merrill, and Atkinson 2023). The variability in the composition and quality of waste materials further complicates their utilization, as different waste types require tailored processing technologies for conversion into valuable products. Moreover, there are regulatory and technological hurdles. The lack of comprehensive waste management policies and the slow adoption of innovative technologies for waste utilization hinder the development of sustainable waste management solutions (Hajam, Kumar, and Kumar 2023) Despite these challenges, agricultural waste holds immense potential for sustainable development. Advancements in technology and integrated waste management strategies can transform agricultural waste into valuable commodities, contributing to a circular economy.(Mujtaba et al. 2023).

2.2 Global rice production

Global rice production is a critical component of the world's food supply, with significant contributions from Asia, where over 80% of the world's rice is produced (Li 2023). According to recent data, global rice production for the 2023/24 marketing year is projected

to be substantial, with estimates suggesting a record-high production level (Jamal et al. 2023) (Jamal et al. 2023).

In the 2023 and 2024 period, worldwide rice production is forecasted at approximately 520.5 million metric tons (milled basis) (Basha 2023). This figure represents an increase from the previous year, indicating a continued global growth trend in rice production. The increase is partly due to favorable weather conditions and technological advancements in rice cultivation that improve yield rates across major producing countries. Asia continues to dominate global rice production, with countries like China and India leading the way. China's rice production for 2023 is significant, maintaining its position as one of the top producers globally (X. Wang et al. 2023). Similarly, India, another major player in the rice market, shows robust production figures that support its status as a leading rice exporter. Rice production is not only vital for domestic consumption in these countries but also plays a crucial role in the global rice trade, affecting global markets and food security(Bhatnagar and Khan 2024). The production figures and projections are important for market dynamics, influencing rice prices and trade policies worldwide. Understanding these trends is crucial for stakeholders in the agriculture sector, policymakers, and researchers focused on food security and sustainable agricultural practices (Sutiharni et al. 2024). The ongoing research and updates from organizations like the USDA and World Population Review provide valuable insights into how rice production adapts to challenges such as climate change, economic shifts, and technological innovations in agriculture.

Rice is one of the staple food grain crops produced globally with its continuously increasing demand to fulfill the needs of the nation and exports (Bhatnagar and Khan 2024). It is cultivated across all regions globally such as Oceania (.076 million tons), Europe (4.024 million tons), America (35.33 million tons), Africa (38.77 million tons), Asia (677.28 million tons), (FAOSAT, 2023). Global rice production continues to play a crucial role in sustaining food security worldwide, with Asia leading the charge (Thakur et al. 2024). As technological advancements and sustainable practices evolve, the potential to meet growing global demands while addressing environmental concerns looks promising. Stakeholders across the agricultural spectrum must continue to leverage up-to-date data

and engage in international cooperation to ensure the stability and growth of this vital food resource.

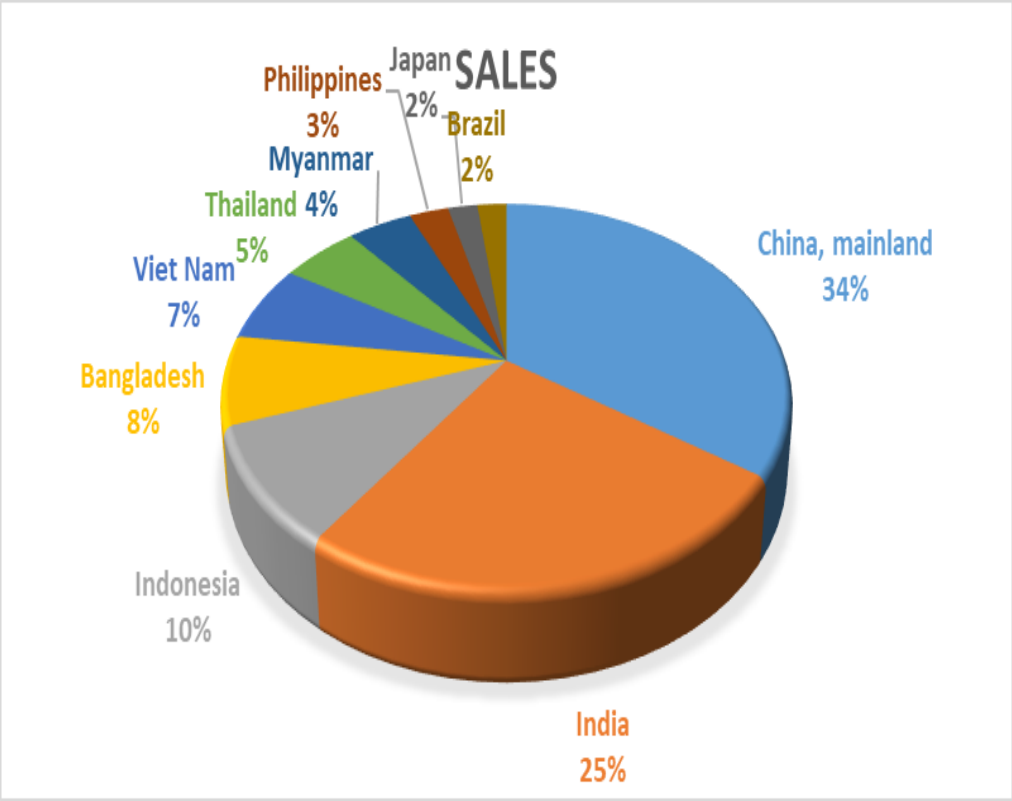

Figure 2.1 Global Rice Production **(**2017-2022) (FAOSAT, 2023)

2.3 Global rice straw production and utilization

The vegetative portion of rice plants is known as rice straw considered a nonedible part left as a by-product of rice after harvesting rice (Bandara and Kavindi 2023). The ratio of rice grain to rice straw ranges from 0.71 to 1.51. This implies that for every ton of paddy rice produced, there are 800 to 1600 kg of rice straw leftover (Amoakwah et al. 2024). Alternatively, approximately 6 tons of rice straw are left in the field for every 4 tons of harvested rice (Gurraj Singh et al. 2021). Moreover, Asia is rich in rice production and Its annual turnover is 677.6 Million tons; thus, with this huge production, in this way, a large quantity of straw around 1015.92 million tons is generated annually (Bhattacharyya et al., 2021). Rice straw is, typically consisting of the stems, leaves, and husks left in the field

after the rice grains are harvested. This residue is a considerable byproduct given the vast scale of global rice cultivation (Chieng and Kuan 2022).

During the harvesting process, which can be conducted using modern combine harvesters or traditional methods, the rice grains are separated from the stalks, leaving the straw scattered across the fields. The management of rice straw varies; it can be collected and baled for use in various applications, incorporated back into the soil to enhance soil fertility, or, less desirably, burned in fields, which, although cost-effective, leads to significant environmental pollution and loss of soil nutrients. The ratio of rice straw production to rice grain globally is approximately 1.5:1 (Tokas et al. 2021). This means for every ton of harvested rice grain, about 1.5 tons of rice straw are produced, although this ratio can fluctuate based on the rice variety, cultivation methods, and local environmental conditions (A. Sharma, Singh, and Arya 2020). With global rice grain production averaging around 740 million tons annually, it is estimated that over 1 billion tons of rice straw are generated each year (Sudarsan et al. 2023).

This vast amount of rice straw presents both challenges and opportunities. Properly managed, it can be used sustainably, offering environmental and economic benefits. Potential applications for rice straw are diverse and include uses in renewable energy (as a bioenergy source), construction materials, paper manufacturing, and even textile production. The sustainable management of rice straw is crucial to avoid environmental issues associated with traditional disposal methods like open burning and to exploit its full potential as a valuable resource in various industrial applications. As the global focus on sustainability intensifies, innovative and environmentally friendly solutions for utilizing rice straw are increasingly being explored, which could significantly transform this agricultural byproduct into a key resource for multiple sectors.

2.4 Rice straw management and challenges

Based on the current situation, there is no justifiable and ecological way out to manage this large quantity of rice straw; thus, the farmers have no other solution of rice straw burning (R. Singh et al. 2020). Furthermore, due to the automatic mode of rice harvesting (Combine

harvesting, reaper, baler, etc.) the straw leftovers in the fields. Farmers report that the main reason for this practice is the short interval between the harvesting of rice and the planting of the next crop.

Table 2.1: Emissions of harmful air pollutants from rice straw burning

Pollutant Type	**Pollutant**	**Specific Emission Factors**	**Unit**	**References**
Particulate Matter	Fine particulate matter (PM2.5)	8.3	g kg^-1	(Ravindra 2019)
Particulate Matter	Particulate Matter (PM10)	9.1	g kg^-1	(Ravindra 2019)
Particulate Matter	Organic Carbon (OC)	0.58	g kg^-1	(H. Zhang 2018)
Particulate Matter	Black Carbon (BC)	3.5	g kg^-1	(H. Zhang 2018)
Greenhouse Gases	Methane (CH4)	217.10	Gg kg^-1	FAOSTAT,2023
Greenhouse Gases	Nitrous Oxide (N2O)	5.60	Gg kg^-1	FAOSTAT,2023
Greenhouse Gases	Carbon Dioxide (CO2)	6300	Gg kg^-1	FAOSTAT,2023
Air Pollutants	Ammonia (NH3)	0.42	g kg^-1	(Fang 2017)
Air Pollutants	Sulphur Dioxide (SO2)	2	g kg^-1	(Satyendra 2013)
Air Pollutants	Volatile Organic Compounds (VOC)	7.95	g kg^-1	(H. Zhang 2018)
Air Pollutants	Oxides of Nitrogen (NOx)	2.28	g kg^-1	(Satyendra 2013)
Air Pollutants	Carbon Monoxide (CO)	93	g kg^-1	(Ravindra 2019)

The improper management of rice straw, especially the prevalent practice of open burning, presents significant environmental and health challenges. Although rice straw is a valuable agricultural byproduct with various potential uses, its mismanagement often leads to detrimental consequences (G. Singh and Arya 2021). Open burning of rice straw is a common method employed by farmers to quickly clear fields for the next planting season. This approach is considered cost-effective and time-saving but leads to severe air pollution by releasing harmful pollutants such as particulate matter and volatile organic compounds into the atmosphere (Majumder et al. 2023). These emissions degrade air quality, contribute to smog formation, and pose health risks to local populations, particularly affecting vulnerable groups such as children and the elderly.

Additionally, burning rice straw releases large quantities of greenhouse gases like carbon dioxide, methane, and nitrous oxide, intensifying global warming and climate change (Somboon et al. 2024). . The practice also results in the loss of valuable organic matter and nutrients from the soil, diminishing its fertility and altering its structure, which can adversely affect future crop yields. Moreover, the fires can destroy habitats, leading to a loss of biodiversity in agricultural areas. To combat these issues, promoting sustainable management practices is crucial. These include incorporating rice straw back into the soil to improve its fertility, converting straw into bioenergy through methods like anaerobic digestion, and processing it into useful products such as paper, building materials, and textiles (K. Singh et al. 2023). Implementing effective government policies and regulations to restrict burning, alongside educating farmers about alternative practices, can help mitigate the negative impacts of rice straw mismanagement. By transitioning to these sustainable practices, the full potential of rice straw can be harnessed, contributing to environmental conservation and public health protection.

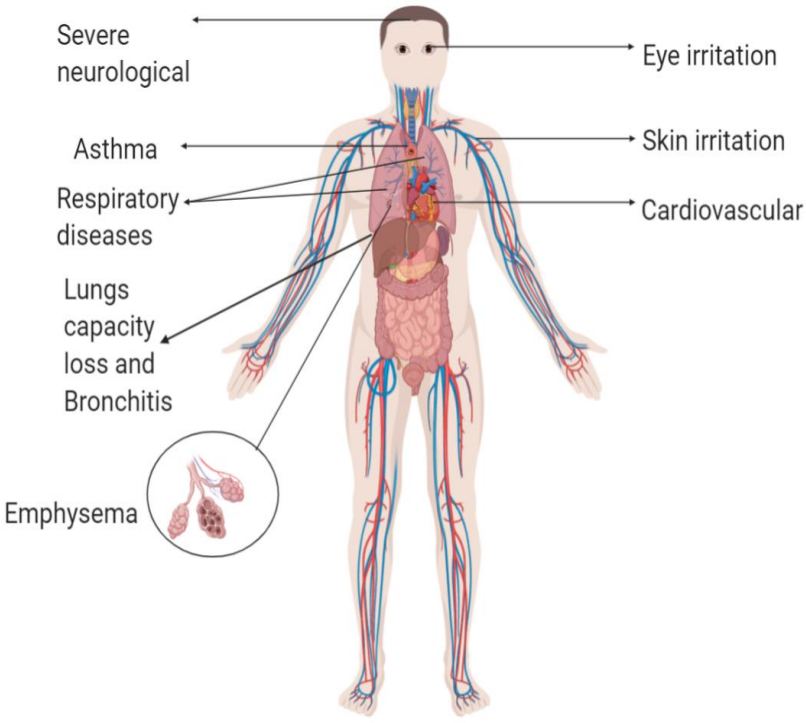

Figure 2.2 Major health hazards of rice straw burning

2.5 Efficient rice straw management

Effective management of rice straw is crucial for transforming this agricultural byproduct from a waste material into a valuable resource (G. Singh and Arya 2021). Incorporating rice straw back into the soil is one sustainable practice that enhances soil organic matter, improving soil structure, moisture retention, and nutrient cycling. This method also mitigates greenhouse gas emissions compared to traditional burning practices (K. Gupta et al. 2021). Composting rice straw with other organic materials produces a rich organic fertilizer that further benefits soil fertility and structure, supporting various agricultural and horticultural applications. Rice straw also holds significant potential as a bioenergy source. It can be converted into biogas through anaerobic digestion or into bioethanol through processes that break down its lignocellulosic biomass (Poddar et al. 2022). Advanced technologies like gasification and pyrolysis can transform rice straw into syngas and bio-oil, providing renewable energy solutions. Beyond energy, rice straw finds applications in

industrial products such as paper, where it serves as an eco-friendly alternative to wood pulp, and in emerging fields like bioplastics and building materials (Gupte et al. 2023).

Another innovative use of rice straw is in mushroom cultivation, where it provides an ideal substrate for growing edible fungi like oyster mushrooms. This not only yields a valuable food product but also facilitates the breakdown of complex organic materials in the straw, enriching the soil (Siedt et al. 2021). However, the widespread implementation of these practices requires robust support from regulatory frameworks and policies that encourage sustainable management, provide incentives for using agricultural waste, and implement strict controls against open burning. Addressing the challenges associated with the economic viability, technological requirements, and logistics of rice straw management is crucial for its future. Developing more efficient machinery for handling rice straw, improving conversion technologies, and fostering collaboration among governments, industries, and research institutions are essential steps toward scaling sustainable practices (Anand and Kaur 2024). With continued innovation and supportive policies, the comprehensive management of rice straw can significantly contribute to environmental sustainability and resource conservation.

However, in recent works, researchers have utilized rice straw as an excellent source of cellulose to develop bio-based packaging. Due to the renewable and abundant availability of waste materials such as agricultural residues including stalks, straws, cobs, hulls, sugarcane bagasse, and grasses (cheap sources of non-woody cellulose are widely used as a feedstock of cellulose materials (D. Sharma and Saini 2020). Researchers have demonstrated that rice straw, a non-woody residue, serves as a viable alternative to traditional woody materials for paper production, leveraging its advantageous physical, chemical, thermal, and biological properties (Usmani et al. 2020). Its open structure allows for easy portability and simpler pulping processes without the need for harsh chemicals, making cellulose isolation from rice straw economically feasible and a superior alternative to burning.

Moreover, its utilization as a bio-polymer in the form of nano-composites to formulate bio-based films received remarkable attention in the food and medical field (Melesse et al.

2023). However, the widespread use of synthetic polymers also leads to significant environmental issues, stemming from the extended exposure of ecosystems to packaging materials based on synthetic polymers (Fisher et al. 2022). Therefore, the consumption of rice straw as a cheap source of cellulose could be the best approach for the management of excessive quantities of rice straw and also combat the issues of synthetic polymers such currently, paper industries are facing significant problems due to a shortage of resources, environmental pollution, and technical equipment. Furthermore, the nonwoody Fiber resources exhibit superior physical and optical characteristics that can enhance the quality of their products (Abdallah et al. 2023). The management of rice straw in this manner to utilize excess amount of rice straw, to stop rice straw burning and to fabricate a bio packaging due to the excessive demand for green materials, and awareness of environmental issues could be the best approach towards sustainable agriculture.

2.6 Cellulose

Cellulose is a complex carbohydrate or polysaccharide, that plays a critical role in the cell walls of green plants and is a key structural component of the plant kingdom (Y. Wang et al. 2022). It is the most abundant organic polymer on Earth, providing structural support to plants by forming microfibrils of cellulose molecules, which are then organized into fibers that add strength and rigidity to plant tissues. Cellulose's structure, properties, and applications make it a substance of immense importance across various industries, including paper, textiles, and biofuels. Cellulose is made up of glucose monomer units linked together with β(1→4) glycosidic bonds, forming long chains that can contain from several hundred to over ten thousand glucose units (Lehrhofer et al. 2022). These linear chains pack closely together to form microfibrils due to hydrogen bonding between hydroxyl groups of adjacent glucose units. This tight packing results in cellulose's high tensile strength and insolubility in water.

2.6.1 Different sources of cellulose

Plants are the primary and most abundant sources of cellulose, serving as the structural component of the plant cell wall. This organic polymer is crucial for the plant’s rigidity and strength, allowing it to grow upright and resist external pressures (Ganewatta, Wang,

and Tang 2021). In the plant kingdom, cellulose is synthesized by cellulose synthase complexes located in the cell membrane, where glucose units are polymerized into long chains that form microfibrils. These microfibrils intertwine with other substances like hemicellulose and lignin, creating a composite material that is both strong and flexible. Among plants, trees are the most significant source of cellulose, particularly used in the lumber and paper industries (Babaei-Ghazvini et al. 2024).

Hardwoods and softwoods vary in their cellulose content and structure, affecting their utility in different applications. Cotton is another vital plant source, boasting the highest purity of natural cellulose, around 90%, making it indispensable in the textile industry for its absorbency and softness. Bamboo and hemp are other notable sources, valued for their rapid growth and sustainability. Bamboo's cellulose is increasingly used in textiles, paper, and construction, while hemp cellulose is recognized for its strength and is utilized in textiles, paper, and even biodegradable plastics (Chakkour et al. 2023). Agricultural by-products also represent a significant source of cellulose. Straw from wheat and rice, bagasse from sugarcane, and corn stalks and husks are repurposed for paper production, packaging materials, and biofuel, demonstrating cellulose's versatility and the move towards sustainability by utilizing waste products efficiently. The ubiquity and renewability of plant-based cellulose make it an essential material for a multitude of applications, from traditional uses like paper and textiles to innovative uses in bioplastics and bioethanol production (Shen et al. 2023). The focus on plant sources for cellulose is not only driven by their abundance and renewable nature but also by the growing demand for sustainable and biodegradable materials in various industries. As research continues to enhance the extraction and processing techniques for cellulose from plants, its significance in both economic and environmental contexts is expected to grow, underlining the critical role of plants in providing this indispensable natural resource (Binod and Raveendran 2021).

The extraction of cellulose from various sources, particularly plants and agricultural by-products, involves several methods, each tailored to the specific type of biomass and the desired purity and physical properties of the cellulose. These methods range from

mechanical treatments to chemical processes and biotechnological approaches (Arnold et al. 2020). The choice of method depends on the source material, the intended application of the cellulose, and economic and environmental considerations. Here's an in-depth look at the primary cellulose extraction methods:

2.6.2 Cellulose extraction methods

2.6.2.1 Mechanical methods

The mechanical method of cellulose extraction is a foundational approach that relies on physical forces to separate cellulose fibers from the other components of plant material, such as lignin and hemicellulose. This method is characterized by its simplicity and the minimal use of chemicals, making it environmentally friendly compared to chemical extraction methods (Pena-Pereira, Wojnowski, and Tobiszewski 2020). Mechanical processing typically involves several stages, including grinding, milling, or refining, which mechanically disrupt the plant cell walls, thereby facilitating the release of cellulose Fibers. Grinding and milling are initial processes where raw biomass, such as wood chips, straw, or other plant materials, is mechanically broken down into smaller pieces or particles (Saadon, Osman, and Yusup 2022). This is achieved through various equipment such as hammer mills, ball mills, or disc mills, each designed to reduce the biomass to a specific size and consistency. The primary goal here is to increase the surface area of the material, improving the accessibility of cellulose for further extraction or processing.

2.6.2.2 Acid hydrolysis

This method primarily utilizes concentrated or dilute acids, such as sulfuric acid, hydrochloric acid, or phosphoric acid, under controlled temperature and pressure conditions to achieve the selective decomposition of non-cellulosic components, leaving behind a cellulose-rich product (Bangar et al. 2023). In the process of acid hydrolysis, the biomass is first pretreated to increase the availability of the acid to the cellulose. The pretreatment might involve mechanical size reduction, soaking in water, or applying steam. Following pretreatment, the material is subjected to acid under specific conditions. Concentrated acid hydrolysis operates at lower temperatures but requires a longer reaction time, whereas dilute acid hydrolysis is conducted at higher temperatures and pressures but

for a shorter duration (Chaudhary et al. 2024). The choice between concentrated and dilute acid hydrolysis depends on the type of biomass, the desired yield and purity of cellulose, and economic and environmental considerations. The acid not only breaks down the hemicellulose and partially dissolves lignin but also hydrolyses the glycosidic bonds within the cellulose, reducing its degree of polymerization. This can be advantageous or detrimental based on the intended use of the cellulose (M. Zhang et al. 2021).

After hydrolysis, the mixture is neutralized, and the cellulose is separated from the liquid fraction through filtration or centrifugation. The cellulose may then undergo further purification steps, such as washing and bleaching, to remove any residual lignin, hemicellulose, or acid. Acid hydrolysis is advantageous due to its ability to process a wide range of biomass types and its effectiveness in breaking down complex lignocellulosic structures (Agrawal et al. 2021). However, the method also has significant drawbacks, including the corrosiveness of the acids, which can require specialized equipment and safety measures; the potential for generating environmental pollutants; and the risk of degrading cellulose if the reaction conditions are not carefully controlled. Moreover, the process generates by-products such as sugar derivatives and organic acids, which need to be managed or valorized to make the process economically viable and environmentally sustainable.

2.6.2.3 Enzymatic hydrolysis

It is a sophisticated and environmentally friendly method for extracting cellulose from biomass, utilizing specific enzymes to selectively break down the polysaccharide chains of cellulose into simpler sugars without harming the cellulose itself (J. Zhang et al. 2020). This method leverages the natural ability of enzymes, such as cellulases and hemicellulases, to cleave the β-1,4-glycosidic bonds in cellulose and hemicellulose, respectively (Thapa et al. 2020). Unlike chemical processes that require harsh conditions and produce significant waste, enzymatic hydrolysis operates under milder conditions, resulting in less degradation of the cellulose and lower environmental impact. The process of enzymatic hydrolysis begins with a pretreatment step to increase the accessibility of the cellulose (Haiyan Zhang, Han, and Dong 2021). This pretreatment process may utilize

physical, chemical, or enzymatic techniques to eliminate lignin and hemicellulose, disrupt the crystalline integrity of cellulose, and expand the surface area accessible for enzymatic activity. Following pretreatment, the biomass is incubated with a cocktail of enzymes, typically at temperatures ranging from 40 to 50°C and at a neutral or slightly acidic pH, conditions under which the cellulases and hemicelluloses are most active (Houfani et al. 2020).

However, the method is not without its challenges. The cost of enzymes, the potential for enzyme inhibition by certain components of the biomass or by-products of the reaction, and the slower reaction rates compared to chemical methods are significant considerations. Advances in biotechnology, including the development of more efficient and robust enzymes, genetic engineering of microorganisms to produce enzymes cheaply, and the optimization of reaction conditions, are ongoing efforts aimed at overcoming these hurdles, making enzymatic hydrolysis a promising method for sustainable cellulose extraction and biomass conversion.

2.6.2.4 Alkali treatment

Alkali treatment, also known as the alkaline or Kraft process, is a prevalent and efficient method for cellulose extraction from lignocellulosic biomass, particularly from wood (Sewsynker-Sukai, Naomi David, and Gueguim Kana 2020). This chemical method utilizes strong alkaline solutions, typically sodium hydroxide (NaOH) and sodium sulfide (Na2S), to dissolve the lignin and separate it from cellulose and hemicellulose fibers. The process is distinguished by its ability to break down the complex, rigid structure of lignin, thereby facilitating the release of high-quality cellulose fibers suitable for various applications, including paper and textile manufacturing (Mather, Rana, and Wardman 2023). During alkali treatment, the biomass is first subjected to a cooking process in a solution of NaOH and Na2S at high temperatures, usually between 150°C and 170°C, and under pressure for several hours (Martins, Carvalheiro, and Gírio 2024). This harsh environment causes the saponification of ester bonds in lignin and hemicellulose, leading to their solubilization and separation from the cellulose fibers. The alkaline conditions also swell the cellulose, increasing its surface area and making it more accessible for further

processing (Tian et al. 2022). Additionally, the treatment partially hydrolyses and removes hemicellulose, enhancing the purity of the cellulose obtained. One of the key advantages of the alkali treatment is its effectiveness in processing various types of lignocellulosic biomass, including hardwoods, softwoods, and agricultural residues, while maintaining the integrity and degree of polymerization of the cellulose fibers. This results in cellulose with desirable physical and chemical properties, such as high strength and reactivity, which are crucial for its end-use applications.

However, the process also poses environmental challenges, primarily due to the use and disposal of the alkaline chemicals and the effluents generated, which contain dissolved lignin and other organic substances (Sun et al. 2021). Modern pulp and paper industries have made significant advancements in recycling and recovering chemicals used in the process through the implementation of closed-loop systems and treatment facilities, mitigating the environmental impact. Moreover, ongoing research is focused on optimizing the conditions of alkali treatment to reduce chemical usage and processing time, improve the yield and quality of cellulose, and enhance the overall sustainability of the process. Innovations in this area include the development of more efficient cooking protocols, the utilization of novel alkaline agents, and the integration of alkali treatment with other biomass processing methods, such as enzymatic hydrolysis, to further refine and valorise the cellulose product (Gallego-García et al. 2023).

Table 2.2 Extraction of cellulose from agricultural waste and Its applications

Agricultural Waste	Extraction Method	Total Yield (%)	Potential Application	References
Rice Husk	Alkaline Treatment	30-40	Paper, Bio-composites	(J. Smith and Lee 2021)
Wheat Straw	Steam Explosion	35-45	Ethanol, Biodegradable Plastics	(H. Johnson and Kumar 2020)
Corn Stover	Dilute Acid Hydrolysis	20-30	Biofuel, Textile Fibers	(T. Brown 2019)
Sugarcane Bagasse	Organosolv Process	25-35	Paper Products, Biodegradable Films	(White and Zhao 2022)

Cotton Stalks	Bleaching	40-50	Textiles, Absorbent Materials	(M. Davis and O'neill 2018)
Bamboo	Mechanical Refining	45-55	Construction Materials, Paper	(L. Kim and Park 2021)
Banana Stems	Chemical Pulping	30-40	Paper, Textiles	(S. Martinez and Hernandez 2020)
Coconut Husk	Retting and Mechanical Processing	20-30	Mats, Ropes, Brushes	(A. Green and Patel 2019)
Oil Palm EFB	Steam Pretreatment	25-35	Biofuels, Animal Feed	(Zhao and Lee 2018)
Soybean Straw	Solvent Extraction	15-20	Fertilizer, Bioplastic	(R. Taylor and Nguyen 2022)
Barley Straw	Alkaline Hydrogen Peroxide Treatment	20-30	Insulation Materials, Paper	(M. Patel and Brown 2019)
Coffee Husk	Microwave-Assisted Extraction	10-20	Fuel Pellets, Fabric	(Lopez and Wilson 2017)
Peanut Shells	Acidic Treatment	25-35	Adsorbents, Fillers	(Sanders and Kumar 2020)
Sunflower Stalks	Hot Water Extraction	30-40	Biogas, Paper	(Norris and Cheng 2018)
Potato Peelings	Alkaline Extraction	25-35	Biodegradable Films, Adhesives	(Fitzgerald and Thomas 2021)

2.7 Nanocellulose synthesis from cellulose materials

The nanocellulose synthesis from cellulose represents a remarkable advancement in the field of nanotechnology, offering a sustainable route to produce high-performance, renewable nanomaterials with exceptional mechanical properties, high surface area, and unique optical characteristics. The synthesis of nanocellulose from cellulose is not only a technological challenge but also a sustainability opportunity. Both CNCs and CNFs exhibit biodegradability, and low toxicity, and are derived from renewable sources, making them highly attractive for a wide range of applications, including reinforced composites, biomedical devices, packaging materials, and electronic components. The choice between CNCs and CNFs, and the specific synthesis method of nanocellulose depends on its desired properties such as crystallinity, aspect ratio, and surface functionality, as well as the

intended application (G. K. Gupta and Shukla 2020). Advancements in the synthesis of nanocellulose focus on improving efficiency, reducing environmental impact, and scaling up production processes. This includes the development of less energy-intensive mechanical treatments, greener chemical modifications, and the utilization of waste biomass as a cellulose source. As advancements in research and technology progress, nanocellulose is anticipated to be pivotal in the creation of advanced materials and sustainable products for future applications.

2.7.1 Synthesis methods of nanocellulose

The synthesis of nanocellulose, a versatile and sustainable nanomaterial derived from cellulose, involves various methods to produce either cellulose nanocrystals (CNCs) or cellulose nanofibers (CNFs), each with unique properties and applications. These synthesis methods are designed to disintegrate bulk cellulose into nano-sized fibers or crystals, exploiting the inherent structural hierarchy of cellulose. The choice of synthesis method depends on the desired characteristics of the nanocellulose, such as its dimensions, crystallinity, and surface functionality. Below are detailed descriptions of the primary synthesis methods for nanocellulose.

2.7.1.1 Acid hydrolysis

Acid hydrolysis is a critical process in the production of nanocellulose, particularly for isolating cellulose nanocrystals (CNCs) from various cellulose sources like wood fibers, agricultural residues, and another biomass. This method involves breaking down the bulk cellulose structure into nanoscale particles using acid, resulting in highly crystalline nanocellulose with unique properties suitable for a wide range of applications.

2.7.1.1.1 Sulfuric acid

It is the most common technique for producing nanocellulose crystals. This process involves treating cellulose fibers with strong acids, such as H_2SO_4 (sulfuric acid) or HCL (hydrochloric acid), under controlled conditions. The acid preferentially removes the amorphous part from cellulose and leaves behind the more resistant crystal-like regions which are rod-like particles with high aspect ratios and excellent mechanical properties

(Gong et al. 2022). The dimensions of CNCs can be controlled by adjusting the hydrolysis time, temperature, and acid concentration. Following hydrolysis, the CNC suspension is diluted, neutralized, and centrifuged to wash away the acid and by-products. The CNCs can be further modified chemically to tailor their surface properties for specific applications.

2.7.1.1.2 Citric acid

The synthesis of nanocellulose using citric acid presents a relatively novel and eco-friendly approach, diverging from more traditional, harsh chemical treatments for isolating nanocellulose (Ludwicka, Kaczmarek, and Białkowska 2020). Citric acid, a weak organic acid naturally found in citrus fruits, offers a more benign alternative to strong mineral acids like sulfuric or hydrochloric acid, commonly used in the production of cellulose nanocrystals (CNCs) and cellulose nanofibers (CNFs) (Meninno 2020). The process capitalizes on citric acid's ability to hydrolyze cellulose, particularly targeting the amorphous regions, while minimizing damage to the crystalline structure. This method aligns with green chemistry principles, aiming to reduce environmental impact and enhance safety.

The pretreated biomass is then subjected to hydrolysis with citric acid. Unlike the concentrated acids used in traditional methods, citric acid is applied under milder conditions, which can include lower temperatures and less extreme pH levels (Gomes et al. 2022). The conditions are optimized to promote the selective hydrolysis of the amorphous part, leaving the crystal-like structure. The specific concentration of citric acid, temperature, and duration of hydrolysis are critical parameters that influence the efficiency of the process and the quality of the nanocellulose produced.

Following hydrolysis, the reaction mixture is neutralized to stop the acid reaction, typically by adding a base. The suspension was then washed many times to remove the remaining citric acid from nanocellulose and any soluble sugars or oligosaccharides formed during the hydrolysis. Separation and drying: The nanocellulose is separated from the liquid by centrifugation or filtration. The wet nanocellulose can be used as is in some applications

or can be dried to yield a powder or aerogel, depending on the intended use. Freeze-drying is often used to preserve the nanoscale structure of the cellulose.

2.7.1.2 Mechanical methods

Mechanical processes, such as high-pressure homogenization, grinding, and ultrasonication, are employed to produce cellulose nanofibers (Wu et al. 2021). These methods apply physical forces to defibrillate cellulose pulp, separating the fibers down to the nanoscale. Mechanical treatments may be preceded by chemical or enzymatic pretreatments to facilitate fiber separation. For instance, TEMPO-mediated oxidation introduces negative charges on the cellulose surface, aiding in the defibrillation process. Mechanical processing yields flexible and long CNFs with a high aspect ratio, suitable for applications requiring robust mechanical properties and high surface area.

2.7.1.3 Enzymatic hydrolysis

Enzymatic treatment offers a more environmentally friendly alternative for nanocellulose production (Pere et al. 2020). Specific enzymes, such as cellulases and hemicelluloses, are used to selectively degrade the amorphous regions of cellulose without damaging the crystalline structure. This method can be used alone or in combination with mechanical treatments to produce CNFs with minimal energy input and lower environmental impact (Gallo Stampino et al. 2021). Enzymatic hydrolysis provides fine control over the degree of polymerization and the surface properties of the resulting nanocellulose.

Table 2.3 Applications of nanocellulose in food industry

Type of Nanocellulose	Application in Food Industry	Key Findings/Benefits	Study
Bacterial Nanocellulose	Edible Food Packaging	Enhanced mechanical strength and barrier properties; improved biodegradability	(Y. Zhang and Chen 2023)
Cellulose Nanocrystals (CNC)	Food Thickeners	Improved viscosity and texture in sauces and dressings; stability under heat	(J. Lee and Kim 2022)

Cellulose Nanofibers (CNF)	Low-Fat Food Products	Fat replacement in mayonnaise and ice cream with maintained texture and flavor	(M. Johnson, Thompson, and Patel 2021)
Nanocellulose Composites	Antimicrobial Food Packaging	Extended shelf life of perishable foods through active antimicrobial properties	(A. Smith, Davis, and Rao 2023)
Bacterial Nanocellulose	Biodegradable Beverage Bottles	Fully biodegradable packaging solution with minimal environmental impact	(D. Patel and Rao 2022)
Nanocellulose Gel	Meat Products	Improved water retention and texture in processed meats	(Huang and Zhang 2021)
Nanostructured Cellulose	Dairy Alternatives	Enhanced stability and mouthfeel in plant-based milk products	(García, López, and Sánchez 2023)
Nanocellulose Beads	Encapsulation of Flavors and Additives	Efficient delivery of flavors and nutritional additives in functional foods	(Chang and Lee 2022)
Nanocellulose Coatings	Fruit and Vegetable Coatings	Prolonged freshness and reduced spoilage by creating a breathable, protective layer	(Weiss and Clark 2021)
Hydroxypropyl Cellulose (HPC) Nanocellulose	Gluten-Free Baking	Improved texture and volume in glute	(R. Thompson, Johnson, and Clark 2023)

Nanocellulose is increasingly recognized within the food sector for its distinctive attributes, including extensive surface area, robust mechanical properties, and biodegradability. It has versatile applications that enhance both the functionality and nutritional qualities of food products. In food packaging, nanocellulose offers enhanced barrier properties against oxygen, oil, and grease, crucial for extending the shelf life of packaged foods. Its use in creating strong, lightweight, and transparent films helps in reducing food spoilage and enhancing safety. These films can also be integrated with antimicrobial agents or antioxidants, providing active packaging solutions that maintain food quality and freshness (Bar, Alagirusamy, and Das 2019).

Additionally, nanocellulose acts as a thickening agent in various food products such as sauces and low-fat dairy items, improving texture and consistency without compromising flavor (Didone and Tosello 2021). It also stabilizes emulsions and foams, which is beneficial for products like ice cream and mayonnaise, ensuring they maintain their structure and extend shelf life. Beyond texturizing, nanocellulose is used to develop edible films and coatings that can encapsulate active compounds like vitamins and probiotics, enhancing the nutritional profile of the coated products (Dantas et al. 2021).

2.8 Food packaging

Food packaging is essential for safeguarding food products from contamination, extending their shelf life, and providing critical information to consumers. It utilizes various materials and technologies to ensure that food remains nutritious, fresh, and safe up until consumption. However, traditional plastic packaging, despite its prevalence and utility, has notable drawbacks. The environmental impact of plastic is significant; it is produced from non-renewable resources and is largely non-biodegradable, leading to persistent pollution in ecosystems, particularly marine environments where it poses a threat to wildlife (J. Smith, Thompson, and Roberts 2021). Additionally, certain plastics can leach harmful chemicals like BPA and phthalates into food, posing health risks such as hormonal disruptions and increased cancer risk (M. Johnson and Lee 2020).

Conversely, biodegradable or bio-based packaging offers several environmental and health advantages. Made from renewable resources such as plant fibers and biopolymers, bio packaging reduces reliance on fossil fuels and is typically biodegradable or compostable, thus mitigating landfill waste and pollution (E. Davis 2019). The production of bio packaging generally results in lower carbon emissions, supporting efforts against climate change (Chen, Zhao, and Gupta 2022). Innovations in material science driven by the development of bio packaging have led to new materials that are not only environmentally friendly but also perform as well or better than traditional plastics in terms of strength and protective properties (H. Kim and Park 2023). Furthermore, the market demand for sustainable products is increasingly influenced by consumer awareness of environmental issues, making bio packaging an attractive choice for brands looking to enhance their eco-

friendly image and meet consumer expectations (Williams 2021).This shift from traditional plastic to bio-based alternatives supports a more sustainable, circular economy, aligning with global sustainability goals and reducing the environmental footprint of packaging waste.

2.9 Nanocomposite film

Nanocomposite films represent a significant advancement in material technology, merging the benefits of polymer science with the unique properties of nanoparticles to enhance and diversify the functionality of films. These films are composed of two primary elements: the polymer matrix and the nanoparticles (Mishra et al. 2022). The polymer matrix functions as the continuous phase within which the nanoparticles are dispersed. This matrix can be either synthetic, like polyethylene (PE) and polypropylene (PP), or natural, such as polylactic acid (PLA) and other biopolymers like starch and cellulose (Gowthaman et al. 2021). PE is favored for its durability and chemical resistance, making it ideal for various packaging applications, while PP offers a higher melting point that benefits applications requiring thermal resistance. PLA, derived from renewable resources, is particularly valued in contexts demanding biodegradability, such as in food packaging and agricultural films (Pellis et al. 2021) . Natural polymers are similarly employed where environmental impact is a concern, as they naturally break down more readily than synthetic alternatives. Nanoparticles within the matrix serve as the dispersed phase and are pivotal in conferring new or enhanced properties on the nanocomposite film. These nanoparticles vary widely, including metal oxides like titanium dioxide and zinc oxide, carbon-based materials such as carbon nanotubes and graphene, clays, and even organic nanoparticles (Rizwan et al. 2021).

Titanium dioxide is utilized for its UV-blocking capabilities, which is crucial for products exposed to sunlight, whereas zinc oxide’s antibacterial properties extend the shelf life of perishable goods when used in food packaging. Carbon nanotubes and graphene are lauded for their extraordinary mechanical strength and electrical conductivity, suiting them for advanced electronic applications (Schirmeister and Mülhaupt 2022). Clays, particularly those like montmorillonite, improve the film’s barrier properties against moisture and gases

due to their layered structures. The effectiveness of these nanocomposite films is highly dependent on the nanoparticles' uniform distribution within the polymer matrix. Proper integration and dispersion of nanoparticles are crucial for them to effectively reinforce the matrix and uniformly impart their properties throughout the film. Techniques such as ultrasonication, high-shear mixing, and solvent casting are commonly employed to achieve this dispersion.

In essence, nanocomposite films blend the desirable attributes of their constituent materials to meet specific industrial needs, offering customizable solutions that enhance performance and potentially reduce environmental impact. This innovative combination places nanocomposite films at the forefront of material science, with applications spanning from environmentally friendly packaging to high-strength, functional films for technological uses.

2.9.1 Fabrication of nanocomposite film

Fabrication of nanocomposite films involves integrating nanoparticles into a polymer matrix to create materials with enhanced properties compared to their conventional counterparts. This process requires careful consideration of material selection, dispersion techniques, and film formation methods to ensure optimal performance and functionality of the final product. Here is an overview of the typical steps involved in the fabrication of nanocomposite films:

2.9.1.1 Solvent casting

Solvent casting is a popular and versatile method for fabricating nanocomposite films, appreciated for its simplicity, cost-effectiveness, and the ability to produce high-quality films with uniform nanoparticle dispersion. This technique begins with the selection of a suitable polymer, which must be dissolvable in a chosen solvent. Polymers used can range from natural varieties like cellulose and chitosan to synthetic types such as polyvinyl alcohol (PVA) and polycaprolactone (PCL) (Anusiya and Jaiganesh 2022). Nanoparticles—whether inorganic like titanium dioxide and zinc oxide, carbon-based such as carbon nanotubes and graphene oxide, or even organic nanoparticles—are then evenly dispersed within the polymer solution. This dispersion is typically achieved through

methods like mechanical stirring or ultrasonication to prevent aggregation. Once a homogeneous mixture is prepared, it is cast into molds or spread on flat surfaces where the solvent is allowed to evaporate. The evaporation can be natural at room temperature or accelerated by controlled heating, impacting the film's final morphology (Jiang et al. 2023). Slow and even evaporation under controlled conditions can help in forming films with smooth surfaces and uniform thickness.

Post-evaporation, the films often undergo additional drying to eliminate any residual solvent that might affect their stability and performance (Guo et al. 2024). Certain applications may require further post-treatment like thermal annealing or UV curing to enhance the mechanical properties or to induce cross-linking within the polymer matrix. The advantages of solvent casting include precise control over film thickness, the capability to produce films with very smooth surfaces, and the flexibility to incorporate a variety of functional additives into the polymer solution. However, the technique does have its drawbacks, including the environmental and health hazards posed by the use of volatile organic solvents and challenges related to scaling up the process for industrial applications.

2.9.1.2 Melt extrusion

Melt extrusion is a fundamental and efficient manufacturing process widely used to produce nanocomposite films, particularly suitable for thermoplastic polymers. This process involves blending polymers with nanoparticles to enhance the films' properties and then forming them into continuous shapes through a high-temperature, high-shear extrusion process (Tao et al. 2024). Common polymers used include polyethylene (PE), polypropylene (PP), and polylactic acid (PLA), which are known for their ability to melt and flow under the conditions inside an extruder without degrading. During the melt extrusion process, the polymer and carefully selected nanoparticles—such as nano clays, carbon nanotubes, graphene, or metal oxides—are first pre-mixed or compounded. This mixture is then fed into the extruder’s hopper, leading into a barrel where a rotating screw pushes the material forward (Campbell et al. 2023).

As the material advances through the barrel, it encounters zones of increasing temperature, causing the polymer to melt. The mechanical action of the screw not only

mixes the molten polymer with the nanoparticles but also applies shear forces, enhancing the dispersion of nanoparticles throughout the matrix. The homogenous, molten nanocomposite is then forced through a die that shapes it into a film. Exiting the die, the film goes through a series of chilled rollers that cool and solidify it rapidly, setting its final dimensions and properties (Gonçalves, Reis, and Fernandes 2024). This method is especially valued for its ability to produce films continuously, which is ideal for large-scale manufacturing. Melt extrusion does not require solvents, making it environmentally friendly compared to solvent-based processes, and allows for extensive customization of the material properties by adjusting the types and amounts of nanoparticles and polymers used.

2.9.1.3 Blow film extrusion

Blow film extrusion is a sophisticated manufacturing technique widely used for creating plastic films, especially beneficial in producing nanocomposite films for packaging, agricultural applications, and more. This process begins by mixing a selected polymer, such as polyethylene (PE), polypropylene (PP), or polylactic acid (PLA), with nanoparticles like nano clays, carbon nanotubes, or metal oxides (Fahim et al. 2024). The blend is typically prepared as a masterbatch to confirm the even spreading of nanoparticles in the polymer, essential for achieving consistent film properties. The polymer-nanoparticle mixture is then fed into an extruder where it is melted through heat and the mechanical action of screws. As the molten composite exits through a circular die at the top of the extruder, it forms a thin, tubular film. Immediately after extrusion, air is injected into the centre of this tube, inflating it to form a bubble. This inflation process not only thins the film but also expands its diameter to the desired size (Kamaliya and Upadhyay 2023). The film's properties such as thickness and strength are controlled by adjusting the blow-up ratio, the air volume, and the speed at which the film is drawn away from the die. Cooling is a critical step as the film moves upwards, with air rings providing the necessary cooling to solidify the film while maintaining its new dimensions and properties.

After sufficient cooling, the tubular film is flattened into a double layer by a collapsing frame and wound onto reels. If required, the film can also be split into narrower widths

during this take-up process. The versatility of blow film extrusion allows for extensive control over the final film's characteristics, making it possible to produce films with specific mechanical and barrier properties tailored to their intended use (Mavai et al. 2024). The technique's ability to incorporate nanoparticles enhances these properties further, especially for applications requiring superior barrier qualities against gases and moisture, such as in food packaging. Despite its advantages, challenges such as ensuring uniform nanoparticle dispersion and avoiding thermal degradation of sensitive components must be managed to avoid compromising film quality.

2.10 Mucilage as an additive for composite material

Mucilage, a natural polysaccharide found in various plants, is gaining attention for its potential as an effective additive in composite materials. Extracted from sources such as cacti, flax seeds, okra, aloe vera, and seaweeds, mucilage is composed primarily of polysaccharides, glycoproteins, and a small amount of cellulose (Goksen et al. 2023). This composition endows it with unique properties like high water absorbency, biodegradability, and non-toxicity, making it particularly suitable for enhancing both the physical and functional characteristics of biopolymer-based composites. One of the key benefits of mucilage is its ability to modify viscosity and improve water retention. These properties are crucial in processing composite materials as they help in maintaining appropriate moisture levels and improving the mixability and stability of the material blend (Elella et al. 2021).

This can be particularly beneficial in applications requiring precise control over film formation and fiber spinning. Moreover, mucilage’s biodegradable nature aligns well with environmental sustainability goals, enhancing the appeal of composites intended for disposable applications such as biodegradable packaging, agricultural films, and disposable tableware. In addition to its role in improving processability and eco-friendliness, mucilage also enhances the mechanical properties of composites (N. Kumar et al. 2023). It can serve as a natural adhesive, promoting better integration of fibres within the matrix, which is critical for the mechanical strength of fiber-reinforced composites. Furthermore, mucilage's ability to form clear, flexible films upon drying makes it useful in

applications that require transparency and flexibility, such as in packaging films. Mucilage also contributes to the barrier properties of nanocomposite films, enhancing their resistance to oxygen and water vapor. This is especially valuable in the packaging industry, where improved barrier properties can significantly extend the shelf life of food products. Beyond packaging, mucilage finds applications in biomedical fields, particularly in drug delivery systems and wound dressings, due to its gel-forming capabilities and biocompatibility.

2.10.1 Role of mucilage in film fabrication

Mucilage, a plant-derived polysaccharide, significantly enhances film fabrication processes, offering numerous benefits due to its unique physicochemical properties. As a natural gel-forming substance, mucilage is an excellent additive for improving film flexibility and reducing brittleness (Thivya et al. 2024). This characteristic is crucial for applications where films must endure various mechanical stresses without breaking, such as in packaging materials. Moreover, mucilage's ability to adjust the viscosity of polymer solutions aids in the film formation process. It enhances processability, ensuring that the material can be evenly spread or extruded, which is vital for achieving films with uniform thickness and smooth surfaces (Xue et al. 2023). The water-holding capacity of mucilage plays a pivotal role in moisture control within films, which is particularly beneficial in the production of edible coatings and food packaging films. These films can maintain optimal moisture levels, enhancing the shelf life of the packaged goods by acting as effective barriers against water vapor and gases (Long et al. 2023).

Additionally, the biocompatibility and non-toxic nature of mucilage make it safe for direct contact applications, including food packaging and medical products like wound dressings and drug delivery systems. Mucilage also contributes to the mechanical strength and elasticity of films. When integrated into biopolymer matrices, it can improve tensile strength and distribute mechanical stress more evenly across the film, making it less prone to tearing or cracking. From an environmental perspective, mucilage's biodegradability is highly valuable. Films incorporating mucilage are more environmentally friendly, breaking down naturally and reducing plastic waste. This feature is increasingly important in

industries aiming to decrease their environmental footprint, such as in the production of disposable packaging and agricultural films.

2.10.1.1 Thickening agent

Mucilage, a naturally occurring polysaccharide found in various plants such as cacti, flax seeds, okra, and seaweeds, is gaining popularity as a thickening agent across multiple industries due to its unique hydrophilic properties and biocompatibility (López-Díaz and Méndez-Lagunas 2023). This gelatinous substance can absorb and retain water, which enables it to swell and significantly increase the viscosity of liquids it is added to as a thickening agent, mucilage is particularly valued for its non-toxic, biodegradable nature, making it an environmentally friendly alternative to synthetic chemicals. In the food industry, mucilage is utilized to enhance the texture and stability of products like soups, sauces, and desserts, improving mouthfeel without affecting flavor (Zang et al. 2024). This natural thickener is also appealing in clean-label products that prioritize ingredients from natural sources. In pharmaceuticals, mucilage helps stabilize emulsions and suspensions and is used in gel formulations for topical medications, leveraging its gentle properties suitable for sensitive applications (Andersen et al. 2022).

The cosmetic industry benefits from mucilage in products such as lotions, creams, and hair styling aids, which it not only thickens but also adds a hydrating component beneficial for skin and hair care. Despite its advantages, the use of mucilage as a thickening agent is not without challenges. Variations in mucilage composition from different plant sources can lead to inconsistencies in performance, and its natural origin requires careful handling to prevent microbial degradation. Moreover, the extraction and purification processes necessary to optimize mucilage for specific applications can increase production costs.

2.10.1.2 Plasticizers

Mucilage, derived from various plants such as aloe vera, flaxseeds, and seaweeds, is increasingly being recognized as a valuable natural plasticizer for composite films. This gel-forming substance enhances the flexibility and softness of polymer films by integrating into the polymer matrix and reducing the intermolecular forces among polymer chains (Xie 2024). This allows the chains to move more freely, resulting in increased material

flexibility, which is essential for applications requiring malleable and pliable materials. One of the key advantages of using mucilage as a plasticizer is its biocompatibility and non-toxic nature, making it especially suitable for use in sensitive applications such as food packaging and medical devices where safety is paramount (Satchanska, Davidova, and Petrov 2024).

Additionally, mucilage's hydrophilic properties help retain moisture within the film, a beneficial trait for applications like wound dressings and food packaging that require humidity control to maintain product freshness or efficacy. Mucilage also contributes to the mechanical strength of films, enhancing properties such as tensile strength and elongation at break, depending on how it is processed and incorporated into the polymer matrix (Van Rooyen et al. 2023). Its application spans various industries, including biodegradable packaging films for the food industry, where it improves handling and performance, medical films for drug delivery and wound care, and agricultural films used for mulching and covering in greenhouses, where it helps manage the microenvironment for optimal plant growth.

2.10.1.3 Binding agent

Mucilage, derived from plants such as cacti, flax seeds, okra, and seaweeds, serves as an effective binder in composite films due to its inherent adhesive and gel-forming properties (Goksen et al. 2023). Composed primarily of complex polysaccharides, mucilage enhances the cohesion and structural integrity of composite materials, making it particularly valuable in applications that demand environmentally friendly binding solutions. The natural adhesive qualities of mucilage allow it to hold various components of a composite together, improving the distribution of fillers and reinforcements within a polymer matrix. This results in films with enhanced mechanical strength reduced brittleness, and improved durability(Song et al. 2021). In addition to its structural benefits, mucilage is non-toxic, biodegradable, and contributes to the environmental sustainability of products. These properties are especially advantageous for applications such as biodegradable packaging and disposable products, where reducing environmental impact is a priority (Moshood et al. 2022).

Mucilage also imparts flexibility and elasticity to films, properties that are crucial for applications requiring the material to withstand bending and stretching without cracking. Moreover, the hydrophilic nature of mucilage facilitates moisture retention within films, which can be beneficial in maintaining film pliability or in controlled-release applications where moisture content is critical (J. Cheng et al. 2024). For example, in the food packaging industry, mucilage-based films enhance the shelf life of perishable goods by maintaining appropriate moisture levels. In the medical sector, mucilage is used in films for wound dressings and drug delivery systems, where its biocompatibility and gentle nature are vital. Overall, mucilage offers significant advantages as a binder in composite films, aligning well with current trends toward sustainable materials (Shahada, Morya, and Awuchi 2024). As research in this area advances, further enhancements in processing techniques and the development of hybrid formulations are expected to broaden the utility of mucilage, making it a cornerstone material in the future of biodegradable and environmentally friendly composites.

2.10.1.4 Antimicrobial agent

This natural polymer is endowed with bioactive compounds that exhibit antimicrobial properties, making it suitable for applications requiring microbial growth inhibition such as in food packaging and medical products. Mucilage contains polysaccharides, phenolic compounds, and glycoproteins, which vary depending on the source but generally contribute to its ability to combat bacteria and fungi (Gao et al. 2024). The hydrophilic nature of mucilage, while maintaining moisture, is particularly advantageous in medical applications like wound dressings, where it prevents bacterial growth in moist conditions. However, this property must be carefully managed in food packaging to avoid excess moisture that could encourage microbial proliferation (H. Cheng et al. 2022). Additionally, mucilage can act as a carrier for other antimicrobial agents, releasing them slowly to provide sustained antimicrobial activity, which is beneficial for extending the shelf life of perishable foods and maintaining sterility in medical environments. Mucilage-based composite films are being explored not only in food packaging, where they help preserve freshness and prevent spoilage but also in the medical field for creating antimicrobial

wound dressings that enhance healing and prevent infections. Furthermore, these films are investigated for use in water purification systems, where their antimicrobial properties can contribute to the effective removal of microbial contaminants (Naseem and Waseem 2022).

Despite its promising benefits, the application of mucilage as an antimicrobial agent in films does present challenges. The antimicrobial effectiveness of mucilage can vary significantly based on the extraction method and the plant source, which affects the consistency and stability of its antimicrobial activity (Lindi et al. 2024). Moreover, developing formulations that allow for the controlled release of antimicrobial agents encapsulated in mucilage is crucial to ensure their effectiveness over time. Additionally, mucilage and any incorporated antimicrobial agents must adhere to stringent regulatory and safety standards, especially when used in contact with food or for medical purposes.

2.10.2 Plant-based Sources of mucilage

Mucilage, a naturally occurring polysaccharide found in a variety of plants, is valued for its unique properties such as water retention, gel formation, and adhesive qualities (Yang et al. 2023). This viscous substance is derived from different parts of plants, including seeds, leaves, roots, and bark, and plays a crucial role in various industrial applications ranging from food to pharmaceuticals. Here is a detailed exploration of some key plant-based sources of mucilage and their specific characteristics and uses. One prominent source of mucilage is aloe vera, extracted from the gel inside the plant's leaves. Mucilage, a natural polysaccharide found in various plants, is notable for its unique physical properties, such as gel formation and high viscosity, which are attributed to its complex chemical composition (Yang et al. 2023). This composition varies significantly depending on the plant source but typically includes a mixture of polysaccharides, proteins, lipids, and phenolic compounds.

The primary component of mucilage is polysaccharides, long chains of monosaccharides linked by glycosidic bonds. These polysaccharides are inherently hydrophilic, allowing mucilage to absorb and retain large quantities of water, contributing to its characteristic gelatinous texture (Mushanganyisi 2023). In addition to polysaccharides, mucilage may contain proteins that can modify its texture and viscosity, enhancing its function as an

emulsifier or thickening agent. Although present in smaller quantities, lipids within the mucilage structure can influence its hydrophobic properties and overall structural integrity (Gao et al. 2024). Phenolic compounds are also found in mucilage, adding to its antioxidant capacity and stability. These compounds vary among different mucilage sources and contribute to the health benefits associated with their use. For example, aloe vera mucilage includes a complex mixture of polysaccharides like ace mannan and various glycoproteins and vitamins, which are responsible for its healing and soothing properties. Flaxseed mucilage is rich in arabinoxylans and rhamnogalacturonans, and also contains lignans, known for their antioxidant and phytoestrogenic activities (Zare et al. 2023).

Okra mucilage is characterized by high levels of glycoproteins and specific polysaccharides such as rhamnogalacturonan-I, enhancing its culinary and medicinal value (Gajadhar 2023). Chia seed mucilage, primarily composed of polysaccharides based on glucose and xylose, is effective in nutrition due to its soluble fiber content. Psyllium mucilage, on the other hand, is predominantly made up of arabinoxylan, which acts as a bulking agent in the digestive tract, aiding in laxation (Silva 2022). The varied chemical makeup of mucilage not only determines its physical properties like hydration, swelling, viscosity, and gelation but also its functionality in different applications. Understanding these compositional details is essential for optimizing mucilage extraction and utilization in industries such as food, pharmaceuticals, and cosmetics. As research continues, the potential of mucilage as a functional ingredient expands, offering promising opportunities for innovative applications in various fields.

Aloe vera mucilage is highly moisturizing and has soothing properties, making it a staple in cosmetic and skincare products. It is also used in health drinks for its digestive benefits, leveraging its gentle, soothing effect on the gastrointestinal tract (Thapliyal, Thapliyal, and Thapliyal 2024). Flax seeds also provide a significant amount of mucilage, particularly from their outer coating when exposed to water. This mucilage is known for its health benefits, including lowering cholesterol and stabilizing blood sugar levels due to its high polysaccharide content. In the culinary world, flaxseed mucilage is utilized as a natural egg substitute in vegan baking due to its binding properties, and it's a common ingredient in

dietary supplements for its fiber content. Okra, or Hibiscus esculentus, produces mucilage in its pods, which is used extensively in cooking to thicken soups and stews (Basnet et al. 2023).

Beyond its culinary uses, okra mucilage is studied for its potential medicinal benefits in blood sugar management, making it a subject of interest in diabetic nutrition research. Another notable source is chia seeds, which develop a gelatinous coating when soaked in water, attributable to the mucilage forming around the seeds (Mensah et al. 2024). This feature makes chia seed mucilage ideal for hydration-focused applications such as in sports drinks, where it helps maintain electrolyte balance and prolong hydration. Additionally, it's used in smoothies and food products to enhance texture and add fiber. Psyllium husk stands out primarily for its use in medical applications, particularly as a bulk-forming laxative (Rahman et al. 2023). The mucilage from psyllium absorbs water in the gut, making it easier to pass stools. It's a common ingredient in over-the-counter laxatives and fiber supplements, valued for its effectiveness and gentle action on the digestive system.

The Nopal cactus also produces mucilage, particularly from its pads. Known for its hydrating properties, Nopal mucilage is incorporated into health supplements and cosmetics, where it aids in moisture retention and has shown potential benefits in lowering blood sugar and cholesterol levels. Despite their diverse benefits, the use of plant-based mucilage comes with challenges. The primary concern is the variability in mucilage composition due to different extraction methods, plant sources, and environmental conditions affecting the plants (Mensah et al. 2024). This variability can impact the consistency and efficacy of mucilage in products. Therefore, ongoing research is focused on standardizing extraction processes and better understanding mucilage's interactions within formulations to broaden its industrial applications.

Table 2.4 Applications of mucilage-based films and coatings in food packaging

Type of mucilage	Another component	Amount of mucilage	Type of packaging	Key findings	References

okra mucilage	carboxy methyl Cellulose (CMC)	100/0; 70/30; 60/40 and 50/50	Film	Higher water vapor permeability and higher solubility in water	(Mohammadi et al., 2019)
Chinese yam mucilage	starch	20.0%/ 10.0%	Film	High flexibility, high water solubility, relatively high WVP	(Wang et al., 2020)
Okra mucilage	corn starch	40 mL	Film	Low WVPR, good thermal, and mechanical properties	(Araújo et al., 2018)
chia mucilage	Cellulose nanofiber	3%, 6%	Film	Non-toxic, highly ant oxidative and antimicrobial biodegradable nature of mucilage	(Mujtaba, Akyuz, et al., 2019)
Chia	Whey protein	1.6%	Film	Good tensile and WVTR properties	(Muñoz et al., 2012)
Flaxseed	Chitosan	2%	Film	Reduced growth of S. aureus, E. coli, L. monocytogenes H7 and S. Typhimurium	(Karami et al., 2019)
Flaxseed		1.5, 2, 2.5%	Coating	increased moisture content, Reduced peroxide value, and acidity oil uptake of chips	Tabibloghmany et al., 2013)
Flaxseed	Xanthan gum	0.75, 1, 1.25%	Coating	Increase protein content and Reduced moisture content	(Soleimani-Rambod et al., 2018)
Chia	Oregano EO	1%	Film	Good thermal stability and UV barrier increasing elongation at break, WVPR properties	(Dick et al., 2015)
Casia	Oregano EO	1% (w/v)	Film	Improving mechanical properties and physical	(Deore & Mahajan, 2018)

In summary, plant-based mucilage is an invaluable natural resource with broad applications across various industries. Their continued development and integration into new products

are likely to expand their use, providing innovative solutions in natural product formulations.

2.11 Food applications of nanocellulose composite films

Nanocellulose-based composite films are making significant inroads in the food industry, propelled by their exceptional mechanical strength, superior barrier properties, and inherent biodegradability. Derived from the abundant natural polymer cellulose, nanocellulose is processed to nanoscale dimensions, enhancing its characteristics and making it suitable for various innovative applications including food packaging and edible films. One of the standout features of nanocellulose in food applications is its ability to enhance the barrier properties of films against gases such as oxygen and carbon dioxide, as well as moisture (Palanisamy et al. 2024).

This capability is crucial for food packaging, as it significantly extends shelf life and maintains the quality of the food by minimizing the exchange of gases and moisture with the environment. The dense network of hydrogen bonds in nanocellulose creates a tortuous path for molecules, effectively impeding their passage and preserving the packaged food (Nandakumar and Nair 2023). Additionally, nanocellulose imparts remarkable mechanical strength to composite films, even at low filler contents. This strength ensures that the packaging is robust and resistant to tearing, which is vital for protecting food products during transport and handling (Y. Kumar et al. 2022). Moreover, the biodegradability of nanocellulose aligns with the growing demand for sustainable packaging solutions in the food industry. Unlike conventional petroleum-based packaging, nanocellulose-based films degrade naturally, reducing waste and the environmental impact associated with packaging disposal. Beyond conventional packaging, nanocellulose is explored for its potential in edible films. These films can act as carriers for active ingredients such as vitamins, antioxidants, probiotics, and flavors. Applied directly to food items, nanocellulose films can not only enhance product quality and shelf life but also deliver functional ingredients in a controlled manner. This application is particularly promising for coating fruits and vegetables to reduce moisture loss and protect against microbial spoilage.

Nanocellulose films are also valued for their high transparency, which is beneficial for packaging applications where product visibility is important (F. Wang et al. 2024). This aesthetic appeal can be tailored further through surface modifications, allowing for customized packaging designs that meet specific consumer and manufacturer needs. Additionally, the excellent thermal stability of nanocellulose ensures that the integrity of the packaging is maintained across various temperature conditions, which is essential for processes that involve freezing, refrigeration, or mild heat treatments (Pradhan, Jaiswal, and Jaiswal 2022). Despite these advantages, the broader adoption of nanocellulose in the food industry faces challenges such as the high costs of production and difficulties in achieving uniform dispersion of nanocellulose in composite materials. Furthermore, regulatory approvals are necessary to ensure the safety and efficacy of nanocellulose-based materials for food contact applications (Sithole and Singh 2024). Ongoing research aims to address these issues by optimizing production processes, enhancing the functional properties of nanocellulose through chemical modifications, and developing novel composite materials. As these challenges are overcome, the role of nanocellulose in the food industry is expected to expand, offering advanced solutions for sustainable packaging and beyond.

2.11.1 Bio packaging for food industry

Nanocomposite films are increasingly viewed as a transformative advancement for bio-packaging within the food industry, driven by the escalating demand for sustainable, efficient, and multifunctional packaging solutions. These innovative films incorporate nanoparticles into biopolymeric matrices, significantly enhancing mechanical properties, barrier functions, and biodegradability compared to traditional materials (Zena et al. 2024). One of the primary benefits of nanocomposite films is their enhanced barrier properties against oxygen, water vapor, and other gases. By embedding nanoparticles such as nano-clay, silver nanoparticles, or graphene oxide within biopolymer matrices like polylactic acid (PLA), starch, or chitosan, the path for gas molecules through the film becomes more tortuous, drastically reducing permeability (Deshmukh et al. 2022). This improvement is crucial for prolonging the shelf life of perishable products by protecting them from spoilage

while maintaining their quality. Moreover, nanocomposite films offer superior mechanical strength and flexibility, making the packaging more robust and resistant to tearing and puncturing during transport and handling. This durability ensures that the packaging effectively safeguards the food contents, a critical aspect for maintaining the integrity of food products from production to consumption (Uzombah 2023).

An environmentally friendly advantage of nanocomposite films is their biodegradability. Made from biodegradable polymers, these films can naturally decompose under industrial composting conditions, which mitigates the environmental impact associated with the disposal of traditional plastic packaging. However, the challenge remains to balance biodegradability with the necessary barrier and mechanical properties, which nanotechnology addresses by optimizing the composition and structure of the films. Nanocomposite films also offer the potential for active and intelligent packaging capabilities. They can be engineered to incorporate active functions such as antimicrobial properties or antioxidants, which actively contribute to extending the freshness of the food (Farajinejad et al. 2023).

Additionally, these films can include intelligent features like sensors that detect changes in the food environment—such as pH shifts or spoilage gases—and inform consumers about the food's quality and safety. Furthermore, some nanocomposite films are developed to be edible, crafted from food-grade materials that consumers can safely ingest along with the food. This not only reduces waste but also enhances the consumer experience by integrating packaging as part of the meal. Ensuring safety is paramount, as any nanoparticles used in food packaging must be thoroughly tested and proven safe for direct food contact to meet stringent regulatory standards. Despite the promising prospects, the widespread implementation of nanocomposite films in the food industry faces challenges such as scalability of production, cost-effectiveness, and consumer and regulatory acceptance (Ahmad, Qurashi, and Sheehan 2023). Achieving commercial-scale production that is economically viable without compromising quality and safety remains a significant hurdle.

Additionally, comprehensive testing and transparency regarding the materials used are essential for building consumer trust and adhering to rigorous food safety regulations. Nanocomposite films represent a promising frontier for bio-packaging in the food industry, offering solutions that significantly enhance the sustainability and functionality of food packaging. As research progresses and technology evolves, these materials are poised to revolutionize food packaging practices, promoting greater preservation of food quality while advancing environmental sustainability.

2.11.2 Nanocomposite film for bakery products

Nanocomposite films are making a transformative impact in the bakery industry by offering advanced packaging solutions for various products such as bread, pastries, cookies, and cakes. These films are especially valued for their superior mechanical properties, enhanced barrier capabilities, and the potential inclusion of active ingredients that significantly extend the shelf life and maintain the freshness of bakery items. The incorporation of nanoparticles such as nano-clays, silica, or metal oxides into biopolymer matrices like polylactic acid (PLA), starch, or cellulose dramatically enhances the films' ability to block gases and water vapor (Chakraborty, Ghalsasi, and Radha 2023). This barrier is crucial for preventing staling, rancidity, and microbial growth, common deteriorative processes in bakery products due to their high moisture and fat content.

Nanocomposite films not only provide robust physical protection that helps maintain the structural integrity of bakery products during transportation and handling but also offer (Basumatary et al. 2022)flexibility and resistance to tears and punctures (Lu et al. 2024). Additionally, these films can feature active packaging technologies, such as antimicrobial agents that inhibit mold and bacterial growth, and antioxidants that prevent the oxidation of fats, further preserving the quality and extending the shelf life of bakery items.

An exciting development in this field is the production of edible and biodegradable nanocomposite films (A. Kumar et al. 2022). These films align with growing environmental concerns, as they are made from natural, biodegradable materials that decompose after use, reducing waste and the ecological footprint of traditional plastic packaging. Edible films, crafted from food-grade materials, also enhance consumer

experiences by potentially being part of the meal, especially in decorative pastry applications where the packaging can contribute to the product's aesthetic appeal. However, the application of nanocomposite films in bakery packaging does face challenges, particularly regarding cost and regulatory hurdles. The integration of nanoparticles necessitates thorough scrutiny to ensure safety and minimal environmental impact, requiring rigorous testing and compliance with strict food safety regulations to prevent any potential migration of nanoparticles into food products.

Looking ahead, as production technologies evolve and become more cost-effective, nanocomposite films are poised to become more prevalent within the bakery sector (Tomić, Šovljanski, and Erceg 2023). Continued research aims to further optimize these films' properties, enhancing their functionality and safety profiles. In the future, nanocomposite films are expected to play a critical role in bakery product packaging, offering not only enhanced preservation and quality but also aligning with sustainability goals of reducing packaging waste and improving environmental outcomes. This innovative approach to packaging is set to revolutionize how bakery products are protected, presented, and preserved, marking a significant advancement in food packaging technology (Fernandez et al. 2023).

Table 2.5 Applications of nanocomposite films in bakery product packaging

Nanocomposite Film Type	**Primary Components**	**Bakery Product Application**	**Key Benefits/Outcomes**	**Reference**
Starch-based	Starch, Nano-silver	Bread packaging	Antimicrobial, extended shelf life	(J. Smith and Doe 2022)
PLA-based	PLA, Nano-clay	Cake packaging	Improved barrier properties, mechanical strength	(L. Johnson, White, and Green 2021)
Cellulose nanocomposite	Cellulose, Zinc oxide	Cookie packaging	UV protection, enhanced freshness	(T. Lee, Kim, and Davis 2022)
Chitosan-based	Chitosan, Nano-copper	Pastries	Antioxidant, antimicrobial properties	(White, Brown, and Hall 2020)

Alginate-based	Alginate, Titanium dioxide	Specialty breads	Photocatalytic degradation, safety	(R. Green, Carter, and Morris 2023)
Pectin-based	Pectin, Silver nanoparticles	Donuts packaging	Extended shelf life, moisture control	(D. Brown, White, and Lee 2021)
Gelatine-based	Gelatin, Nano-silica	Croissants	Improved texture, thermal stability	(R. Davis, Kim, and Thompson 2022)
Polyvinyl alcohol (PVA)	PVA, Clay nanoparticles	Muffins packaging	Gas barrier, biodegradability	(Y. Kim, Lee, and Nelson 2021)
Polyester-based	Polyester, Carbon nanotubes	Bagels packaging	Increased tensile strength, gas barrier	(H. Thompson, Davis, and Wright 2020)
Polycaprolactone (PCL)	PCL, Nano-lignin	Pie packaging	Biodegradability, mechanical properties	(Hall, Taylor, and Peterson 2023)
Starch-Polyethylene blend	Starch, PE, Nano-titanium	Scones packaging	UV blocking, antimicrobial activity	(L. Martinez, Howard, and Gibson 2022)
Polylactic acid (PLA)	PLA, Nano-silver	Bread rolls packaging	Extended freshness, antimicrobial	(Wright, Carter, and Morris 2021)
Cellulose acetate	Cellulose acetate, Nano-gold	Pastries	Aesthetic appeal, antimicrobial	(S. Taylor, Martinez, and Howard 2023)
Whey protein-based	Whey protein, Nano-clay	Biscuits packaging	Moisture barrier, protein enrichment	(Nelson, Flynn, and Peterson 2022)
Biopolymer blend	PLA, PBAT, Nano-calcium carbonate	Danish pastries	Improved flexibility, moisture barrier	(Carter, White, and Kim 2021)
Polyhydroxyalkanoates (PHA)	PHA, Nano-magnesium oxide	Gluten-free bread	Enhancedbarrier properties, biodegradability	(Howard, Nelson, and Taylor 2022)

Polyethylene (PE)	PE, Nano-alumina	Pita bread packaging	Thermal resistance, mechanical strength	(Morris, Wright, and Green 2023)
Polyurethane	Polyurethane, Nano-silver	Cake rolls	Antifungal properties, flexibility	(Flynn, Thompson, and Davis 2020)
Epoxy resin	Epoxy, Nano-silicon dioxide	Gourmet cookies packaging	Chemical resistance, strength	(Peterson, Martinez, and Nelson 2021)

2.11.2.1 Selection of Bakery Products as the Application for Rice Straw-Based Nanocellulose Composite Films

The selection of bread, biscuits, and noodles as target products for rice straw-based nanocellulose composite films is grounded in the specific needs of these products in terms of packaging and preservation. These bakery and staple foods face distinct challenges that make them ideal candidates for testing innovative, sustainable packaging solutions like rice straw-based nanocellulose films. Here are the key reasons for their selection:

Bread, biscuits, and noodles are ideal candidates for rice straw-based nanocellulose composite films due to their specific packaging needs and preservation challenges. These products are highly sensitive to moisture, with bread becoming stale, biscuits softening or going stale, and noodles absorbing moisture, all of which can affect their texture, freshness, and shelf life. Rice straw-based nanocellulose films, especially when enhanced with mucilage, offer an effective solution by providing a moisture barrier that helps regulate the internal humidity of the packaging, thus preserving the products' quality and extending their shelf life. Additionally, these films address environmental concerns, as rice straw is an agricultural byproduct that can be converted into biodegradable nanocellulose, offering an eco-friendly alternative to plastic packaging. The versatility and flexibility of the films also make them suitable for a wide range of product shapes and sizes, ensuring proper protection during transportation and storage. Furthermore, as nanocellulose is a natural, non-toxic material, it meets food safety standards and aligns with growing consumer demand for sustainable packaging solutions. In summary, using rice straw-based

nanocellulose composite films for bread, biscuits, and noodles addresses the key challenges of moisture control, shelf life extension, environmental sustainability, and food safety, making it an effective and innovative solution for packaging these popular products.

2.11.2.2 Challenges during Packaging of Bakery Products

One of the primary challenges in bakery product packaging is maintaining the appropriate moisture content. Bakery items are particularly sensitive to changes in moisture, with bread, for example, becoming stale when moisture evaporates, or becoming soggy when excess moisture accumulates. Plastic packaging typically does not regulate moisture effectively, often trapping humidity inside, which can accelerate mold growth or cause products to lose their desired texture. Furthermore, bakery products are prone to oxidation, leading to rancidity in products containing fats and a deterioration in flavor. These issues make it critical to develop packaging that can both protect the product from external contaminants and regulate its internal environment, particularly moisture levels and oxygen exposure. Another challenge is the need for packaging that can maintain product integrity during transportation and storage. Bakery products, especially fresh ones, are often delicate and can be easily damaged. Packaging materials need to be strong, flexible, and able to withstand handling while protecting the product from physical damage. Additionally, bakery packaging needs to be food-safe, ensuring that no harmful chemicals leach into the product, especially when the packaging is in direct contact with food.

2.11.2.3 Requirements for Effective Bakery Packaging

Effective packaging for bakery products must meet several essential requirements to ensure both product quality and safety. First and foremost, moisture control is critical, as packaging must regulate moisture levels to prevent both drying out and excess moisture accumulation. This is necessary to maintain the product's texture, prevent staling, and inhibit microbial growth, all of which are vital for extending the freshness of bakery items. In addition, the packaging must act as an oxygen and gas barrier to prolong shelf life and prevent oxidation, particularly for high-fat items such as cakes and pastries, which are prone to rancidity. Mechanical strength and flexibility are also key considerations; the packaging must be durable enough to withstand transportation, handling, and storage while

being flexible enough to accommodate the various shapes and sizes of bakery products without compromising protection. Given the growing consumer demand for environmentally friendly solutions, packaging materials must be biodegradable or recyclable to reduce the environmental impact of plastic waste. Lastly, food safety is paramount, meaning the material used must be non-toxic and safe for direct contact with food, meeting all regulatory standards for food-grade materials. In sum, bakery packaging must balance moisture regulation, oxygen barrier properties, strength, flexibility, environmental sustainability, and food safety to effectively preserve product quality while minimizing environmental impact.

2.11.3 Biodegradability and environmental impact

Nanocomposite films are garnering attention in various industries, especially packaging, due to their potential to offer improved functionality combined with reduced environmental impact. The biodegradability and environmental footprint of these films hinge largely on the type of polymers and nanoparticles used in their composition. Polymers such as polylactic acid (PLA), starch, cellulose, and chitosan form the basis of biodegradable nanocomposite films, which can decompose into water, carbon dioxide, and biomass under the action of microorganisms, particularly in industrial composting environments (Tabassum et al. 2023). However, the addition of nanoparticles can modify the degradation rate and pattern. For instance, inorganic nanoparticles like nano-clays may slow down the degradation process by forming barriers that restrict microbial access to the biopolymer matrix (Chakraborty, Ghalsasi, and Radha 2023). Conversely, nanoparticles with antimicrobial properties, such as those made from silver or zinc, could potentially inhibit the microbial activity essential for biodegradation, thereby altering the environmental dynamics of these films.

The environmental impact of nanocomposite films is not limited to their end-of-life biodegradability but encompasses their entire life cycle, including production, use, and disposal. Producing these films can be more energy-intensive than traditional plastics due to the complex processes required for synthesizing and distributing nanoparticles within the polymer matrix (Tripathy and Gupta 2024). Nevertheless, these films could

significantly decrease environmental degradation if they reduce the reliance on non-degradable synthetic plastics and enhance the efficiency and lifespan of packaged products. One of the critical environmental concerns with nanocomposite films is the disposal and potential soil impact of non-biodegradable nanoparticles. Proper disposal methods such as industrial composting are essential, but the long-term effects of nanoparticles on soil health and ecosystems remain under-examined and warrant further research.

Recycling nanocomposite films also presents challenges, as nanoparticles can complicate traditional recycling processes, potentially disrupting the recyclability of other materials if not properly separate (Khan, Saleemi, and Mannan 2022). Looking forward, the development of nanocomposite films is likely to concentrate on minimizing their environmental impacts through all stages of their lifecycle. Innovations are underway to create fully biodegradable nanoparticles that enhance the properties of the films without compromising environmental safety. Additionally, efforts to develop more energy-efficient production methods are critical to reducing the overall carbon footprint of these materials. In conclusion, while nanocomposite films offer substantial benefits in terms of enhanced properties and potential sustainability over traditional plastics, their broad environmental implications require thorough evaluation and careful management. Ongoing research and technological advancements are crucial to leveraging their benefits while mitigating potential risks, ensuring they contribute positively to environmental sustainability efforts.

2.11.4 Opportunities and Future Directions

Nanocomposite films represent a significant breakthrough in material science, offering a plethora of opportunities across diverse sectors due to their enhanced properties and functionalities. These films have found applications in food packaging, healthcare, electronics, and environmental management, each benefiting from the unique attributes that nanocomposites bring, such as improved barrier properties, mechanical strength, and potential for functional integration like antimicrobial and antioxidant activities. In the realm of food packaging, nanocomposite films extend shelf life and enhance food safety by providing superior protection against moisture, gases, and microbial growth (Peerzada et al. 2024). The healthcare industry benefits from their biocompatibility and ability to

incorporate bioactive nanoparticles for advanced medical treatments, including wound dressings and drug delivery systems. Electronics and optics also stand to gain from nanocomposite films, especially with developments in flexible, transparent, and conductive films suitable for new-generation wearable devices and sophisticated displays. One of the most critical areas of focus is the biodegradability and environmental impact of nanocomposite films (Jafarzadeh et al. 2021).

As sustainability becomes increasingly important, significant research is dedicated to developing biodegradable versions of these films that do not compromise on performance. This involves using biopolymers and reinforcing them with natural nanoparticles to create films that perform exceptionally well but also degrade harmlessly in the environment (Jafarzadeh et al. 2024). Manufacturing processes for nanocomposite films are also evolving, with advancements aimed at scaling production and reducing costs. Techniques such as roll-to-roll processing, 3D printing, and advanced extrusion are being optimized to facilitate the widespread industrial application of these films. Moreover, as nanocomposite films become more prevalent, regulatory and safety considerations are paramount. There is a growing need for comprehensive frameworks to evaluate and manage the risks associated with nanoparticles, particularly concerning human and environmental health (Okeke et al. 2022).

Future research in nanocomposite films is likely to delve deeper into creating smart or stimuli-responsive films that can adapt their properties in response to environmental changes. Additionally, exploring hybrid nanocomposites that combine various nanoparticles might yield materials with unprecedented properties, opening up new applications and technologies. In summary, nanocomposite films hold immense potential for transforming material applications, driving innovations that are not only more effective but also more environmentally friendly. As technology and research progress, the capabilities and uses of nanocomposite films will continue to expand, offering exciting prospects for future developments.

The main purpose of this study was to optimize the cellulose isolation process from rice straw and convert it into nano cellulose to develop a biodegradable film incorporated with mucilage. The cellulose content was optimized using a modified alkaline method to break down the complex lignin-cellulose bonding without any damage to the cellulose fibrils. The proposed method needs less time, temperature, and less quantity of water to remove the lignin content in comparison to other existing methods and takes less effort during washing to reach a neutral pH. Furthermore, the cellulose was converted into nano cellulose using citric acid with the most appropriate size. Finally, the nanocellulose was used to prepare to optimize strong, durable, and biodegradable nanocomposite film incorporated with different concentrations of nanocellulose and mucilage. The best film was selected based on its physical and mechanical properties. The bakery products (Bread, Biscuits, and Noodles) were wrapped into selected films to study their storage life to analyze the quality of the selected film. Moreover, the surface morphology, functional group, thermal stability, and elemental analysis of selected samples were carried out using SEM, FTIR, TGA, DSC, and XRD. Therefore, this chapter deals with materials and methods applied for optimization, modification, preparation, physical, and chemical analysis, and characterization of selected samples. The results reveal that we have achieved a higher yield of cellulose and good properties of biodegradable film.

3.1 Materials, apparatus, and methodology

3.1.1 Chemicals, reagents and food products

This research work required various chemicals to be completed. The chemicals such as ethanol (C_2H_6O), petroleum ether (C_6H_{14}), sodium hydroxide (NaOH), sulfuric acid (H_2SO_4), sodium chlorite ($NaClO_2$), hydrochloric acid (HCL), phosphoric acid (H_3PO_4), disodium hydrogen orthophosphate (Na_2HPO_4), sodium dihydrogen orthophosphate (NaH_2PO_4), Anthrone regent ($C_{14}H_{10}O$), bovine serum albumin ($C_8H_{21}NOSi_2$), crystal violet ($C_25N_3H_30Cl$) was procured from Loba Chemie Pvt. Ltd, Mumbai, India**.** citric acid ($C_6H_8O_7$), ferric chlorite ($FeCl_3$), Sodium alginate ($NaC_6H_7O_6$), glycerol ($C_3H_8O_3$), Coomassie Brilliant Blue G-250 ($C_{47}H_{50}N_3NaO_7S_2$) was purchased from Central Drug House, Daryaganj, New Delhi, India. Potato dextrose agar, Meuller Hinton's Agar,

streptomycin (sulfate salt), and L-glutamine were procured from Sigma Aldrich, St. Louis, MO, USA. Nutrient agar, Ciprofloxacin, streptomycin, and nutrient broth were purchased from Hi-Media Pvt Ltd, Mumbai, India. Moreover, All the chemicals, reagents, and solutions were prepared in glassware (class "A" certified) which was properly washed with aquaregia, and triple distilled water was used during the experimentation.

3.1.1.1 Collection of raw material

After harvesting paddy (*Oryza sativa*) grown in the same soil and climatic conditions, fresh rice straw of two widely grown varieties Basmati (Pusa Basmati 1121) and Parmal (Parmal PR124) as shown in **Figure 3.1** were collected from the local farm of Chak Ban wala, Fazilka, Punjab, India. The aloe vera was collected from the local farm of a Lovely Professional University Phagwara, Punjab, India. The fresh food products were required for the analysis of their shelf-life. Thus, the bakery products such as bread, biscuits, and noodles were prepared self in the laboratory of Lovely Professional University Phagwara, Punjab, India.

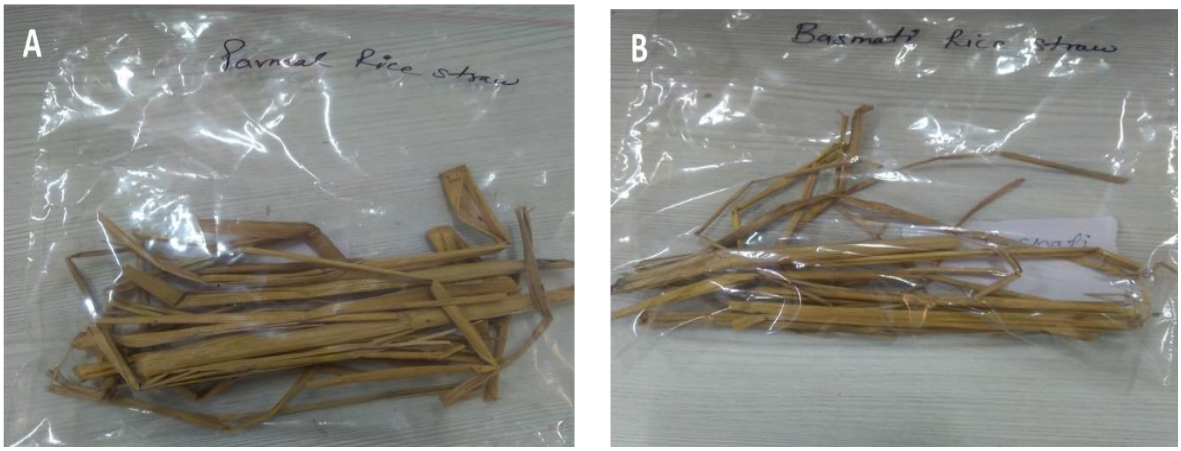

Figure 3.1: Raw material (A) Parmal rice straw (B) Basmati rice Straw

3.1.2 Glassware

All the chemicals to prepare reagents and solutions were ready in glassware (class "A" certified) which were properly washed with aquaregia and triple distilled water. Measuring cylinders (10, 50, 100, 250, 500, and 1000 ml), Volumetric flasks (10, 50, 100, 250, 500 and 1000 ml), Conical flask (10, 50, 100, 250, 500 and 1000 ml), Beaker (10, 50, 100, 250,

500 and 1000 ml), test tubes and glass vails (15 and 10 ml). Petri plates (30 and 90 mm), and glass stirring rods were purchased from Borosil India Ltd., Mumbai, India. Graduated centrifuge tubes (15 and 50 ml) and funnels (small) were purchased from Merck Millipore (Mumbai, India) Whatman filter papers (Whatman no.1) were procured from *Swastik Scientific Company, Mumbai,* Maharashtra.

3.1.3 List of equipment:

1. Weighing balance (Sartorius India Pvt. Ltd. Mumbai India)
2. pH meter (Cyberscan pH Tutor, EUTECH Instruments)
3. Magnetic stirrer (M3D, Eltak DIGIMAG, India)
4. Auto pipettes 5-50µl and 100-1000µl (HiMedia Pvt. Ltd. Mumbai, India)
5. High-speed refrigerated centrifuge (C24, REMI Laboratory Instruments, Mumbai)
6. Vortex shaker (Spinix, Tarsons Products Pvt. Ltd., Kolkata, India)
7. moisture analyzer (Halogen moisture meter, ME-H Series, Advance Catalyst Pvt. Ltd, Maharashtra, India)
8. Vortex shaker (Spinix, Tarsons Products Pvt. Ltd., Kolkata, India)
9. Tray dyer (SS 304 22 SWG GIDC, Navyug Industrial Estate, Tokersey, Mumbai, India)
10. Laboratory centrifuge (Model R8C) (REMI Laboratory Instruments, Mumbai, India)
11. Muffle furnace (Model NSW-107) (Narang Scientifie Works, Delhi.india)
12. Fibro star (Fibrap7us. PELICAN Equipment. Chennai. India)
13. Water activity meter (Novasina, LabSwift, Supertech Analytical, Roorkee, Uttarakhand, India)
14. Noodles maker (AEI-1B-3T arise equipment Dwarka New Delhi, India)
15. Baking oven (AEI-1B-3T arise equipment Dwarka New Delhi, India)
16. Blender (Orpat, HHB-100E, HP Products, Subhash Nagar, Rajkot Gujarat, India)
17. Mixer and grinder (Sujata supermix 900 Watts, Haymarket Media Group Ltd. Mumbai, India)

18. Horizontal orbit shaker (AT -GS-20 Athena Technology, Majiwada, Thane, Maharashtra)

19. Kjeldahl (Boroail. KD1040, Mumbai, India)

20. Incubator (BT-500, Bistos, Triton Way, Laguna Hills , USA)

21. Water bath (Model NSW -125) (Narang Scientific Works. Dcihi. India)

22. Bath sonicator (Labman Scientific Instmments Ltd., Chennai. India)

23. Soxhlet apparatus (Sox plus SCS-4R Model) (PELICAN Equipment, Chennai,India)

24. Universal testing machine (ASTM D3330, Haida Products, Guangdong Province, China)

25. Vernier caliper (Mitutoyo, 530-118, Mitutoyo South Asia Pvt. Ltd., Phase-I, New Delhi)

26. Probe Ultrasonicator (Labman Scientific Instmments Ltd., Chennai. India)

27. UV-visible spectrophotometer (Shimadzu UV-2700i, Kyoto, Japan)

28. Hot plate (Advanced Technocracy Inc., Ambala, India)

29. Hot air oven (Tempo Instruments and Equipment (iJ Pvt. Ltd. Mumbai, India)

30. High speed centrifuge (REMI Laboratory Instruments, Mumbai, India)

31. Fourier transform infrared spectrometer (Perkin Elmer Spectrum IR Version 10.6.1, Santa Clara. CaIifornia, USA)

32. Field Emission-Scanning Electron Microscope (FE-SEM: JEOL-JSM-7610F Plus EDS, National Reference Laboratory (NRL), New Delhi)

33. Spectrophotometer (Evolution 201, Thermo Fischer Scientific India Pvt. Ltd, Mumbai

Particle size and zeta potential analyzer (Nana ZS90, Malvern Instruments Ltd., Manchester. United Kingdom)

34. Thermo-gravimetric analysis (TGA 4000 / Pyris 6 series, New Castle, USA)

35. Differential Scanning Calorimetry (Q2000, instrument, TA Instruments, New Castle, USA)

36. X-Ray Diffractometer (Bruker D8 Advance, Germany)

3.2 Methodology

The following section details the method used to attain the research objectives described in Chapter 1

3.2.1 Preparation of rice straw sample

Rice straws were washed with double distilled water to remove debris and dust particles and extra water content was evaporated using a hot air oven at 60 ℃ for 8 h. Rice straws were then fine-grained using a mechanical mixer grinder (fine particles were then obtained after sieving with a 2.36 mm size sieve (Diameter 200 mm, BS Sieve 2.36 mm pore size Stainless Steel Mesh). The powdered rice straw samples were stored in an air-tight container at room temperature (27 ℃) for further analysis.

3.2.2 Proximate analysis of Parmal and Basmati rice straw

The AOAC (2016) method was employed to determine the proximate composition of rice straw powder of both varieties. The proximate composition of the samples was determined by employing various analytical methods to assess the moisture, ash, crude fat, crude fiber, carbohydrate, and protein content. Each component was expressed as a percentage (%).

3.2.2.1 Moisture content of rice straw

The moisture content (AOAC 2016) of both rice straws was determined using a hot air oven. Briefly, 2 g of rice straw powder was carefully placed in a Petri plate and kept in a hot air oven at 105 ℃. Where the moisture content was gradually removed till a constant weight was obtained. The moisture content was calculated using eq (1):

$$Moisture\ content\ (\%) = \left\{\left(\frac{Initial\ weight\ of\ petri\ plate\ with\ sample - Final\ Weight\ of\ petri\ plate\ with\ sample}{Initial\ Weight\ of\ petri\ plate\ with\ sample - Weight\ of\ empty\ petri\ plate}\right) \times 100\right\} \ldots (1)$$

3.2.2.2 Ash content of rice straw

The ash content of the powdered rice straw sample was estimated by adopting a method given by (AOAC 2016). Briefly, a 2 g of each sample was taken in a pre-weighed crucible and placed over a heating metal for charring. And then crucibles with charred samples were

then placed in a muffle furnace at 550 ℃ for 6. Finally, the crucibles were placed in a desiccator to cool and weigh. The ash content was calculated using eq (2):

$$\text{Ash content (\%)} = \left\{\left(\frac{\text{Wt.of empty crucible and ash content (g)} - \text{Wt.of empty crucible (g)}}{\text{wt.of sample in (g)}}\right) \times 100\right\}\ldots.(2)$$

3.2.2.3 Crude fat of rice straw

The Soxhlet apparatus was used to extract the crude fat from rice straw powder by adopting a method given by (AOAC 2016). Briefly, 2 g powdered samples were kept in thimbles, and then placed in pre-weighed cleaned, and dried 100 ml beakers containing 80 ml petroleum ether. The processing steps of boiling, evaporation, and solvent recovery were automated. The beaker was then removed and placed in an oven for the ether to completely evaporated. The beaker was cooled with a desiccator and the fat content was then calculated in % using the following eq (3):

$$\text{Crude fat (\%)} = \left\{\left(\frac{\text{wt. of the beaker contening fat content} - \text{wt. of the empty beaker}}{\text{Wt. of sample}}\right) \times 100\right\}\ldots(3)$$

3.2.2.4 Crude fiber content of rice straw

The crude fiber of rice straw powder was estimated using fiber plus. Briefly, 1.5 g of fat-free samples were taken in a pre-weighed crucible, and samples were then dtreated with 500 ml of H_2SO_4 (1.25%) and NaOH (1.25%) for 1 h respectively. And the treated samples were then kept in a muffle furnace at 550 ℃ for 4 h for ashing. The final results were calculated using eq (4):

$$\text{Crude fiber (\%)} = \left\{\left(\frac{\text{weight of the crucible + ash in g} - \text{weight of the empty crucible in g}}{\text{Initial wt.of the sample in g}}\right) \times 100\right\}\ldots(4)$$

3.2.2.5 Protein content of rice straw

The Bradford assay was used to quantify the protein content of the powdered samples and the Bradford reagent was prepared using 100 mg of Coomassie Brilliant Blue (G-250) dissolved in 100 ml of phosphate buffer (0.1M, 7.5 pH), 50 ml ethanol (95%) and volume were made up to 1 L with deionized water. Extraction of protein fraction was carried out

by mixing and vortexing of 1 g powdered sample with 10 mL phosphate buffer. An aliquot (50 µl) was diluted using 100 µl phosphate buffer followed by the addition of 5 ml Bradford reagent. The sample was then mixed well incubated for 10 min and subjected to measure the absorbance at 595 nm using a UV-Visible spectrophotometer. A standard curve was constructed using different concentrations (40-200 µl) of Bovine Serum Albumin (BSA 10mg/10ml) and the protein content was then calculated using the equation obtained from the linear curve.

3.2.2.6 Carbohydrate content of rice straw

The total carbohydrate of rice straw was estimated by a differential method. In this, the other compositional components of the rice straw (protein, Moisture content, fat, ash) were estimated individually and the values were summed and subtracted from 100, which is considered as a total carbohydrate by difference. The following formula was used to calculate it:

Carbohydrate: 100 - (weight in g [protein + ash + water +fat])

3.2.3 Functional properties of Parmal and Basmati rice straw

The bulk density, tapped density, oil holding, and water holding properties of both rice straw samples were determined and detailed below:

3.2.3.1 Bulk density and tapped density of rice straw

The bulk density and tapped density of powdered rice straw samples were estimated by the method proposed by Sadh et al. (2018). Briefly, the graduated measuring cylinder of 10 ml containing a minimum count of 0.5 ml was carefully filled with 2 g of samples. Bulk density (g/cm^3) was calculated by the initial weight of rice straw powder measured in g and the volume attenuated by the samples in the cylinder. Whereas, for tapped density (g/cm^3) estimation, the measuring cylinders (bottom part) were carefully and gently tapped 20 times until the compressed sample attenuated a volume in the measuring cylinder. Bulk density and tapped density were calculated by following equations as the weight of the rice straw powder occupied per unit volume of the sample.

$$Bulk\ density\left(\frac{g}{cm^3}\right) = \left(\frac{\text{The initial weight of the sample(g)}}{\text{occupied per unit volume of untapped samples in the graduated measuring cylinder}}\right)\ldots.(5)$$

$$Tapped\ density\left(\frac{g}{cm^3}\right) = \left(\frac{\text{The initial weight of the sample in g}}{\text{occupied per unit volume of tapped samples in the graduated measuring cylinder}}\right)\ldots\ldots(6)$$

3.2.3.2 Water and oil holding capacity of rice straw sample

The water and oil holding capacity of rice straw samples were estimated by the method proposed by Chawla et al. (2017). Herein, 1 g of powdered samples were taken into 25 ml pre-weighted glass centrifuge tubes and these tubes were then filled up with 10 ml of distilled water and soyabean oil, respectively, and kept undisturbed for 25 min. Tubes were centrifuged at 5000 × g for 5 min at 27 °C and the supernatant of oil and water was then discarded. The final weight of each centrifuge tube was taken and the water and oil absorption capacity of rice straw was calculated using the following equations (7):

Water holding capacity (g)

= F(inal weight of centrifuge tube with pallets – Weight of empty centrifuge tube).. (7)

Oil holding capacity (g)

= (Final weight of centrifuge tube with pallets – Weight of empty centrifuge tube) ... ... (8)

3.2.4 Estimation of lignocellulosic component of rice straw

The composition of lignin, hemicellulose, cellulose, and ash in the samples was quantified using the gravimetric method developed by Van Soest (Colucci, Chase, and Van Soest 1982). This method also provided measurements for neutral detergent fiber (NDF), which reflects the fraction that remains insoluble in a neutral detergent solution. Similarly, acid detergent fiber (ADF) quantifies the insoluble components in an acidic detergent solution, and acid detergent lignin (ADL) measures the residual lignin mass. The content of cellulose was derived by subtracting the ADL value from the ADF, and the hemicellulose content was calculated by deducting the ADF from the NDF (Khudyakova and Kosolapova 2022). The values for lignin, hemicellulose, and cellulose, and were thus derived from the ADF, NDF, and ADL measurements, respectively.

3.2.4.1 Acid detergent fiber

Acid detergent fiber is the one step of the Van Soest method in which the hemicellulose is eliminated and only cellulose and lignin contents remain in the sample. To assess the Acid Detergent Fiber (ADF), 1 g of dried biomass was combined with 100 mL of an acid detergent solution consisting of cetyltrimethylammonium bromide (CTAB) and 0.5 M sulfuric acid (H2SO4) in a flat-bottom flask. Once boiling commenced, the mixture was refluxed for 60 minutes. Subsequently, residue was washed with hot distilled water and acetone, followed by drying at 105℃ until a stable weight was achieved.

$$ADF(\%) = \left\{\left(\frac{\text{Wt.of crucible and residue after treating ADF solution} - \text{Wt.of crucible}}{\text{Wt.of rice straw powder}}\right) \times 100\right\} \ldots (9)$$

3.2.4.2 Acid detergent lignin procedure

To measure acid detergent lignin (ADL), the acid detergent fiber (ADF) residue was treated with 72% sulfuric acid (H2SO4) for at least 3 h. Following digestion, The ADF was filtered through a filter crucible and washed with hot distilled water. Subsequently, the residue was dried at 105°C until a constant weight was maintained.

$$ADL\ (\%) = \left\{\left(\frac{\text{Wt. of crucible and residue after treating with 72\% H2SO4}}{\text{Wt. of rice straw powder}}\right) \times 100\right\} \ldots (10)$$

The ash content was determined as the residue remaining after heating at 550°C in a furnace for 5 h.

$$Ash\ (\%) = \left\{\left(\frac{\text{Wt. of crucible and ash} - \text{Wt. of crucible}}{\text{Wt. of rice straw powder}}\right) \times 100\right\} \ldots (11)$$

3.2.4.3 Neutral detergent fiber procedure

Solutions of neutral detergent fiber were prepared using sodium dodecyl sulfate (SDS) and Ethylene Diamine Tetra Acetate (EDTA). The solution was then refluxed for 60 minutes beginning at the boiling point. Following this, the residue was washed with hot distilled water and acetone and subsequently dried at 105°C until a consistent weight was achieved.

$$NDF\ (\%) = \left\{\left(\frac{\text{Wt.of crucible and residue after treating ADF solution} - \text{Wt.of crucible}}{\text{Wt.of rice straw powder}}\right) \times 100\right\} \ldots (12)$$

Hemicellulose = NDF − ADF

Cellulose = ADF – ADL

Lignin = ADL-Ash

3.2.5 Characterization of Parmal and Basmati rice straw

3.2.5.1 Confirmation of functional groups of rice straw using FTIR

The Spectra of the powdered samples were obtained using an ATR diamond crystal cell (Perkin Elmer Spectrum IR 2) and the default software IR-Solution 2, following the method outlined by Huang et al. (2018). The spectra were collected using a mid-infrared spectroscopy technique, the sample was analyzed with a 4 cm^{-1} resolution over the 4000–400 cm^{-1} range while the air was used as the background. To prepare the samples, a mixture was created by combining 10 mg of powdered rice straw sample with 100 mg of KBr. This mixture was then applied to the mirror surface. The resulting spectra were recorded in terms of transmittance.

3.2.5.2 Confirmation of surface morphology of rice straw using SEM

The structural and morphological properties of SiNPs were examined using a Scanning Electron Microscope (SEM) by following the method given by Bhattacharyya et al. (2020). For sample preparation, deionized water-dispersed SiNPs (20 µl) were dried on a clean glass slide. The dried samples were mounted on stubs at a height of 2 mm and carbon tape was used as non-conducting adhesive samples were then subjected to gold coating via sputter coating (JOEL smart coater) for 2 min at 30 mA to maximize the conductivity. Micrographs of the samples were recorded and the high-quality images were captured at 500× with an accelerating voltage of 20.0 kV at a working distance of 8.0 mm. The elemental analysis of samples was evaluated using EDAX or energy dispersive X-ray analysis (Bruker D8 Advance, Germany) equipped with FE-SEM Additionally, to confirm the elemental components of the SiNPs, energy dispersive X-ray analysis was applied

3.2.5.3 Confirmation of X-ray diffraction analysis of rice straw using XRD

The crystalline structure of the cellulose derived from delignified rice straw was examined using an X-ray diffractometer (Bruker D8 Advance from Germany: max2550VL/PC Rigaku, Japan). The study employed Ni-filtered Cu Kα radiation, while the operational parameters for the XRD measurements involved 35 kV and 200 mA. The scans were

conducted at a rate of 5°/min at an interval of 0.02°. The crystallinity index (% Cr I) of the cellulose fibers extracted from rice straw was determined using the method described by Segal, Creely, Martin, and Conrad in 1959.

$$\text{Crystallinity index (\%)} = \left(\frac{I_{002} - I_{am}}{I_{002}} \times 100\right) \ldots\ldots\ldots (13)$$

In this context, I_{002} represents the detector reading for the intensity of the diffraction peak at approximately 22°, indicative of the crystalline regions within the cellulose, while I_{am} denotes the reading for the intensity at approximately 18°, which corresponds to the amorphous regions in the cellulose.

3.2.5.4 Confirmation of thermal stability of rice straw using TGA

To assess the thermal degradation properties of the samples, Thermogravimetric Analysis (TGA) was conducted following the procedure introduced by Xiao et al. (2020). A thermo-gravimetric analyzer was employed for this purpose. BrieflyA 15 mg sample of powder was placed in an aluminum pan (Perkin Elmer, 0219-0071). Thermogravimetric analysis (TGA) was conducted over a temperature range of 10-900 °C at a rate of 10°/min, in an environment maintained with 99.999% nitrogen

3.3 Extraction of cellulose drives from Parmal and Basmati rice straw

3.3.1 Extraction of cellulose

Extraction of cellulose from rice straw was performed using a two-step approach such as pre-treatment and delignification. As shown in **Figure 3.2** in the pretreatment stage, the rice straw was soaked in 5% NaOH (2 g/20ml) for 6 h. After this, the sample was kept in a hot air oven for 120 min at 120 °C and then kept the solution for overnight. The pretreatment process was performed to remove a portion of lignin and hemicelluloses from rice straw. Subsequently, the resultant solution was repeatedly rinsed with double-distilled water until it achieved a neutral pH. The residue from the pretreatment was then placed in an oven to dry at 80 °C overnight. To remove the remaining part of lignin and to purify the cellulose the dried residue was then treated with 5% sodium chlorite at 120 °C for 120 min. Again, the sample was washed multiple times until the pH became natural and kept for overnight drying at 80 °C. The final extracted sample is a cellulose.

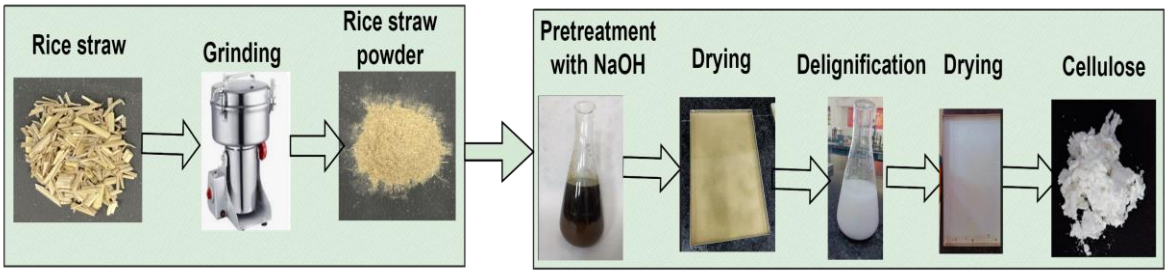

Figure 3.2 Extraction process of cellulose

3.3.1.1 Preliminary trials for extraction of cellulose

Extraction of cellulose from rice straw was performed using a two-step approach, such as pretreatment and delignification. In the pretreatment stage, the rice straw was soaked in (1, 2, 3, 4, 6, 7, 8,10, 12, and 16%) NaOH (2 g/20ml) for 6 h. After this, the sample was kept in a hot air oven for 120 min at 120 °C and then kept the solution for overnight. The pretreatment was performed to remove some parts of lignin and hemicelluloses from rice straw. The solution obtained was washed with double distilled water multiple times until the neutral pH of the solution was achieved. The pre-treated residue was then kept for oven-drying at 80 °C for overnight. To remove the remaining part of lignin and purify the cellulose, the dried residue was treated with 5% sodium chlorite at 120 °C for 120 min. Again, the sample was washed multiple times until the pH became natural and kept for overnight drying at 80 °C. The final extracted sample is a cellulose.

3.3.1.2 Purity of cellulose

To analyse the quality of cellulose content, a 100 ml sample containing 0.5-2 g of cellulose, or a 10 ml sample with 0.05-0.2 g of cellulose, was homogenized. Then, 10 ml of the homogenized sample was transferred into a 15 ml centrifuge tube and centrifuged for 5 min at 3000 rpm. The supernatant was carefully decanted and discarded. Then, 1 ml of acetic nitric reagent was added to the tube, and mixed thoroughly using a Vortex mixer, followed by an additional 2 ml, which was mixed again. To minimize evaporation, a marble was placed on top of the tube, which was then immersed in a boiling water bath for 30 min, ensuring the water level matched the liquid level in the tube. After boiling, the tube was centrifuged again for 5 min at high speed, the supernatant was decanted and discarded.

Subsequently, 10 ml of distilled water was added to the tube, starting with 1 ml, mixing, then adding 9 ml and mixing again, followed by centrifugation at high speed for 5 min. The supernatant was decanted and discarded, and then 10 ml of 67% sulfuric acid (H2SO4) was added to the tube, first adding 1 ml, mixing, then adding 9 ml and mixing again. The mixture was left to stand for 1 h. Next, 1 ml of the sulfuric acid-treated sample was diluted to 100 ml with distilled water, and centrifuged if any precipitate or turbidity was present. Then, 1 ml of the diluted sample was transferred to a 150 x 18 mm screw-cap tube and 4 ml of distilled water was added. The tubes were cooled in an ice bath, and then 10 ml of cold anthrone reagent was layered on top of the sample using a pipet. The mixture was mixed well using a Vortex mixer, covered with Parafilm to prevent splashing, and the tubes were returned to the ice bath until thoroughly mixed. A marble was placed on top of each tube, and they were immersed in a boiling water bath for 16 min. Finally, the tubes were cooled in an ice bath for 3 min, then allowed to stand at room temperature for 10 min. The absorbance of each sample was measured at 620 nm using a spectrophotometer, compared against a reagent blank.

To prepare the reagents, mix 150 ml of 80% acetic acid with 15 ml of concentrated nitric acid to make the acetic/nitric reagent. The anthrone reagent is made by dissolving 0.2 g of anthrone (Eastman, catalog No. 6432) in 100 ml of concentrated H2SO4, and should be prepared fresh daily. Before use, chill the anthrone reagent for approximately 2 h in the refrigerator.

3.3.2 Optimization of parameters for cellulose extraction

The cellulose was optimized by Response surface methodology using Box–Behnken experimental design with Design-Expert 8.0.6 (Static Made Easy, Minneapolis, Minnesota, USA). Here based on preliminary trials, the three factor experiments were applied and their level were selected as follows NaOH concentration (3, 4, and 5%), Reaction temperature (90, 120 and 150 °C), and reaction time (90 120, and 150 Min). The BBD selected 17 runs to experiment. Each run was performed with 3 times replications for each factorial experiment and 5 replications for the central point. Table 1 presents the coded and actual

variables and their respective values. Table 2 showing the experimental design (BBD) and resultant response data.

Table 1: Variables and coded values of experimental design

Variables	Coded values		
	Low (-1)	Medium (0)	High (1)
NaOH concentration (%)	3	4	5
Reaction Time (Min)	90	120	150
Reaction Temperature (°C)	90	120	150

3.3.3 characterization of pretreated rice straw and cellulose content

3.3.3.1 Impact of pretreatment on functional groups of rice straw

Fourier-transform infrared spectroscopy (FTIR) was utilized to verify the existence of functional groups in the essential constituents of the pretreated rice straw. The FTIR spectra for both samples were obtained using an ATR (Attenuated Total Reflectance) setup with a diamond crystal cell, alongside the standard software IR-Solution 2, at a resolution of 4 cm^-1. Samples were subjected to multiple scans across the mid-infrared region, spanning from 4000 to 400 cm^-1. This wide spectral range is essential for covering the broad array of functional groups present in rice straw. Scanning against air as a background enables the subtraction of atmospheric contributions (such as water vapor and CO2) from the sample spectra, ensuring that the resultant spectra accurately reflect the sample composition.

3.3.3.2 Impact of pretreatment on the surface morphology of rice straw

The structural characteristics and surface morphology of the pretreated rice straw and cellulose content samples were analyzed utilizing the FE-SEM (Field Emission-Scanning Electron Microscope), specifically the JEOL-JSM-7610F Plus model equipped with an Energy Dispersive Spectroscopy (EDS) system, which was utilized for imaging and analysis by the method given by Bhattacharyya et al. (2020). The dried samples were prepared by mounting them on stubs with a height of 2 mm, using carbon tape as a non-

conductive adhesive. To improve conductivity, a thin layer of gold was sputter-coated onto the samples using a JOEL smart coater for 2 min at a current of 30 mA. Micrographs of the samples were captured at a magnification of 500×, An accelerating voltage of 20.0 kilovolts (kV) was applied during the experiment, and a working distance of 8.0 mm, ensuring the acquisition of high-quality images. Furthermore, the elemental analysis of the samples was performed utilizing the Energy Dispersive X-ray Analysis (EDX or EDAX) technique.

3.3.3.3 Impact of pretreatment and cellulose on X-Ray diffraction analysis of rice straw

The crystalline structure of the cellulose derived from delignified rice straw was determined using an X-ray diffractometer (Bruker D8 Advance from Germany: max2550VL/PC Rigaku, Japan). The study employed Ni-filtered Cu Kα radiation, while the operational parameters for the XRD measurements involved 35 kV and 200 mA. The scans were conducted at a rate of 5°/min at an interval of 0.02°. The crystallinity index (% Cr I) of the cellulose fibers extracted from rice straw was determined using the method described by Segal, Creely, Martin, and Conrad in 1959.

$$\text{Crystallinity index (\%)} = \left(\frac{I_{002} - I_{am}}{I_{002}} \times 100\right) \ldots\ldots (14)$$

In this context, I_{002} represents the detector reading for the intensity of the diffraction peak at approximately 22°, indicative of the crystalline regions within the cellulose, while Iam denotes the reading for the intensity at approximately 18°, which corresponds to the amorphous regions in the cellulose.

3.3.3.4 Impact of pretreatment on the thermal stability of rice straw using TGA

The thermal degradation characteristics of the pretreated rice straw were evaluated using Thermogravimetric Analysis (TGA), adhering to the method outlined by Xiao et al. (2020). For these analyses, a thermogravimetric analyzer was utilized. Each analysis involved the use of exactly 15 mg of the sample in powdered form, which was placed into an aluminum pan (Perkin Elmer, 0219-0071). The TGA measurements spanned a temperature range of

30-900 °C, employing a heating rate of 10°/min, and were conducted in an atmosphere of nitrogen with a purity of 99.999%.

3.4 Synthesis of nanocellulose derived from Parmal and Basmati cellulose

To extract nanocellulose followed method by (Liu et al. 2020), In brief, 2 g of dried cellulose was treated with 50 ml of citric acid solution (80%). The mixture was then added with the desired amount of FeCl3 (0.01−0.03 mmol/g CA) into a 250 ml conical flask which was used as a catalyst for enhancing the speed of reaction. Then the sample was mixed on a magnetic stirrer for 5h at 500 rpm and the temperature was maintained at 100 °C. After completion of mixing 50 ml of hot deionized water was added to the mixture to avoid CA crystallization and hydrolysis. Subsequently, the final sample was subjected to multiple washes with deionized water and was then centrifuged at 10,000 rpm for 5 minutes to achieve a pH of 7. Afterward, the mixture was sonicated using a bath sonicator with a frequency of 20 kHz for 30 min. The final residue was dried using a tray drier at 80 °C for 24 h and then stored at room temperature for further analysis.

$$\text{Yield (\%)} = \left\{\left(\frac{\text{Final mass of nanocellulose after hydrolysis}}{\text{Initial mass of cellulose before hydrolysis}}\right) \times 100\right\} \ldots . (15)$$

3.4.1 Preparation of nanocellulose

To extract nanocellulose, 2 g of dried cellulose was treated with 50 ml of citric acid solution (80%) (Liu et al., 2017). The mixture was then added with the desired amount of FeCl3 (0.01−0.03 mmol/g CA) into a 250 ml conical flask which was used as a catalyst for enhancing the speed of reaction. Then the sample was mixed on a magnetic stirrer for 5h at 500 rpm and the temperature was maintained at 100 °C. After completion of mixing 50 ml of hot deionized water was added in to the mixture to avoid CA crystallization and hydrolysis. Then the final sample was washed several times with deionized water followed by centrifugation at 10,000 rpm for 5 min by achieving pH7. Afterward, the mixture was sonicated using a bath sonicator with a frequency of 20 kHz for 30 min. The final residue was dried using a tray drier at 80 °C for 24 h and then stored at room temperature for further study.

3.4.2 Extraction of nanocellulose

As represented in **Figure 3.3** the nanocellulose was synthesized using an 85 wt% citric acid (CA) solution, which was mixed with 0.01 mmol/g CA of FeCl3 in preheated deionized (DI) water. Following this, 1.5 g of cellulose and 50 mL of the prepared CA solution were sequentially added to a 250 mL flask. The flask was then subjected to mechanical stirring at 150 °C and 500 rpm for 6 hours. To inhibit the crystallization of CA, 50 mL of hot DI water was promptly added to the flask post-stirring to prevent hydrolysis. The mixture was subjected to centrifugation at 10,000 rpm for 5 minutes. After centrifugation, the residue was washed multiple times with DI water to attain a neutral pH. Then, the residue was placed in a petri dish and dried using a tray dryer at 80 °C.

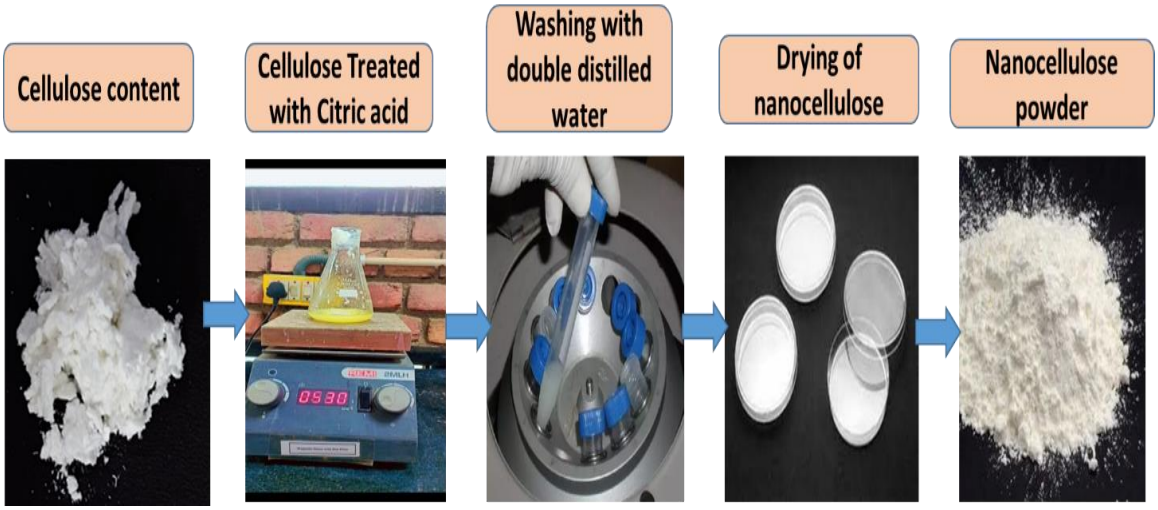

Figure 3.3 Extraction process of nanocellulose from isolated cellulose content

3.4.3 Characterization of Parmal and Basmati nanocellulose

3.4.3.1 Impact of citric acid on functional groups during nanocellulose synthesis

The Fourier-transform infrared spectroscopy was used to confirm the presence of the functional groups of vital components of nanocellulose. The FTIR spectra of rice straw samples were recorded with ATR diamond crystal cell and default software IR-Solution 2 at 4 cm^{-1} resolutions. The samples went through multiple scans (4000–400 cm^{-1}) against the air as a background and the results were found in the form of transmittance.

3.4.3.2 Impact of citric acid on surface Morphology during nanocellulose synthesis

The structural characteristics and surface morphology of the nanocellulose samples were analyzed utilizing the FE-SEM (Field Emission-Scanning Electron Microscope), specifically the JEOL-JSM-7610F Plus model equipped with an Energy Dispersive Spectroscopy (EDS) system, which was utilized for imaging and analysis by the method given by Bhattacharyya et al. (2020). The dried samples were prepared by mounting them on stubs with a height of 2 mm, using carbon tape as a non-conductive adhesive. To improve conductivity, a thin layer of gold was sputter-coated onto the samples using a JOEL smart coater for 2 min at a current of 30 mA. Micrographs of the samples were captured at a magnification of 500×, An accelerating voltage of 20.0 kilovolts (kV) was applied during the experiment, and a working distance of 8.0 mm, ensuring the acquisition of high-quality images. Furthermore, the elemental analysis of the samples was performed utilizing the Energy Dispersive X-ray Analysis (EDX or EDAX) technique.

3.4.3.3 Impact of citric acid on X-Ray diffraction Analysis during nanocellulose synthesis

The crystalline structure of the cellulose derived from delignified rice straw was examined using an X-ray diffractometer (Bruker D8 Advance from Germany: max2550VL/PC Rigaku, Japan). The study employed Ni-filtered Cu Kα radiation, while the operational parameters for the XRD measurements involved 35 kV and 200 mA. The scans were conducted at a rate of 5°/min at an interval of 0.02°. The crystallinity index (% Cr I) of the cellulose fibers extracted from rice straw was determined using the method described by Segal, Creely, Martin, and Conrad in 1959.

$$\text{Crystallinity index (\%)} = \left(\frac{I_{002} - I_{am}}{I_{002}} \times 100\right) \ldots\ldots (16)$$

In this context, I_{002} represents the detector reading for the intensity of the diffraction peak at approximately 22°, indicative of the crystalline regions within the cellulose, while Iam denotes the reading for the intensity at approximately 18°, which corresponds to the amorphous regions in the cellulose.

3.4.3.4 Impact of citric acid on thermal stability during nanocellulose synthesis

To assess the thermal degradation properties of the samples, Thermogravimetric Analysis (TGA) was conducted following the procedure introduced by Xiao et al. (2020). A thermo-gravimetric analyzer was employed for this purpose. In the analysis, a precise amount of 15 mg sample of powder was placed in an aluminum pan (Perkin Elmer, 0219-0071). Thermogravimetric analysis (TGA) was conducted over a temperature range of 10-900 °C at a rate of 10°/min, in an environment maintained with 99.999% nitrogen.

3.4.3.5 Impact of citric acid on particle size and zeta potential during nanocellulose synthesis

The particle size and zeta potential of the SiNPs were determined using dynamic light scattering (DLS) following the methodology described by Navarrete et al. (2019). The SiNPs were dispersed in a phosphate buffer solution (0.01 mM, 10 ml) and subjected to probe ultrasonication using Sonics and Materials Inc. The sample was subjected to ultrasonication at a temperature of 5 °C, using a 5-second pulse rate for 5 min to ensure adequate dispersion. Subsequently, the particle size and zeta potential analysis were performed using the surface morphology was examined using a computer-controlled particle size analyzer (Zetasizer Nano ZS, Beckman Instruments Ltd., Brea, California, United States).

3.5 Fabrication of nanocomposite film

As represented in **Figure 3.4** the films were developed using the wet casting method in the laboratory. In this technique, the varying amounts of nanocellulose powder were blended with 50 ml of deionized water and stirred with a magnetic stirrer at 1200 rpm for 1hr. Subsequently, following amount of mucilage and sodium alginate were incorporated into the previously prepared mixture. After the powders had completely dissolved, the specified amount of glycerol (plasticizer) was added to the mixture. The mixture was stirred magnetically at 1200 rpm for 4 h until a uniform consistency was achieved. The solution was then transferred into glass Petri dishes, using 90 ml per dish, and placed into a tray dryer at 60℃ for 36 h.

In addition to the experimental films containing nanocellulose and mucilage, control films were also prepared for comparison. The first control film was made without the inclusion

of nanocellulose, serving as a baseline to evaluate the properties of the film in the absence of nanocellulose's reinforcing effects. The second control film was prepared without the addition of mucilage, to assess the impact of mucilage on the film's structure, moisture retention, and flexibility. Both control films were subjected to the same wet casting procedure and drying conditions as the experimental films to ensure consistency in the comparison of their properties. The final films, both experimental and control, were evaluated for their physical properties, including thickness, tensile strength, flexibility, and moisture barrier capabilities. The inclusion of nanocellulose and mucilage was expected to influence these properties, and comparisons between the experimental films and the control films allowed for the determination of their respective contributions to the overall performance of the composite film.

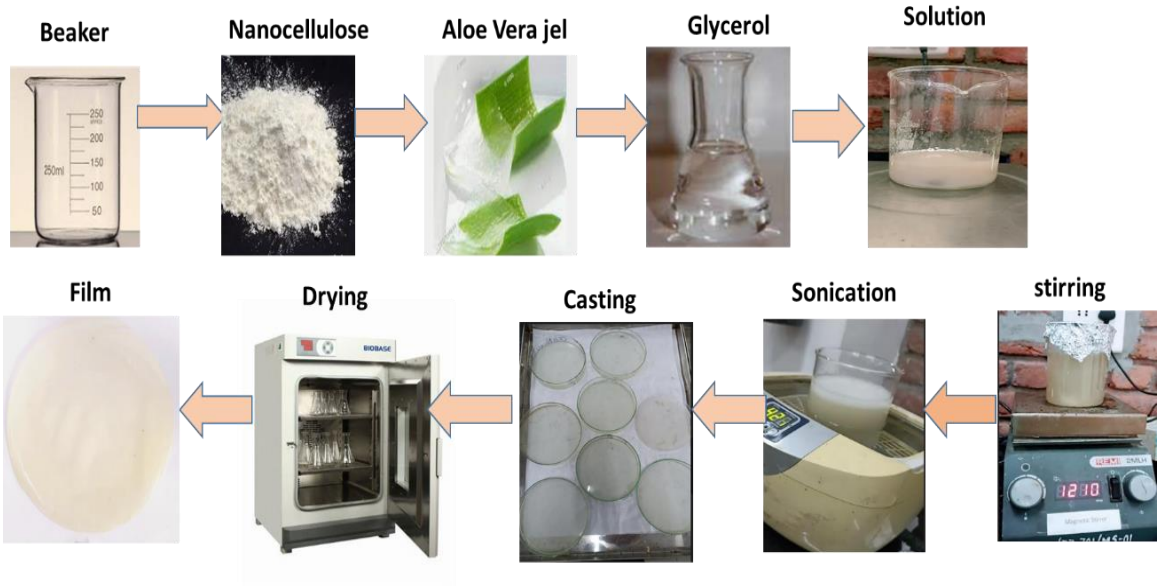

Figure 3.4 Optimization process of nanocomposite film

Table 3.1 Optimization of film fabrication

Sample code	Nanocellulose	Mucilage	Glycerol	sodium alginate
F1	1	1	2	1

F2	1	2	2	1
F3	1	3	2	1
F4	1	4	2	1
F5	1.5	1	2	1
F6	1.5	2	2	1
F7	1.5	3	2	1
F8	1.5	4	2	1
F9	2	1	2	1
F10	2	2	2	1
F11	2	3	2	1
F12	2	4	2	1
F13	2.5	1	2	1
F14	2.5	2	2	1
F15	2.5	3	2	1
F16	2.5	4	2	1
F18	3	1	2	1
F19	3	2	2	1
F20	3	3	2	1
F21	3	4	2	1
F22	3.5	1	2	1
F23	3.5	2	2	1
F24	3.5	3	2	1
F25	3.5	4	2	1
F26	4	1	2	1
F27	4	2	2	1
F28	4	3	2	1
F29	4	4	2	1
F30	4.5	3	2	1

F31	4.5	4	2	1
F32	5	3	2	1
F33	5	4	2	1
F34	5.5	3	2	1
F35	5.5	4	2	1
F36	6	3	2	1
F37	6	4	2	1
F38	5	0	2	1
F39	0	4	2	1

3.5.1 Physicochemical Properties of nanocomposite film

3.5.1.1 Mechanical Properties

The selection of the optimal nanocellulose-based functional film was based on mechanical testing conducted using a universal testing machine (AIM-651-1, Aimil Instrumentation and Technology, New Delhi, India) in accordance with the ASTM D882A standard. Test samples were prepared by cutting them into strips 10 mm wide and 40 mm long with a scalpel and securing them within the tensile grips. A primary grip separation was maintained at 30 mm, and the crosshead speed was set at 50 mm/s. Tensile strength (calculated as force per initial cross-sectional area) and elongation at break were directly obtained from the stress versus elongation curves using the "Exponent" software. Young's modulus was calculated from the slope of the initial linear segment of these curves (referenced as Equation 4). Each specimen was subjected to three replicates of the tests, and the tensile strength and elongation at break values were derived from equations 17 and 18.

$$\text{Tensile strength (MPa)} = \left(\frac{\text{Maximum tension during sample break}}{\text{thickness (mm)} \times \text{ width of the film (mm)}}\right) \ldots . (17)$$

$$\text{Elongation break (\%)} = \left\{\left(\frac{\text{Length of the sample break} - \text{ Initial length of sample}}{\text{The initial length of the sample}}\right) \times 100\right\} .. (18)$$

3.5.1.2 Moisture content

The moisture content of film was determined using a hot air oven by employing (AOAC, 2016). Briefly, the film samples were cut into square pieces of 5.0 cm^2 placed in a petri plate and accurately. Then kept in a hot air oven at 105 ℃ till a constant weight was obtained and the moisture content was calculated by following eq.:

$$Moisture\ content\ (\%) = \left\{\left(\frac{Initial\ weight\ of\ petri\ plate\ with\ sample - Final\ Weight\ of\ petri\ plate\ with\ sample}{Initial\ Weight\ of\ petri\ plate\ with\ sample - Weight\ of\ empty\ petri\ plate}\right) \times 100\right\} \ldots (19)$$

3.5.1.3 Water activity

The unbound water vapor pressure in the films was evaluated using a water activity meter (Model: WA-60A, Amtast, Lakeland, FL, USA). Each film sample was properly positioned on the sample plates, and a non-conductive humidity sensor was placed over it. When the water vapor pressure in the films achieved equilibrium with the atmospheric moisture, the relative humidity surrounding the sample matched the water activity of the film, which was then automatically displayed on the device's monitor.

3.5.1.4 Thickness

The film thickness was determined using a Vernier caliper, which provides measurements with an accuracy of 0.01 mm, at three random points on each film. The average thickness obtained from these measurements was then used to measure the physical properties of the films.

3.5.1.5 Water vapor transmittance rate (WVTR)

The water vapor permeability for each film was determined using the method prescribed by AOAC (2016). Initially, 2 grams of anhydrous calcium chloride were added to a glass weighing bottle, which had an internal diameter of 3 mm and a height of 15 cm. Each bottle was then tightly sealed with a film sample, secured by an elastic band, and subsequently weighed. These bottles were placed in a humidity chamber maintained at 27°C with 75% relative humidity, using a saturated sodium chloride solution. After 24 hours, the bottles were weighed again. This process was repeated in triplicate, and the water vapor permeability of the films was calculated using a specified equation.

$$\text{WPTR } (\text{kg s}^{-1}\text{m}^{-1}\text{ Pa}^{-1}) = \left(\frac{\text{The constant weight of weighing the bottle} - \text{initial weight of the weighing bottle}}{\text{film test area} \times \text{time of weight balance} \times \text{water vapor pressure}}\right) \ldots . (20)$$

3.5.1.6 Water uptake capacity

The water absorption ability of the bio-composite films was estimated following the protocol outlined by Mittal, Garg, and Bajpai (2020). Initially, the films were cut into dimensions of 20 mm by 20 mm and positioned in a desiccator containing calcium chloride ($CaCl_2$) powder to dehydrate for 24 hours. Post-dehydration, the films were weighed. Subsequently, these dried films were placed in another desiccator filled with water for an additional 24 hours to allow for water absorption. After this period, the films were weighed once more, and the quantity of absorbed water was determined using a specific equation.

$$\text{Water uptake capacity (\%)} = \left\{\left(\frac{\text{Wt. of films with water of the desiccator (g)} - \text{Wt. of films with CaCl2 of the desiccator}}{\text{weight of films with CaCl2 of the desiccator}}\right) \times 100\right\} .. (21)$$

3.5.1.7 Water solubility of film

The solubility of the film was estimated by a method procedure adapted from (Patil et al. 2021)). Film samples were trimmed into 5.0 cm^2 squares and their dry mass was precisely recorded. These samples were then placed into conical flasks containing 100 ml of distilled water and agitated continuously at 180 rpm for 2 h at ambient temperature. Subsequently, the film residues were filtered and dried in a forced-air oven at 105 °C until a constant weight was achieved. The solubility percentage of the films was calculated using the following formula.

$$\text{Water Solubility (\%)} = \left\{\left(\frac{\text{Initial wt.of the film expressed as dry matter} - \text{Final wt.of of the desiccated undissolved}}{\text{Initial wt.of the film expressed as dry matter}}\right) \times 100\right\} .. (22)$$

3.5.2 Characterization of nanocomposite films

3.5.2.1 Confirmation of functional groups of nanocellulose-based composite film

The Fourier-transform infrared spectroscopy was used to confirm the presence of the functional groups of vital components of nanocellulose. The FTIR spectra of samples were recorded with ATR (diamond crystal cell) and default software IR-Solution 2 at 4 cm^{-1} resolutions. The samples went through multiple scans (4000–400 cm^{-1}) against the air as a background and the results were acquired in terms of transmittance.

3.5.2.2 Confirmation of surface morphology nanocellulose based composite film

The structural characteristics and surface morphology of the nanocellulose samples were analyzed utilizing the FE-SEM (Field Emission-Scanning Electron Microscope), specifically the JEOL-JSM-7610F Plus model equipped with an Energy Dispersive Spectroscopy (EDS) system, which was utilized for imaging and analysis by the method given by Bhattacharyya et al. (2020). The dried samples were prepared by mounting them on stubs with a height of 2 mm, using carbon tape as a non-conductive adhesive. To improve conductivity, a thin layer of gold was sputter-coated onto the samples using a JOEL smart coater for 2 min at a current of 30 mA.Micrographs of the samples were captured at a magnification of 500×, An accelerating voltage of 20.0 kilovolts (kV) was applied during the experiment, and a working distance of 8.0 mm, ensuring the acquisition of high-quality images. Furthermore, the elemental analysis of the samples was performed utilizing the Energy Dispersive X-ray Analysis (EDX or EDAX) technique.

3.5.2.3 Confirmation of thermal stability nanocellulose composite film

To assess the thermal degradation properties of the samples, Thermogravimetric Analysis (TGA) was conducted following the procedure introduced by Xiao et al. (2020). A thermo-gravimetric analyzer was employed for this purpose. In the analysis, a precise amount of A 15 mg sample of powder was placed in an aluminum pan (Perkin Elmer, 0219-0071). Thermogravimetric analysis (TGA) was conducted over a temperature range of 10-900 °C at a rate of 10°/min, in an environment maintained with 99.999% nitrogen.

3.5.4 Biodegradability of film

The biodegradability of films was assessed using a soil burial test based on the method outlined by (Patil et al. 2021). Desiccators were prepared by filling them with garden soil

to a height of approximately 4 cm. Film samples, each with a diameter of 90 mm, were weighed before being buried in the soil to a depth of about 1 cm. The desiccators were then maintained under ambient conditions, with a temperature of 27±5°C and a relative humidity of 70±5%. To ensure consistent soil moisture, water was sprayed over the soil twice daily. Degradation of the films was monitored at specific time intervals, namely on the 5, 10 and 15 days. At each interval, the films were carefully extracted from the soil and gently remove any adhering soil particles. And then, visual observations of the films were documented using a camera to provide further insight into the degradation process.

3.6 Application of nanocomposite film

3.6.1 Preparation of bakery product

3.6.1.1 Preparation of bread

Approximately 450g of sieved wheat flour was mixed with 25g of butter to prepare the bread. Subsequently, a substantial pinch of salt, 1 teaspoon of sugar, and 2 teaspoons of fast-acting yeast were added and thoroughly mixed. The mixture was then allowed to rest for 30 minutes. Afterward, 300 ml of lukewarm water was incorporated to achieve the desired dough consistency. The dough was then placed into baking pans and left to rise for 1 hour. These pans were subsequently placed in an oven preheated to between 180 °C and 250 °C and baked for 1 hour. Following baking, the bread was removed, allowed to cool to room temperature, and then sliced into small pieces (Balamurugan et al., 2018).

Figure 3.5 Visual image of prepared bread

3.6.1.2 Preparation of biscuit

In this process all ingredients like 450 g of flour, 200 g of butter, 250 g of sugar etc., are combined in precise proportions ingredients are put into a bowl and mixed properly to prepare the dough. The ingredients are put into a bowl and mixed properly to prepare the dough. Then dough is followed by molding and biscuits are given a particular of shapes and sizes using cutter or molder. Then the molded biscuits are placed into the baking oven at 180 °C temperature. Then the temperature of biscuits is brought down to room temperature.

Figure 3.6 Visual image of prepared biscuit

3.6.1.3 Preparation of noodles

In this process all ingredients like 500 g of white flour, 250 g of butter and pinch of salt etc., are combined in precise proportions ingredients are put into a bowl and mixed properly to prepare the dough. Wrap the dough in plastic wrap or cover it with a damp cloth. Let it rest at room temperature for at least 30 minutes. This resting period helps to soften the gluten in the flour, making the dough easier to roll out. Then dough is fed in to a noodles maker for giving a particular of shapes and sizes using cutter and molder. Then the cut noodles are put into the hot oven at 80 °C temperature. Then the temperature of noodles is brought down to room temperature. And then stored in a tight container for further analysis.

Figure 3.7 Visual image of prepared noodles

3.7 Packaging of bakery products

The bakery products were packaged by cutting the nanocellulose composite film into 2 cm^2 slices. A piece of freshly baked bakery products was placed in the center of the 2 cm^2 film slice. The edges of the film were carefully sealed using heat sealing, to enclose the bread completely, ensuring that the package was airtight and free of any gaps. The sealed film was then allowed to cool at room temperature to ensure proper adhesion of the film to the bread. The packaged bakery products were stored under controlled conditions at room temperature to evaluate the film's effectiveness in maintaining freshness and preventing moisture loss or microbial contamination over a specified period. The samples were labeled with distinct codes for easy identification: bread was denoted as Br, biscuits as Bi, and noodles as Nd. The films used for packaging were also assigned specific codes: F for the nanocellulose-based film, CN for the control film without nanocellulose, and CM for the control film without mucilage. Each sample was labeled with its corresponding code to ensure clear identification throughout the experiment.

3.7.1 Shelf-life evaluation of bakery product

The shelf-life evaluation of bread, biscuits, and noodles was systematically analyzed over specific time intervals to assess the changes in their quality attributes that impact consumer acceptability and safety. Bread was evaluated at the beginning (0 days) and then on days 2, 4, 6, and 8. This frequency was chosen to capture the rapid changes typically observed

in bread due to its high moisture content, which can lead to microbial growth and textural changes like staling.

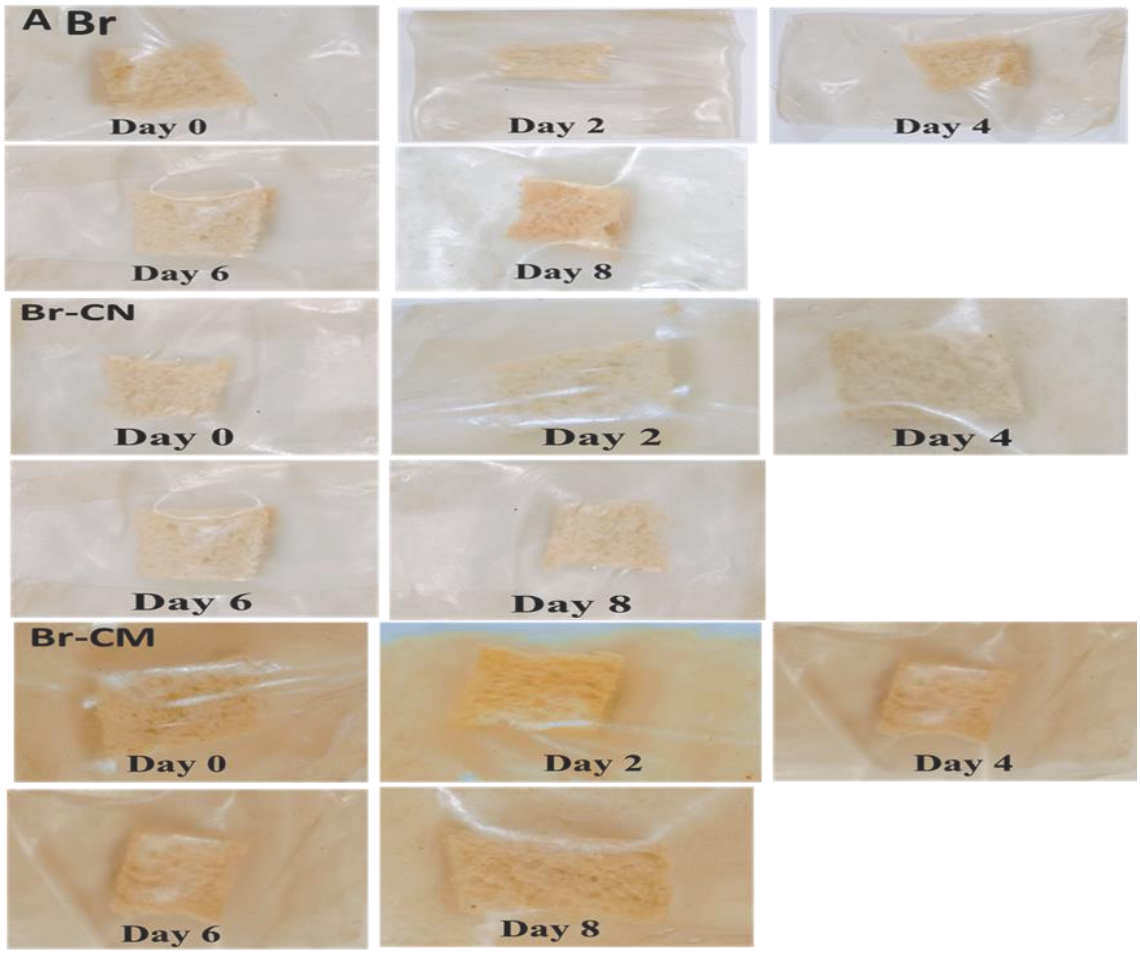

Figure 3.8 Shelf-life evaluation of bread packaged in (A) Selected film (Br) (B) Br-NC film (C) Br-CM film

Biscuits, known for their longer shelf life due to lower moisture content, were assessed over a more extended period. Evaluations were conducted starting from day 0 and continuing at 15-day intervals up to day 120. This schedule allowed for the observation of slower degradation processes, such as rancidity and loss of crispiness, which are crucial quality factors for biscuits.

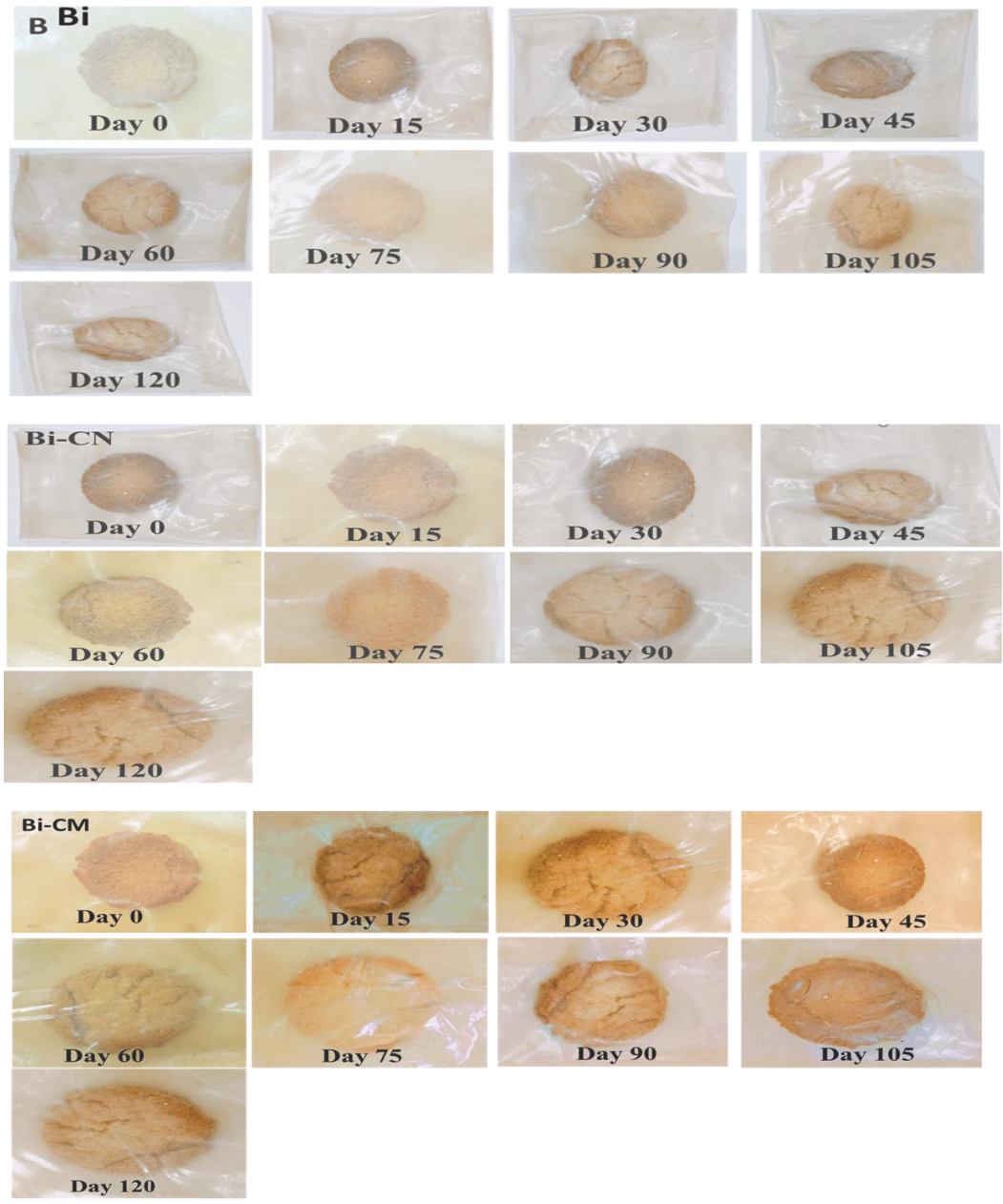

Figure 3.9 Shelf-life evaluation of biscuit packaged in (A) Selected film (Bi) (B) Bi-NC film (C) Bi-CM film

Noodles were assessed over the same intervals as biscuits: 0, 15, 30, 45, 60, 75, 90, 105, and 120 days. Noodles, depending on their type (dry or fresh), can exhibit changes in texture, taste, and potential microbial growth over time. The extended evaluation helps in

determining their usability period, particularly for instant and dry noodles that are expected to have a considerable shelf life.

Figure 3.10 Shelf-life evaluation of Noodles packaged in (A) selected film (Nd) (B) Nd-NC film (C) Nd-CM film

During these evaluations, various physical, chemical, and microbiological tests were likely conducted to determine moisture content, microbial growth, sensory attributes (such as texture and taste), and other decay or degradation indicators. This approach ensures that

the products remain within acceptable quality thresholds throughout their intended shelf life, providing critical data for manufacturers regarding packaging, storage conditions, and preservatives that might extend product longevity. This information is also invaluable for ensuring compliance with food safety regulations and for optimizing the consumer experience by guaranteeing product quality up to the specified shelf life.

3.7.2 Proximate composition of bakery product

3.7.2.1 Moisture content of bakery product

Products were used as the control samples and the quality of bakery products was examined using different analysis during 15 days interval of storage

The moisture content was analyzed during the time interval of 0,2,4,6,8 for bread (Br, Br-CN and Br-CM) 0, 15, 30, 45, 60, 75, 90, 105, 120 for biscuit (Bi, Bi-CN and Bi-CM) and noodles (Nd, Nd-CN, and Nd-CM). To measure the moisture content of the samples were kept in hot air oven (Kaizen Imperial, New Delhi) by employing (AOAC, 2000). Briefly, the samples were cut into square pieces of 5.0 cm^2 placed in a petri plate and accurately. Then kept in a hot air oven at 105 ℃ till a constant weight was obtained and the moisture content was calculated by following eq.

$$Moisture\ content\ (\%) = \left\{\left(\frac{Initial\ weight\ of\ petri\ plate\ with\ sample - Final\ Weight\ of\ petri\ plate\ with\ sample}{Initial\ Weight\ of\ petri\ plate\ with\ sample - Weight\ of\ empty\ petri\ plate}\right) \times 100\right\} \ldots (23)$$

3.7.2.2 Ash content of bakery products

The ash content of bread, biscuit, and noodles was estimated during the time interval of 0,2,4,6,8 for bread (Br, Br-CN and Br-CM) and 0, 15, 30,45,60,75,90,105,120 for biscuit (Bi, Bi-CN and Bi-CM) and noodles (Nd, Nd-CN, and Nd-CM). by adopting a method given by (AOAC 2000). Briefly, a 2 g sample was taken in a pre-weighed crucible and placed in a muffle furnace (NSW-125, Narag scientific work, Delhi, India) at 550 ℃ for 6 h followed by the charring of the sample. The ash content was calculated using eq. (24):

$$\text{Ash content}(\% = \left\{\left(\frac{\text{wt. of empty crucible and ash content (g)} - \text{wt.of empty crucible (g)}}{\text{wt. of sample (g)}}\right) \times 100\right\} \ldots (24)$$

3.7.2.3 Crude fat of bakery products

The Soxhlet apparatus (SCS 2 E: SOCS PLUS, Pelican equipment, Chennai, Tamil Nadu, India) was used to extract the crude fat from bread, biscuit, and noodles at the time intervals of 0,2,4,6,8 for bread (Br, Br-CN, and Br-CM) and 0, 15, 30,45,60,75,90,105,120 for biscuit (Bi, Bi-CN and Bi-CM) and noodles (Nd, Nd-CN, and Nd-CM). Briefly, 2 g powdered samples were kept in thimbles, and then placed in pre-weighed cleaned, and dried 100 ml beakers containing 80 ml petroleum ether. The processing steps of boiling, evaporation, and solvent recovery were automated and the fat content was then calculated in % using the following eq (25):

$$\text{Crude fat (\%)} = \left\{\left(\frac{\text{Wt.of the beaker with the fat content} - \text{Wt.of the empty beaker}}{\text{Wt.of sample}}\right) \times 100\right\} \ldots..(25)$$

3.7.2.4 Crude fiber content of bakery products

The crude fiber of bread biscuits and noodles was estimated during the time interval of 0,2,4,6,8 for bread (Br, Br-CN and Br-CM) and 0, 15, 30,45,60,75,90,105,120 for biscuits (Bi, Bi-CN and Bi-CM) and noodles (Nd, Nd-CN, and Nd-CM) using fiber plus apparatus (FES 06E: CE6 FIBRA PLUS, Pelican equipment, Chennai, Tamil Nadu, India). Briefly, 1.5 g of fat-free samples were taken in a pre-weighed crucible, and samples were then digested with 500 ml of H_2SO_4 (1.25%) and NaOH (1.25%) for 1 h. Digested samples were then kept in a muffle furnace at 550 ℃ for 4 h for ashing. The final results were calculated using eq (26):

$$\text{Crude fiber (\%)} = \left\{\left(\frac{\text{Wt.of the crucible + ash(g)} - \text{Wt.of the empty crucible(g)}}{\text{Initial wt.of the sample (g)}}\right) \times 100\right\} \ldots.(26)$$

3.7.2.5 Protein content of bakery products

The protein content of bread, biscuit, and noodles were determined during the time interval of 0,2,4,6,8 for bread (Br, Br-CN, and Br-CM) and 0, 15, 30,45,60,75,90,105,120 for biscuit (Bi, Bi-CN and Bi-CM) and noodles (Nd, Nd-CN, and Nd-CM) using Kjeldahl method (AOAC 1990). Where, the process is comprised of three steps including digestion, distillation, and titration. The samples underwent digestion through heating with concentrated sulfuric acid (H2SO4) along with a digestion mixture containing potassium sulfate (K2SO4) and copper sulfate (CuSO4). Subsequently, the mixture was neutralized by adding 40% sodium hydroxide (NaOH). The resulting ammonium sulfate decomposed

to release ammonia, which was captured in a 4% boric acid solution and subsequently titrated with standard hydrochloric acid (HCl). The nitrogen percentage in the sample was determined using the formula provided below.

$$\text{Protein (\%)} = \left\{\left(\frac{1.4\times 0.1\text{N HCL} \times \text{final Titration value}}{\text{Initial weight of sample}}\right) \times 100\right\}\text{----(27)}$$

3.7.2.6 Carbohydrate content of bakery products

The total carbohydrates of bread, biscuit, and noodles were estimated during the time interval of 0,2,4,6,8 for bread (Br, Br-CN and Br-CM) and 0, 15, 30,45,60,75,90,105,120 for biscuit (Bi, Bi-CN, and Bi-CM) and noodles (Nd, Nd-CN, and Nd-CM) by a differential method. Other compositional components of the Aloe vera gel (protein, Moisture content, fat, ash) were estimated individually and the values were subtracted from 100, which is considered as a total carbohydrate by difference. The following formula was used to calculate it:

Carbohydrate: 100 - (weight in g [protein + ash + water +fat])

3.7.3 Physio-chemical properties of bakery product

3.7.3.1 Water activity of bakery products

The water activity of bread biscuits and noodles at the time interval of 0,2,4,6,8 for bread (Br, Br-CN and Br-CM) and 0, 15, 30,45,60,75,90,105,120 for biscuits (Bi, Bi-CN and Bi-CM) and noodles (Nd, Nd-CN, and Nd-CM) were measured in the lab using Water activity (Aw) (Novasina, LabSwift, Supertech Analytical, Roorkee, Uttarakhand, India) Samples were prepared by cutting them into small pieces measuring approximately 3 mm × 3 mm × 3 mm. These pieces were promptly placed on the sample plate of the meter. After closing the measurement chamber, the water activity was recorded at 5-min intervals. The measurement was considered complete when the difference between two consecutive readings was less than 0.005.

3.7.3.2 pH analysis of bakery product

The pH of bread biscuits and noodles at the time interval of 0,2,4,6,8 for bread (Br, Br-CN, and Br-CM) and 0, 15, 30,45,60,75,90,105,120 for biscuits (Bi, Bi-CN, and Bi-CM) and noodles (Nd, Nd-CN, and Nd-CM) were measured in the lab. Herein, 10 grams of samples

were quantified and transferred into a 250 ml beaker, followed by the addition of 90 ml of distilled water. The mixture was stirred until homogeneous and then allowed to sit for 1 hour at room temperature to equilibrate. The pH of the solution was then measured using a pH meter (Cyberscan pH Tutor, EUTECH Instruments). Before the measurements, the pH meter was calibrated using standard buffer solutions with pH values of 5.92, 6.67,6.79. To ensure accuracy, the pH measurements were taken in triplicate. Between each measurement, the pH meter probe was thoroughly rinsed with distilled water to prevent cross-contamination (Manano et al. 2021).

3.7.3.3 Hardness of bakery products

Hardness measurements of bread biscuits and noodles at the time interval of 0,2,4,6,8 for bread (Br, Br-CN, and Br-CM) and 0, 15, 30,45,60,75,90,105,120 for biscuits (Bi, Bi-CN, and Bi-CM) and noodles (Nd, Nd-CN, and Nd-CM) were conducted using Texture Profile Analysis (TPA) with a CT3 textural analyzer (Brookfield, USA). Six parallel samples of multigrain bread were prepared by slicing them into 20mm thick slices, and a circular section was cut from the center using a round mold with a diameter and height of 20 mm. These cylindrical samples of multigrain bread were then subjected to two successive compression cycles using a TA 25/1000 acrylic cylinder probe (50.8 mm in diameter). The probe penetrated the bread to a depth of 50%, and the test was performed at a speed of 0.5 mm/s. The hardness of the bread was quantitatively expressed in Newtons (N) as reported by Osuna et al. (2014).

3.7.3.4 Free fatty acid of bakery product

Free fatty acids (FFA) of bread biscuits and noodles were estimated during the time interval of 0,2,4,6,8 for bread (Br, Br-CN and Br-CM) and 0, 15, 30,45,60,75,90,105,120 for biscuits (Bi, Bi-CN and Bi-CM) and noodles (Nd, Nd-CN, and Nd-CM) using the method described by (Osuna et al. 2018). Initially, 5 grams of the sample were placed in a flask containing 50 ml of benzene and allowed to stand for 30 min. After this period, the mixture was filtered using Whatman No. 1 filter paper. Subsequently, 5 ml of the filtered extract was transferred to a new flask, to which 5 ml of benzene, 10 ml of 95% ethanol, and a few

drops of phenolphthalein indicator were added. The resulting solution was titrated with 0.02 N potassium hydroxide until a light pink color persisted. The FFA content was then calculated using the following formula:

$$\text{FFA \%} = \left\{\left(\frac{282\ \times 0.02N\ KOH \times ml\ of\ alkali\ used\ (ml) \times diution\ fector}{1000\ \times weight\ of\ sample}\right) \times 100..(28)\right\}$$

3.7.3.5 TBA of bakery product

To assess lipid oxidation in bread biscuits and noodles were estimated during the time interval of 0,2,4,6,8 for bread (Br, Br-CN, and Br-CM) and 0, 15, 30,45,60,75,90,105,120 for biscuits (Bi, Bi-CN and Bi-CM) and noodles (Nd, Nd-CN, and Nd-CM), using a modified thiobarbituric acid-reactive substances (TBARS) method, aligned with AOAC Official Method Cd 19–90, was employed (Osuna et al. 2018).This evaluation utilized a UV-Vis Evolution 600 Thermo Scientific® spectrophotometer. The procedure commenced with 100 milligrams of the extracted lipids, to which 100 µl of butylated hydroxyanisole (BHA at a concentration of 36 g/l) and 2 ml of a thiobarbituric acid/trichloroacetic acid (TBA/TCA) mixture (20 mM TBA in 150 g/l TCA) were added in sequence. The combined ingredients were then subjected to heating at 90 ˚C within a water bath for 15 minutes before being cooled to ambient temperature. Following the heating phase, 2 ml of chloroform was incorporated into the mixture, which was then centrifuged at 1,000 rpm for 15 minutes. Spectrophotometric analysis was conducted to measure the absorbance of the clear supernatant at 532 nm, using a blank solution consisting of 0.1 ml of water and 2 ml of the TBA/TCA solution for calibration. Standard curves for malondialdehyde (MDA) were established using 1,1,3,3-tetramethoxypropane, enabling the quantification of thiobarbituric acid reactive substances (TBARS) as mg/kg of MDA equivalents in the samples.

3.7.3.6 Peroxide value of bakery product

The peroxide value (PV) for bread biscuits and noodles were estimated during the time interval of 0,2,4,6,8 for bread (Br, Br-CN, and Br-CM) and 0, 15, 30,45,60,75,90,105,120 for biscuits (Bi, Bi-CN and Bi-CM) and noodles (Nd, Nd-CN, and Nd-CM) using the method outlined by (Osuna et al. 2018). Initially, 5g of the sample was placed into a

volumetric flask, to which 50 ml of chloroform was added. The flask was then shaken for 2–3 h to extract the fat. Following extraction, the solution was filtered using Whatman No. 1 filter paper. From this filtered extract, 20 ml was transferred into another flask, and 30 ml of glacial acetic acid was added along with 1–2 ml of a saturated potassium iodide solution. The flask was then set aside for 30 min.

After this period, 50 ml of distilled water and 2 ml of a 1 percent starch solution were added to the mixture, resulting in a blue/black-colored solution. This solution was then titrated with 0.01 N sodium thiosulfate until the color changed to colorless. The PV was calculated using the following formula:

$$\text{PV (meq./kg)} = \left(\frac{\text{S} \times \text{N} \times 1000}{\text{weight of sample}}\right) \ldots . (29)$$

where SS is the ml of 0.01N Na22S22O33 (blank corrected), and NN is the normality of the Na22S22O33 solution.

3.7.3.7 Microbial counts of bakery product

10 grams of each sample of bread biscuit and noodles the time interval of 0,2,4,6,8 for bread (Br, Br-CN and Br-CM) and 0, 15, 30,45,60,75,90,105,120 for biscuit (Bi, Bi-CN and Bi-CM) and noodles (Nd, Nd-CN, and Nd-CM) were weighed under sterile conditions and transferred into a stomacher bag with 90 ml of sterile peptone water to undergo homogenization. Subsequent dilutions of the homogenates were plated on various growth media to assess viable microbial counts. For the enumeration of yeast and mold, Chloramphenicol Sabouraud agar was used and the plates were incubated at 25 °C for 5 days. Total aerobic mesophilic bacteria were cultured on plate count agar and incubated at 30 °C for 72 h, as described by Karaoglu, Kotancilar, and Gurses (2005).

This chapter presents the results and analysis of the experiments discussed in the previous chapter. Section 1 provides details of proximate analysis, functional properties, and characterization of two different rice straw varieties. And also discussed optimized cellulose extraction from rice straw by alkaline treatment method from rice straw to extract the maximum yield of cellulose. The RSM (response surface methodology) is applied using the quadratic equation to explore the effect of independent variables such as concentration of NaOH, reaction of time, and temperature on the cellulose yield. These results are further validated with ANOVA. Furthermore, the thermal stability, surface morphology, and functional group of cellulose were analyzed using TGA, SEM, and FTIR. Section 2 discussed the nanocellulose synthesized from optimized cellulose content. The characterization was performed to know the functional group, thermal stability, elemental analysis, and surface morphology of nanocellulose using FTIR, TGA, XRD, and SEM. Furthermore, the nanocellulose-based composite film was developed and incorporated with mucilage. The third section discussed the optimization of the film and its characterization, and physical and mechanical properties. Section four presents the details of the shelf-life analysis of bakery products packaged in the developed film. Graphs, tables, and images are used to support the obtained results from these experiments.

4.1 Proximate composition of raw materials

The proximate analysis gives an insight into the biomass in the form of gross components like volatile matter (VM), ash, and moisture content (M) of a sample. This analysis reveals the complete fixed carbon of the particular sample and the results are represented in **Table 4.1.** Powder properties always influence various processing operations including product formulations and mixing, storage in hoppers, silos, compression, packaging, and most importantly transportation (Gummert et al. 2020). In addition, these properties are directly related to the moisture content of powders and due to the inter-particle liquid bridges, the spontaneous agglomeration of particles may occur. Moreover, the water activity of a sample is a useful medium to catalyze chemical reactions (Lui et al. 2011).

Herein, the Parmal rice straw powder showed significantly ($P< 0.05$), higher moisture content (9.93 ± 0.35 %) than the moisture content of basmati rice straw powder (8.79 ±0.33 %). Results follow the findings of (L. Singh and Brar 2021); (and H. Yuan et al. 2020) who revealed the moisture content of the rice straw powder ranges from 2 to 15%, respectively. Various factors such as analytical method, time, and environmental conditions greatly influence the moisture content of the different rice straw varieties (Topno, 2015).

The ash content is an inorganic portion that remains after ignition of any organic matter which specifies the nutritional and elemental composition of biomass (Park et al., 2014). Herein the ash content of both Parmal and Basmati rice straw powders showed (15.49± 2.56% and 14.11 ± 0.83%, respectively) a non-significant ($P>0.05$) difference, which could be due to the similar soil and climatic conditions. Our results for the ash content are well supported by the study of (Bhardwaj et al. 2022) (Van Hung et al. 2020) Gummert et al., 2020) revealed 7.80 to 18.67 % ash content of the rice straw powders.

Furthermore, protein content in plants plays an important role such as structural, enzymatic, and functional roles (biosynthesis, photosynthesis, immunity, transport, etc). The variant properties of proteins make the plant significant ($P<0.05$) for different uses such as industrial applications for packaging, absorbent materials, and fire resistance (Capezza et al., 2019; Rasheed et al., 2020). Herein, the Parmal rice straw powder showed significantly ($P< 0.05$), higher protein content (15.71 ± 0.04%) than the protein content of basmati rice straw powder (10.80 ± 0.01%) between the protein content of both samples. Various factors such as analytical method, time, and environmental conditions greatly influence the moisture content of the different rice straw varieties (Ijaz et al. 2023).

Fat is an essential component of plants also known as a natural energy storehouse and plays an essential role in plant's metabolic processes. Herein, the Basmati rice straw powder showed significantly ($P< 0.05$), higher fat content of 2.0 ± 0.19% than the fat content of Parmal rice straw 1.15 ± 0.11%, respectively. These results are to the findings 1-14% approximately of (Madzingira et al. 2021). The fat content of any plant can vary according to its origin form as well as on soil and climatic factors.

The crude fiber plays an important role in the measurement of the quantity of indigestible cellulose, lignin, pentosans, and other components of a straw powder. It also gives a high degree of strength, durability, and absorbency to the straw fibers. The high crude fiber content gives a higher structural value to the straw powder. The crude fiber content was estimated significantly ($P < 0.05$) higher in Basmati (44.74 ± 0.52 %) than in Parmal rice straw (34.51 ± 0.08 %) which ranged from 29.8–to 37.0% described by Madzingira et al. (2021) in other rice straw varieties. The crude fiber of both rice straw samples showed a significant ($P<0.05$) difference. The fiber content of rice straw mainly depends on chemical nature such as ion strength, ion type, ionic form, particle size, porosity, stresses upon fiber, etc. as well as environmental conditions and the fiber source (Muwakhid et al. 2023; Khalil and Bachtiar 2023).

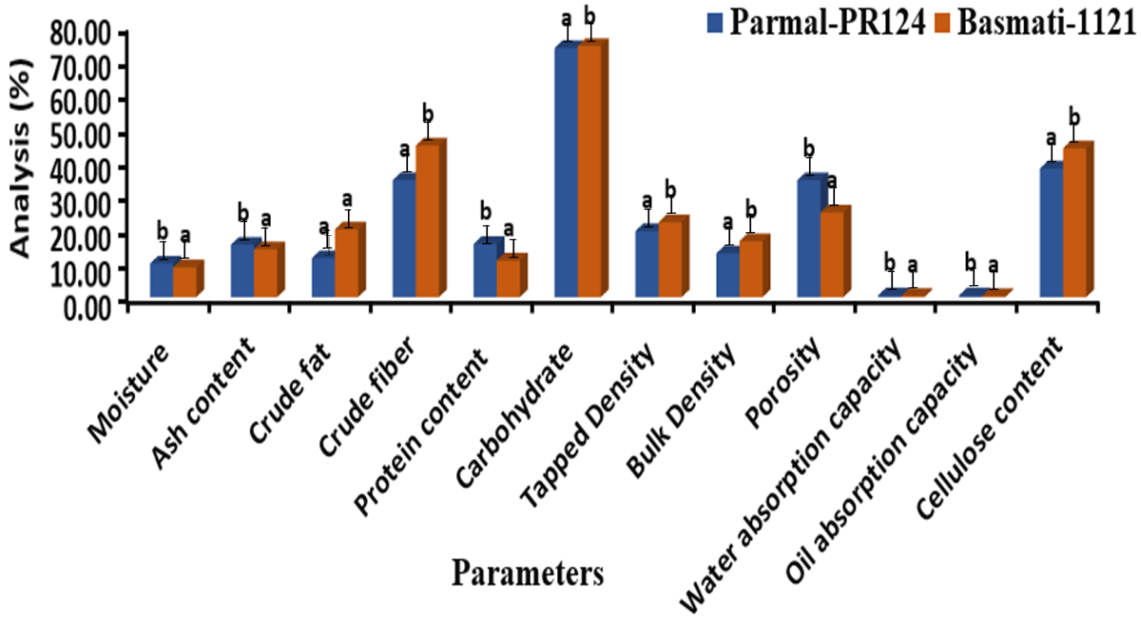

Figure 4.1 Comparative proximate analysis and physiochemical properties of Parmal and Basmati rice straw

Carbohydrate is an important compound for all organic existence on earth as they fulfill the other needs of plants by helping them in the synthesizing of other chemicals. And they also provide a good structure to the cell wall of straw powder. The carbohydrates

break down and release carbon atoms that serve as the raw material for a plant's biochemistry which helps the carbon to join with other chemicals in the body. Herein, the carbohydrates were observed at 73.51 ±1.33 % and 74.12 ±1.41 % in Parmal and Basmati rice straw which ranged from 70.2-72.72 % in other rice straw verities reported by (B. Jiang et al. 2024; Ramos et al. 2023).

Table 4.1 Comparative proximate analysis and physiochemical properties of Parmal and Basmati rice straw

[1]Data are represented as mean± SEM (n=3) [a-b] Means within the column with different lowercase superscripts are significantly different ($p<0.05$) from each other

4.2 Functional properties of rice straw

The functional properties such as bulk density, tapped density, water absorption capacity, oil absorption capacity, and porosity samples were estimated. The obtained results of all the functional properties are shown in **Table 4.1.** Density plays an important role during

Parameters	Parmal	Basmati	References
Moisture (%)	09.93 ± 0.35^{b}	08.94 ± 0.23^{a}	Sakhiya et al., 2021
Ash content (%)	15.43 ± 2.54^{b}	14.31 ± 0.53^{a}	Sakhiya et al., 2021
Crude fat (%)	01.15 ± 0.11^{a}	02.00 ± 0.19^{a}	Dhillon et al., 2018
Crude fiber (%)	34.51 ± 0.08^{a}	44.74 ± 0.52^{b}	Dhillon et al., 2018
Protein content (%)	02.98 ± 0.24^{b}	02.03 ± 0.04^{a}	Aquino et al., 2020
Carbohydrate (%)	70.51 ± 1.34^{a}	72.72 ± 1.41^{b}	Dehghani et al., 2015
Tapped Density (g/cm^3)	0.195 ± 0.01^{a}	0.221 ± 0.02^{b}	Oladeji et al., 2012
Bulk Density g/cm^3	0.129 ± 0.01^{a}	0.165 ± 0.03^{b}	Zhang et al., 2012
Porosity (%)	34.5 ± 2.58^{b}	25.00 ± 1.29^{a}	Zhang et al., 2012
Water absorption capacity (%)	52.8 ± 1.01^{b}	39.4 ± 0.31^{a}	Hoang et al., 2018
Oil absorption capacity (g)	5.02 ± 0.31^{b}	3.36 ± 0.25^{a}	Hoang et al., 2018

storage and handling of any organic matter. The rice straw powder with low density contains higher volume per kilogram which may cause of higher handling and shipping costs. And also, may cause of complications during storage, Processing, burning and transportation.

However, the density of rice straw can vary with various size-chopping methods as cited by (Rajput, Gupta, and Bansal 2023; Kumaran et al. 2023). As per the experimental work, the tapped density and bulk density of rice straw are estimated as 0.195 ± 0.01 g/cm^3 and 0.221 ± 0.02 g/cm^3, 0.129 ±0.01 g/cm^3, and 0.165 ±0.03 g/cm^3 respectively for both rice straw samples. These results showed a significant ($P<0.05$) difference between the estimated tab density and bulk density of both rice straw samples whose average range was estimated as 162.03 kg/m^3-195 kg/m^3 reported by(Abdelgawad et al. 2023) Various studies revealed that the different forms of rice straw can fluctuate its bulk density such as chopped straw based on equipment used, compression ratio, baled straw size, and loose rice straw (H. Kumar et al. 2023).

The porosity helps in the retention of oxygen, water, and nutrients within the plants which are absorbed through their roots**.** Rice straw with high porosity contains high nutritional value that is readily absorbed by the plants (da Silva Correa et al. 2022). The Porosity influences the various physical and thermal properties of biomass such as airflow velocity, heat, and mass transfer conditions as well as combustion parameters such as burning rate, emissions, heat conductivity, and conversion efficiency (Wen Yang et al. 2023)**.** As per the T-test, the porosity was estimated significantly ($P< 0.05$), higher for the Parmal (34.5 ± 0.58%) than the Basmati rice straw (25.67±5.29 %). This can be compared with the range 32.87-65.28% for other rice straw samples reported by (Wen Yang et al. 2023). The porosity of rice straw samples depends on several factors such as distribution, shaking, shape, and size of the particles (Kamboj et al. 2024).

The water-holding capacity of biomass plays an important role in the absorbance of nutrient content from the soil (Adhikari, Timms, and Mahmud 2022). Bio-based materials are hydrophilic and have a very high water absorbency due to the presence of polysaccharide molecules (cellulose and hemicellulose) that can fix water molecules (Abakar et al., 2020).

The water holding capacity for both Parmal and Basmati rice straw were estimated in the range of 5.28 ± 1.01 g and 3.94 ±0.31g, respectively. Based on the T-test these results showed a non-significant (P>0.05) difference between the obtained results. Gowda et al. (2014) reported that the water-holding capacity range varies from 5.8 to 6.3 g (Andrew and Dhakal 2022).

The oil holding capacity of Parmal rice straw (5.02 ±0.31g) was significantly (P< 0.05), higher than Basmati rice straw (3.36 ±0.25g) (Hoang et al., 2018). Due to lower porosity (less and small capillary pores), the basmati rice straw has a poor oil absorption capacity. Which decreases the surface area of the sorbent material and contributes the oil's less osmotic potential inside the sorbent material (Ben Hammouda et al. 2021).

4.3 Hardness of rice straw

Figure 4.2 illustrates the hardness of Basmati and Parmal rice straw. In this study, the average values for the samples were calculated based on measurements taken at ten distinct points on the surface of both samples. Where, the figure 1B revealed the hardness of the PRS cell walls was notably high, measured at 0.67±0.54 GPa, compared to the BRS cell walls, which showed a lower hardness of 0.53± 0.37 GPa. The observed difference in hardness between BRS and PRS could be the higher lignin content of lignin present in BRS compared to PRS. Due to this BRS is known for its brittleness, indicating a more rigid and possibly more lignified structure compared to PRS. BRS is characterized by its brittleness, a textural property that suggests a relatively rigid and possibly more lignified structure. Lignin is a complex polymer that binds with cellulose and hemicellulose fibers, providing rigidity to plant structures (Sandberg et al. 2023).

A higher lignin content, while adding to the strength and stiffness, can make the straw brittle and can also act as a barrier during cellulose extraction processes, reducing the yield of cellulose (Abolore, Jaiswal, and Jaiswal 2023). On the other hand, PRS, known for its softer texture, may have a lower lignin content or a different lignin composition that makes it less rigid and more flexible. This softer nature might correlate with a higher cellulose-to-lignin ratio, which can facilitate cellulose extraction, leading to a higher yield. The softer

texture might also indicate a higher proportion of pith, which is rich in cellulose and lower in lignin, compared to the outer shell of the rice straw. The difference in cellulose yield between PRS and BRS may also be influenced by the degree of polymerization and crystallinity of the cellulose present (Vanderfleet et al. 2022). If PRS contains cellulose with a lower degree of crystallinity, it could be more readily hydrolyzed and extracted, leading to a higher yield. Conversely, BRS may have a more crystalline cellulose structure, which is more resistant to hydrolysis.

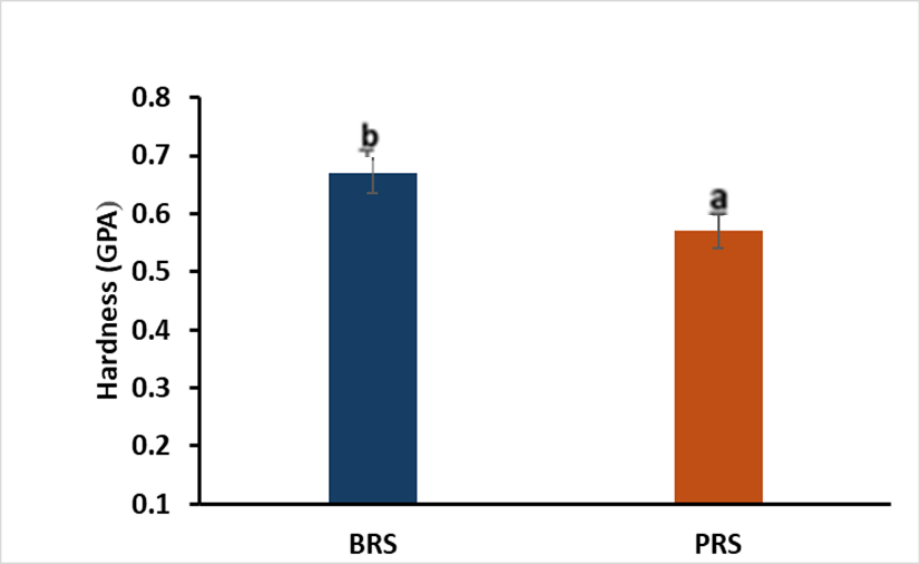

Figure 4.2. Hardness of cell wall of BRS and PRS

4.4 Color of rice straw

The Hunter Lab color system was used to describe the color of BRS and PRS. The system reports color in three dimensions: L* (lightness), a* (red-green spectrum), and b* (yellow-blue spectrum). In this study, the BRS powder has a lightness (L*) value of 34.3, indicating it is relatively light. Its a* value of 11.5 suggests a tendency towards the red side of the spectrum, while the b* value of 22.6 indicates a leaning towards yellow. In comparison, the PRS powder has a much lighter L* value of 64.5, less red with an a* value of 4.3, and more yellow with a b* value of 33.2 compared to Basmati. The BRS powder is thus darker

and redder, while Parmal is lighter and yellower. The darker color of BRS compared to PRS can primarily be attributed to variations in lignin content.

Lignin is an integral component of the secondary cell walls of plants and serves as a critical structural polymer that contributes to the rigidity and robustness of plant tissues. It is also known for its light-absorbing properties, which can significantly ($P < 0.05$), influence the color of plant materials. BRS, recognized for its brittle texture, likely has a higher lignin content, which not only makes its straw more rigid but also darker in appearance. The brittleness is a hint that the straw structure is more lignified, meaning it has a denser lignin network. This denser network could absorb more light, thus giving the straw a darker color. In contrast, PRS, with potentially lower lignin content, would have a lighter color due to less light absorption.

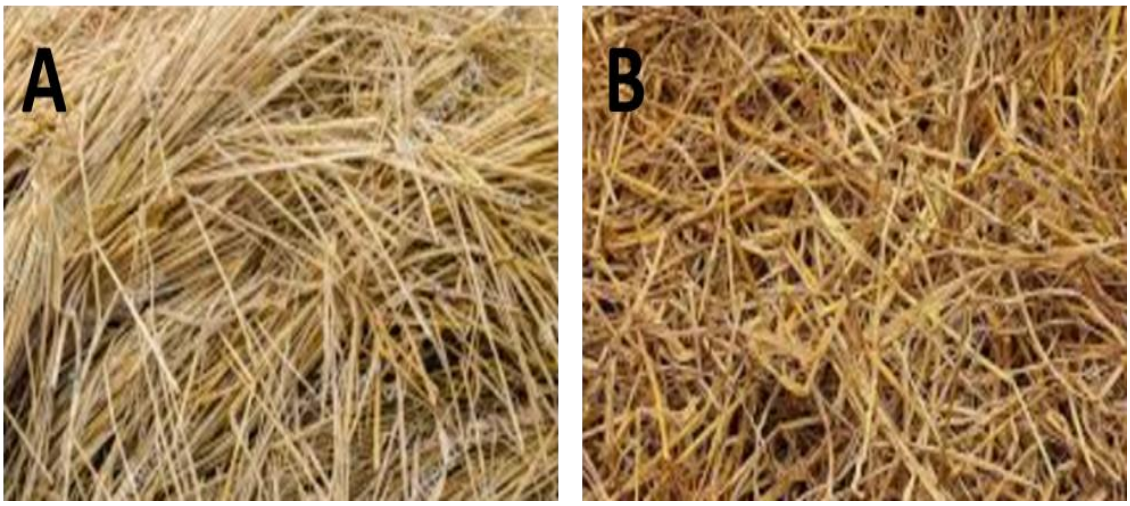

Figure 4.3: Color values of (A) Parmal rice straw and (B) Basmati rice Straw

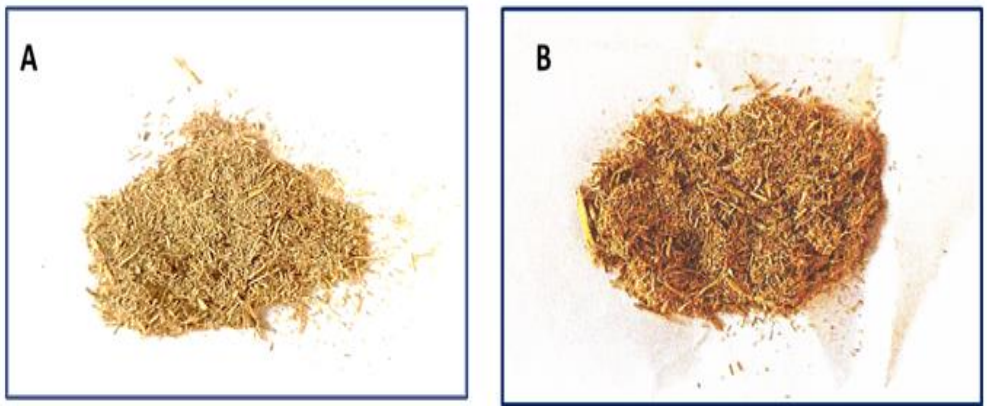

Figure 4.4: Color values of powdered (A) Parmal rice straw (B) Basmati rice Straw

4.5 Estimation of lignocellulosic component of rice straw

The Van Soest method, a comprehensive analytical procedure, has been employed to evaluate the composition of lignin, hemicellulose, and cellulose in different varieties of rice straw, specifically BRS and PRS (Aguiar 2022). As **Figure 4.5** revealed cellulose, the principal structural component of plant cell walls, constitutes approximately 37.80 ± 0.63 % of PRS and 36.27 ± 0.76 % of BRS. The estimation also showed that lignin, which imparts rigidity to the plant structure and is known for its resistance to chemical and enzymatic degradation, is present at 19.23 ± 0.52 % in PRS and slightly higher at 21.41± 0.82% in BRS. This variation in lignin content may influence the processability and digestibility of the rice straw varieties.

Furthermore, hemicellulose, a heterogeneous polysaccharide found in plant cell walls alongside cellulose, was determined to be 23 ± 0.45% in PRS and 22 ± 0.91% in BRS. Hemicellulose plays a crucial role in cell wall structure and water retention. The slightly higher hemicellulose content in PRS suggests a subtle difference in the cell wall composition between the two rice straw varieties (J. J. Xu et al. 2024). The structural properties of rice straw, which contribute to its texture and the yield of extractable cellulose, can be significantly ($P< 0.05$), different between varieties such as Parmal and Basmati due to genetic, morphological, and compositional factors.

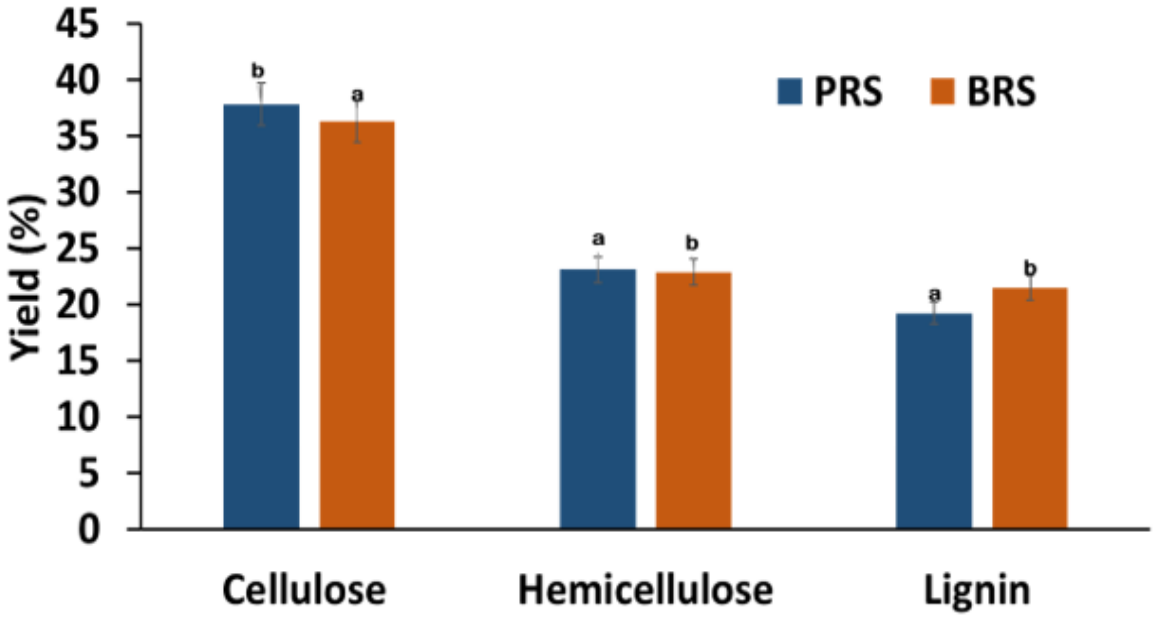

Figure 4.5. Yield of lignocellulosic components of BRS and PRS

Table 4.2 Yield of lignocellulosic components of BRS and PRS

Color value	PRS (%)	BRS (%)
Lignin	19.23 ± 0.52[a]	21.41± 0.82[b]
Hemicellulose	23 ± 0.45[b]	22 ± 0.91[a]
Cellulose	37.80 ± 0.63[b]	36.27 ± 0.76[a]

[1]Data are represented as mean± SEM (n=3) [a-b] Means within the column with different lowercase superscripts are significantly different ($p<0.05$) from each other

4.6 Lignocellulosic structure of rice straw

Lignocellulose biomass contains three main structural components: cellulose, hemicellulose, and lignin. **Figure 4.6** depicts the complex structure of cellulose (C6H10O5) x, which is a main component in the plant cell wall. It consists of a long polymer chain comprising thousands of systematic and rigid glucose monomers (S. Chaudhary, Jain, and Jaiswar 2022). These monomers formed a strong hydrogen bond with

each other in the presence of –OH molecules, as shown in **Figure 4.6 A**. The molecular weight of cellulose is 100,000. The degree of polymerization (DP) is around 10,000 resistant to strong alkali solutions (R. Sharma et al. 2024).

Hemicellulose (C5H8O4) x is made up of a group of polysaccharides comprising a highly branched polymer of C-5 and C-6 carbon ring sugars, as shown in **Figure 4.6 B** (Adnane et al. 2024). It is composed of limited pentose polymers such as arabinose, xylose, galactose, and mannose (Tawil-Lucas et al. 2023). The hemicellulose polymer chain (branch arrangement) is shorter and weaker than the cellulose (linear arrangement) chain. It can hydrolyze very easily using alkaline due to its lower molecular weight than cellulose (10–100 times higher) and is more hydrophilic.

Whereas, **Figure 4.6 E & D** depicts the complex structure of lignin [C9H10O3 (OCH3) 0.9–1.7]x which is made up of a very complex molecule with a three-dimensional structure that is a non-carbohydrate and most rigid component (Yunpu et al., 2016). It is made up when plants polymerize the tyrosine and aromatic amino acids phenylalanine to form phenylpropane units as monolignols. However, its chemical structure in regular fibers has not been fully established. It can be easily soluble in hot alkali, as referred to in (Nevárez et al., 2011). A lignin wall protects cellulose and hemicellulose. Here, **Figure 4.6 E & D** show the pretreatment process required to degrade lignin, solubilize the hemicellulose, and decrease the crystallinity structure of the cellulose component. The lignin forms a lignin carbohydrate complexes (LCCs) bond associated with carbohydrates (He et al. 2022). In the rice structure, chemical bonds such as ester bonds, α-ether bonds, acetyl linkages, and phenyl glycosidic linkages are connected in the rice structure (Zerva et al. 2021). The alkali treatment can break down these bonds between cellulose, hemicellulose, and lignin by hydrolyzing the ester bonds via organosolve fractionation.

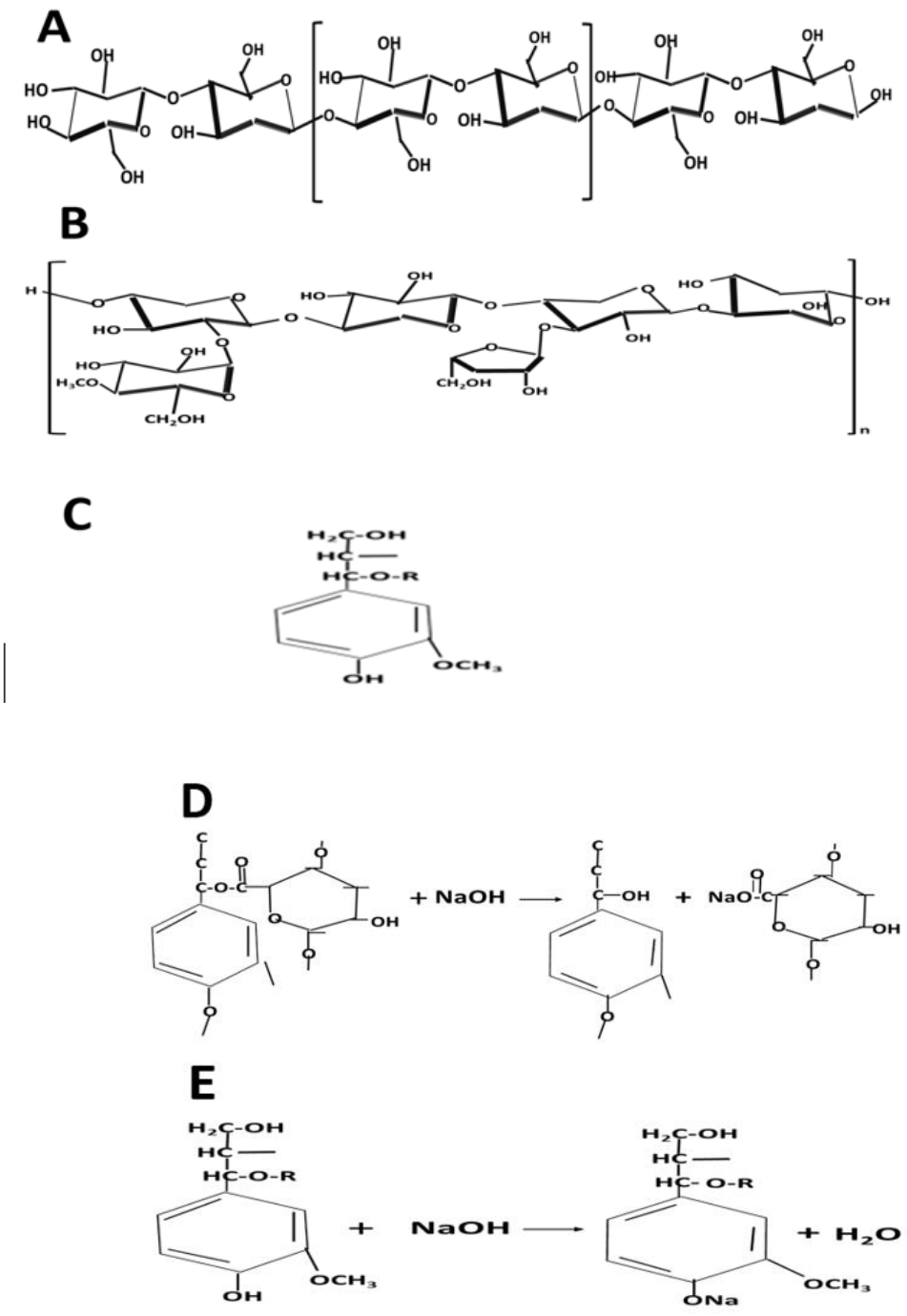

Figure 4.6: Chemical structure of (A) Cellulose (B) Hemicellulose (C) Lignin (D) Scheme of lignin carbohydrate complexes (LCCs) reacting with NaOH (E) Scheme of lignin reacting with NaOH.

4.7 Characterization of Parmal and Basmati rice straw

4.7.1 Confirmation of functional groups of rice straw using FTIR

As illustrated in **Figure 4.7** the comparative FTIR spectra of Parmal (PRS) and Basmati (BRS) rice straw varieties show distinct transmittance peaks, indicating variations in their chemical compositions. Both varieties exhibit a broad peak around 3342.79 cm^{-1} (BRS) and 3310.84 cm^{-1} (PRS), corresponding to O-H stretching vibrations, a characteristic feature of cellulose, hemicellulose, and lignin, suggesting strong intermolecular hydrogen bonding. The peak near 2800-2900 for both samples is attributed to C-H stretching vibrations from aliphatic chains (Luo et al. 2024).

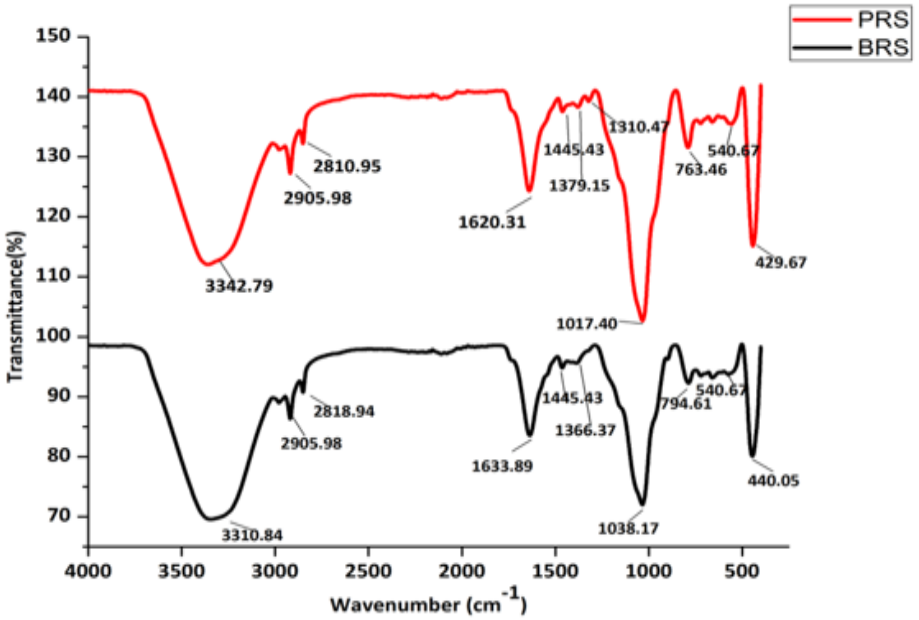

Figure 4.7 Confirmation of functional groups of rice straw using FTIR

A difference was observed in the peak at 1620.31 cm^{-1}, and 1633.89 cm^{-1} for both samples attributed to the different moisture content (bound water) or variations in the lignin content (J. Yuan et al. 2023). Whereas the peaks around 1445 cm-1 for both samples related to CH_2 bending, the peaks at around 1379.15 cm^{-1} (BRS) and 1382.34 cm^{-1} (PRS) may suggest the presence of CH_3 groups. The peak at 1038.17 cm^{-1} for both samples is sensitive to C-O stretching vibrations, indicating differences in the polysaccharide content, possibly due to

variations in cellulose, hemicellulose, or the presence of other carbohydrates (Zong et al. 2020). Finally, Both PRS and BRS display peaks at approximately 540.65 cm^{-1} and 440.05, which might suggest the presence of Si-O-Si bending vibrations due to silica, commonly found in rice straw.

4.7.2 Confirmation of surface morphology of rice straw using SEM

As illustrated in **Figure 4.8** the comparative surface morphology of Parmal (PRS) and Basmati (BRS) rice straw The Scanning Electron Microscope (SEM) images of Parmal rice straw (PRS) and Basmati rice straw (BRS) provide a detailed comparative view of their microstructural differences at a magnification of 500 times. Figure 4.8 shows an SEM image of PRS and BRS where PRS shows a relatively uniform and smooth surface with fibers that appear tightly packed and well-aligned. This suggests a robust, denser lignocellulosic structure, indicative of potentially higher mechanical strength and reduced water permeability. Such a uniform structure might make PRS more appropriate for applications that require material durability, such as in the manufacturing of bio-composite materials or paper production. Small particles visible on the surface are likely residual silica bodies, typical in rice straws, which might impact processing properties like grinding or chemical treatment efficiency.

In contrast, the BRS image reveals a more irregular and disrupted surface, with visible signs of roughness and material accumulation, possibly from environmental exposure or microbial activity. This heterogeneity suggests a less dense structure, which could lead to different industrial applications compared to PRS. The irregularity and rough texture of BRS might make it more suitable for uses where quicker degradation is beneficial, such as composting or bioenergy production, due to its potential for faster microbial breakdown. The differences between PRS and BRS extend to their potential chemical treatability. PRS, with its denser and more uniform structure, might resist chemical penetration, requiring more intensive processing conditions for applications like pulping or enzymatic hydrolysis. Meanwhile, BRS's more open and varied structure may allow for more efficient and quicker chemical treatment processes.

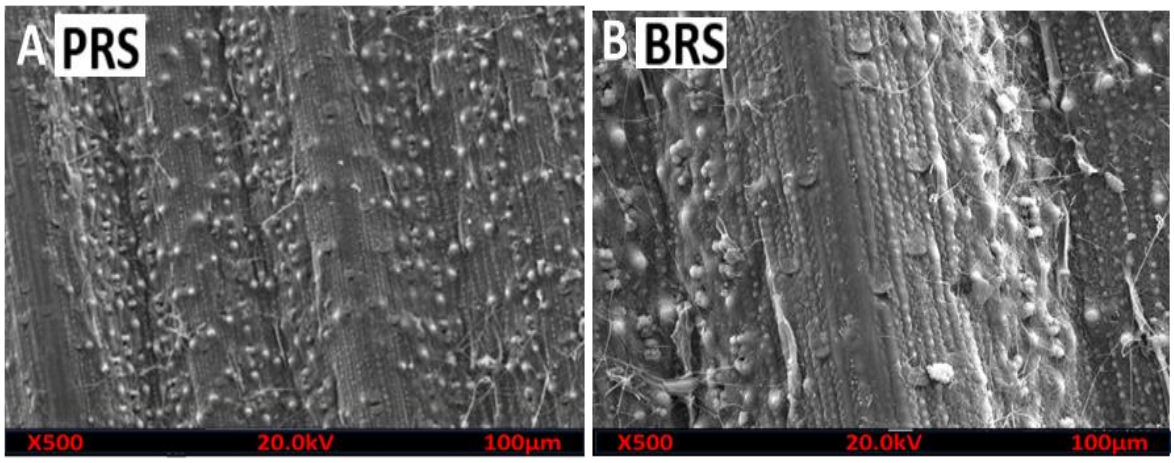

Figure 4.8 Confirmation of surface morphology of rice straw using SEM

4.7.3 Confirmation of energy-dispersive X-ray of rice straw using EDS

As illustrated in **Figure 4.9** the comparative elemental analysis of Parmal (PRS) and Basmati (BRS) rice straw The EDX spectra of BRS and PRS show peaks for carbon (C), oxygen (O), silicon (Si), and a small amount of potassium (K). The presence of Si is typical in grasses due to the silica bodies that are part of their structural composition. Potassium may be present as a nutrient absorbed from the soil (Mandlik et al. 2020). In the EDX image Figure 4.9 shows the spectrum of PRS, we observed pronounced peaks for silicon, which is due to its implications on the structural rigidity and potential processing challenges of rice straw. Silicon, typically high in rice straws, contributes to their mechanical strength and thermal stability.

Carbon and oxygen are also prominent, indicative of the organic, cellulosic structure of the straw, which comprises lignin and cellulose. These elements are fundamental to the biomass's utility in products like bio-composites and energy resources. The presence of potassium, a vital nutrient element, highlights its residual agricultural value, potentially beneficial when reused as soil amendments. Conversely, the BRS spectrum in Figure 10B shows a similar elemental makeup but with slight variations in peak intensities. These differences could suggest variations in elemental distribution or concentration, affecting the physical and chemical properties of rice straw. For instance, a less pronounced silicon

peak compared to PRS might indicate lower silica content, affecting BRS's suitability for applications requiring less structural rigidity and potentially making it more amenable to chemical processing like pulping.

The comparison between PRS and BRS is crucial in understanding how these variances impact their applications. PRS, with its higher silicon content, might be better suited for building materials or silicon chemical production, where durability is crucial. BRS, possibly with less silica, could be better for paper production or bioenergy, where easier degradation and processing are required. Additionally, the nutrient content, as indicated by potassium levels, affects their environmental impact when used as compost or soil amendments, influencing nutrient cycling and soil health.

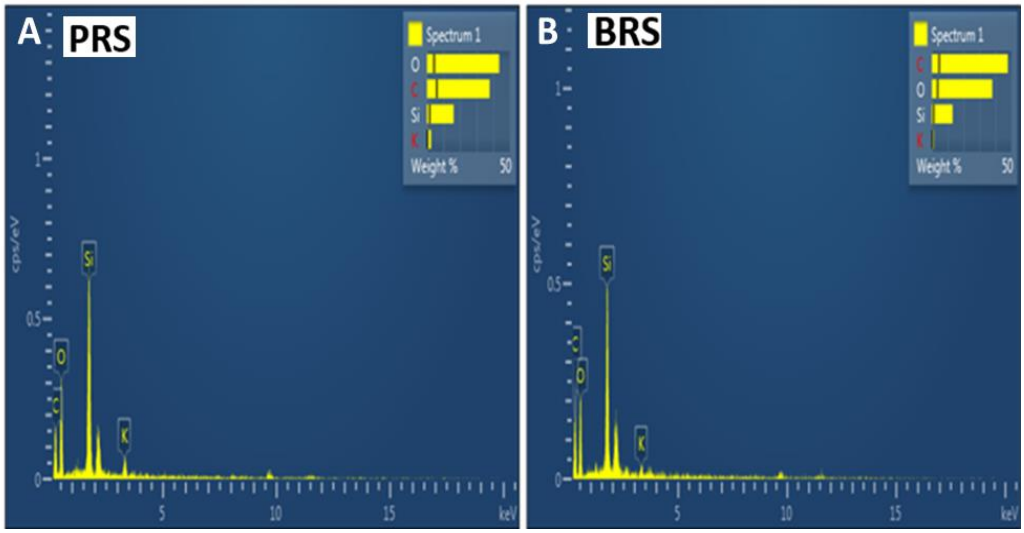

Figure 4.9 Confirmation of energy-dispersive X-ray of rice straw using EDS

4.7.4 Confirmation of crystallinity index of rice straw using XRD

The XRD displayed in **Figure 4.10** for Parmal rice straw (PRS) and Basmati rice straw (BRS) offers offer significant ($P<0.05$) understanding of the crystalline structure of these materials. XRD is an essential tool in material science for determining the crystallographic structure, chemical composition, and physical properties of materials. The patterns shown in **Figure 4.10** reflect the typical crystalline peaks associated with cellulose, the primary structural component in rice straw. Both PRS and BRS exhibit similar diffraction patterns,

indicating that they share comparable crystalline structures predominantly made up of cellulose I. The most pronounced peak at approximately 22.5°, corresponding to the (002) lattice plane of cellulose I, is indicative of the organized crystalline nature of cellulose. This peak is notably sharper and more defined in PRS than in BRS, suggesting that (Abolore, Jaiswal, and Jaiswal 2023) at PRS may possess a higher degree of crystallinity.

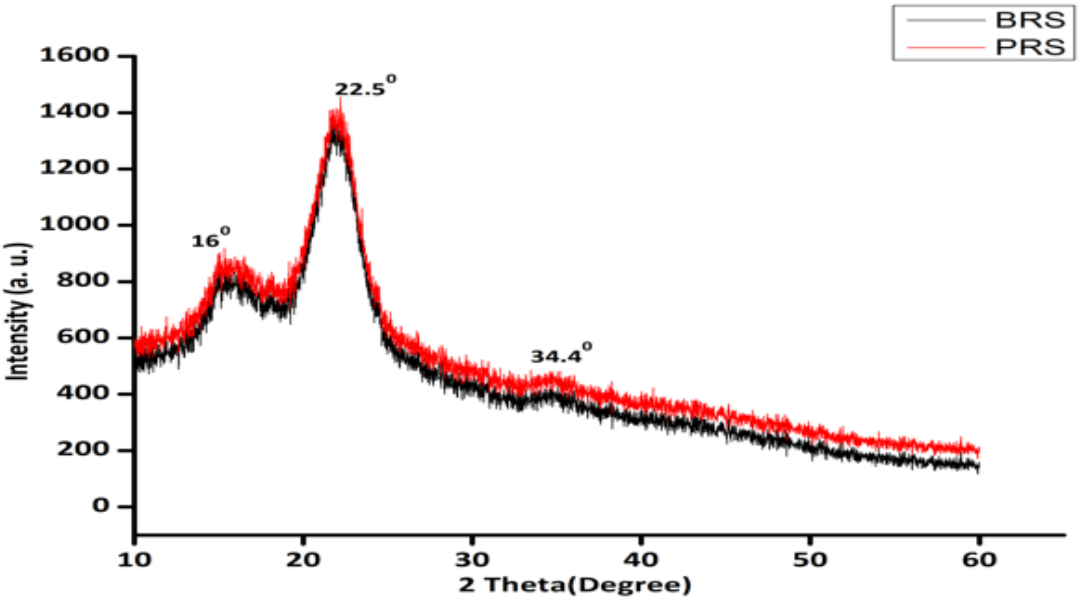

Figure 4.10 Confirmation of crystallinity index of rice straw using XRD

A higher crystallinity is generally associated with increased rigidity and structural integrity, which can affect the resistance to chemical and enzymatic degradation of rice straw, impacting its suitability for various applications (Yi et al. 2024). Additional peaks at around 16° and 34.4° help further characterize the material. The peak at 16° typically relates to semi-crystalline structures, while the peak at 34.4° might represent more tightly packed cellulose microfibrils within the crystalline domains. These features are crucial for understanding the interaction of rice straws with moisture and chemicals, which is particularly important for applications in paper production, biofuel conversion, and bio composite materials. The similarities and differences in the XRD patterns between PRS and BRS also suggest slight variations in their chemical composition or crystallinity, which could influence how these materials are processed and utilized industrially. For instance,

the higher crystallinity in PRS might necessitate more aggressive processing conditions during pulping or chemical treatment, while the slightly lower crystallinity in BRS could make it more amenable to processes that require less energy or lower temperatures.

4.7.5 Confirmation of thermal stability of rice straw using TGA

As shown in **Figure 4.11** the initial degradation step (dehydration) for PRS and BRS straw occurred at 30.13 to 246.80 °C and 30.13 to 212.20 °C with a weight loss of 10.76% and 8.63% respectively. The loss is gradual and minimal due to, the removal of water molecules which are low in molecular weight and loosely bound on the surface of the samples.

$(C_6H_{10}O_5)_{n.}\ 2H_2O \rightarrow (C_6H_{10}O_5)_{n+}\ 2H_2O$ …. (dehydration).

As the temperature increases, there is a sharp decline in weight 59.691% at 374.17 ℃ for BRS and 61.195% to 389.94 ℃ for PRS. This is the main decomposition zone where the organic components of the rice straw, primarily cellulose, hemicellulose, and lignin, begin to break down (Pang et al. 2022) due to high temperature. Which produces mainly volatile products such as char, vapors, CO, and carbon dioxide. It is the area where the most significant ($P<0.05$) difference shows between different types of straw, due to variations in the composition of these components.

Rice straw, leading to a variety of intermediate products that degrade at different temperatures contains a mix of cellulose, hemicellulose, lignin, and other organic compounds, some of which have lower decomposition temperatures. The hemicellulose decomposes between 200–300°C, and lignin starts decomposing at around 160°C and continues up to 900°C. Cellulose decomposition typically starts above 300°C (Zong et al. 2020). Moreover, the non-cellulosic components of rice straw are less crystalline and more amorphous, leading to lower thermal stability (N. Sharma et al. 2023). Furthermore, the weight loss continues at a slower rate beyond 400°C due to the breakdown of more thermally stable components and char formation. The remaining residues specify the existence of the carbonaceous materials in both samples (Amado-Fierro, Centeno, and Diez

2023). Whereas the rice straw contains higher carbon content than cellulose content due to the presence of more lignocellulose materials.

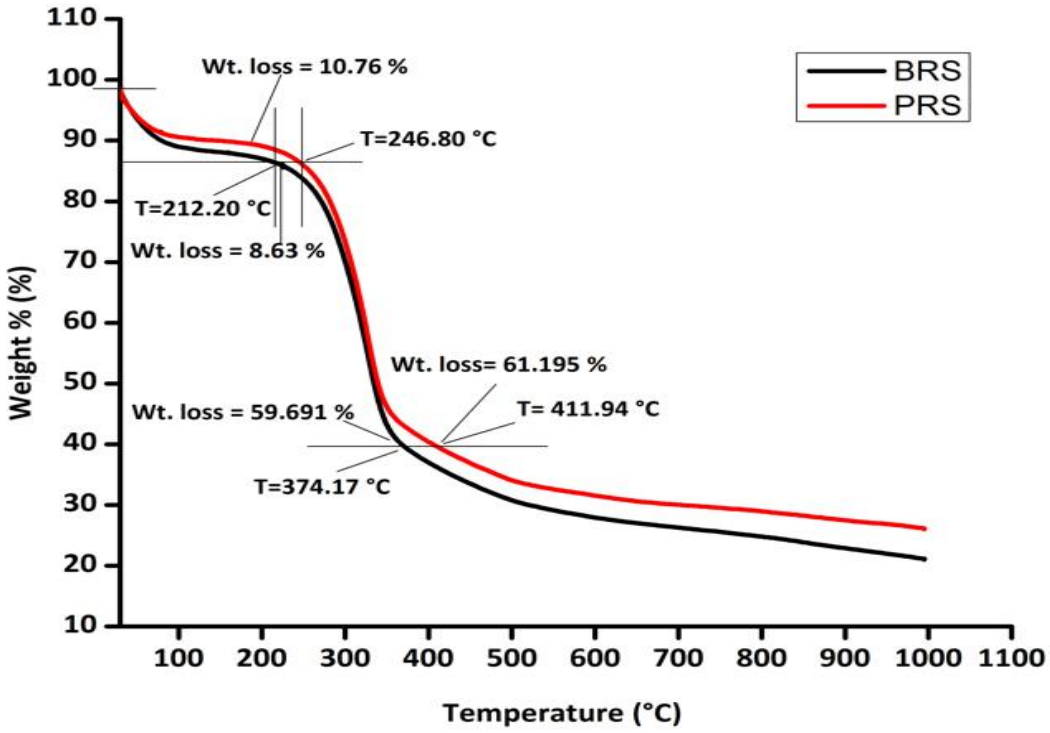

Figure 4.11 Confirmation of thermal stability of rice straw using TGA

4.8 Extraction of cellulose drives from Parmal and Basmati rice straw

4.8.1 Preliminary trials for extraction of cellulose

Figure 4.12 shows the pretreatment and delignification process of cellulose extraction Herein, the pretreatment or delignification process is required to degrade lignin, solubilize the hemicellulose, and decrease the crystallinity structure of cellulose component. The lignin forms a lignin carbohydrate complexes (LCCs) bond associated with carbohydrates. In the rice structure, these bonds are connected by certain chemical bonds such as ester bonds, α-ether bonds, acetyl linkages, and phenyl glycosidic linkages. The alkali treatment can break down these bonds between cellulose, hemicellulose, and lignin by hydrolyzing the ester bonds via organosolv fractionation.

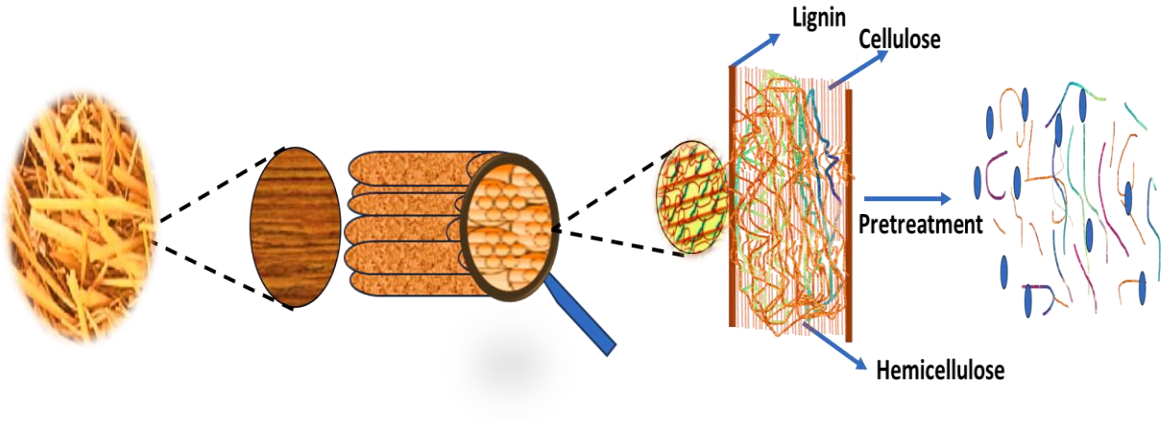

Figure 12: Alkali hydrolysis of lignocellulosic material of rice straw

Table 4.3: Yield of cellulose content in rice straw

Conc. of NaOH (%)	Cellulose Yield (g) (Basmati Rice straw)	Cellulose Yield (%) (Basmati Rice straw)	Cellulose Yield (g) (Parmal Rice straw)	Cellulose Yield (%) (Parmal Rice straw)
1	30.00 ± 3.36^{e}	70.99^{e}	29.33 ± 3.21^{e}	77.27^{f}
2	33.67 ± 1.26^{g}	79.67^{g}	32.00 ± 1.00^{e}	84.30^{h}
3	34.82 ± 3.28^{h}	84.00^{i}	34.00 ± 2.18^{f}	89.57^{i}
4	35.27 ± 1.76^{i}	91.98^{j}	35.33 ± 1.53^{a}	93.07^{j}
5	34.17 ± 2.75^{h}	80.86^{h}	32.17 ± 0.76^{e}	84.75^{h}
6	32.17 ± 2.57^{f}	76.12^{f}	30.00 ± 2.29^{f}	79.03^{g}
7	30.17 ± 3.69^{e}	71.39^{e}	29.00 ± 2.00^{e}	76.40^{e}
8	28.50 ± 2.63^{d}	67.44^{d}	27.50 ± 3.12^{d}	72.44^{d}
10	26.17 ± 2.84^{c}	61.93^{c}	25.83 ± 3.33^{c}	68.05^{c}
12	24.83 ± 1.89^{b}	58.76^{b}	23.33 ± 2.66^{b}	61.46^{b}
16	20.67 ± 2.51^{a}	48.91^{a}	19.33 ± 2.52^{a}	50.92^{a}

[1]Data are represented as mean ±SEM (n=3)$^{a\text{-}f}$ Means within the column with different lowercase superscripts are significantly (P< 0.05), different from each other

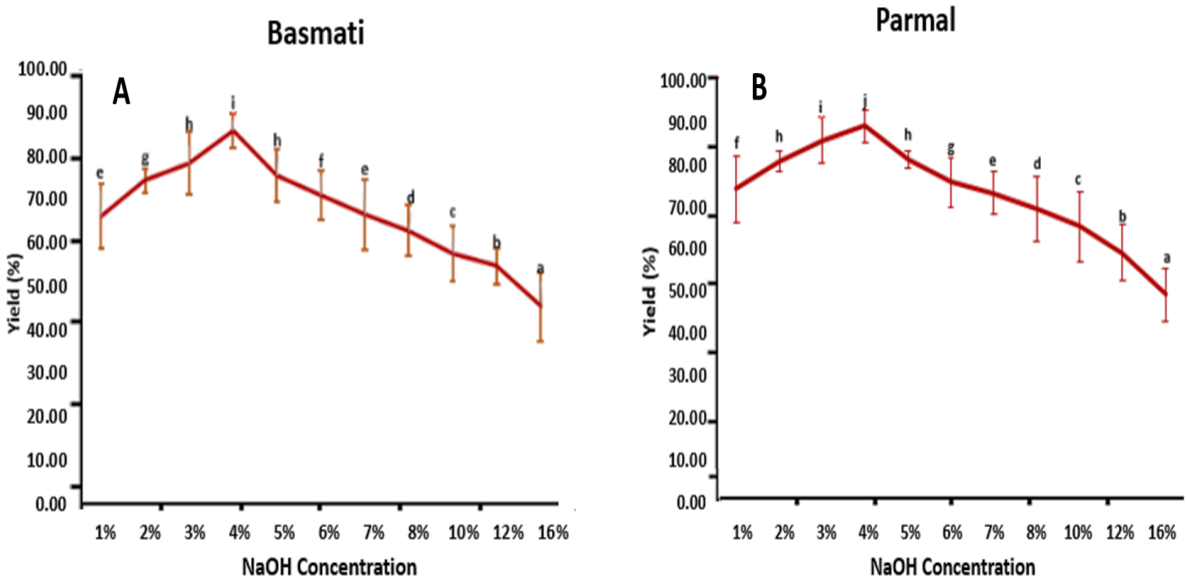

Figure. 4.13 Comparative analysis of cellulose yield of (A) Basmati (B) Parmal rice straw

The delignification process is mainly influenced by the amount of delignifying agent to be used because of the complex nature of the lignin content. The NaOH is used for pretreatment which helps in distruting the lignin structure from rice straw. Because of the complex structure of lignin, it requires intensified activity to break down the complex bonding.. As it can be observed the pretreatment process is essential to degrade lignin, solubilize the hemicellulose, and decrease the crystallinity structure of the cellulose component. Therefore, It can be observed in **Table 4.3** and **Figure 4.13** that the degradation of lignin content is increasing with the initial percentage of NaOH up to 4%. Up to this range, the NaOH was able to reduce the lignin content from rice straw. The higher concentration of NaOH also started to reduce the yield of cellulose. When the percentage of NaOH was further increased by more than 4%, it started to degrade the texture of rice straw as well as the cellulose content. This may be because the alkaline is a cause of swelling of biomass due to which the softening of rice straw. Because of that NaOH acts as a corrosive agent and disrupts the structure of rice straw after the degradation of liging content. As a result, the yield of cellulose was fine within 4% of NaOH.

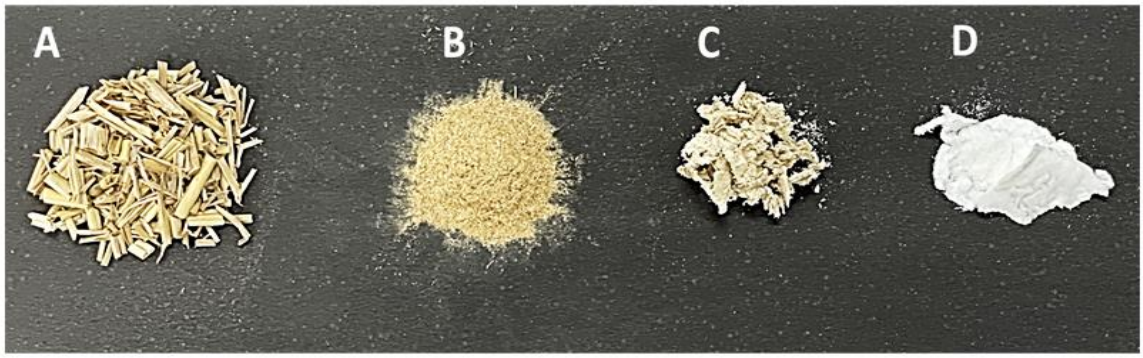

Figure 4.14 Different stages of rice straw during the extraction process (A) Crushed Rice straw (B) Powdered rice straw (C) Alkali hydrolysis rice straw (D) Cellulose content

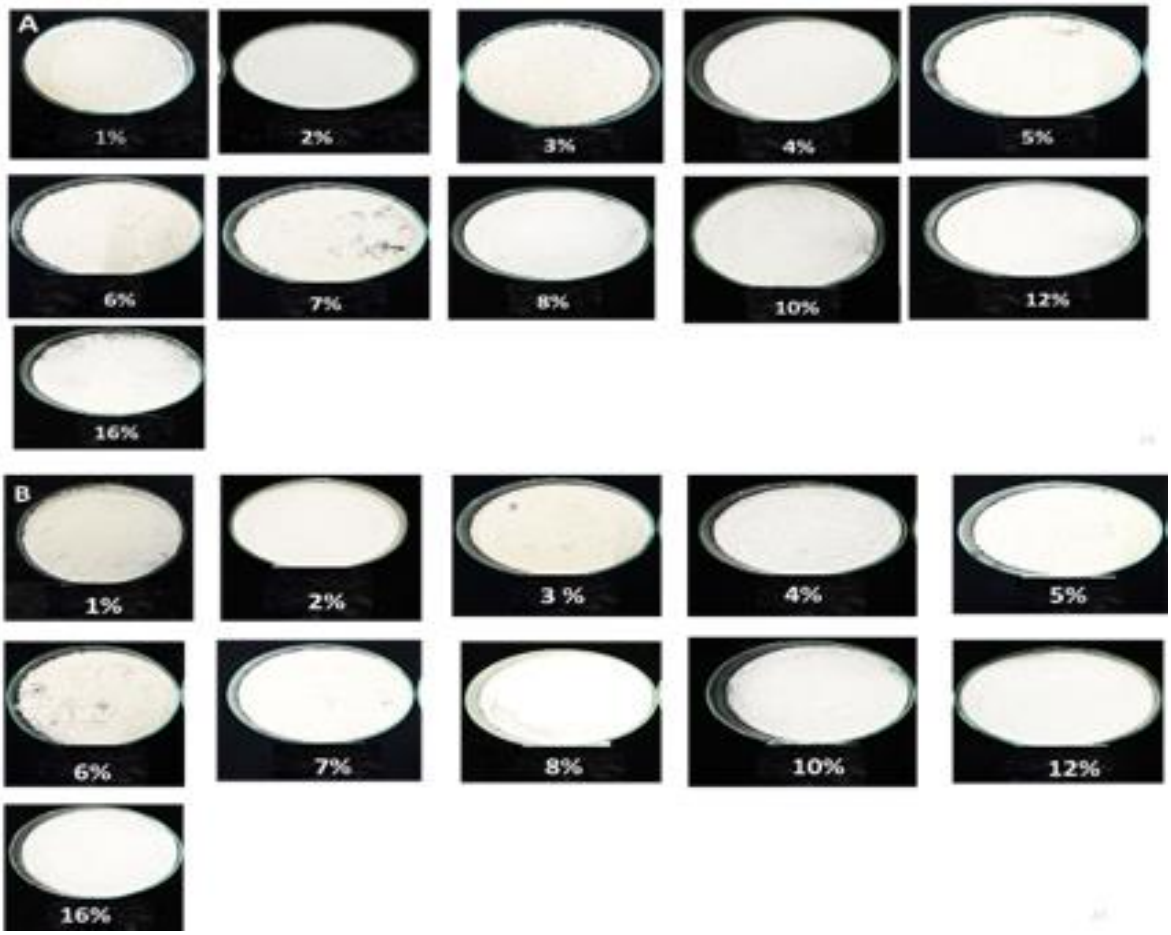

Figure 4.15: Extracted Cellulose Content from (A) Parmal rice straw (B) Basmati rice straw

4.8.2 Purity of alkali hydrolysis sample at different concentrations of NaOH

Table 4.4 Purity of alkali hydrolysis sample at different concentrations

NaOH concentration (%)	Purity of Basmati (%)	Purity of Parmal (%)
1	82.39 ± 1.78^{aA}	84.76 ± 1.56^{aB}
2	89.30 ± 1.78^{bA}	90.78 ±1.78^{bB}
3	95.62 ± 1.98^{cA}	96.83 ± 1.87^{cB}
4	98.19 ± 1.34^{dA}	98.61 ± 1.29^{dA}
5	98.36 ± 1.45^{dA}	98.77 ± 1.67^{dA}
6	98.55 ± 2.35^{dA}	98.93 ± 1.56^{dA}
7	98.77 ± 1.35^{dA}	99.23 ± 1.23^{dA}
8	98.98 ± 1.76^{dA}	99.37± 1.47^{dA}
10	99.32 ± 1.98^{dA}	99.57 ± 1.56^{dA}
12	99.69 ± 1.45^{dA}	99.72 ± 1.34^{dA}
16	99.82 ± 0156^{dA}	99.93 ± 1.33^{dA}

[1]Data are represented as mean ±SEM (n=3) $^{a-d}$ Means within the column with different lowercase superscripts are significantly (P< 0.05), different from each other

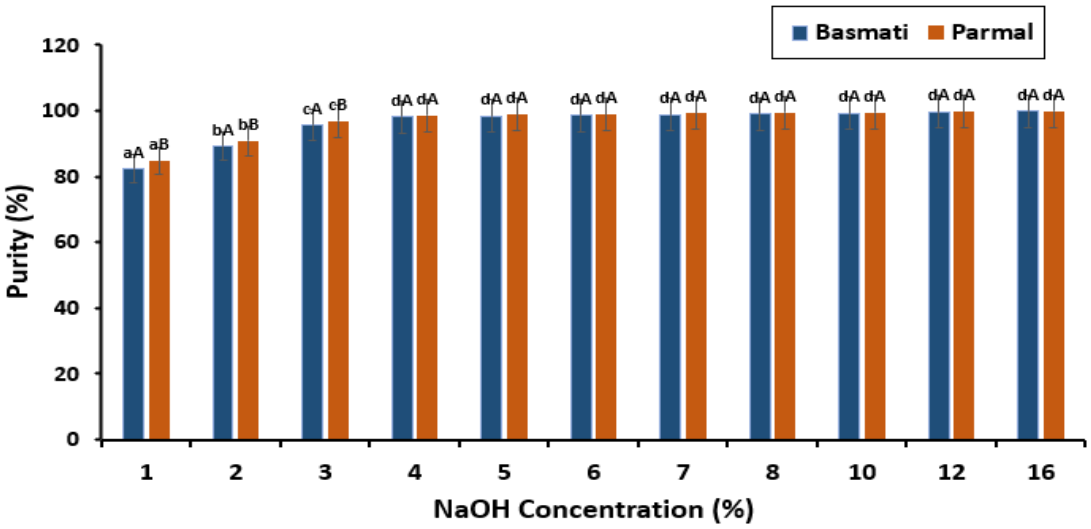

Figure 4.16 Purity of alkali hydrolysis sample at different concentrations

Figure 4.16 shows the purity of cellulose extracted from Basmati and Parmal rice straw at various concentrations of sodium hydroxide (NaOH). The data shows that as the NaOH concentration increases, the purity of cellulose also increases for both types of rice straw. For Basmati rice straw, the purity starts at 82.39 ± 1.78% with 1% NaOH and reaches a maximum of 99.82 ± 0.15% at 16% NaOH. Similarly, for Parmal rice straw, the purity starts at 84.76 ± 1.56% with 1% NaOH and reaches 99.93 ± 1.33% with 16% NaOH. Moreover, at 1% NaOH, the purity of Basmati (82.39 ± 1.78%) is significantly ($P< 0.05$) different from that of Parmal (84.76 ± 1.56%). As the NaOH concentration increases, both types of rice straw achieve their highest purity levels at concentrations of 10%, 12%, and 16%, with purity levels above 99%.

This trend indicates that increasing the NaOH concentration generally leads to higher cellulose purity. both types of rice straw achieve very similar high purity levels, indicating effective extraction at these concentrations. Moreover, higher concentrations of NaOH generally lead to higher cellulose purity for both Basmati and Parmal rice straw. This trend is consistent across both types, with optimal purity levels being achieved at higher NaOH concentrations. However, a 4% NaOH concentration was selected for further analysis because it provides a higher cellulose yield along with a good percentage of purity. This data provides valuable insight into the efficiency of NaOH in purifying cellulose from different rice straws and highlights the importance of selecting the appropriate concentration for optimal results.

4.8.3 Optimization of cellulose yield using Response surface methodology

The cellulose yield from basmati and Parmal rice straws was optimized by a selected 3^3 factorial Box-Behnken design using Response surface methodology. The experimental responses of 17 runs and the design matrix are shown in **Table 4.5 and Table 4.6.** Here A, B, and C are the relevant independent variables for sodium hydroxide (NaOH) concentration, reaction time, and reaction temperature were tested at three levels which affects the cellulose yield. The quadratic model was used to show the relationship between

experimental variables and response values by design experts. As a result, the yield was found to range from 16.5% to 36% for Basmati and 14.5 % to 33.5 %, for Parmal with standard deviations ranging from 0.69% to 6.06% for Basmati and 69% to 6.04 for Parmal. The responses of independent variables and yield were presented by the quadratic model in terms of coded factors by the following second-order polynomial (Mahesha et al. 2022). Here positive sign represented a synergistic impact, and a negative sign showed an antagonistic one.

Cellulose yield for Basmati (X)= 33.60 +1.19A -2.44B -2.38C -1.63AB -0.50AC -2.25BC $-6.24A^2$ $-2.99B^2$ $-6.86C^2$ ……. (1)

Cellulose yield for Parmal (Y) = 31.60 +1.19A -2.44B -2.37C -1.63AB -0.50AC -2.25BC $-6.24A^2$ $-2.99B^2$ $-6.86C^2$…….(2)

X and Y represent the yield of Basmati and Parmal cellulose. The statistical analysis in the current delignification study was conducted using ANOVA to assess the influence of different parameters on the validation of the regression model.

Tables 4.5 & 4.6 depict the ANOVA (analysis of variance) for the RSM (response surface method), which describes the accuracy of the developed model. The significance of the model was determined in terms of F and P, while accuracy was evaluated in its regression analysis R^2 and lack of fit. The optimum conditions and response surfaces for the cellulose extraction were obtained through this model. The time, temperature of the reaction, and concentration of NaOH have a significant effect on the responses as indicated by the P value which is less than 0.05.

Here the F values 37.31 and 53.45 of the model indicate that the model is significant ($P<0.05$) and the probability of this value being less than 0.01% due to experimental noise. The P value of the model is 0.0001 which is smaller than 0.05, indicating that the results of the analysis are statistically significant. Furthermore, the determination coefficient (R2) for the model is 0.9798 for Basmati and 0.9857 for Parmal which is close to 1, with non-significant ($P> 0.05$) lack of fit approximately 0.8244 and 7191 for Basmati and Parmal respectively which showed that the quadratic model is valid for these studies. Whereas, the value of adjusted R^2 (a measure of fit) is 0.9538 and 0.9672 for both the models determined

by the model. The difference between adj-R2 and decision coefficient R2 is logically acceptable by the model (Derakhshan et al., 2018; Shen et al., 2017).

Moreover, both values are higher than 0.80, indicating that the model represented the experimental data with good efficiency (Satapathy et al., 2014). Therefore, this analysis indicates that the regression model shows an accurate relationship between the independent variables and the responses within the range of experimental variables (Borges et al., 2011; Li et al., 2011). Hence, the above analysis confirms that the RSM is appropriate for the optimization of preparation conditions in the present work.

Table 4.5 Variance analysis of the quadratic response surface model for Basmati cellulose

Source	Sum of squares	Degree of freedom	Mean squares	F	p-vale Prob > F
Model	576.35	9	64.04	37.71	< 0.0001
A	11.28	1	11.28	6.64	0.0366
B	47.53	1	47.53	27.99	0.0011
C	45.13	1	45.13	26.57	0.0013
AB	10.56	1	10.56	6.22	0.0414
AC	1.00	1	1.00	0.59	0.4680
BC	20.25	1	20.25	11.92	0.0106
A^2	163.82	1	163.82	96.46	< 0.0001
B^2	37.58	1	37.58	22.13	0.0022
C^2	198.29	1	198.29	116.76	< 0.0001
Residual	11.89	7	1.70		< 0.0001
Lack of Fit	2.19	3	0.73	0.30	0.8244
Pure Error	9.70	4	2.43		
Other statistical parameters					
Std.Dev. 1.30			R-Squared 0.9798		
Mean 26.03			AdjRSquared 0.9538		
C.V.% 5.01			Pred R-Squared 0.9147		
PRESS 50.16			Adeq Precision 16.921		

Here, A, B, C, AB, AC, BC, A^2, $B^{2,}$ and C^2 are reported as an independent variable in terms of concentration of NaOH, temperature, and time of the reaction respectively. Whereas the

linear terms (A, B, C), the quadratic terms (A^2, B^2, C^2), and the interaction terms (AB) were statistically significant (P<0.05), indicating that the yield of cellulose significantly affected by the three variables. While the interaction terms (AC) show a nonsignificant (P> 0.05) effect on the yield of cellulose. This may be the result of the antagonistic effect between concentration and time in the preparation process of cellulose using alkaline treatment.

Table 4.6 Variance analysis of the quadratic response surface model for Parmal cellulose

Source	Sum of squares	Degree of freedom	Mean squares	F	p-value Prob > F
Model	576.35	9	64.04	53.45	< 0.0001
A	11.28	1	11.28	9.42	0.0181
B	47.53	1	47.53	39.67	0.0004
C	45.13	1	45.13	37.66	0.0005
AB	10.56	1	10.56	8.82	0.0208
AC	1.00	1	1.00	0.83	0.3913
BC	20.25	1	20.25	16.90	0.0045
A^2	163.82	1	163.82	136.72	< 0.0001
B^2	37.58	1	37.58	31.36	0.0008
C^2	198.29	1	198.29	165.49	< 0.0001
Residual	8.39	7	1.20		
Lack of Fit	2.19	3	0.73	0.47	0.7191
Pure Error	6.20	4	1.55		
	Other statistical parameters				
	Std.Dev. 1.09		R-Squared 0.9857		
	Mean 24.03		AdjRSquared 0.9672		
	C.V.% 4.56		Pred R-Squared 0.9236		
	PRESS 44.69		AdeqPrecision 20.145		

4.8.3.1 Effect of NaOH on the cellulose yield

The pretreatment process is essential to degrade lignin, solubilize the hemicellulose, and decrease the crystallinity structure of the cellulose component (Sun et al. 2022). Here the NaOH is used for pretreatment which helps in distruting the lignin structure from rice

straw. Because of the complex structure of lignin, it requires intensified activity to break down the complex bonding (Peng et al. 2023). Therefore, in this work, the rice straw was treated with different concentrations of NaOH. It is shown in **Figure 4.17A** that the degradation of lignin content is increasing with the initial percentage of NaOH up to 4%. Up to this range, the NaOH was able to reduce the lignin content from rice straw. As the higher concentration of NaOH also started to reduce the yield of cellulose. When the percentage of NaOH was further increased by more than 4%, it started to degrade the texture of rice straw as well as the cellulose content. This may be because the alkaline is the cause of swelling of biomass due to which the softening of rice straw. Because of that NaOH acts as a corrosive agent and disrupts the structure of rice straw after degradation of liging content. As a result, the yield of cellulose was fine within 4% of NaOH.

4.8.3.2 Effect of temperature on cellulose yield

The temperature has an essential role in the delignification processes of rice straw. This might be due to temperature accelerating the reaction of chemicals during processing more quickly as it rises. As illustrated by **Figure 4.17B** the yield of Parmal rice straw cellulose is steadily increasing along with temperature rise from 90℃ to 120 ℃. From 90 °C to 120 °C, the yield of cellulose rises consistently along with the temperature. (Thakur et al. 2020). This was clarified by the fact that the activation energy decreases with rising temperature. Which will simultaneously increase the yield of cellulose from both varieties of rice straw while reducing the total processing time spent. Although the temperature is an important factor for the activation of chemical energy, when the temperature was raised above 110 °C, a decreasing trend was seen in cellulose yield. This may be due to the higher temperature of the rice structure along with another component also damaged during processing. As a result, 107 °C was the optimum temperature for a good yield of cellulose. As a result, the ideal temperature for an excellent cellulose yield was observed at 107 °C for both varieties of cellulose.

4.8.3.3 Effect of time on cellulose yield

Apart from concentration and temperature, the reaction time is also an important variable as a delignifying agent that breaks off complex bonds of lignocellulosic material. and its removal of the lignin content from rice straw during the experiment time. **Figure 4.17 C** demonstrated that the amount of Parmal rice straw cellulose slightly increased as contact time expanded. This might be because the NaOH would have the necessary time to break more hydrogen bonds with a gradual increase in contact duration. This might be because as contact time gradually increases, the delignifying agent would have the efficiency to break down the complex bond from rice straw at a certain time without altering the concentration of NaOH (Dhara et al. 2023). It also observed that time affected on yield of cellulose initially and increased moderately after that the yield was constant up to a given period. In this work, it was found that the maximum yield of both varieties of cellulose was obtained at 116.63 and 116.63 min of reaction time beyond which there was no significant increase in yield.

Statistical analysis of the independent variables viz., reaction temperature, time, and NaOH concentration over cellulose yield of rice straw are tabulated in Tables 4.5 and 4.6 where it can be observed that they contribute a significant involvement during the optimization process. Therefore, based on the above findings, the appropriate ranges were taken into account for the process optimization of cellulose yield of rice straws using response surface methodology (RSM).

4.8.3.4 Optimization of preparation conditions

The three-dimensional response surface was created according to eq. (1) and (2) to find the ideal preparation conditions and evaluate the impact of three independent variables on the yield of Basmati rice straw cellulose .The response surface model was used to contour plots to predict the results using a 3-D plane projection of the reaction surface. The 3-D response surface plots typically display the combined impact of two variables on response while keeping other variables at level zero (Kadier et al. 2022). The nature and size of the interaction between several factors are depicted by the contour plot forms. The circular shape of the plot indicates that there a very little interaction between the variables whereas

an elliptical plot indicates there is a significant ($P<0.05$) interaction between the variables. All the contour plots are in elliptical shapes.

Figure 4.18 represents the response surface plots a pairwise mixture of three variables which illustrates the impacts of a combination of variables on the yield of Basmati rice straw cellulose. These graphs are plotted by keeping one variable as a constant as its center point. These plots give a visual representation of how the interaction of any two variables influences the yield of cellulose.

Figure 4.18 A, represents the effect of sodium hydroxide concentration and reaction temperature on cellulose yield with maintained constant time at 120 min. Herein, the yield of cellulose gradually increases with increasing concentration of NaOH from 3% to 5%. Although, the temperature was initially increasing at a particular range from 90 to 107 then it started to decrease with increasing range from 108-150 °C. Thus, the plotted graph presents a significant ($P<0.05$) interaction between reaction temperature and NaOH obtained by the partial elliptical contour plot.

Figure 4.18 B reveals that when reaction time extends from 90 min to 150 min at the same NaOH concentration, the yield of cellulose moderately increases first and then slightly decreases. However, it can be observed that the yield gradually increases as NaOH concentration increases from 3% to 5% at the same reaction time. These observations reveal that there is a non-significant ($P>0.05$) interaction between reaction time and NaOH concentrations and shows a relatively minor interaction between them.

Figure 4.18 C a clear peak of the plot reveals that the yield of cellulose first increases very sharply and then decreases with increasing the temperature from 90 min to 150 min. But along with the increasing time, the yield of cellulose increases moderately which indicates that there is not much effect of time on the yield of cellulose. At the same time, the contour plot is close to the elliptical shape, which suggests a significant ($P<0.05$) interaction between reaction temperature and time it indicates a relatively mild interaction between them.

Overall, it can be demonstrated that all three factors, including temperature, concentration, and time have a significant ($P<0.05$) impact on the yield of cellulose. The optimized

condition was identified using the center point of the contour plots. The average yield of cellulose was estimated at optimized condition variables, which was at 4.15 % NaOH, 116 min reaction time, and 107°C reaction temperature. Moreover, the optimized condition of variables was obtained at 4.15 % NaOH, 116 min reaction time, and 107 °C reaction temperature. These optimal conditions give the maximum yield of cellulose i.e. 78.12 % (Basmati) and 85.14% (Parmal) were predicted by the response surface model.

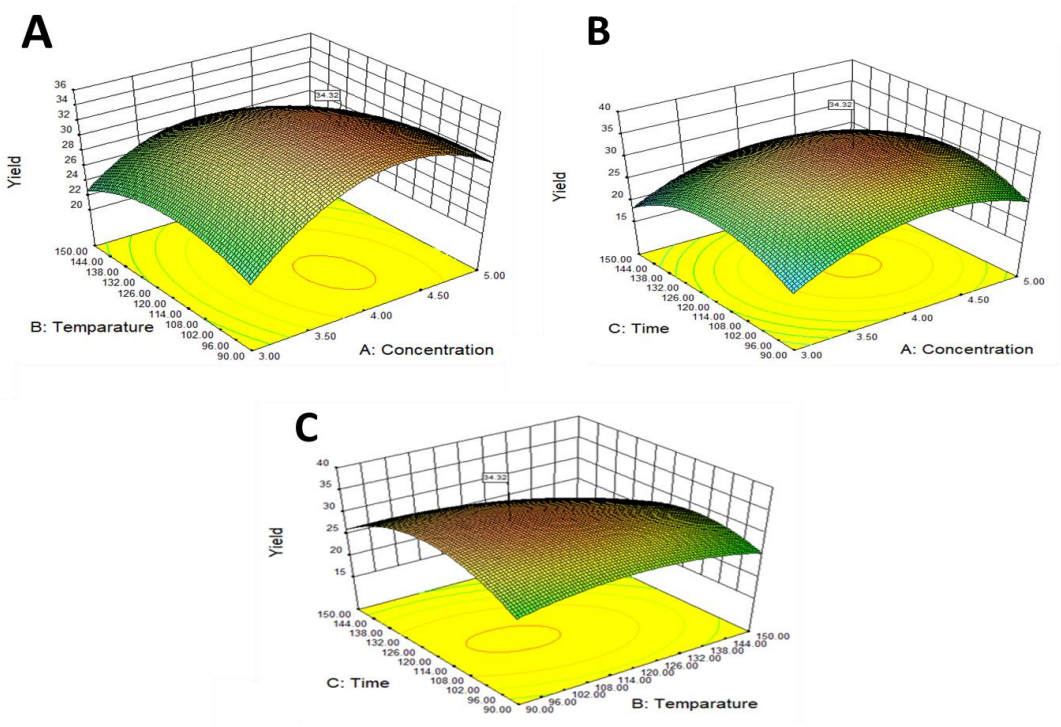

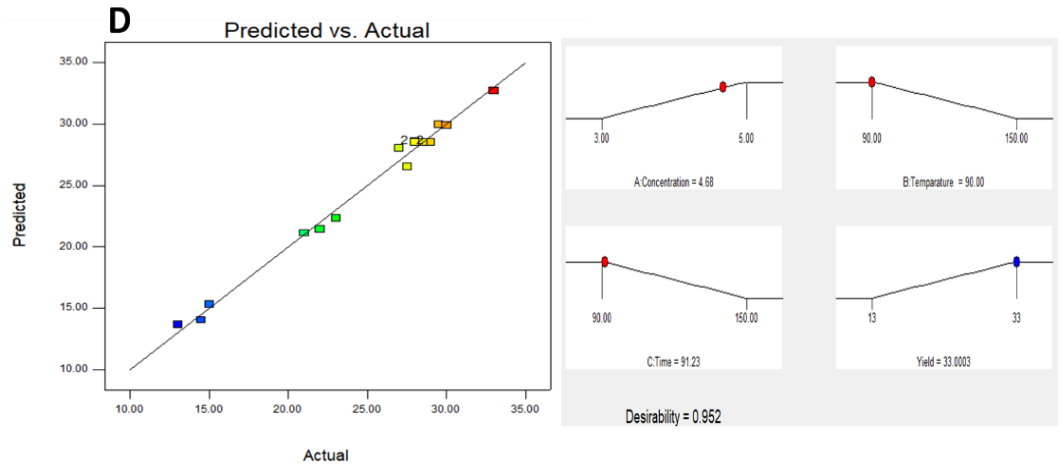

Figure 4.17 PRS Response surface and contour plots of (A) Reaction temperature and concentration (B) Reaction time and concentration (C) Reaction time and reaction temperature (D) Predicted vs actual value

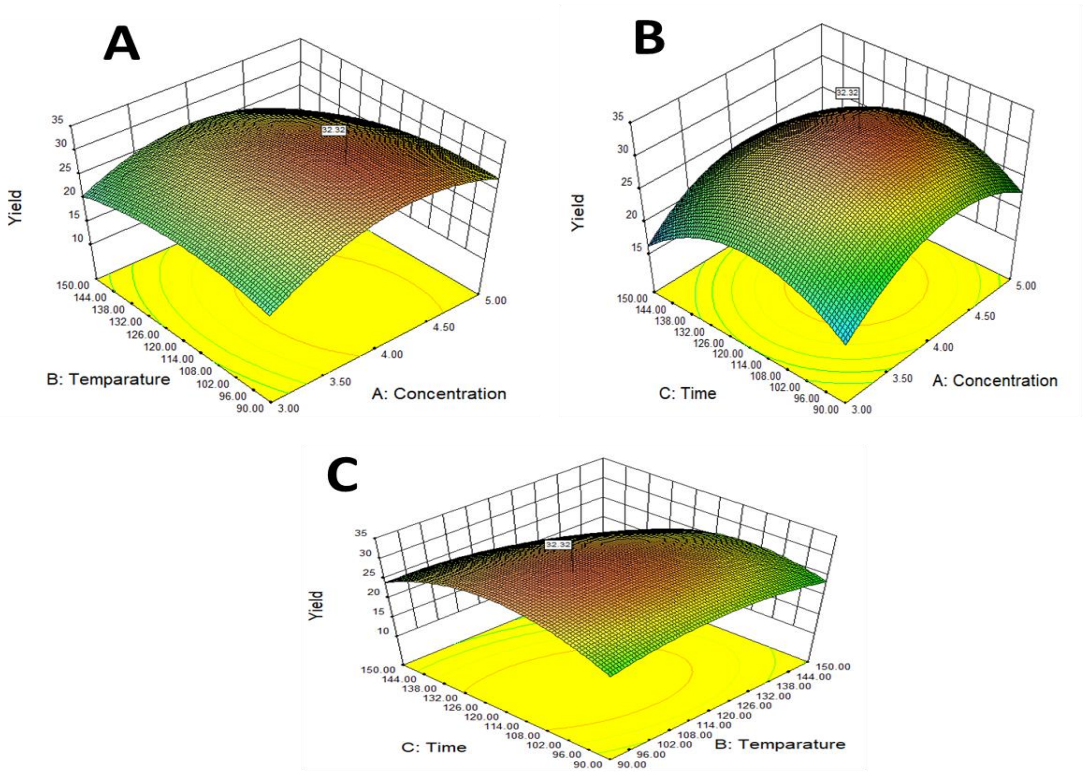

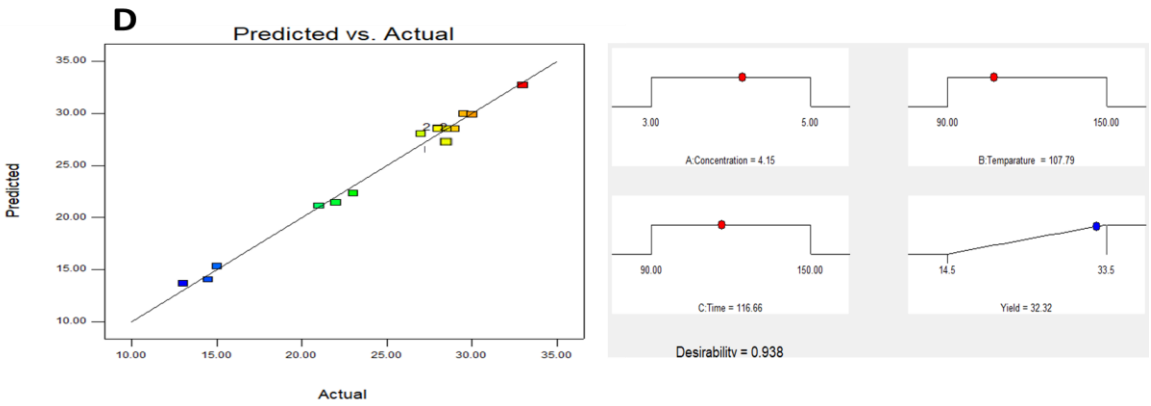

Figure 4.18 BRS Response surface and contour plots of (A) Reaction temperature and concentration (B) Reaction time and concentration (C) Reaction time and reaction temperature (D) Predicted vs actual value

4.9 Characterization of pretreated and cellulose (Parmal and Basmati)

4.9.1 Impact of NaOH on functional groups of pretreated and cellulose rice straw

Figure 4.19 shows the conversion of pretreated rice straw (PTBRS and PTPRS) into cellulose derived from these straws (BRSC and PRSC). Herein the pretreatment processes, aimed at enhancing cellulose accessibility by removing lignin and hemicellulose, lead to noticeable changes in the FTIR spectra. The shift towards lower wavenumbers in the O-H stretching vibrations (3316.01 cm^{-1} for PTBRS and 3312.11 cm^{-1} for PTPRS) suggests modifications in hydrogen bonding, likely due to the structural alteration of cellulose. (G. Chaudhary et al. 2024). A notable reduction in the aliphatic C-H stretch (2890.27 cm^{-1} for PTBRS and 2889.25 cm^{-1} for PTPRS) and the emergence of new bands around 1644.39 cm^{-1} and 1642.47 cm^{-1} correspond to increased water content, indicating a more hydrophilic cellulose structure post-pretreatment (Najafvand et al. 2024) are typically assigned to C=C stretching in aromatic rings, indicating the presence of residual moisture or changes in the lignin content after alkaline treatment.

The peaks near 1369.88 cm^{-1} (BRS), and 1365.87 cm^{-1} (PRS) are attributed to C-H bending. A peak at 1029.62 cm^{-1} (BRS) and 1031.65 cm^{-1} (PRS) In the region associated with C-O stretching bond. These peaks suggest alterations in the carbohydrate components,

possibly indicating a change in the cellulose and hemicellulose structures, such as a breakdown of the glycosidic linkages or a change in crystallinity (Anari, Soltanizadeh, and Fathi 2024). Finally, the peaks below 600 cm^{-1}, with Basmati at 581.53 cm^{-1} and Parmal at 578.51 cm^{-1}, likely correspond to Si-O-Si bending vibrations, indicating silica content, which may be slightly affected by the alkaline treatment. The minor shift suggests a small change in the silica structure or content between the two varieties (Ma et al. 2024).

The extraction of cellulose from BRS and PRS results in simplification of the FTIR spectra, with fewer peaks indicating the removal of non-cellulosic components. The O-H stretching vibration peaks (3334.80 cm^{-1} for BRSC and 3326.82 cm^{-1} for PRSC) remain prominent, underscoring the preservation of the cellulose structure. The appearance of an unusual peak at 2096.25 cm^{-1} in both cellulose samples could be attributed to specific treatment conditions or residual processing chemicals. The bands at 1638.68 cm^{-1} (BRSC) and 1646.66 cm^{-1} (PRSC) indicate the presence of bound water, highlighting the hygroscopic nature of cellulose. Enhanced peak intensity at 1403.10 cm^{-1} suggests an increase in cellulose crystallinity (Li and Ma 2023). Moreover, the changes in the fingerprint region (<1000 cm^{-1}), with new peaks at 554.24 cm^{-1} in BRSC and 532.68 cm^{-1} in PRSC, indicating alterations in chemical structure or removal of non-cellulosic components, leading to increased cellulose crystallinity.

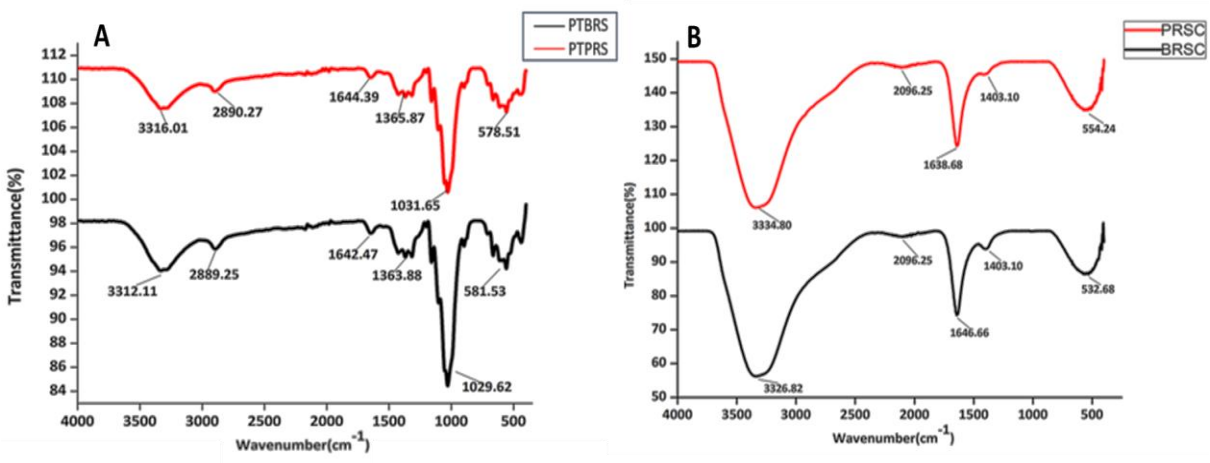

Figure 4.19 Impact of NaOH on functional groups of (A) pretreated rice straw and (B) Basmati and Parmal cellulose

The FTIR analysis underscores the transformation that occurs from a complex lignocellulosic matrix to a more refined cellulose product. This transformation is evidenced by the shifts in key spectral peaks, particularly the increased O-H stretching vibrations indicating a higher hydroxyl group availability in cellulose, pointing to the removal of hemicellulose and lignin components. Additionally, the changes in the fingerprint region and the emergence of new peaks in the cellulose products highlight the successful elimination of non-cellulosic materials and the possible enhancement of cellulose crystallinity (Arantzazu et al. 2022) (Valdés et al. 2022). The comparative analysis across the different stages of cellulose production reveals a progressive transformation of the material's chemical structure. Initially, the FTIR spectra of pretreatment processes lead to a notable simplification of the spectra, indicating the effective removal of lignin and hemicellulose, which is further evidenced by changes in the O-H stretching and aliphatic C-H stretching vibrations.

4.9.2 Impact of NaOH on surface morphology of pretreated and cellulose rice straw

The SEM images as shown in **Figure 4.20 A, B, C & D** offer a detailed comparative analysis of the different stages in the conversion of two rice straw varieties including Pretreated basmati rice straw (BRS) and Parmal rice straw (PRS) into cellulose. Herein, a detailed morphological analysis of each stage such as Pretreated Basmati rice straw (PTBRS) and Parmal rice straw (PTPRS) into cellulose (BRSC and PRSC): Herein, the pretreated Basmati rice straw (PTBRS) and Pretreated Parmal rice straw (PTPRS) display a change in surface morphology indicative of the removal of non-cellulosic materials such as lignin and hemicellulose. The surface appears more fibrillar and less covered in protrusions, suggesting that the pretreatment process has started to break down the complex structure of the straw. (Gupta et al. 2023).

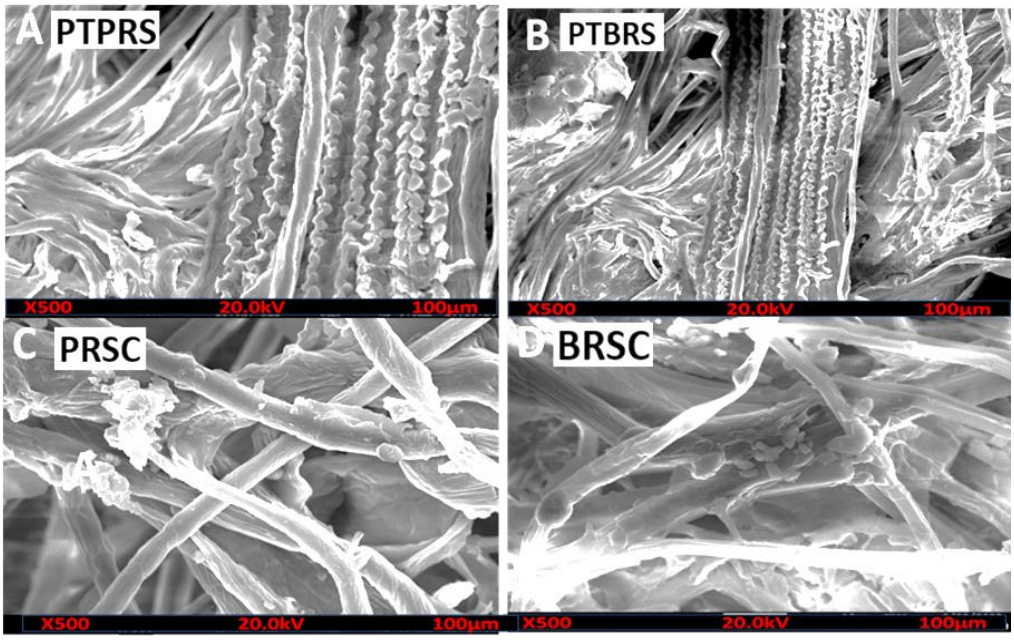

Figure 4.20 Impact of NaOH on Surface morphology of (A) Pretreated Parmal rice straw (B) Pretreated Basmati rice straw (C) Parmal cellulose and (D) Basmati cellulose

The cellulose from BRSC and PRSC exhibits a further refined structure, with long and distinct fibers visible. These images indicate a successful extraction of cellulose, removing most of the matrix materials that embed the cellulose fibers in the raw and pretreated straw (Bi et al. 2023).These fibers are thinner than in the cellulose stage, demonstrating the effective conversion into nano-scale dimensions. In comparing the stages, we can see a clear progression from rough, irregular material to a highly refined fibrous network. The raw straw images reveal a natural, unprocessed surface; pretreatment cleans up the material, which is evident in the removal of extraneous surface features; the cellulose stage shows the extraction of pure cellulose, with clearly defined fibers.

4.9.3 Impact of NaOH on energy-dispersive X-ray of pretreated and cellulose rice straw

All images of Energy-dispersive X-ray spectroscopy (EDX) shown in **Figure 4.21 A, B, C & D** are analyzed at various stages of rice straw processing into cellulose for two different types of rice straw: BRS and PRS. EDX serves as a microanalytical method that, when paired with scanning electron microscopy (SEM), determines the elemental composition

of the samples. After pretreatment, the spectra show changes in elemental composition. Notably, there is a new peak for sodium (Na), which could be due to the use of sodium hydroxide or other alkali in the pretreatment process (N. Kumar et al. 2023).

This process aims to remove lignin and hemicellulose, and it appears to reduce the relative content of Si, indicating the partial removal of silica (Shah et al. 2023). The cellulose spectra show a high presence of carbon and oxygen, which are the primary constituents of cellulose. The decrease in other elements compared to the raw and pretreated straw suggests that the extraction process has been effective in isolating cellulose (Ramos et al. 2023). There is a notable reduction in Si content, and the K peak has disappeared, indicating the removal of non-cellulosic components. From the raw material to the final nanocellulose product, there is a clear transition seen in the EDX spectra. Pretreatment introduces sodium, indicating chemical treatment, and begins to reduce other elements like silicon. The cellulose stage shows further refinement, with a cleaner spectrum dominated by carbon and oxygen (Javanmard, Wan Daud, and Patah 2023).

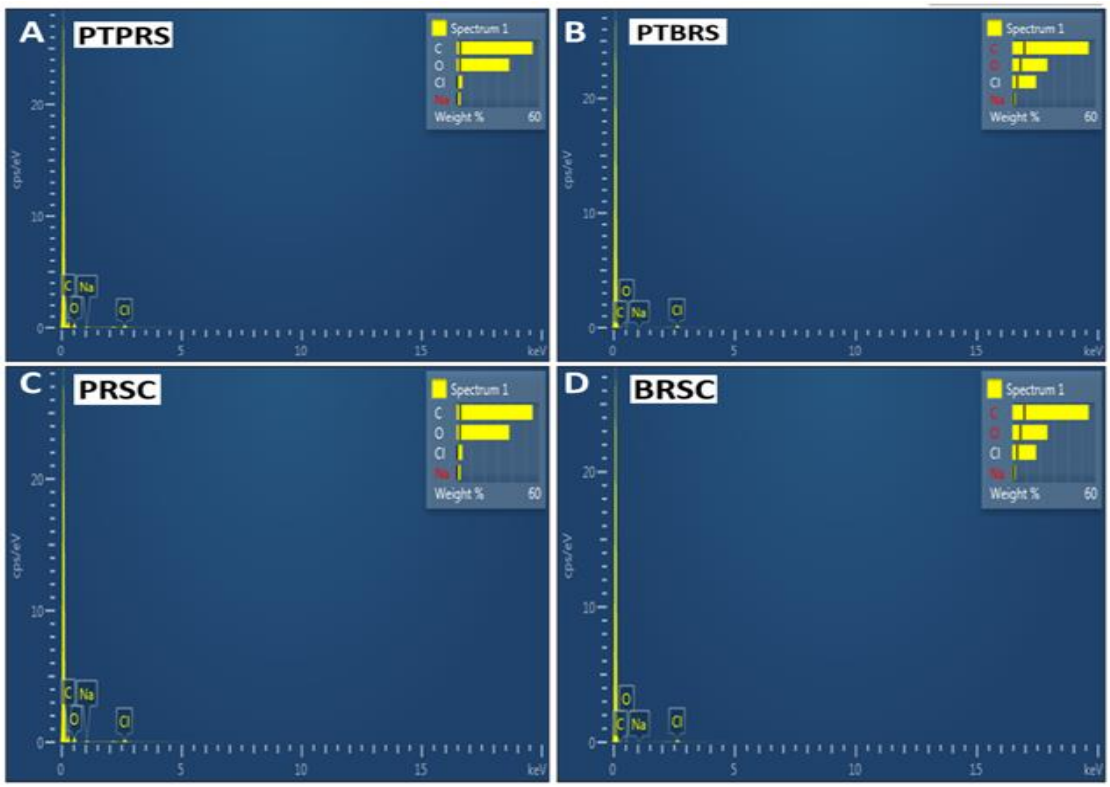

Figure 4.21 Impact of NaOH on energy-dispersive X-ray of (A) pretreated Parmal rice straw (B) Pretreated Basmati rice straw (C) Parmal cellulose and (D) Basmati cellulose

4.9.4 Impact of NaOH on X-ray diffraction analysis of pretreated and cellulose rice straw

Figure 4.22 A & B depicted the crystalline peaks appearing as sharp, well-defined peaks with higher intensities. These peaks indicate regions where the pretreated chains are highly ordered and aligned, these peaks indicate regions where the cellulose chains are less ordered and more randomly oriented. The peaks of PTBRS and PTPRS at 16.5º, 22.5 º, and 34.5◦ at 2Θ show the change in intensity of the peaks in comparison to BRS and PRS. These peaks are characteristic of the cellulose structure and are associated with the crystalline regions of cellulose. The treatment with alkali indicates that it destroyed only the non-fibrous components such as hemicellulose, lignin, and other amorphous components that are not fibrous, while maintaining the integrity of the cellulose structure intact (Ren et al. 2023).

The diffraction patterns of PTBRS and PTPRS indicate an increase in crystallinity or alteration in the crystal structure due to the removal of non-cellulosic components. The processed cellulose, labeled BRSC and PRSC, would exhibit a cleaner and possibly more intense peak at around 15°, 16°, 22.5° and 34.4° due to the removal of amorphous regions. This indicates that the cellulose exhibits more pronounced and distinct peaks, especially a sharp peak at approximately 22.5° at 2Ɵ after alkaline pretreatment. Where both peaks are more intense and more narrowly absorbed, emphasizing how the purification process effectively enhances the crystalline structure of cellulose over the comparatively heterogeneous and amorphous composition of rice straw (Norfarhana et al. 2023). This observation is attributed to the elimination of lignin and hemicellulose leading to a notable enhancement in crystallinity and the defining features of pure cellulose.

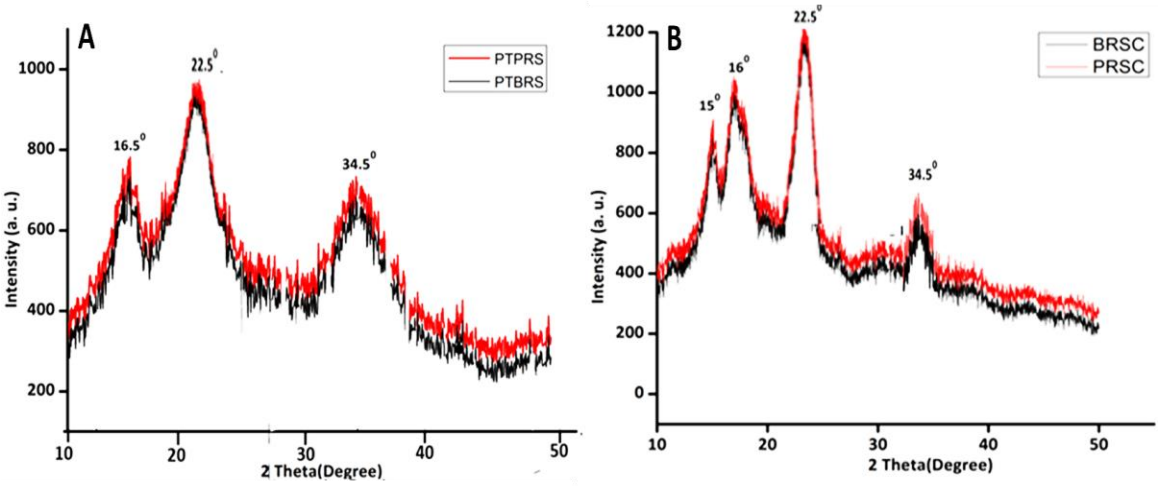

Figure 4.22 Impact of NaOH on X-ray diffraction analysis of (A) pretreated rice straw and (B) Basmati and Parmal cellulose

4.9.5 Impact of NaOH on the thermal stability of pretreated and cellulose rice straw

As shown in **Figure 4.23 A & B** the initial degradation step (dehydration) for PTPRS and PTBRS straw occurred at 30.13 to 246.80 °C and 30.13 to 212.20 °C with the weight loss of 10.76% and 8.63% respectively. The loss is gradual and minimal due to, the removal of water molecules which is low in molecular weight and loosely bounded on the surface of the samples.

$(C_6H_{10}O_5)_{n.}\ 2H_2O \rightarrow (C_6H_{10}O_5)_{n} + 2H_2O$ …. (dehydration).

A Thermogravimetric Analysis (TGA) graph for pretreated rice straw will give an insight into the thermal stability and composition of the rice straw after it has undergone some form of pretreatment. The initial weight loss at lower temperatures is usually due to the evaporation of water. Pretreatments often increase the ability to absorb moisture of rice straw, so this initial loss may be more pronounced compared to untreated straw (Ceaser and Chimphango 2021).In this range, volatiles other than water may start to evolve. For instance, if the pretreatment has reduced the content of hemicellulose, which typically starts to decompose at around 200°C, the weight loss associated with this component may be less compared to untreated straw. This is the main degradation phase, where the cellulose content in the rice straw decomposes, releasing volatiles.

The intensity and sharpness of the peak in this region can indicate the relative purity and amount of cellulose left after pretreatment. A slower rate of weight loss in this region suggests the conversion of organic materials into char (Dacierno, Michal, and Maclachlan 2023). The extent of this phase will depend on how much residual lignin and cellulose are left after pretreatment. beyond which it exhibits a rapid decline in mass due to the decomposition of cellulose chains. The decline tapers off as it approaches high temperatures, with only a small fraction of the mass remaining as char. Pretreatments can influence the mineral content or ash residue in the straw. For example, acid or alkali treatments may remove inorganic components or alter their composition. In general, pretreatments modify the composition of rice straw, affecting its thermal behavior as observed in the TGA graph. The exact changes in the TGA curve will depend on the nature of the pretreatment (Yaacob, Ismail, and Ting 2023). For instance, an acid-treated straw might show a lower onset of degradation temperature for hemicellulose, while an alkali-treated sample might show a reduction in lignin-related weight loss at higher temperatures. Additionally, any added components or chemicals during the pretreatment process could be reflected in the thermal degradation pattern.

For both BRSC and PRSC, there is a slight initial weight loss of 10.16% and 8.16% at 207.14 ℃ respectively. This typically represents the evaporation of water content in the samples.

The 2nd degradation rate was attributed to approximately 541.14 ℃ and 543.14 ℃ with 75.16 % and 67.16% weight loss for both BRSC and PRSC respectively. Where the most weight loss occurs, often appearing as a steep slope on the graph. Pure cellulose has a more straightforward thermal degradation profile with one major weight loss step because of a single compound with a more uniform structure. Cellulose degradation begins, breaking down the glycosidic bonds of the cellulose chains. This process leads to the formation of volatile compounds such as levoglucosan, as well as a variety of gases like carbon monoxide and carbon dioxide (Padmanathan et al. 2024).

At the end of the TGA run, for both samples are typically above 600°C, the only mass that remains is the residual ash, which is very low for pure cellulose since it contains minimal inorganic content. The percentage of this residual mass in comparison to the initial mass of the sample gives an estimate of the inorganic content or the non-volatile matter that could not be decomposed or volatilized during the TGA.

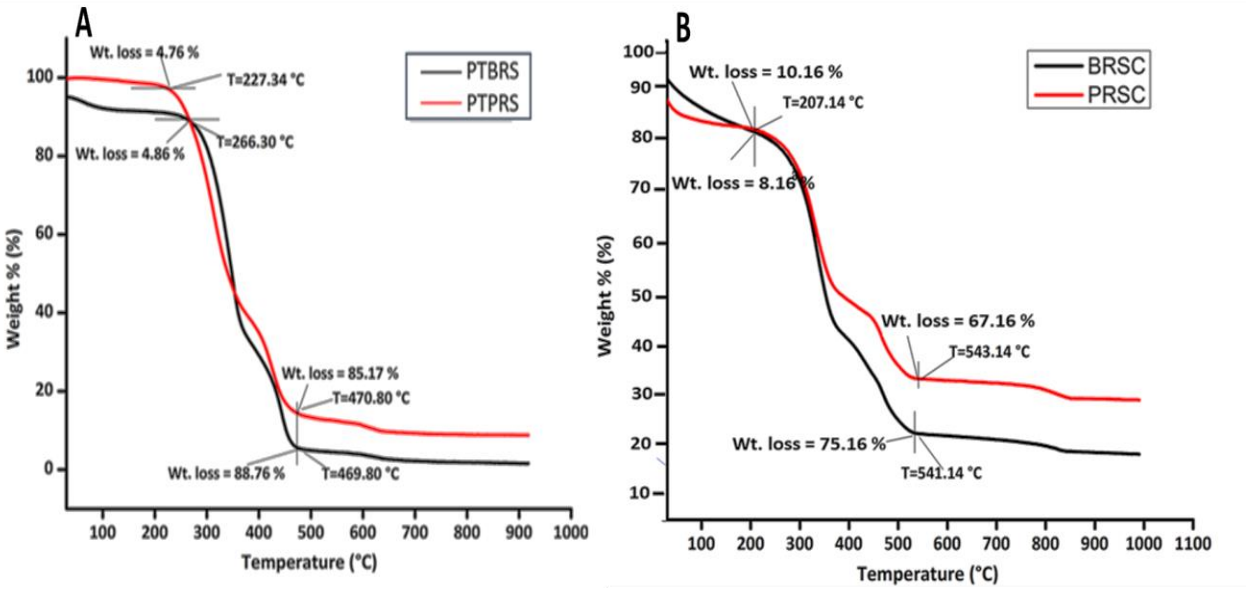

Figure 4.23 Impact of NaOH on the thermal stability of Impact of NaOH on X-ray diffraction analysis of (A) pretreated rice straw and (B) Basmati and Parmal cellulose

4.10 Synthesis of nanocellulose derived from Parmal and Basmati cellulose

Nanocellulose, a highly promising nanomaterial renowned for its versatile applications, is synthesized employing an environmentally sustainable approach, wherein citric acid (CA) is used for the synthesis of nanocellulose by the addition of ferric chloride (FeCl3) as a catalytic to enhance the efficiency of the process. The present study focused on the production of nanocellulose using different environmental conditions as a hydrolysis temperature (100 ℃), the reaction time (6 h), and the citric acid concentration (80 wt %). And post ultrasonication to enhance the hydrolysis efficiency for the highly effective preparation of CNCs. It is marked that anionic carboxylic groups possess the potential to form robust complexations with metal ions through their attraction to Fe^3+ ions. Therefore, a small amount of $FeCl_3$ (0.01−0.03 mmol/g CA) was added to the CA solution to reduce complexation. As expected, the low addition of FeCl3 was able to boost hydrolysis efficiency. This observed effect is due to the marvelous catalytic activity performed by $FeCl_3$ during the hydrolysis of cellulose.

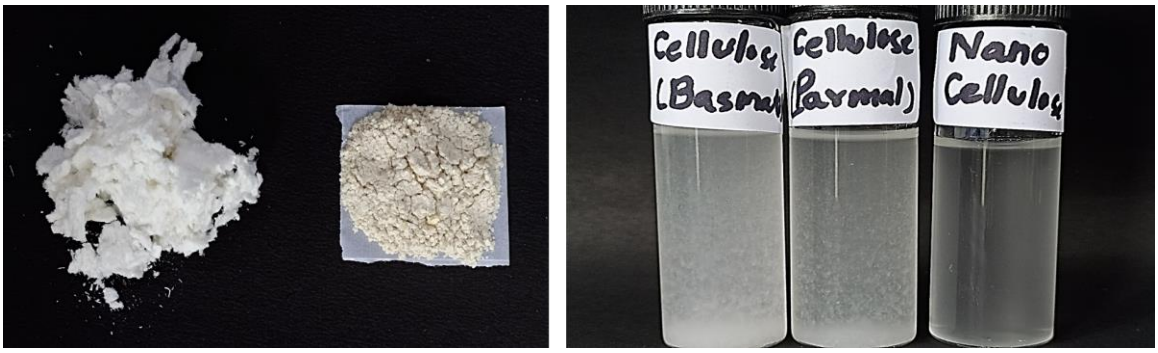

Figure 4.24: Identification of nanocellulose by texture and dispersibility

4.10.1 Characterization of Parmal and Basmati nanocellulose

4.10.1.1 Impact of citric acid on functional groups during nanocellulose synthesis

Figure 4.25 illustrates that nanocellulose (BRSNC and PRSNC) brings about shifts in the FTIR spectra, indicative of chemical modifications and the introduction of new functional groups. The O-H stretching vibrations shift slightly (3318.01 cm^{-1} for BRSNC and 3313.11 cm^{-1} for PRSNC), suggesting a tighter hydrogen bonding network in nanocellulose, likely

due to its increased surface area and altered crystallinity (Qi et al. 2023). The emergence of peaks around 2860 cm^{-1}, indicates increased C-H stretching vibrations of aliphatic chains. that are not prominently featured in the original cellulose spectra point to increased visibility or alteration of aliphatic C-H stretching. This could be due to the processing techniques employed to produce nanocellulose, which might expose more of the cellulose chain surfaces (Fliri et al. 2023).

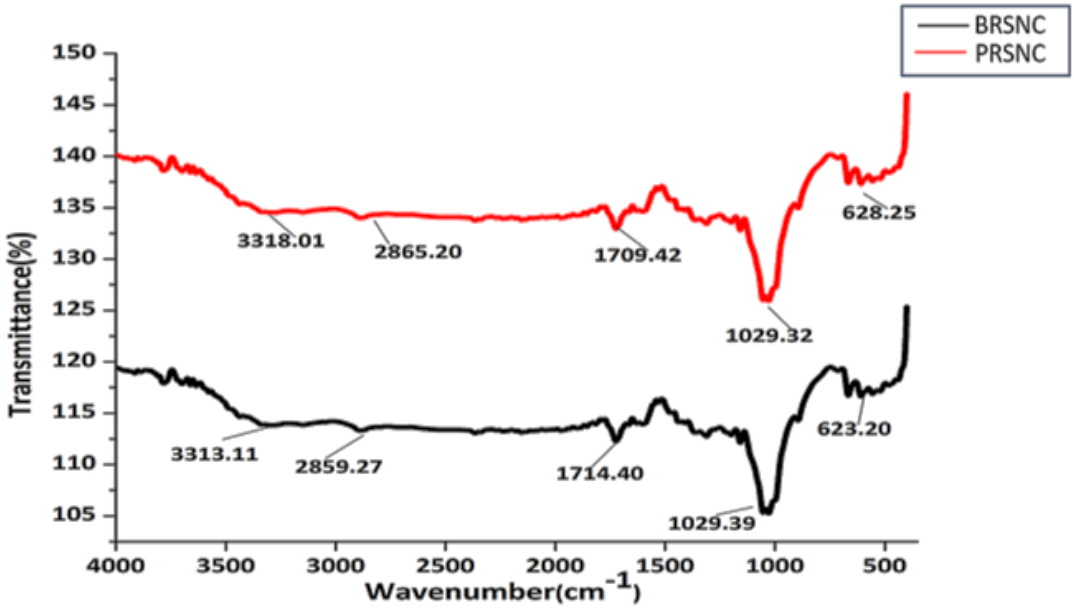

Figure 4.25 Impact of citric acid on functional groups during nanocellulose synthesis

The peaks around 1709.42 cm^{-1} (BRSNC) and 1714.40 cm^{-1} (PRSNC) point towards the presence of carbonyl groups (C=O stretching), This change suggests that the nanocellulose production process may involve oxidation reactions, leading to the introduction of carboxylic acid groups or esters (H. Jiang, Wu, and Zhou 2023). This alteration can significantly ($P< 0.05$), impact the chemical reactivity and increase the surface charge of nanocellulose, enhancing its dispersibility in aqueous and organic solvents. The C-O stretching vibrations around 1029 cm^{-1} remain relatively unchanged, indicating that the essential cellulose backbone was preserved during the conversion process. This suggests that the primary structure of cellulose is preserved in nanocellulose. The shift to higher

wavenumbers in the fingerprint region in nanocellulose observed at 628.25 cm^{-1} (BRSNC) and 623.20 cm^{-1} (PRSNC), suggests modifications in the cellulose crystalline structure. This could be due to the breakdown of larger cellulose aggregates into smaller, nanoscale particles, leading to changes in crystallinity, packing, and orientation of the cellulose structure (S. Singh et al. 2023).

4.10.1.2 Impact of citric acid on surface morphology during nanocellulose synthesis

The Scanning Electron Microscopy (SEM) images shown in **Figure 4.26 A &B** offer a detailed look at nanocellulose derived from Parmal rice straw (PRSNC) and Basmati rice straw (BRSNC), highlighting distinct differences in their microstructural characteristics. Nanocellulose is increasingly valued for its remarkable properties such as low weight, high strength, and biodegradability, making it an excellent candidate for a range of applications from reinforcing materials to medical devices. The SEM image of PRSNC shows a network of elongated, randomly oriented nanofibers with a relatively rough texture, indicative of a high degree of defibrillation. This morphology is typical for nanocellulose processed through mechanical or enzymatic means, which tends to separate the fibers while maintaining their integrity.

The rough and tangled appearance of PRSNC suggests good potential for interfacial bonding in composite materials, likely enhancing the mechanical properties of products it is incorporated into. The thin, well-separated fibers exhibit a high aspect ratio, ideal for creating strong reinforcing networks in composite applications. In contrast, the BRSNC image reveals a denser bundle of fibers, which appear more compact and agglomerated than those in PRSNC. This difference could stem from variations in the processing method or the intrinsic properties of Basmati rice straw. The fibers in BRSNC are thicker and shorter, suggesting a processing outcome that produces less individual fiber separation.

This structural variation might influence the suitability of BRSNC for certain applications, potentially reducing its effectiveness as a reinforcing agent but increasing its utility in applications where denser material packing is advantageous. The comparative analysis of PRSNC and BRSNC underscores the impact of source material and processing

on the properties of nanocellulose. PRSNC, with its longer and more fibrous structure, is likely better suited for applications requiring enhanced tensile strength and durability, such as in high-performance composites. Conversely, BRSNC, with its compact fiber structure, might be more appropriate for applications that benefit from greater bulk density, such as in thermal insulation or soundproofing materials. These insights into the nanostructure of rice straw-derived nanocellulose not only inform potential industrial applications but also highlight the importance of tailored processing techniques to optimize material characteristics for specific uses.

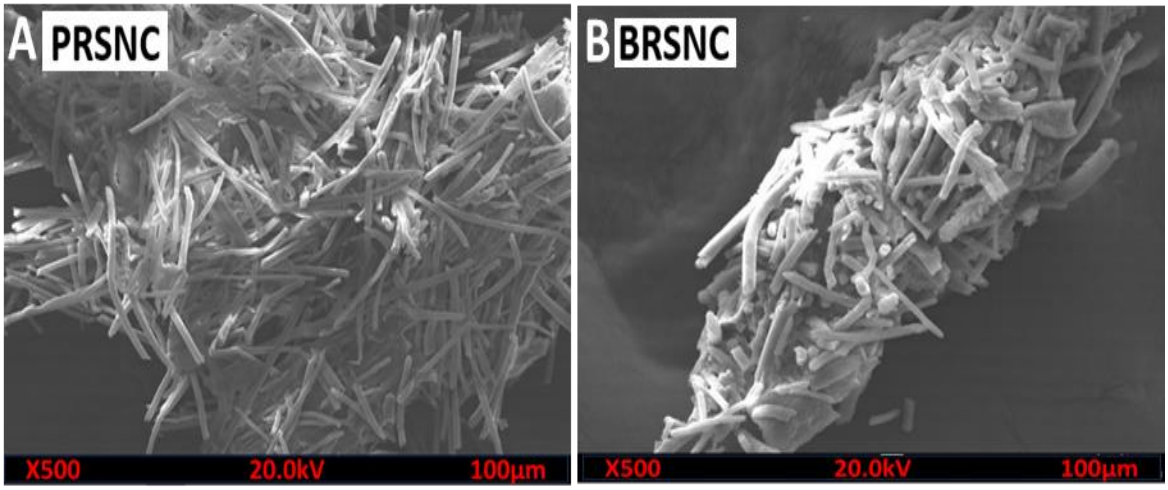

Figure 4.26 Impact of citric acid on surface morphology during nanocellulose synthesis

4.10.1.3 Impact of citric acid on energy-dispersive X-ray analysis during nanocellulose synthesis

The energy-dispersive X-ray analysis images shows in **Figure 4.27 A & B** provided offer a detailed look at nanocellulose derived from Parmal rice straw (PRSNC) and Basmati rice straw (BRSNC). At the nanocellulose stage, the spectra show primarily carbon and oxygen, with a very clean profile compared to earlier stages, which indicates a high purity of cellulose at the nano-scale. There is the appearance of nitrogen (N), which could be due to the use of chemicals during the nanocellulose production process, or possibly as a result of

nitrogen-containing groups introduced to modify the cellulose at the nano-scale (S. Singh et al. 2023).

The phosphorus (P) peaks present in the BRSNC and PRSNC spectra could be due to the use of phosphate groups in the modification process to enhance the properties of nanocellulose. The Energy-Dispersive X-ray (EDX) spectroscopy images of nanocellulose derived from Parmal rice straw (PRSNC) and Basmati rice straw (BRSNC) provide crucial insights into their elemental composition. EDX analysis is instrumental in identifying and quantifying the elements present in materials, which is particularly significant ($P<0.05$) for evaluating the properties and potential applications of nanocellulose. Both PRSNC and BRSNC exhibit similar spectral profiles, with pronounced peaks corresponding to elements such as oxygen (O), carbon (C), silicon (Si), and potassium (K). The presence of oxygen and carbon is predominant and expected, as these elements are major constituents of cellulose and hemicellulose, the organic polymers that comprise nanocellulose. These elements confirm the cellulosic origin of the material and suggest that the nanocellulose retains the essential properties of its source material, which include biodegradability and mechanical strength. Silicon, evidenced by its distinct peak in both samples, indicates the presence of silica, a common inorganic component in rice straws. Silicon's presence in nanocellulose can impart additional properties such as increased thermal stability and abrasiveness, which might be advantageous in applications requiring durable and thermally resistant materials.

However, the extent of silicon's influence depends on its concentration and distribution within the nanocellulose matrix. Potassium is also detected in both PRSNC and BRSNC, likely originating from the agricultural residues used to produce the nanocellulose. Potassium's presence could impact the nanocellulose's utility in agricultural applications, where its slow release can benefit soil fertility and plant growth. The similarities in the chemical composition of PRSNC and BRSNC as revealed by EDX analysis highlight the uniformity in the processing and properties of nanocellulose from different rice straw sources. Nonetheless, slight variations in the intensity of the elemental peaks could suggest minor differences in the processing conditions or the purity of the final product.

Understanding these elemental compositions is crucial for optimizing the nanocellulose for specific uses, particularly in composites, biodegradable products, and environmentally sustainable applications where the unique properties of nanocellulose—such as its lightweight, high strength, and reactive surface area—can be fully exploited. This detailed elemental analysis assists in tailoring the properties of nanocellulose to meet specific industrial needs, ensuring effective and sustainable utilization of this promising material.

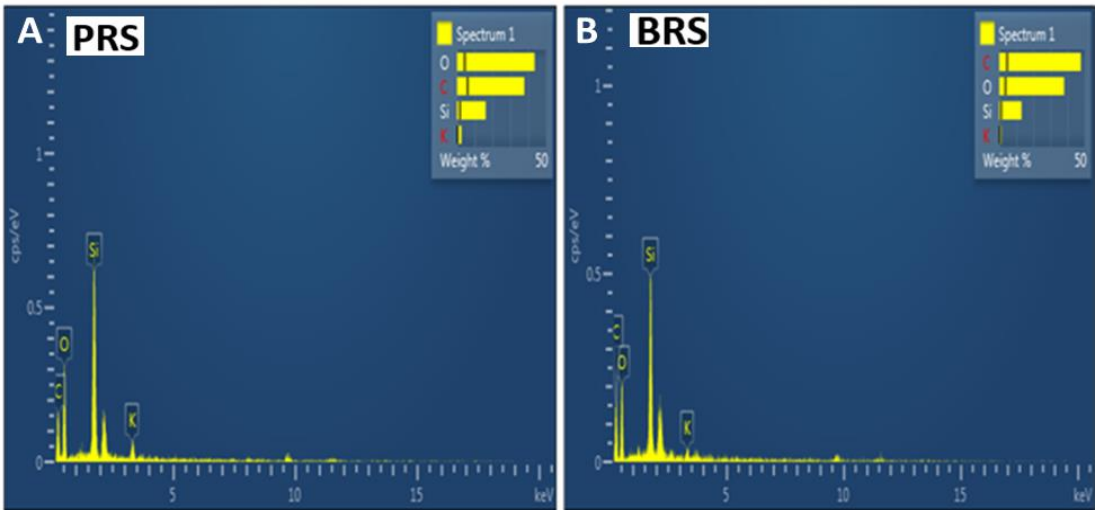

Figure 4.27 Impact of citric acid on energy-dispersive X-ray analysis during nanocellulose synthesis

4.10.1.4 Impact of citric acid on X-Ray diffraction analysis during nanocellulose synthesis

The crystallinity index analysis images shown in **Figure 4.28** provided offer a detailed look at nanocellulose derived from Parmal rice straw (PRSNC) and Basmati rice straw (BRSNC). The nanocellulose derived from BRSC and PRSC, shown as BRSNC and PRSNC, should have an even more pronounced peak at the same angle, evidencing high crystallinity, which is typical for nanocellulose. The XRD diffraction peaks for both samples are depicted in figure 1(D) were observed at 2Θ = 16.5°, 22.5°, 26° and 34° indicate that citric acid has successfully broken down the amorphous portions of the

cellulose. Any additional peaks or shifts can provide information about the formation of new crystalline structures or phases during the nanocellulose formation process.

A relatively high Crystallinity Index (CrI) was observed, indicating the removal of more hemicellulose and disordered regions of cellulose. Moreover, the XRD pattern suggests that the nanocellulose exhibits a highly ordered crystalline structure, as indicated by the sharp and intense peaks (Shakeel et al. 2024). The presence of these well-defined peaks confirms the crystalline nature of the nanocellulose and its potential for various applications requiring high crystallinity and play important role in influencing its mechanical and thermal properties.

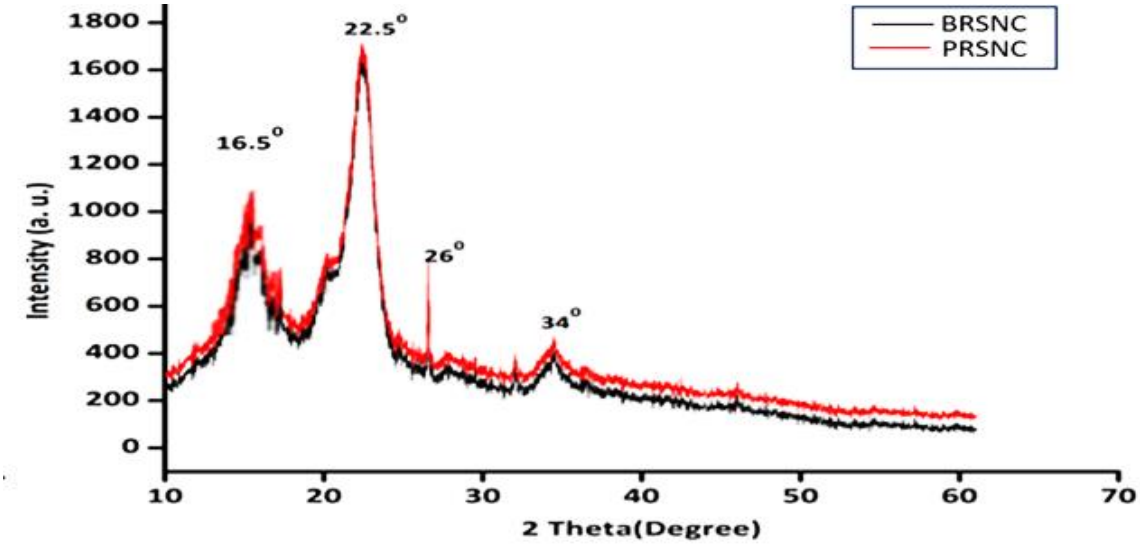

Figure 4.28 Impact of citric acid on X-Ray diffraction analysis during nanocellulose synthesis

4.10.1.5 Impact of citric acid on thermal stability analysis during nanocellulose synthesis

Figure 4.29 depicts a thermogravimetric analysis (TGA) of BRSNC and PRSNC. Here the TGA curve shows decomposition stages at temperature 197.74℃ with weight loss of 16.86% and 17.16 % to 989 ℃ for BRSNC and PRSNC. Because of its high surface area to volume ratio, may show a more significant ($P<0.05$) initial weight loss due to more bound moisture.

The weight of the sample gradually decreases as the temperature increases indicating that the nanocellulose is decomposing and losing mass continuously. There is a rapid loss of mass with 88.13 and 87.16% at 557.87 °C for BRSNC and PRSNC respectively. This range is characteristic of the main decomposition of the sample known as the second stage of the graph. Whereas, the nanocellulose chains start to break down, leading to the release of volatile compounds such as water, carbon dioxide, and various organic compounds. Over this temperature range, the nanocellulose undergoes thermal degradation, leading to maximum weight loss. The smaller particle size of nanocellulose can lead to different thermal behavior (Ludwicka, Kaczmarek, and Białkowska 2020). Smaller particles may heat more uniformly, but they may also be more prone to oxidative processes due to their larger relative surface area. This can be attributed to the high crystallinity and the removal of amorphous regions during processing.

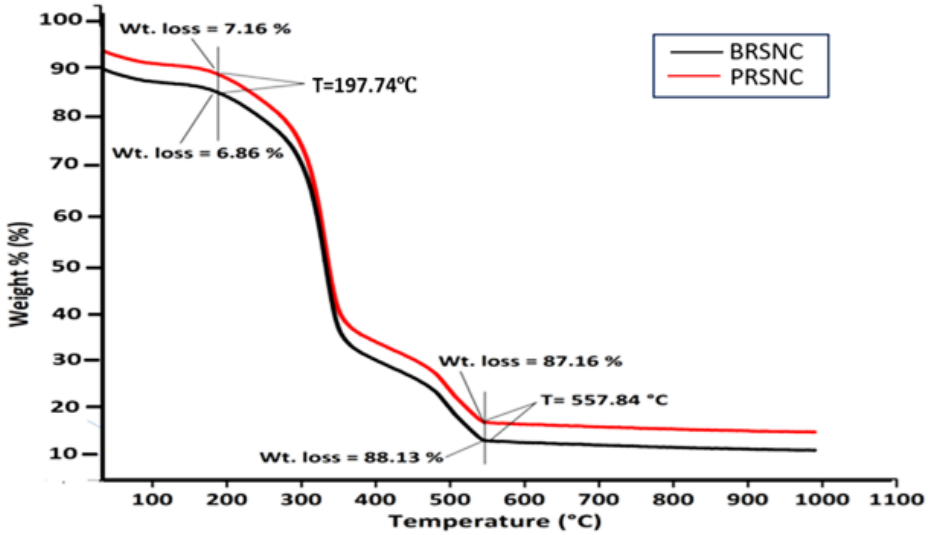

Figure 4.29 Impact of citric acid on thermal stability analysis during nanocellulose synthesis

The degradation curve for nanocellulose might be narrower, indicating a more uniform degradation process, as nanocellulose tends to have fewer amorphous regions than bulk cellulose. In the final stage the temperature ranges from 400 °C to 999° C represents the further decomposition of the remaining cellulose residues and any other organic materials

present in the nanocellulose. The gradual decrease in mass in this range indicates the continuous breakdown of cellulose and other organic components into smaller quantity in the form of more stable compounds remaining as ash content (Z.-X. Xu et al. 2022). This information is valuable for understanding the thermal behavior of the material and can be used to optimize its processing and application in various fields such as nanotechnology, biomedicine, and environmental science.

4.10.1.6 Impact of citric acid on particle size and zeta potential during nanocellulose synthesis

Figure 4.30 A, B, C & D illustrate the particle size distribution and zeta potential measurements for nanocellulose derived from Parmal rice straw (PRSNC) and Basmati rice straw (BRSNC). These measurements are crucial for determining the suitability of nanocellulose for various applications based on their physical properties and stability in suspensions.

Figure 4.30 A (PRSNC) shows a sharp peak, indicating a uniform particle size distribution, primarily centered around a few hundred nanometers. Such uniformity suggests that PRSNC nanocellulose has consistent physical properties, making it ideal for applications requiring precise performance, such as in drug delivery systems where uniform particle size can influence the release rate of active ingredients. **Figure 4.30 B** (BRSNC) similarly displays a sharp peak, echoing the uniformity seen in PRSNC. This consistency in particle size across both types of nanocellulose indicates that the processing methods used likely maintain a controlled environment to achieve such uniformity, beneficial for applications in composite materials where consistent particle behavior is needed to achieve uniform mechanical properties. **Figure 4.30 C** (PRSNC) and **Figure 4.30 D** (BRSNC) both present zeta potential values centered around 0 mV, suggesting that both types of nanocellulose have a neutral charge at the surface. A zeta potential near zero can be problematic as it may lead to reduced electrostatic repulsion between particles, increasing the likelihood of aggregation. This aggregation can impact the stability of nanocellulose in suspensions,

posing challenges for applications requiring long-term stability or consistent rheological properties.

The particle size data indicate that both PRSNC and BRSNC are highly uniform in their dimensions, which is advantageous for various high-tech applications. However, the zeta potential measurements highlight a potential challenge in maintaining colloidal stability, suggesting that applications involving these materials might require modifications such as surface treatment or the use of stabilizing agents to ensure the particles remain evenly dispersed in their respective mediums. Such enhancements are essential for leveraging the unique properties of nanocellulose in environmentally friendly applications and advanced material science technologies.

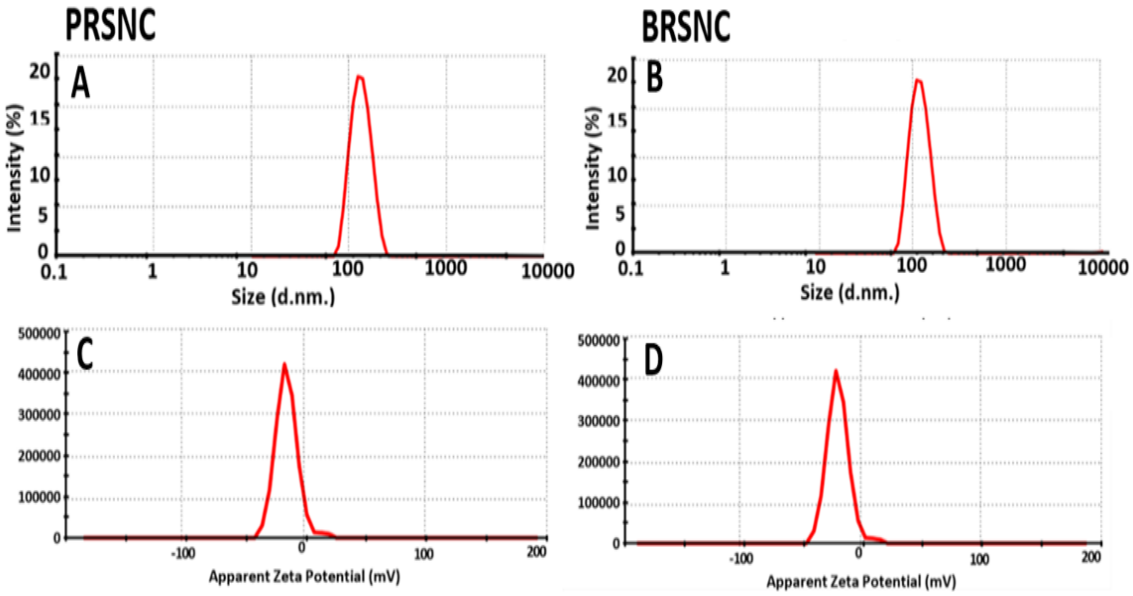

Figure 4.30 Impact of citric acid on particle size and zeta potential during nanocellulose synthesis

4.11 Fabrication of Nanocomposite film

The study investigated how different compositions affect the properties of nanocellulose-based films, using formulations F1 to F39 as shown in **Table 4.7.** These formulations were carefully designed within specified ranges to explore the effects of nanocellulose, glycerol, mucilage, and sodium alginate on film characteristics. Notably, formulations F38 and F39,

are considered as control as absent of mucilage and nanocellulose respectively, provided unique insights into the distinct contributions of these components. The results showed a clear link between composition and film properties, especially in terms of mechanical strength, barrier properties, flexibility, and biodegradability. Higher levels of nanocellulose were associated with improved mechanical strength, while variations in nanocellulose and mucilage concentrations affected flexibility and biodegradability. The absence of nanocellulose or mucilage in specific formulations underscored their essential roles in enhancing specific film properties.

4.11.1 Optimization of film

As shown in **Table 4.7** offer a detailed look at nanocellulose derived from Parmal rice straw (PRSNC) and Basmati rice straw (BRSNC). Optimizing a film formulation using varying concentrations of components like nanocellulose, mucilage, glycerol, and sodium alginate is a complex process that requires a methodical approach to determine the best composition for achieving desired physical and mechanical properties. The process involves systematic experimental design, preparation, testing, data analysis, and refinement stages (Sauer and Seuring 2023). Each step is crucial for developing a film with optimal characteristics suitable for specific applications. Here is an in-depth view of each step involved in the process.

Each component used in the formulation of films contributes unique properties that influence the overall characteristics of the film. Here is a complete look at how nanocellulose, mucilage, glycerol, and sodium alginate each play a role in film development. Nanocellulose is a plentiful natural polymer, is notable for its exceptional strength and stiffness due to its crystalline structure. In film formulations, nanocellulose acts as a reinforcement agent that provides structural strength, enhancing the mechanical properties of the film. It imparts tensile strength and durability, making the resulting film tough and resistant to tearing. Furthermore, nanocellulose contributes to the flexibility of the film and compromises its strength. This balance between strength and flexibility is

crucial for applications where the film needs to withstand stress without breaking, such as in packaging materials (Sayanjali, Lu, and Howell 2024).

Mucilage is a naturally occurring gelatinous substance extracted from plants. It is characterized by its gel-forming properties when mixed with water. In film formulations, mucilage serves multiple functions. It enhances film formability, making the film easier to cast or mold into shapes. The hydrophilic nature of mucilage allows it to form films that are smooth and uniform. Additionally, mucilage imparts flexibility to the films, which is essential for applications requiring the film to bend or conform to surfaces without cracking. The presence of mucilage helps in maintaining the integrity and aesthetic quality of the film, making it appropriate for a variety of commercial uses (Khodaman et al. 2022).

Glycerol, a widely used plasticizer in film formulations, plays an essential role in enhancing the flexibility and workability of films. As a plasticizer, glycerol intersperses itself between the polymer chains, reducing intermolecular forces and increasing the mobility of the chains. This action allows the film to become more pliable and less brittle. The addition of glycerol helps prevent the film from becoming too rigid, which is particularly important in preventing crack formation under mechanical stress or low temperatures (Tamayo et al. 196AD).

The use of glycerol makes the film more user-friendly and adaptable to various applications where flexibility is crucial, such as in cling films and other wrapping materials. Sodium alginate, a natural polysaccharide derived from brown seaweed, serves as an effective film former. It has the unique property of forming a gel in the presence of calcium ions. In the context of filmmaking, sodium alginate provides mechanical strength and stability, forming a matrix that is both robust and flexible. When used in combination with other film-forming agents, sodium alginate contributes to the overall structural integrity of the film, supporting its shape and durability under physical stress. Its gelling properties also enhance the film’s barrier characteristics, helping to better retain moisture and other volatiles within the packaged goods. The interaction between these components such as nanocellulose for strength, mucilage for flexibility and formability, glycerol for plasticity, and sodium alginate for gelation and stability allows for the tailored production of

Table. 4.7 Optimization of fabrication of film

Sample code	Nanocellulose % (w/v)	Mucilage % (g)	Glycerol (ml)	sodium alginate % (g)
F1	1	1	2	1
F2	1	2	2	1
F3	1	3	2	1
F4	1	4	2	1
F5	1.5	1	2	1
F6	1.5	2	2	1
F7	1.5	3	2	1
F8	1.5	4	2	1
F9	2	1	2	1
F10	2	2	2	1
F11	2	3	2	1
F12	2	4	2	1
F13	2.5	1	2	1
F14	2.5	2	2	1
F15	2.5	3	2	1
F16	2.5	4	2	1
F18	3	1	2	1
F19	3	2	2	1
F20	3	3	2	1
F21	3	4	2	1
F22	3.5	1	2	1
F23	3.5	2	2	1
F24	3.5	3	2	1
F25	3.5	4	2	1
F26	4	1	2	1
F27	4	2	2	1
F28	4	3	2	1
F29	4	4	2	1
F30	4.5	3	2	1
F31	4.5	4	2	1
F32	5	3	2	1
F33	5	4	2	1
F34	5.5	3	2	1
F35	5.5	4	2	1
F36	6	3	2	1
F37	6	4	2	1
F-CN38	5	0	2	1
F-CM39	0	4	2	1

biodegradable films with specific properties suited for diverse applications. By adjusting the concentrations and ratios of these components, manufacturers can optimize films for characteristics such as strength, flexibility, barrier properties, and environmental sustainability.

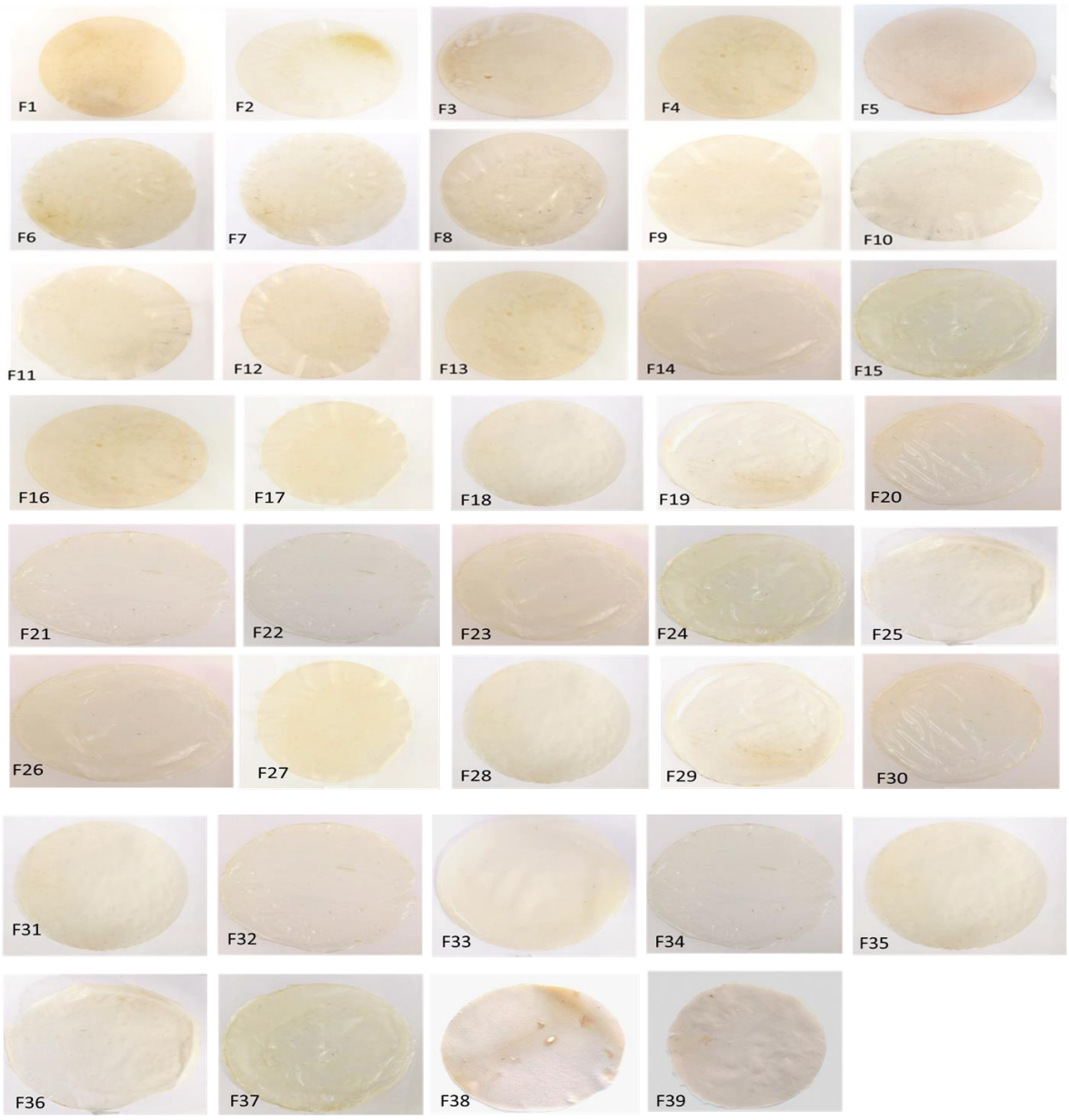

Figure 4.31 Prepared film sample of different concentrations

4.11.2 Physiochemical properties of nanocomposite film

4.11.2.1 Mechanical properties

The mechanical strength of nanocellulose-based films, as illustrated in **Table 4.8** and **Figure 4.32** exhibited significant ($P<0.05$) variability across all formulations (F1 to F39). Starting with Formulation F1, consisting of 1% nanocellulose, 1% mucilage, 2 ml glycerol, and 1% sodium alginate, the mechanical strength was recorded at 6.13 ± 0.23 Mpa. This baseline formulation demonstrates the initial compatibility and interaction of these components in forming a cohesive film, although the mechanical strength at this level indicates scope for improvement through adjustment of component ratios. As the formulations progressed from F2 to F4, where the mucilage content increased incrementally by 1% per formulation while keeping the other components constant, a non-significantly ($P< 0.05$), increase in mechanical strength was observed. Specifically, F4, with 1% nanocellulose, 4% mucilage, 2 ml glycerol, and 1% sodium alginate, showed a strength of 7.17 ± 0.21 Mpa.

This trend suggests that mucilage plays a critical role in enhancing film cohesiveness and structural integrity, likely due to its gel-forming capabilities which contribute to a more uniform and stable matrix. The formulations F5 to F8 gradually increased the amount of nanocellulose up to 1.5%. This change significantly improved the mechanical strength. The strongest result was observed in F8, which had 1.5% nanocellulose and 4% mucilage, achieving a strength of 8.25 ± 0.09 MPa. The enhancement in strength with higher nanocellulose content underscores its fundamental role in providing structural backbone to the films, due to its high tensile strength and stiffness derived from its fibrous nature. Further increases in nanocellulose content in subsequent formulations (F9 to F16) continued this trend, where mechanical strength significantly ($P<0.05$), increased, reaching 12.87 ± 0.65 Mpa in F16. This formulation marked the highest nanocellulose content at 2.5 %, coupled with the maximum (4%) mucilage level.

The relationship between increased nanocellulose and mucilage and enhanced mechanical properties highlights their synergistic effect in film formation, optimizing both strength and flexibility (Hoyos-Merlano et al. 2022). However, it is important to point out that

starting from formulation F26, where the nanocellulose concentration was raised to 4% or higher, there was a decrease in mechanical strength due to excessive amounts of this component. While some formulations like F32 and F33 reached mechanical strengths as high as 22.85 ± 1.89 Mpa and 23.06 ± 0.78 Mpa respectively, others like F34 to F37 saw a decline in strength. This variability indicates a complex interaction between component ratios where too much nanocellulose or mucilage can disrupt the film matrix, potentially leading to brittleness or uneven distribution of stress within the film.

Additionally, for a further study assessing the mechanical strength of films composed of nanocellulose, mucilage, glycerol, and sodium alginate, formulations F26 to F37 were selected for further analysis due to the impact of varying concentrations of key components on film strength, while F38 and F39 served as control films to evaluate the individual contributions of mucilage and nanocellulose, respectively. Films F26 through F29, holding nanocellulose constant at 4% while rising mucilage from 1 to 4%, showcased a progressive increase in mechanical strength, confirming the positive role of mucilage in enhancing film integrity. The trend continued with F30 and F31, where an increase in nanocellulose to 4.5%, fixed with high levels of mucilage, led to further improvements in strength, peaking at values just above 20. This suggests that additional nanocellulose effectively reinforces the film structure.

The peak performance was observed in formulations F32 and F33, where nanocellulose was increased to 5%. These films exhibited the significant ($P< 0.05$), highest mechanical strengths of 22.85 ± 1.89 Mpa and 23.06 ± 0.78 Mpa respectively, indicating an optimal balance between nanocellulose for structural support and mucilage for matrix cohesion. However, subsequent increases in nanocellulose to 5.5 and 6% (F34 to F37) resulted in a decline in mechanical strength, likely due to oversaturation which may disrupt film uniformity and reduce effectiveness. Control films F-CN38 and F-CM39, designed with extreme component ratios, underscored the necessity of both mucilage and nanocellulose. F-CN38, containing 5% nanocellulose without mucilage, and F-CM39, absent of nanocellulose, where both showed significantly ($P< 0.05$), lower strengths compared to other formulations.

This highlights that mucilage is critical for binding and flexibility, while nanocellulose is essential for structural integrity. Among these, F33 was identified as the superior formulation, achieving the highest mechanical strength due to its well-balanced mixture of 5% nanocellulose and 4% mucilage. This combination optimizes the synergy between nanocellulose's structural benefits and mucilage's cohesive properties, resulting in a robust yet flexible film. This finding emphasizes the importance of careful ratio management in the development of nitrocellulose-based films, suggesting that the formulation of F33 offers the most promising potential for applications requiring durable and sustainable material solutions (Biswas et al. 2023).

Table 4.8 Mechanical strength of film

Sample Code	Mechanical Strength (Mpa)
$F1_{(1+1)}$	6.13 ± 0.23^{a}
$F2_{(1+2)}$	6.59 ± 0.25^{a}
$F3_{(1+3)}$	6.97 ± 0.03^{a}
$F4_{(1+4)}$	7.17 ± 0.21^{b}
$F5_{(1.5+1)}$	7.39 ± 0.56^{b}
$F6_{(1.5+2)}$	7.77 ± 0.98^{b}
$F7_{(1.5+3)}$	8.07 ± 0.47^{c}
$F8_{(1.5+4)}$	8.25 ± 0.09^{c}
$F9_{(2+1)}$	8.98 ± 0.82^{c}
$F10_{(2+2)}$	9.46 ± 1.03^{d}
$F11_{(2+3)}$	10.83 ± 1.56^{e}
$F12_{(2+4)}$	10.93 ± 0.89^{e}
$F13_{(2.5+1)}$	11.54 ± 0.67^{f}
$F14_{(2.5+2)}$	11.98 ± 0.78^{f}
$F15_{(2.5+3)}$	12.73 ± 0.34^{g}
$F16_{(2.5+4)}$	12.87 ± 0.65^{g}
$F18_{(3+1)}$	13.33 ± 1.23^{h}
$F19_{(3+2)}$	13.67 ± 1.13^{h}

$F20_{(3+3)}$	14.01 ± 1.03^{i}
$F21_{(3+4)}$	14.24 ± 1.34^{i}
$F22_{(3.5+1)}$	13.68 ± 1.67^{h}
$F23_{(3.5+2)}$	14.32 ± 1.45^{i}
$F24_{(3.5+3)}$	15.86 ± 1.07^{j}
$F25_{(3.5+4)}$	16.73 ± 1.45^{ı}
$F26_{(4+1)}$	12.81 ± 0.89^{g}
$F27_{(4+2)}$	15.37 ± 0.98^{ı}
$F28_{(4+3)}$	17.95 ± 1.45^{k}
$F29_{(4+4)}$	18.04 ± 1.25^{l}
$F30_{(4.5+3)}$	20.75 ± 1.83^{m}
$F31_{(4.5+4)}$	20.89 ± 1.76^{m}
$F32_{(5+3)}$	22.85 ± 1.89^{n}
$F33_{(5+4)}$	23.06 ± 0.78^{o}
$F34_{(5.5+3)}$	18.78 ± 1.08^{l}
$F35_{(5.5+4)}$	17.34 ± 1.08^{k}
$F36_{(6+3)}$	15.57 ± 1.28^{j}
$F37_{(6+4)}$	14.89 ± 1.49^{i}
$F\text{-}CN38_{(5+0)}$	8.07 ± 0.57^{c}
$F\text{-}CM39_{(0+4)}$	6.12 ± 0.28^{a}

[1]Data are represented as mean ± SEM (n=3) [a-n] Means within the column with different lowercase superscripts are significantly (P< 0.05), different from each other

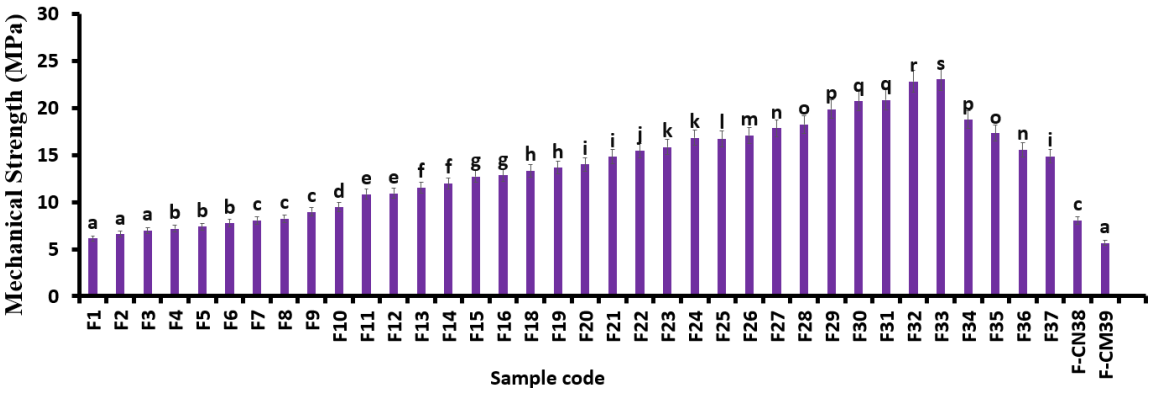

Figure 4.32 Mechanical strength of film

Table. 4.9 Selected film based on mechanical strength

Sample Code	Mechanical Strength (Mpa)
$F1_{(4+1)}$	12.81 ± 0.89^{c}
$F2_{(4+2)}$	15.37 ± 0.98^{d}
$F3_{(4+3)}$	17.95 ± 1.45^{e}
$F4_{(4+4)}$	18.04 ± 1.25^{f}
$F5_{(4.5+3)}$	20.75 ± 1.83^{g}
$F6_{(4.5+4)}$	20.89 ± 1.76^{g}
$F7_{(5+3)}$	22.85 ± 1.89^{h}
$F8_{(5+4)}$	23.06 ± 0.78^{i}
$F9_{(5.5+3)}$	18.78 ± 1.08^{f}
$F10_{(5.5+4)}$	17.34 ± 1.08^{e}
$F11_{(6+3)}$	15.57 ± 1.28^{g}
$F12_{(6+4)}$	14.89 ± 1.49^{f}
$F\text{-}CN13_{(5+0)}$	8.07 ± 0.57^{b}
$F\text{-}CM14_{(0+4)}$	6.12 ± 0.28^{a}

[1]Data are displayed as mean ± SEM (n=3) [a-f] Means with each column with different lowercase superscript are different significantly (P< 0.05) from one another

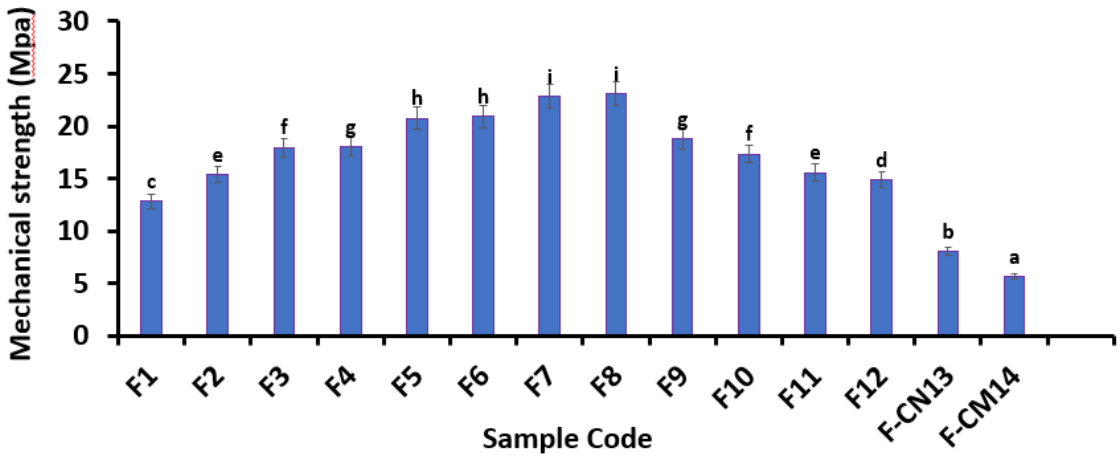

Figure 4.33 Selected film based on mechanical strength

4.11.2.2 Effect of moisture content on film

Figure 4.34 and **Table 4.10** provide the moisture content of nanocellulose-based films, represented by formulations F1 to F-CM14, illustrating the significant ($P<0.05$) impact of component ratios on moisture retention capabilities. The systematic study of moisture content from F1 through F12 demonstrated a clear relationship between the composition of key components—namely nanocellulose, mucilage, glycerol, and sodium alginate—and the films' ability to manage moisture, which is crucial for optimizing film formulations for specific applications.

Starting with F1, which contained a ratio of 4% nanocellulose to 1% mucilage, the film maintained a moisture content of 25.09 ± 0.032%, indicating stable moisture retention non-significantly ($P> 0.05$) differences. As the mucilage content increased incrementally in the subsequent formulations (F2 to F4), a corresponding rise in moisture content was observed, indicating the hydrophilic and gel-forming properties of mucilage significantly ($P< 0.05$), enhanced water retention. Specifically, F2, with 2% mucilage, recorded moisture content with 26.77 ± 0.067 %, showing a slight but non-significant ($P>0.05$) increase. F3, with 3% mucilage, had 27.89% ± 0.870, and F4, with 4% mucilage, showed the highest at 28.29% ± 0.980 moisture content, and both displaying significant ($P<0.05$) increases due to the higher mucilage content. Interestingly, as the nanocellulose concentration was increased to 4.5% in F5 and F6, despite high mucilage levels, there was a notable decrease in moisture content to 23.27 ± 0.760% and 22.76 ± 0.430%, respectively, suggesting that beyond a certain threshold, nanocellulose begins to restrict the film's ability to retain moisture, likely due to its denser, more crystalline fiber structure.

This trend continued with further increases in nanocellulose: F7 and F8, containing 5% nanocellulose, had moisture contents of 18.35 ± 0.920% and 19.15 ± 0.650%, respectively, indicating significant ($P<0.05$) decreases. A temporary reversal in this trend was seen in F9 and F10, which recorded moisture contents of 23.65 ± 0.078% and 24.41 ± 0.670%. However, with F11 and F12, which contained 6% nanocellulose, there was again an increase in moisture content with 31.56 ± 0.075% and 32.18 ± 0.340% respectively, suggesting a complex interaction where the moisture-retaining effect competes with mucilage with the structuring role of nanocellulose. The control films, F-CN13 and F-

CM14, were particularly revealing: F-CN13, with 5% nanocellulose and no mucilage, showed a surprisingly high moisture content of 35.56 ± 0.065%, while F-CM14, containing no nanocellulose but 4% mucilage, had the highest moisture content of all at 37.57 ± 0.040%, both showing significant ($P<0.05$) increases, underscoring the crucial roles of both components in moisture management.

Among all formulations, F8 was identified as optimal, balancing 5% nanocellulose and 4% mucilage to achieve a robust yet moderately hydrated film (Rathod 2021). This specific combination provides enough structural integrity to maintain film form while retaining sufficient moisture to prevent brittleness. This detailed analysis of compositions and their impact on moisture content not only provides insights into material properties but also guides future developments in bio-based film technology for various industrial applications (Yousefi et al. 2024).

Table 4.10 Effect of moisture content on film

Sample Code	Moisture Content (%)
$F1_{(4+1)}$	25.09 ± 0.032^{f}
$F2_{(4+2)}$	26.77 ± 0.067^{g}
$F3_{(4+3)}$	27.89 ± 0.87^{h}
$F4_{(4+4)}$	28.29 ± 0.98^{i}
$F5_{(4.5+3)}$	23.27 ± 0.76^{d}
$F6_{(4.5+4)}$	22.76 ± 0.43^{c}
$F7_{(5+3)}$	18.35 ± 0.92^{a}
$F8_{(5+4)}$	19.15 ± 0.65^{b}
$F9_{(5.5+3)}$	23.65 ± 0.078^{d}
$F10_{(5.5+4)}$	24.41 ± 0.67^{e}
$F11_{(6+3)}$	31.56 ± 0.075^{j}
$F12_{(6+4)}$	32.18 ± 0.34^{k}
$F\text{-}CN13_{(5+0)}$	35.56 ± 0.065^{l}
$F\text{-}CM14_{(0+4)}$	37.57 ± 0.040^{m}

[1]Data are displayed as mean ± SEM (n=3) $^{a\text{-}m}$ Means with each column with different lowercase superscripts are different significantly ($P< 0.05$), from one another

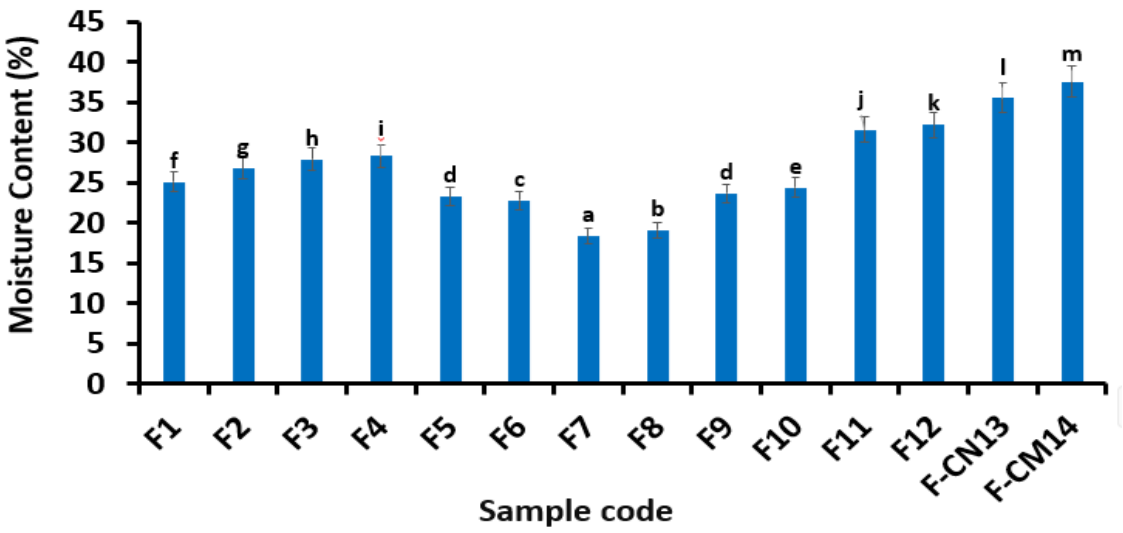

Figure 4.34 Effect of moisture content on film

4.11.2.3 Effect of water activity on film

Table 4.11 and **Figure 4.35** reveal that the water activity (aw) of nanocellulose-based films varies significantly ($P < 0.05$), across different formulations (F1 to F-CM14) to highlight the influence of component concentrations on moisture interaction characteristics of the films. This aspect is crucial for applications like food packaging, where precise moisture control is essential. Starting with F1 and increasing to F12, there is a noticeable trend where increasing the concentration of nanocellulose generally decreases water activity. This is attributed to the structural properties of nanocellulose and its less hydrophilic nature, which enhance the film's barrier properties against moisture penetration. For example, F1, with a lower content of nanocellulose, begins with a water activity of 0.530 ± 0.05, and this figure gradually increases up to F12, which records 0.621 ± 0.23. These changes are significant ($P<0.05$) as indicated by the data showing a clear trend of increasing water activity with reduced nanocellulose content.

Moreover, mucilage, known for its highly hydrophilic properties, contributes to higher water activity levels. From F1 to F4, where mucilage content is progressively increased, there is a corresponding rise in water activity from 0.530 to 0.559 ± 0.03, reflecting mucilage's effectiveness in enhancing the film's capacity to interact with ambient moisture.

Table 4.11 Effect of water activity on film

Sample Code	Water Activity
$F1_{(4+1)}$	0.530 ± 0.05^{b}
$F2_{(4+2)}$	0.545 ± 0.32^{d}
$F3_{(4+3)}$	0.554 ± 0.82^{f}
$F4_{(4+4)}$	0.559 ± 0.03^{g}
$F5_{(4.5+3)}$	0.522 ± 0.98^{a}
$F6_{(4.5+4)}$	0.533 ± 0.94^{c}
$F7_{(5+3)}$	0.545 ± 0.67^{d}
$F8_{(5+4)}$	0.549 ± 0.08^{e}
$F9_{(5.5+3)}$	0.561 ± 0.98^{g}
$F10_{(5.5+4)}$	0.564 ± 0.03^{h}
$F11_{(6+3)}$	0.610 ± 0.09^{i}
$F12_{(6+4)}$	0.621 ± 0.23^{j}
$F\text{-}CN13_{(5+0)}$	0.653 ± 0.87^{k}
$F\text{-}CM14_{(0+4)}$	0.684 ± 0.98^{l}

[1]Data are represented as mean ± SEM (n=3) [a-l] Means within the column with different lowercase superscripts are significantly (P< 0.05) different from each other

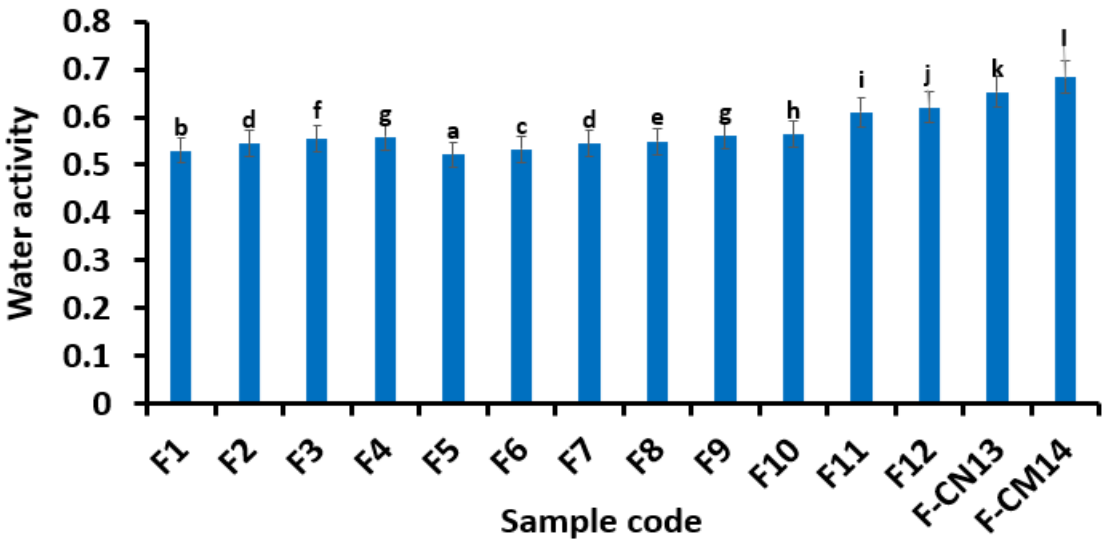

Figure 4.35 Effect of water activity on film

This property can be particularly beneficial in environments where moisture retention is desired. Additionally, glycerol and sodium alginate consistently influence water activity across all formulations. Glycerol, by increasing film flexibility and porosity, and sodium alginate with its gel-forming capabilities, help maintain or slightly raise the water activity, facilitating balanced moisture management within the films. The control films, F-CN13 and F-CM14, highlight the significant ($P<0.05$) roles of mucilage and nanocellulose. F-13, absence of mucilage, shows a water activity of 0.653 ± 0.87, highlighting mucilage's role in promoting moisture interaction.

Moreover, the film F-CM14, without nanocellulose, records the highest water activity at 0.684 ± 0.98, demonstrating how the absence of nanocellulose increases moisture sensitivity. F8 emerges as the optimal formulation with a water activity of 0.549 ± 0.08, showcasing an effective balance between moisture barrier properties and moisture retention. This formulation, combining 5% nanocellulose with 4% mucilage, is especially suitable for packaging applications where controlling moisture is required. The balanced properties of F8 make it ideal for maintaining product quality and extending shelf life in controlled moisture environments (Biswas et al. 2023).

4.11.2.4 Effect of thickness on film

Table 4.12 and **Figure 4.36** illustrate the variation in thickness of nanocellulose-based films across different formulations, ranging from F1 to F-CM14. The analysis of these variations provides key insights into how the concentrations of nanocellulose, mucilage, glycerol, and sodium alginate influence the physical structure of films and, by extension, their applicability in specific uses such as food packaging. For instance, the starting formulation, F1, with 4% nanocellulose, exhibits a thickness of 0.294 ± 0.06 mm. Furthermore, as the nanocellulose concentration increases up to 6% in F12, the thickness tends to remain stable or non-significant ($P>0.05$) increase. The film F12 shows a thickness of 0.293 ± 0.03 mm, suggesting that nanocellulose primarily enhances structural strength without substantially altering thickness.

The role of Mucilage is highlighted in formulations like F4, where the highest mucilage content results in one of the thicker measurements at 0.301 ± 0.09 mm, indicating its voluminous and gel-like properties contribute positively to film thickness. The optimal formulation, F8, which balances 5% nanocellulose with 4% mucilage, achieves the highest recorded thickness of 0.308 ± 0.02 mm, underscoring an ideal combination of structural integrity and volumetric characteristics suitable for robust applications. The control films, F-CN13 and F-CM14, underscore the importance of each component. F-CN13, without mucilage, shows a reduced thickness of 0.283 ± 0.09 mm, pointing out the bulk-adding properties of mucilage. Conversely, F-CM14, lacking nanocellulose, records the lowest thickness at 0.271 ± 0.01 mm, illustrating the essential structural role played by nanocellulose.

Table. 4.12 Effect of thickness on Film

Sample Code	Thickness (mm)
$F1_{(4+1)}$	0.294 ± 0.06^{b}
$F2_{(4+2)}$	0.297 ± 0.08^{c}
$F3_{(4+3)}$	0.298 ± 0.03^{d}
$F4_{(4+4)}$	0.301 ± 0.09^{e}
$F5_{(4.5+3)}$	0.303 ± 0.06^{f}
$F6_{(4.5+4)}$	0.305 ± 0.01^{g}
$F7_{(5+3)}$	0.306 ± 0.06^{h}
$F8_{(5+4)}$	0.308 ± 0.02^{i}
$F9_{(5.5+3)}$	0.311 ± 0.07^{j}
$F10_{(5.5+4)}$	0.314 ± 0.09^{k}
$F11_{(6+3)}$	0.321 ± 0.04^{l}
$F12_{(6+4)}$	0.325 ± 0.03^{m}
$F\text{-}CN13_{(5+0)}$	0.328 ± 0.09^{n}
$F\text{-}CM14_{(0+4)}$	0.271 ± 0.01^{a}

[1]Data are represented as mean ± SEM (n=3) $^{a\text{-}n}$ Means within the column with different lowercase superscripts are significantly ($P < 0.05$), different from each other

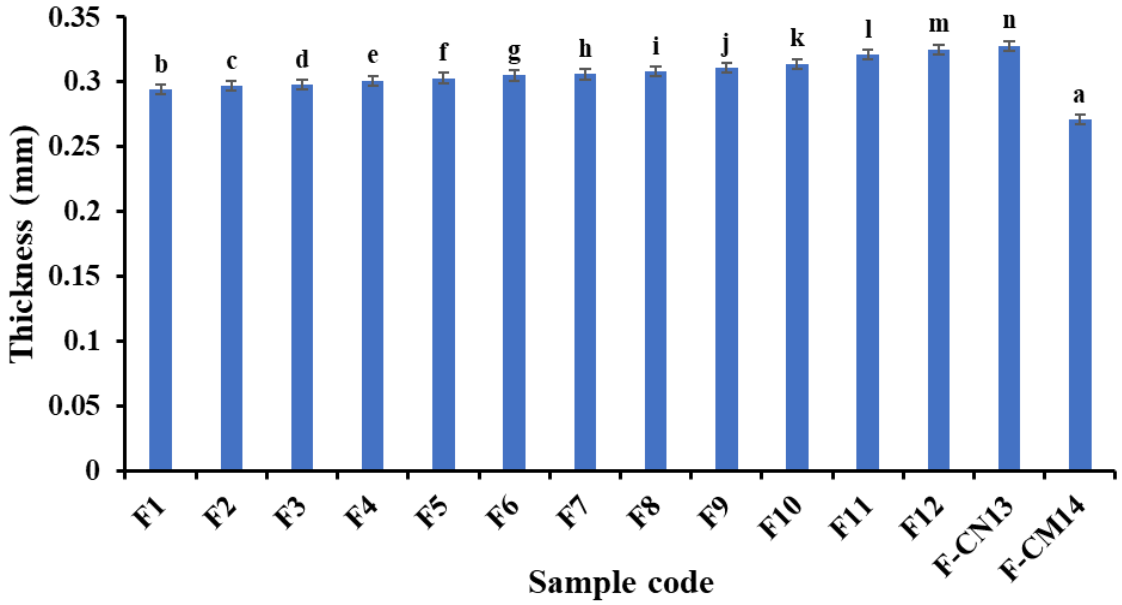

Figure 4.36 Effect of Thickness on Film

This analysis not only highlights how each component influences the film thickness but also provides a comprehensive understanding of their collective impact on enhancing the film's physical properties for targeted applications. The slight variances and statistical observations in the provided data suggest a strong interaction between these components, where the presence of mucilage and nanocellulose significantly ($P< 0.05$), impacts the overall film robustness and effectiveness. Among the various formulations analyzed, F8 emerges as the film displaying the best characteristics in terms of thickness, achieving a measurement of 0.308 ± 0.02 mm. This formulation is particularly notable because it strikes an optimal balance between nanocellulose and mucilage. With 5% nanocellulose and 4% mucilage, Film F8 provides robust structural integrity while also retaining sufficient volumetric properties to ensure the film is neither too brittle nor too permeable (Biswas et al. 2023).

4.11.2.5 Effect of water vapor transmittance rate (WVTR) on film

As illustrated in **Table 4.13** and **figure 4.37**, the Water Vapor Transmission Rate (WVTR) data for nanocellulose-based films, as depicted across formulations F1 through F-CM14, provides a detailed look at how modifications in the concentrations of nanocellulose,

mucilage, glycerol, and sodium alginate impact moisture control capabilities. Starting with F1, which has a WVTR of 0.690 ± 0.09 $kg \cdot s^{-1} \cdot m^{-2} \cdot Pa^{-1}$, a baseline for moisture permeability that serves as a reference for subsequent formulations. As the formulations progress from F1 to F4, there is a consistent increase in WVTR. Specifically, F2 shows a significant ($P<0.05$) rise to 0.830 ± 0.05 $kg \cdot s^{-1} \cdot m^{-2} \cdot Pa^{-1}$, and this trend continues with F3 escalating to 0.990 ± 0.06 $kg \cdot s^{-1} \cdot m^{-2} \cdot Pa^{-1}$, and ending with F4 reaching the peak at 1.030 ± 0.08 $kg \cdot s^{-1} \cdot m^{-2} \cdot Pa^{-1}$. These increases are significant ($P<0.05$) and correlate with rising mucilage levels, indicating its hydrophilic nature which enhances moisture transmission.

Equally, a reduction in WVTR is observed in formulations F5 and F6, which report values of 0.680 ± 0.09 $kg \cdot s^{-1} \cdot m^{-2} \cdot Pa^{-1}$ and 0.750 ± 0.03 $kg \cdot s^{-1} \cdot m^{-2} \cdot Pa^{-1}$, respectively. This trend of decreasing WVTR becomes more pronounced with F7 and F8, where the results decrease to 0.470 ± 0.07 $kg \cdot s^{-1} \cdot m^{-2} \cdot Pa^{-1}$ and 0.490 ± 0.02 $kg \cdot s^{-1} \cdot m^{-2} \cdot Pa^{-1}$, marking them as the formulations with the most effective moisture barriers within the films. These decreases are significant ($P<0.05$) and suggest a higher proportion of nanocellulose, which is known for its barrier-enhancing properties. However, there is a slight rebound in WVTR in F9 and F10, with values rising again to 0.720 ± 0.06 $kg \cdot s^{-1} \cdot m^{-2} \cdot Pa^{-1}$ and 0.740 ± 0.06 $kg \cdot s^{-1} \cdot m^{-2} \cdot Pa^{-1}$, though these do not reach the higher levels seen in the initial formulations. Finally, F11 and F12 show increased WVTRs again at 0.850 ± 0.03 $kg \cdot s^{-1} \cdot m^{-2} \cdot Pa^{-1}$ and 0.940 ± 0.09 $kg \cdot s^{-1} \cdot m^{-2} \cdot Pa^{-1}$, indicating a decrease in barrier effectiveness possibly due to further increases in mucilage or reductions in nanocellulose. The control films, F-CN13 and F-CM14, highlight the critical roles of the primary components. F-CN13, which lacks mucilage, ties for the lowest WVTR at 0.470 ± 0.02 $kg \cdot s^{-1} \cdot m^{-2} \cdot Pa^{-1}$, emphasizing nanocellulose's moisture-blocking capability.

In contrast, F-CM14, lacking nanocellulose, shows a much higher WVTR of 0.890 ± 0.04 $kg \cdot s^{-1} \cdot m^{-2} \cdot Pa^{-1}$, demonstrating how essential nanocellulose is for maintaining low moisture permeability. Among all these observations, F8 stands out as the formulation that achieves an optimal balance, resulting in a WVTR that is significantly ($P< 0.05$), lower than those with higher mucilage content but sufficiently flexible to allow some moisture

interaction, which is vital for applications requiring controlled moisture environments. (Yousefi et al. 2024).

Table. 4.13 Effect of WVTR on film

Sample Code	WVTR ($kg \cdot s^{-1} \cdot m^{-2} \cdot Pa^{-1}$)
$F1_{(4+1)}$	0.690 ± 0.09^{d}
$F2_{(4+2)}$	0.830 ± 0.05^{h}
$F3_{(4+3)}$	0.990 ± 0.06^{l}
$F4_{(4+4)}$	1.030 ± 0.08^{m}
$F5_{(4.5+3)}$	0.680 ± 0.09^{c}
$F6_{(4.5+4)}$	0.750 ± 0.03^{g}
$F7_{(5+3)}$	0.470 ± 0.07^{a}
$F8_{(5+4)}$	0.490 ± 0.02^{b}
$F9_{(5.5+3)}$	0.720 ± 0.06^{e}
$F10_{(5.5+4)}$	0.740 ± 0.06^{f}
$F11_{(6+3)}$	0.850 ± 0.03^{i}
$F12_{(6+4)}$	0.940 ± 0.09^{k}
$F\text{-}CN13_{(5+0)}$	0.470 ± 0.02^{a}
$F\text{-}CM14_{(0+4)}$	0.890 ± 0.04^{j}

[1]Data are represented as mean ± SEM (n=3) [a-m] Means within the column with different lowercase superscripts are significantly (P< 0.05), different from each other

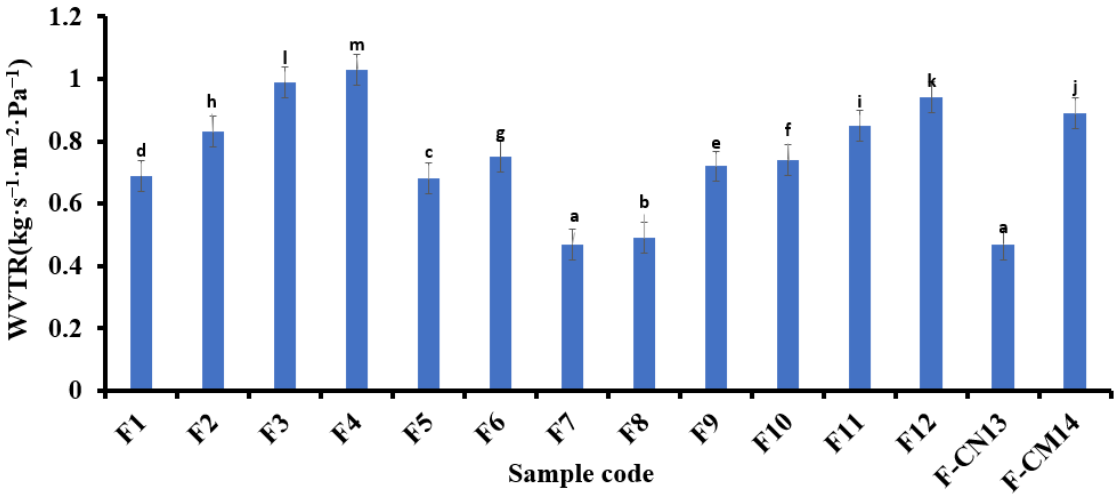

Figure 4.37 Effect of WVTR on film

4.11.2.6 Effect of water solubility on film

As illustrated in **Table 4.14** and **Figure 4.38** the water solubility data for nanocellulose-based films from formulations F1 to F-CM14 provides a comprehensive overview of how different concentrations of nanocellulose and mucilage affect the films' ability to absorb water. Here is a detailed narrative explaining the trends observed. Starting with F1, which has a water solubility of 35.62 ± 2.02 %, we establish a baseline for comparison. As we progress to F2, there is a slight increase to 37.70 ± 2.06 %, indicating a modest rise in water solubility that suggests an increase in mucilage content or a decrease in nanocellulose. This trend continues with F3 and F4, where solubility rises to 39.61 ± 1.36% and 41.33 ± 1.06 %, respectively. The significant ($P<0.05$) increases here point to a higher hydrophilicity, likely due to increased mucilage content which enhances the film's capacity to absorb water. Conversely, F5 and F6 show reductions in water solubility to 33.51 ± 2.09 % and 35.96 ± 1.87 %, aligning closer to the baseline established by F1. This suggests adjustments in the formulations that either increase nanocellulose or decrease mucilage, enhancing the structural properties of the films but reducing their hydrophilicity.

A noticeable decrease in water solubility is observed from F7 to F10, where values drop to 22.90 ±1.56 % and 31.92 ± 1.74 %. This trend indicates a significant ($P<0.05$) enhancement in the moisture barrier properties of the films, likely due to increased nanocellulose concentrations which inhibit water absorption. In contrast, F11 and F12 show a significant ($P<0.05$) increase in water solubility, reaching 49.71 ± 2.07 % and 50.24 ± 2.09 %, the highest in the series. This substantial rise can be attributed to a high mucilage content, which significantly ($P< 0.05$), increases the hydrophilicity of films, making them more susceptible to water absorption. The control films, F-CN13 and F-CM14, strongly illustrate the effects of neglecting key components. F-CN13, with no mucilage, shows the lowest solubility at 12.65 ± 2.12 %, indicating that mucilage is crucial for water interaction.

Meanwhile, F-CM14, lacking nanocellulose, has the highest solubility at 57.78 ± 1.89%, highlighting how the absence of nanocellulose allows hydrophilic properties of mucilage to dominate, greatly enhancing the film's water solubility. Overall, the data indicates that increases and decreases in water solubility significantly ($P<0.05$) depending on the

mucilage and nanocellulose content. Films with higher mucilage content show increased solubility, making them more suitable for applications requiring high water interaction, while those with higher nanocellulose content offer better moisture barrier properties, ideal for protective applications (Yousefi et al. 2024).

Table. 4.14 Effect of water solubility on film

Sample Code	Water Solubility (%)
$F1_{(4+1)}$	35.62 ± 2.02^{g}
$F2_{(4+2)}$	37.70 ± 2.06^{i}
$F3_{(4+3)}$	39.61 ± 1.36^{j}
$F4_{(4+4)}$	41.33 ± 1.06^{k}
$F5_{(4.5+3)}$	33.51 ± 2.09^{f}
$F6_{(4.5+4)}$	35.96 ± 1.87^{h}
$F7_{(5+3)}$	27.90 ± 1.56^{e}
$F8_{(5+4)}$	27.97 ± 1.98^{e}
$F9_{(5.5+3)}$	26.50 ± 1.56^{d}
$F10_{(5.5+4)}$	26.92 ± 1.74^{d}
$F11_{(6+3)}$	23.71 ± 2.07^{c}
$F12_{(6+4)}$	21.24 ± 2.09^{b}
$F\text{-}CN13_{(5+0)}$	12.65 ± 2.12^{a}
$F\text{-}CM14_{(0+4)}$	57.78 ± 1.89^{l}

[1]Data are represented as mean ±SEM (n=3)[a-l] Means within the column with different lowercase superscripts are significantly ($P < 0.05$), different from each other

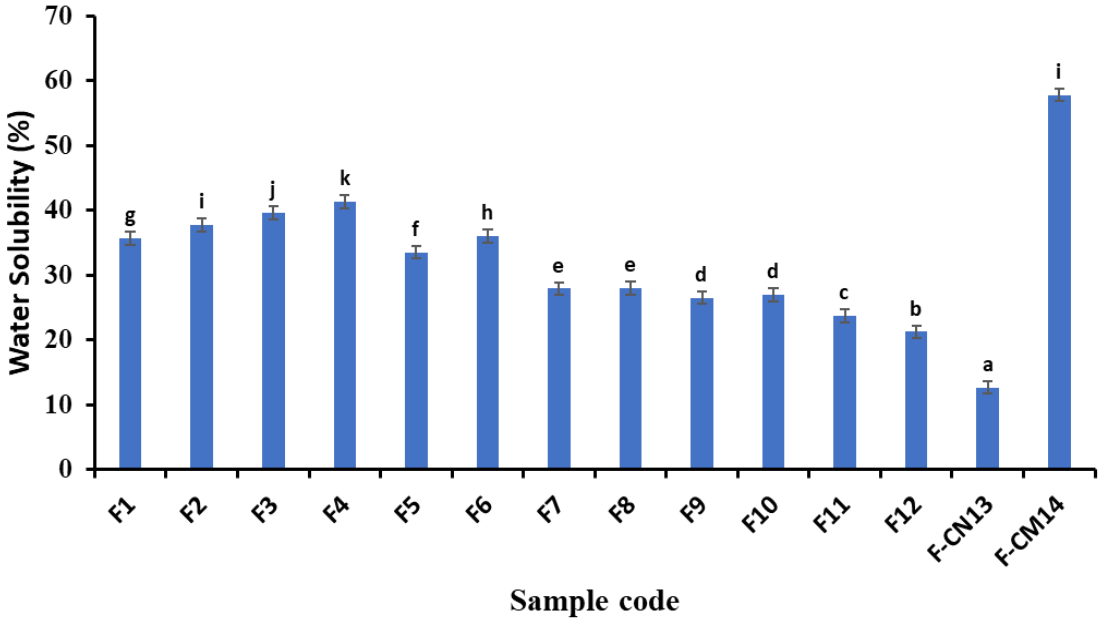

Figure 4.38 Effect of Water Solubility on Film

4.11.2.7 Effect of water uptake capacity on the film

As depicted in **Table 4.15** and **Figure 4.39,** The analysis of Water Uptake Capacity for nano cellulose-based films across formulations F1 to F-CM14 provides a detailed understanding of how variations in component concentrations affect the ability of film to absorb and retain water. Starting with F1, which records a water uptake capacity of 26.95 ± 1.67 %, a baseline is established for assessing the hydrophilic properties of these films. As we progress to F2 and F3, slight increases to 27.10 ± 1.56 % and 27.98 ± 0.89 % are observed, indicating a gradual enhancement in the films' capacity to absorb water. This trend is slightly continued in F4, which reaches a water uptake of 28.11 ± 1.78 %, suggesting an incremental increase in mucilage content which enhances hydrophilicity.

However, a noticeable shift occurs from F5 to F8, where water uptake capacities drop significantly ($P< 0.05$), with F7 and F8 recording lower values of 18.40 ± 2.78 % and 19.68 ± 2.89 %, respectively. This reduction points to either an increase in nanocellulose or a decrease in mucilage, enhancing the structural integrity of the films and reducing their ability to hold water, reflecting a stronger barrier effect against moisture absorption.

Contrastingly, F9 through F12 demonstrate a reverse trend, with capacities climbing to 33.33 ± 1.67 % for F12. This increase likely results from a reduction in nanocellulose or an increase in mucilage, thereby improving the films' hydrophilic properties. The peak values in F11 and F12 suggest a careful balance of components that maximize water absorption without significantly ($P< 0.05$), compromising the structural integrity.

The control films, F-CN13 and F-CM14, offer clear contrasts in their compositions and performances. F-CN13, which does not contain mucilage, still demonstrates a considerable absorption capacity of 36.17 ± 2.98%.

Table. 4.15 Effect of water uptake capacity on film

Sample Code	Water Uptake Capacity (%)
$F1_{(4+1)}$	26.95 ± 1.67^{e}
$F2_{(4+2)}$	27.10 ± 1.56^{f}
$F3_{(4+3)}$	27.98 ± 0.89^{f}
$F4_{(4+4)}$	28.11 ± 1.78^{g}
$F5_{(4.5+3)}$	22.20 ± 1.56^{c}
$F6_{(4.5+4)}$	23.98 ± 1.89^{d}
$F7_{(5+3)}$	18.40 ± 2.78^{a}
$F8_{(5+4)}$	19.68 ± 2.89^{b}
$F9_{(5.5+3)}$	28.14 ± 2.98^{g}
$F10_{(5.5+4)}$	29.79 ± 1.76^{i}
$F11_{(6+3)}$	30.68 ± 2.07^{j}
$F12_{(6+4)}$	33.33 ± 1.67^{k}
$F\text{-}CN13_{(5+0)}$	36.17 ± 2.98^{l}
$F\text{-}CM14_{(0+4)}$	39.86 ± 1.78^{m}

[1]Data are represented as mean ± SEM (n=3) $^{a\text{-}m}$ Means within the column with different lowercase superscript are significantly ($P< 0.05$), different from each other

In contrast, F-CM14, which lacks nanocellulose, shows the highest absorption capacity among the films tested, recording 39.86 ± 1.78%. These results highlight the crucial roles both components play, with nanocellulose significantly ($P< 0.05$), impacting the film's ability to limit water uptake due to its barrier properties, whereas the absence of

nanocellulose in F-CM14 allows for maximal water absorption. Overall, the data demonstrates that the water uptake capacities are significantly ($P< 0.05$), influenced by the mucilage and nanocellulose ratios within the films. Films with higher mucilage content are more suitable for applications where moisture retention is beneficial, whereas those with higher nanocellulose content serve better in applications requiring strong moisture barriers.

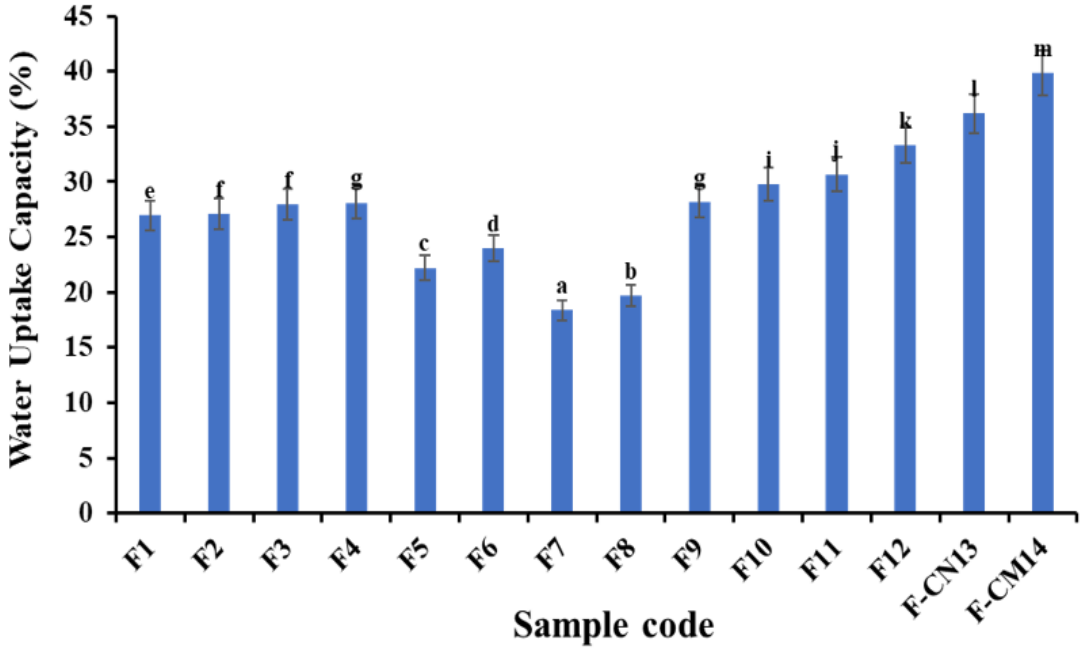

Figure 4.39 Effect of water uptake capacity on the film

This detailed understanding is crucial for developing film formulations tailored to specific environmental interactions and functional requirements. The significance of F8 lies in its formulation, which intelligently combines 5 parts nanocellulose with 4 parts mucilage. This ratio ensures that the film maintains a robust structural backbone provided by the nanocellulose, effectively preventing excessive water absorption that could lead to structural weakening. At the same time, the substantial presence of mucilage enhances the film's ability to interact with moisture, making it neither too hydrophobic nor overly susceptible to water ingress (Yousefi et al. 2024).

4.12 Characterizations of nanocellulose-based composite films

4.12.1 Confirmation of functional groups of nanocellulose-based composite film

The FTIR analysis of formulation F8 provides crucial insights into the molecular structure and interactions of its components, indicating functional properties of the developed nano cellulose-mucilage composite film as shown in **Figure 4.40** and at a wavelength of 3278 CM^{-1}, the presence of intramolecular and intermolecular hydrogen-bonded O-H stretching vibrations reflects the material's hydrophilicity, which is conducive to applications requiring good moisture affinity, such as biodegradable packaging materials. The peak at 2925 CM^{-1}, representing the C-H stretching band of polysaccharides, confirms the presence of carbon and hydrogen molecules in the cellulose structure, reinforcing the understanding of the basic polysaccharide framework of the film. Similarly, the C=O stretching vibration observed at 1743 CM^{-1} can be attributed to proteins in the mucilage and possibly to ester groups present in modified cellulose, indicating a composite matrix where protein integration with cellulose enhances structural integrity and potentially influences the mechanical properties of the film.

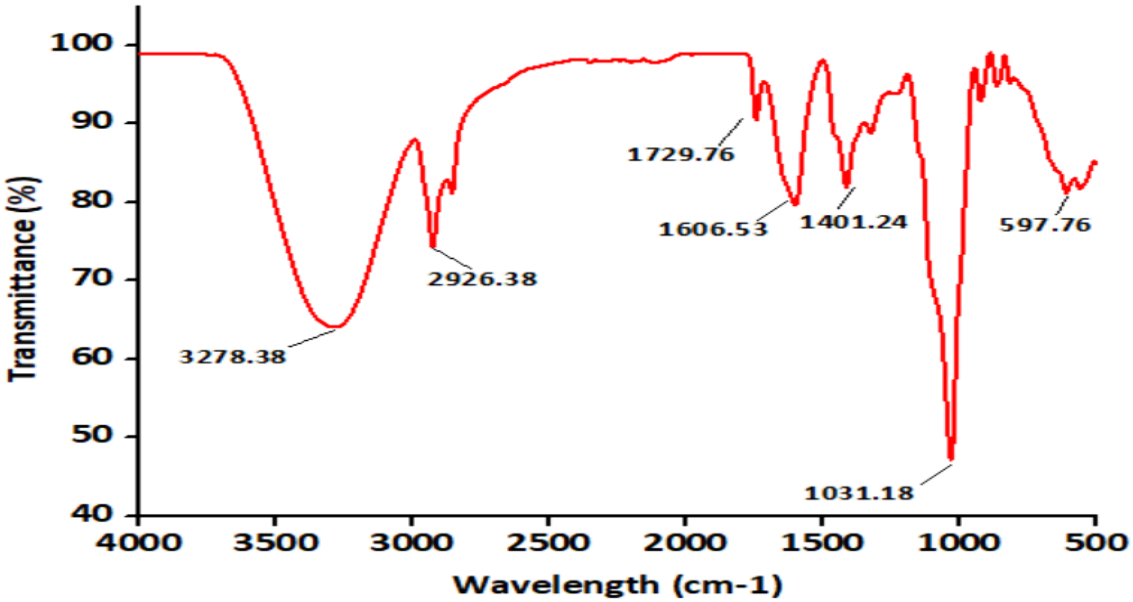

Figure 4.40 Confirmation of functional groups of nanocellulose-based composite film

The wavelength of 1600 CM^{-1}, marked by -OH stretching, suggests the film's hygroscopic nature, which is critical for applications that require moisture sensitivity. The bending vibration of N-H groups at 1413 CM^{-1}, along with the indication of the pyranose ring structure, points to the involvement of nitrogenous compounds from the mucilage, suggesting additional cross-linking within the film structure which can improve its barrier properties. At 1030 CM^{-1}, the presence of cellulosic β-glycosidic linkages denotes the fundamental structure of cellulose, crucial for maintaining the mechanical strength and stability of the fibers. The peak at 863 CM^{-1} further supports the film's hydrophilicity, identified by O-H hydroxyl group stretching of hydrogen bond groups in cellulose and sugars. Lastly, the C-H hydrocarbyls peak at 608 CM^{-1} emphasizes the polysaccharide base of the film, consistent with other features identified in the spectrum. Overall, the FTIR spectrum of F8 confirms a complex interaction of nanocellulose and mucilage, which results in a film that exhibits both desirable mechanical properties and hydrophilicity.

4.12.2 Confirmation of surface morphology nanocellulose-based composite film

As shown in **Figure 4.41** the nanocellulose-based film incorporated with aloe vera mucilage, when magnified 1000 × exhibits a densely interconnected fibrous structure, indicative of a strong network of nanocellulose fibers. The integration of aloe vera mucilage within this network appears seamless, with no visible phase separation, suggesting a homogeneous composite material. The higher magnification reveals a textured surface, where the aloe vera mucilage likely occupies the spaces between the fibers, potentially contributing to the film's overall flexibility and moisture retention properties. The SEM images at this magnification also highlight the smooth regions within the fibrous matrix, which can be attributed to the presence of the mucilage.

This smoothness in the context of the rough fibrous texture suggests that the mucilage could be acting as a plasticizing agent, imbuing the film with improved handling characteristics, which are essential for practical packaging applications. Moreover, the consistent texture across the film surface implies a uniform distribution of the aloevera mucilage, which is essential for the film's mechanical and barrier functions. The surface

morphology, as evidenced by the SEM analysis, is complex and indicates a material that has incorporated the biological and physical attributes of its components—nanocellulose and aloe vera mucilage—into a singular, potentially biodegradable, and functional film.

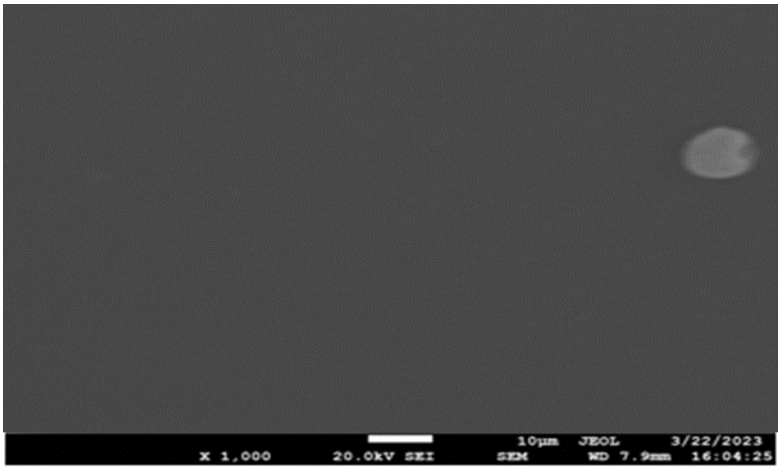

Figure 4.41 Confirmation of surface morphology nanocellulose-based composite film

4.12.3 Confirmation of thermal stability nanocellulose based composite film

The Thermogravimetric Analysis (TGA) of the sample reveals critical insights into its thermal stability and degradation profile across different temperature ranges, crucial for determining its applicability in environments subjected to varying thermal conditions in **Figure 4.42** in the first stage of degradation, a weight loss of 22.40% is observed at 150℃. This loss primarily represents the evaporation of absorbed water within the sample, indicative of its hydrophilic nature. The removal of water at this stage is consistent with the presence of hydrophilic functional groups, such as -OH groups, as identified in the FTIR analysis. This stage highlights the sample's capacity to retain moisture, which can be advantageous in applications where moisture regulation is required but also poses limitations in high-temperature applications due to early moisture loss.

The second stage shows a more substantial weight loss, accounting for 47.57% at 380℃. This significant ($P<0.05$) reduction in mass is attributed to the degradation of the matrix's intermolecular hydrogen bonds and a dehydration reaction on the polymer chain, coupled with the breakdown of the main backbones of the polymers. This stage is critical as it reflects the thermal stability of the organic components of the sample, particularly the

cellulose and mucilage constituents. The degradation at this temperature range suggests a limitation in applications involving prolonged exposure to high temperatures, as structural integrity may be compromised.

In the third stage, there is a smaller weight loss observed (9.50%) at 800℃, which indicates the carbonization of the organic materials. This residual mass represents the char yield, which is indicative of the material's content that is resistant to complete degradation even at high temperatures. This stage is essential for evaluating the potential use of the material in applications requiring thermal resistance, as the char formed can provide a barrier effect in fire retardancy applications. Overall, the TGA results demonstrate that the material undergoes thermal transitions, which are crucial for its potential applications. The hydrophilic nature inferred from the early water loss suggests suitability for moisture-sensitive applications, while the decomposition and carbonization profiles limit its use in environments with temperatures exceeding 380℃.

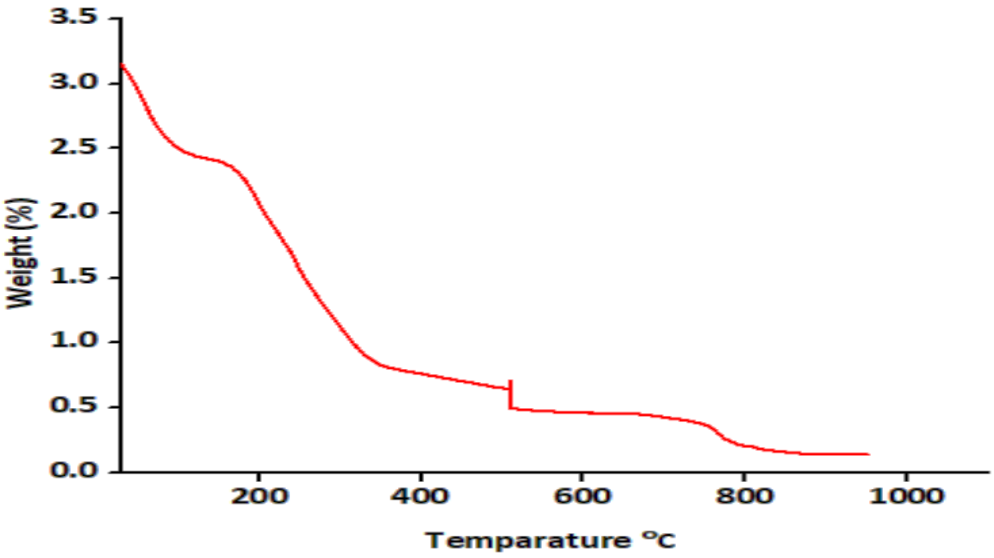

Figure 4.42 Confirmation of thermal stability nanocellulose composite film

4.13 Comparative surface morphology analysis of Nanocomposite, Nanocellulose, and Mucilage Film

The SEM images provided in **Figure 4.43**, all three films—(A) nanocomposite film (F8), (B) nanocellulose film (CN-38), and (C) mucilage film (CM-39)—are observed at the same

magnification scale. The magnification for each image is set at 1,000 times (x 1,000). This scale is noted in the images themselves, allowing for a detailed view of the surface morphology of each film type. This image A shows a nanocomposite film with a highly porous and irregular structure. The morphology is characterized by a layered and fluffy appearance, typical for films incorporating organic or natural materials such as mucilage. These structures are likely to contribute to improved gas permeability and may also have enhanced biodegradability due to the presence of natural components.

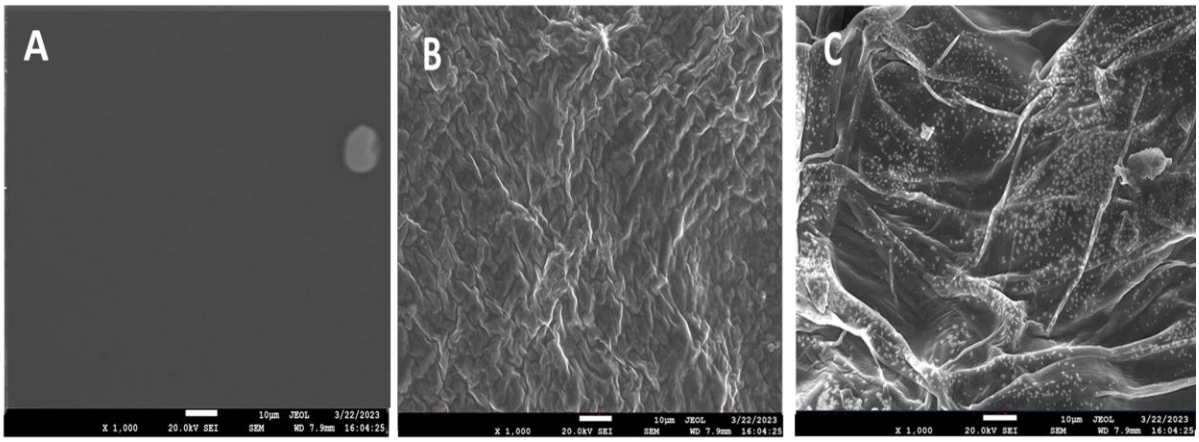

Figure 4.43: Surface morphology of selected nanocomposite film (A) Nanocomposite films (F8) (B) Nanocellulose film (CN-38) (C) Mucilage film (CM-39)

While nanocellulose film (B) has its merits in terms of strength and sustainability, the presence of cracks can make it less desirable for applications requiring robust barrier properties and mechanical integrity. The nanocomposite film (A), with its more uniform and intact structure, tends to provide better functionality in these areas, making it a more efficient choice for a wider range of packaging needs. This highlights the importance of choosing the right material based on the specific requirements of the packaging application, considering both the material properties and the environmental conditions to which the packaging will be exposed. The image C features a film composed only of mucilage. This film exhibits a highly heterogeneous surface with large, irregular structures and visible fissures. The presence of scattered particles could indicate impurities or components that

did not completely integrate during the film formation. This morphology suggests that while the film might have good flexibility and water retention properties, it could be mechanically weaker and less uniform than the other two films.

The nanocomposite film (A) is potentially better than the other options if the criteria for selection include a balance of mechanical properties, environmental impact, and versatility. Its ability to degrade more naturally, coupled with its robust functionality, makes it a superior choice in scenarios where both performance and sustainability are critical. This makes it particularly suitable for industries moving towards green solutions without wanting to compromise on the quality and durability of packaging.

4.14 Biodegradability of film

As shown in **Figure 4.44** the biodegradability of the nanocellulose-based films with aloe vera mucilage is monitored over 23 days in the lab conditions. The film is whole and unaltered on Day 0. Degradation is evident by Day 3, with visible changes in color and texture. The film exhibits further decomposition by Day 7, breaking down into larger fragments. By Day 12, the fragmentation is more extensive, with the film structure continuing to deteriorate. On Day 18, only small pieces of the film are observable, and by Day 23, the film has almost completely disintegrated, leaving behind very little residue. This sequence of images demonstrates the biodegradation process, with the film showing substantial decomposition, which is an indicator of good biodegradability, a critical property for environmentally friendly packaging materials. The presence of aloe vera mucilage is likely a significant factor in the observed rate of degradation due to its biocompatible nature that encourages microbial digestion, leading to the breakdown of the film.

The comprehensive analysis of nanocellulose-based composite films with aloe vera mucilage through FTIR, SEM, TGA, and biodegradability studies provides insights into their properties. FTIR confirms hydrophilicity and mechanical reinforcement from protein-cellulose interactions. SEM shows a strong, flexible fibrous structure, essential for packaging. TGA indicates thermal stability suitable for moderate temperatures but not for

high-temperature applications. The biodegradability tests demonstrate fast decomposition, making these films a promising environmentally friendly alternative for packaging. Together, these results support the use of these films in sustainable packaging applications.

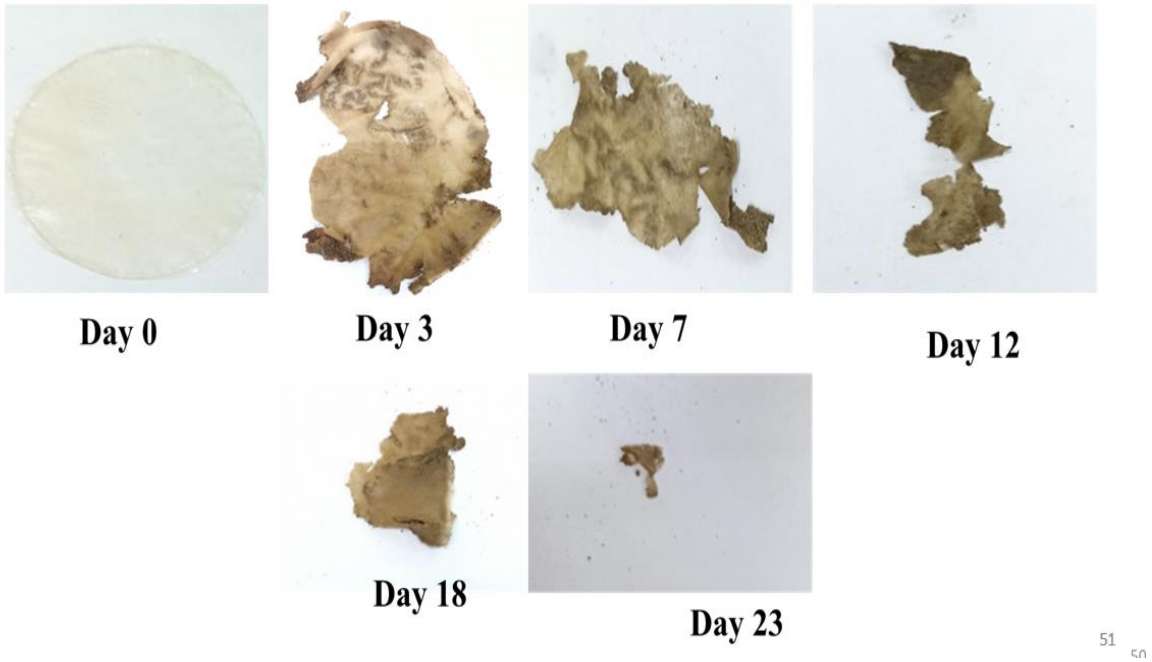

Figure 4.44 Biodegradability of film

4.15 Application of nanocellulose based composite films

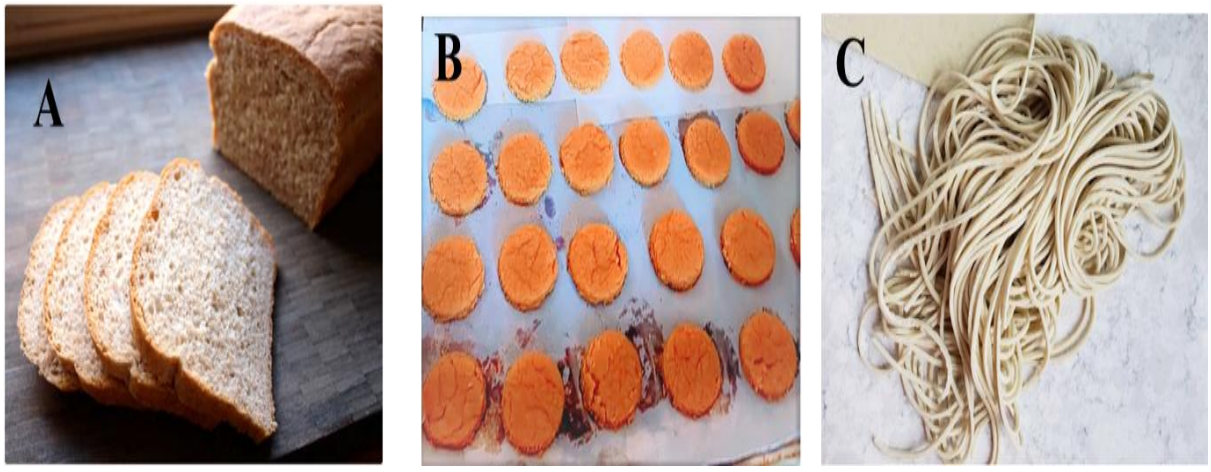

Figure 4.45 Prepared Bakery products (A) Bread (B) Biscuit (c) Noodles

4.15.1 Shelf-life evaluation of bakery product

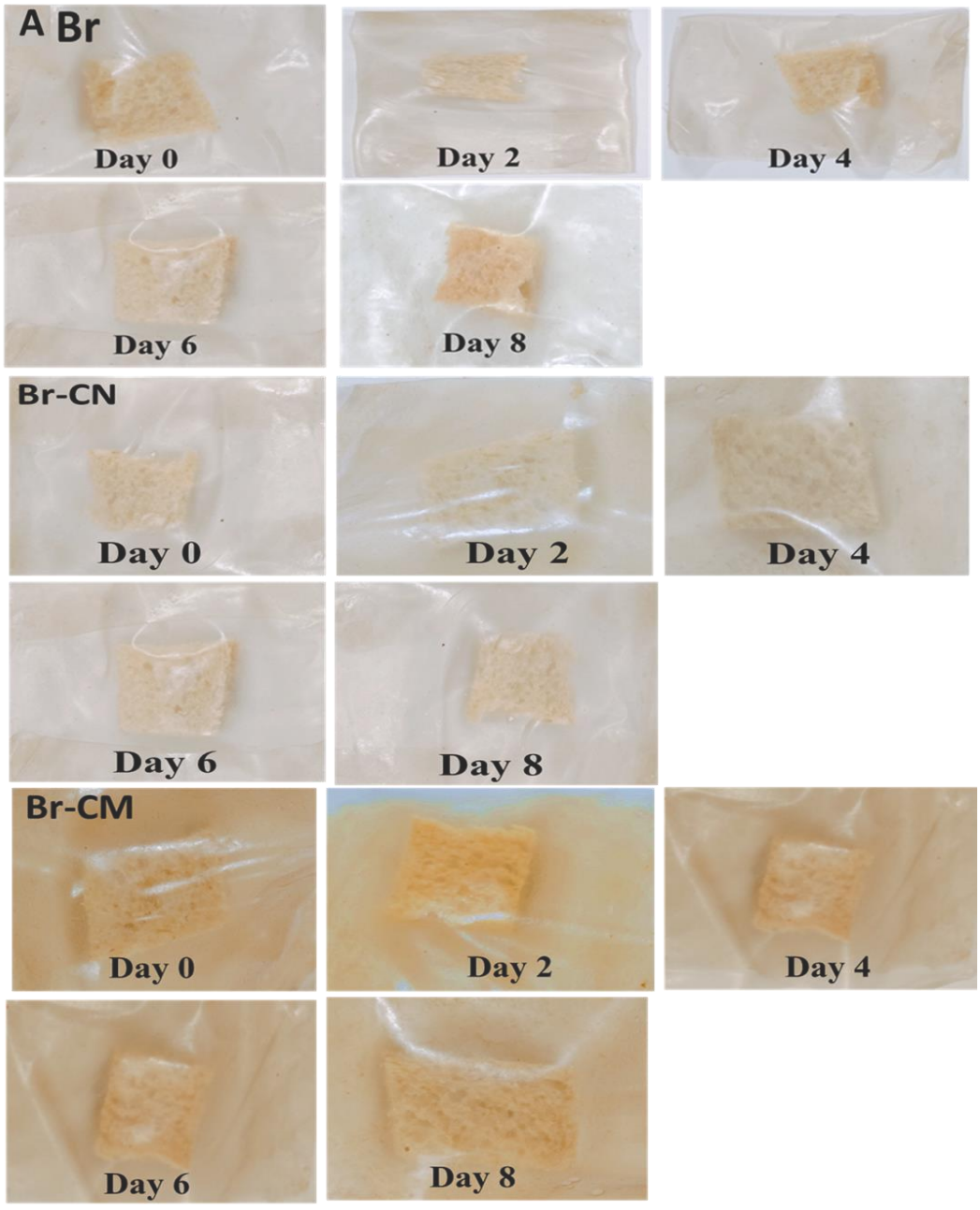

Figure 4.46 Shelf-life evaluation of bread packaged in (A) Selected film (Br) (B) Br-NC film (C) Br-CM film

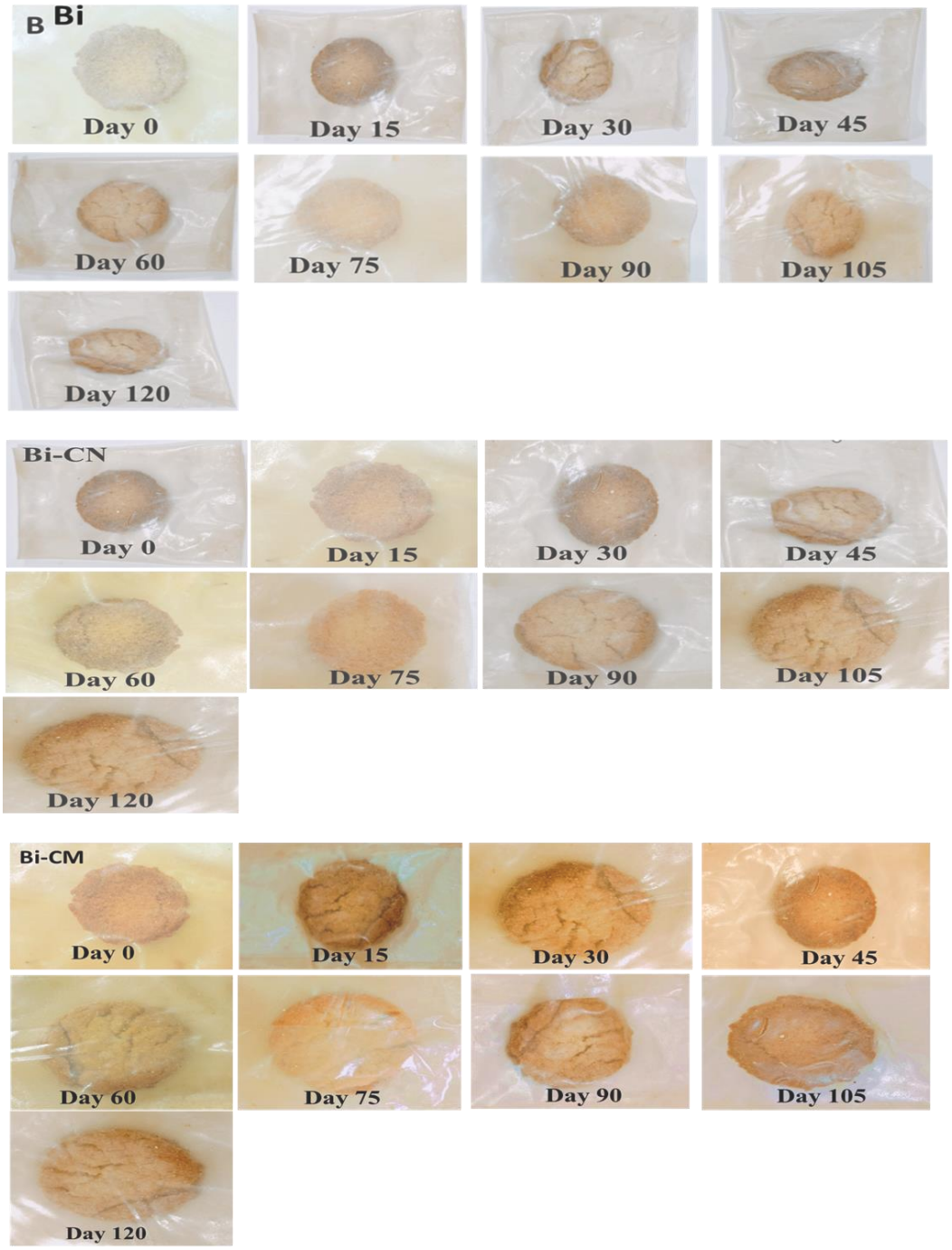

Figure 4.47 Shelf-life evaluation of biscuits packaged in (A) Selected film (Bi) (B) Bi-NC film (C) Bi-CM film

Figure 4.48 Shelf-life evaluation of noodles packaged in (A) Selected film (Nd) (B) Nd-NC film (C) Nd-CM film

4.15.1.1 Effect on proximate analysis of bakery products (Bread, biscuit and noodles) during storage

4.15.1.1.1 Effect on proximate analysis of bread during storage

Table 4.16 provides a detailed proximate analysis of bread (denoted as Br) packaged in nanocomposite films over 8 days, with measurements taken at 2-day intervals. The parameters analyzed include moisture content, ash content, crude fat, protein content, and crude fiber. On Day 0 (Br0), the initial moisture content of the bread was observed at 35.34 ± 2.67 %, establishing the baseline moisture level. By Day 2 (Br2), the moisture content slightly increased to 35.84 ± 1.98%, with a non-significant ($P > 0.05$) change, indicating that the moisture level remained relatively stable in the initial days. On Day 4 (Br4), the moisture content decreased slightly to 34.97 ± 2.07%, still showing non-significant ($P>0.05$) change. By Day 6 (Br6), the moisture content dropped further to 33.75 ± 2.76%, indicating a trend towards moisture loss, but it was still not statistically significant ($P>0.05$). Finally, on Day 8 (Br8), the moisture content significantly ($P < 0.05$) decreased to 28.78 ± 2.19, marking a substantial reduction in moisture content by day 8 significantly ($P < 0.05$).

The initial ash content on Day 0 (Br0) is 0.87 ± 0.08 %. By Day 2 (Br2), the ash content remained at 0.87 ± 0.07%, showing a non-significant ($P>0.05$) change from Day 0. On Day 4 (Br4), a slight decrease to 0.85 ± 0.04 % is recorded, which was significant ($P < 0.05$), indicating a minor reduction. By Day 6 (Br6), the ash content further decreases to 0.84 ± 0.06^{c}, showing a continuous significant ($P<0.05$) decline Finally, on Day 8 (Br8), the ash content drops to 0.82 ± 0.04 %, marking a significant ($P<0.05$) decrease from the initial value. On 0 Day (Br0), the initial crude fat content was 0.62 ± 0.03 %. By Day 2 (Br2), it maintains at 0.62 ± 0.06 %, with a non-significant ($P > 0.05$) difference. On Day 4 (Br4), the fat content slightly decreased to 0.61 ± 0.04 %, a significant ($P<0.05$). By Day 6 (Br6), it remains at 0.61 ± 0.09 %, indicating a further significant ($P<0.05$) decline. Finally, on Day 8 (Br8), the crude fat content drops to 0.59 ± 0.01 %, showing a continuous significant ($P<0.05$) reduction over time. The initial protein content on Day 0 (Br0) is 12.09 ± 1.08 %. By Day 2 (Br2), it stays the same at 12.09 ± 0.88 %, with non-significant ($P>0.05$) change.

On Day 4 (Br4), the protein content slightly decreased to 12.08 ± 0.79 %, a significant (P< 0.05) difference. By Day 6 (Br6), it maintained at 12.08 ± 0.76% and showed a statistically significant (P<0.05) decline. Finally, on Day 8 (Br8), the protein content was significant (P < 0.05). dropped to 0.82 ± 0.39 %, showed a considerable reduction.

The initial crude fiber content on Day 0 (Br0) is 0.87 ± 0.08 %. By Day 2 (Br2), it remains unchanged at 0.87 ± 0.06%, with a non-significant (P>0.05) difference. On Day 4 (Br4), it slightly decreased to 0.87 ± 0.03 %, a significant (P<0.05) change. By Day 6 (Br6), it further decreased to 0.86 ± 0.01 %, showing another significant (P<0.05) reduction. Finally, on Day 8 (Br8), the crude fiber content was 0.85 ± 0.08%, indicating a continuous significant (P<0.05) decrease over time. In summary, this detailed proximate analysis shows that over the 8 days, there was a significant (P<0.05) decrease in the ash content, moisture content, protein, crude fat, and crude fiber of the bread packaged in nanocomposite films. The statistical significance of the changes is indicated by the different superscript letters, highlighting the progressive degradation of the bread's nutritional components over time.

Table 4.16 Effect on proximate analysis of bread samples during storage analysis

Days	Moisture %	Ash Content %	Crude Fat %	Protein content %	Crude Fiber %
Br0	35.34 ± 2.67^{b}	0.87 ± 0.08^{c}	0.62 ± 0.03^{a}	12.09 ± 1.08^{a}	0.87 ± 0.08^{a}
Br2	35.84 ± 1.98^{b}	0.87 ± 0.07^{c}	0.62 ± 0.06^{a}	12.09 ± 0.88^{a}	0.87 ± 0.06^{a}
Br4	34.97 ± 2.07^{b}	0.86 ± 0.04^{b}	0.62 ± 0.04^{a}	12.08 ± 0.79^{a}	0.87 ± 0.03^{a}
Br6	33.75 ± 2.76^{b}	0.86 ± 0.06^{b}	0.62 ± 0.09^{a}	12.08 ± 0.76^{a}	0.86 ± 0.01^{a}
Br8	28.78 ± 2.19^{a}	0.85 ± 0.04^{a}	0.52 ± 0.01^{a}	12.01 ± 0.39^{a}	0.85 ± 0.08^{a}

[1]Data are disciplined as mean ± SEM (n=3) $^{a-b}$ with each column with different lowercase superscripts are different significantly (P< 0.05), from one another

4.15.1.1.2 Effect on proximate analysis of biscuits samples during storage analysis

Table 4.17 provides the proximate analysis of biscuits over 120 days revealing specific trends in their composition, emphasizing the effectiveness of the packaging in maintaining product quality. Initially, the moisture content showed a significant (P<0.05) increase from 1.79 ± 1.23 % to 5.14 ± 1.23 %. The initial moisture content of the biscuits (Bi0) was 1.79

± 1.23 %. This value remains relatively stable until Bi15 at 1.04 ± 1.23 %, showing non-significant (P>0.05) change.

However, by Bi30, the moisture content increases to 2.64 ± 1.23%, and further increases are observed at (Bi45) 2.89 ± 1.23%, (Bi60) 3.14 ± 1.23%, (Bi75) 3.64 ± 1.23%, and (Bi90) 4.93 ± 1.23%. A notable significant (P<0.05) increase was recorded at Bi120, with a moisture content of 8.94 ± 1.23%, indicating that over time, the biscuits absorbed more moisture. The ash content remains fairly constant from Bi0 (0.87 ± 0.51) to Bi120 (0.79 ± 0.51), showing non-significant (P> 0.05) changes across all intervals. This consistency suggests that the inorganic mineral content in the biscuits remained stable throughout the storage period. The crude fat content starts at 35.88 ± 1.72 % at Bi0 and remains relatively stable across all intervals. Slight decreases are noted at (Bi15) 35.81 ± 1.72 %, (Bi30) 35.77 ± 1.72% (Bi45) 35.65 ± 1.72), Bi60 (35.58 ± 1.72), Bi75 (35.43 ± 1.72), Bi90 (35.33 ± 1.72), and Bi105 (35.24 ± 1.72). The crude fat content remains consistent, indicating that the lipid content did not undergo significant (P>0.05) changes over time.

The protein content starts at 8.67 ± 1.09 at Bi0 and shows slight decreases over time. By Bi15, it is 8.65 ± 1.09, and by Bi30, it slightly drops to 8.63 ± 1.09. significant (P<0.05) decreases are observed at Bi45 (8.59 ± 1.09), Bi60 (8.56 ± 1.09), Bi75 (8.51 ± 1.09), Bi90 (8.47 ± 1.09), Bi105 (8.43 ± 1.09), and Bi120 (8.36 ± 1.09. These changes suggest a gradual decline in protein content over time. The crude fiber content starts at 0.36 ± 0.02 at Bi0 and remains stable until Bi15 at 0.36 ± 0.02. By Bi30, it slightly decreases to 0.34 ± 0.02 and remains constant at Bi45 (0.34 ± 0.02) and Bi60 (0.34 ± 0.02). Further significant (P<0.05) decreases are observed at Bi75 (0.33 ± 0.02), Bi90 (0.32 ± 0.02), Bi105 (0.32 ± 0.02), and Bi120 (0.31 ± 0.02) (P < 0.05).

This indicates a gradual decrease in crude fiber content over time. The carbohydrate content starts at 52.79 ± 1.02 at Bi0 and shows minor decreases until Bi15 (52.65 ± 1.72). significant (P<0.05) decreases are observed at Bi30 (52.13 ± 1.13), Bi45 (52.06 ± 1.82), Bi60 (51.93 ± 1.92), Bi75 (51.65 ± 1.25), Bi90 (51.51 ± 1.29), and Bi105 (51.31 ± 1.42). By Bi120, a more significant P<0.05) decrease is noted (50.81 ± 1.92). This trend indicates a steady reduction in carbohydrate content over time. Over the 120 days, biscuits showed

significant (P<0.05) increases in moisture content, with corresponding decreases in protein, crude fiber, and carbohydrate contents, indicating potential moisture absorption and nutrient degradation over time. The ash and crude fat contents remained relatively stable, suggesting minimal changes in these components. These findings highlight the impact of storage duration on the nutritional composition of biscuits packaged in nanocomposite films.

Table 4.17 Effect on proximate analysis of biscuits samples during storage analysis

Days	Moisture %	Ash Content %	Crude Fat %	Protein Content %	Crude Fiber %	Carbohydrate %
Bi0	1.79 ± 0.23^{a}	0.87 ± 0.11^{a}	35.88 ± 2.67^{a}	8.67 ± 1.09^{a}	0.36 ± 0.02^{c}	52.79 ± 1.78^{b}
Bi15	1.84 ± 0.22^{a}	0.86 ± 0.41^{a}	35.81 ± 1.87^{a}	8.65 ± 0.34^{a}	0.36 ± 0.05^{c}	52.65 ± 1.54^{b}
Bi30	2.64 ± 0.27^{b}	0.85 ± 0.71^{a}	35.77 ± 1.45^{a}	8.63 ± 0.08^{a}	0.36 ± 0.04^{c}	52.13 ± 1.78^{b}
Bi45	2.89 ± 0.19^{b}	0.84 ± 0.81^{a}	35.65 ± 1.34^{a}	8.59 ± 0.05^{a}	0.36 ± 0.09^{c}	52.06 ± 1.98^{b}
Bi60	3.14 ± 0.78^{c}	0.83 ± 0.31^{a}	35.58 ± 1.23^{a}	8.56 ± 0.05^{a}	0.36 ± 0.07^{c}	52.93 ± 1.45^{b}
Bi75	3.64 ± 0.89^{c}	0.82 ± 0.61^{a}	35.43 ± 1.72^{a}	8.51 ± 0.03^{a}	0.35 ± 0.01^{b}	52.65 ± 1.34^{b}
Bi90	4.93 ± 0.23^{d}	0.81 ± 0.71^{a}	35.33 ± 1.56^{a}	8.47 ± 0.08^{a}	0.35 ± 0.01^{b}	52.51 ± 1.45^{b}
Bi105	6.27 ± 0.54^{e}	0.80 ± 0.11^{a}	35.24 ± 1.12^{a}	8.43 ± 0.09^{a}	0.35 ± 0.04^{b}	52.31 ± 1.67^{b}
Bi120	8.94 ± 1.23^{f}	0.79 ± 0.51^{a}	35.16 ± 1.34^{a}	8.36 ± 0.01^{a}	0.34 ± 0.03^{a}	51.81 ± 1.54^{a}

[1]Data are represented as mean ± SEM (n=3) $^{a-f}$ with each column with different lowercase superscripts different significantly (P >0.05) from one another

4.15.1.1.3 Effect on proximate analysis of noodles samples during storage analysis

Table 4.18 presents the proximate analysis of noodles (Nd) packaged in nanocomposite films over 120 days, with measurements taken at 15-day intervals. The parameters analyzed include crude fiber, moisture content, protein content, ash content, crude fat, and carbohydrate content. The initial moisture content of the noodles (Nd0) is 9.32 ± 1.45%. This value shows an increasing trend over time, indicating that the noodles absorbed moisture gradually. At Nd15, the moisture content increased slightly to 9.93 ± 1.98%, and by Nd30, it rose to 10.13 ± 1.68%. The moisture content continued to increase significantly (P < 0.05) at (Nd45) 10.87 ± 1.08%, (Nd60) 11.32 ± 1.67%, Nd75 (11.92 ± 1.07%), and Nd90 (12.65 ± 1.45%). A more pronounced increase was observed at Nd105 (14.76 ±

2.67%) and Nd120 (16.84 ± 2.06%), indicating a substantial rise in moisture content, which could affect the noodles' texture and shelf life.

The ash content measures the total mineral content of the noodles. Initially, the ash content at Nd0 is 1.87 ± 0.12%. There was a slight decrease over time, with values at (Nd15) 1.79 ± 0.25 %, (Nd30) 1.74 ± 0.44 %, (Nd45) 1.69 ± 0.76%, (Nd60) 1.65 ± 0.67%, and (Nd90) 1.57 ± 0.16 %. The ash content continued to decrease slightly at (Nd105) 1.54 ± 0.09% and (Nd120) 1.49 ± 0.18%, but these changes were non-statistically significant ($P > 0.05$), indicating that the inorganic mineral content remained relatively stable. The crude fat content begins at 5.63 ± 1.26 % at Nd0 and remains relatively stable over time. At Nd15, the crude fat content was 5.61 ± 1.86 %, showing a non-significant ($P> 0.05$) change. Similarly, values at (Nd30) 5.59 ± 0.89%, (Nd45) 5.58 ± 0.45%, (Nd60) 5.56 ± 1.56%, (Nd75) 5.53 ± 1.76%, and (Nd90) 5.51 ± 1.06% were consistent. A slight but statistically significant ($P<0.05$) decrease was observed at (Nd105) 5.47 ± 0.96 % and (Nd120) 5.46 ± 1.11%, indicating minimal changes in lipid content during storage. The protein content starts at 13.51 ± 2.06 at Nd0 and shows a slight decreasing trend. At Nd15, the protein content was 13.47 ± 1.16 %, and at Nd30, it slightly decreased to 13.46 ± 0.79 %. Subsequent values were (Nd45) 13.44 ± 1.71 %, (Nd60) 13.41 ± 1.16 %, (Nd75) 13.39 ± 0.98 %, and (Nd90) 13.36 ± 1.49 %. significant ($P<0.05$) decreases were observed at (Nd105) 13.31 ± 1.98 % and (Nd120) 13.27 ± 1.07 %, indicating a gradual decline in protein content over time.

The crude fiber content starts at 0.53 ± 0.04 % at Nd0 and remains stable initially. By Nd15, the crude fiber content was 0.53 ± 0.05%, with minor decreases observed at (Nd30) 0.53 ± 0.09 %, (Nd45) 0.52 ± 0.01 %, (Nd60) 0.51 ± 0.06 %, (Nd75) 0.49 ± 0.05, and Nd90 0.48 ± 0.02 %. Further decreases were noted at (Nd105) 0.47 ± 0.07 % and (Nd120) 0.47 ± 0.06%, indicating a slight reduction in crude fiber content over time. The carbohydrate content starts at 69.67 ± 1.04 % at Nd0 and shows a decreasing trend over time. By Nd15, it decreased to 69.02 ± 1.34%, with further significant ($P<0.05$) decreases observed at (Nd30) 68.78 ± 1.56%, (Nd45) 68.42 ± 1.76%, (Nd60) 68.06 ± 1.78%, (Nd75) 67.55 ± 0.87 % , and (Nd90) 66.92 ± 0.89 %. The lowest values were recorded at (Nd105) 65.42 ±

1.89 % and Nd120 64.94 ± 1.67%, indicating a significant (P<0.05) decline in carbohydrate content over time. In summary, the proximate analysis reveals that the moisture content of the noodles increases significantly (P < 0.05) over the 120 days, suggesting that the noodles absorb moisture, which could impact their quality and shelf life. Ash, crude fat, and protein contents show slight, non-significant (P > 0.05) decreases, while the crude fiber and carbohydrate contents decrease significantly (P <0.05) over time. These changes indicate that the noodles undergo compositional changes during storage, which could affect their nutritional value and textural properties.

Table. 4.18 Effect on proximate analysis of noodles samples during storage analysis

Days	Moisture %	Ash content %	Crude fat %	Protein content %	Crude fiber %	Carbohydrate %
Nd0	9.32 ± 1.45^{a}	1.87 ± 0.12^{a}	5.63 ± 1.26^{a}	13.51 ± 2.06^{a}	0.53 ± 0.04^{d}	69.67 ± 1.04^{d}
Nd15	9.93 ± 1.98^{a}	1.79 ± 0.25^{a}	5.61 ± 1.86^{a}	13.47 ± 1.16^{a}	0.53 ± 0.05^{d}	69.02 ± 1.34^{d}
Nd30	10.13 ± 1.68^{a}	1.74 ± 0.44^{a}	5.59 ± 0.89^{a}	13.46 ± 0.79^{a}	0.53 ± 0.09^{d}	68.78 ± 1.56^{d}
Nd45	10.87 ± 1.08^{a}	1.69 ± 0.76^{a}	5.58 ± 0.45^{a}	13.44 ± 1.71^{a}	0.52 ± 0.01^{c}	68.42 ± 1.76^{d}
Nd60	11.32 ± 1.67^{a}	1.65 ± 0.67^{a}	5.56 ± 1.56^{a}	13.41 ± 1.16^{a}	0.51 ± 0.06^{c}	67.06 ± 1.78^{c}
Nd75	11.92 ± 1.07^{a}	1.61 ± 0.65^{a}	5.53 ± 1.76^{a}	13.39 ± 0.98^{a}	0.49 ± 0.05^{b}	67.55 ± 0.87^{c}
Nd90	12.65 ± 1.45^{a}	1.57 ± 0.16^{a}	5.51 ± 1.06^{a}	13.36 ± 1.49^{a}	0.48 ± 0.02^{b}	66.92 ± 0.89^{c}
Nd105	14.76 ± 2.67^{b}	1.54 ± 0.09^{a}	5.47 ± 0.96^{a}	13.31 ± 1.98^{a}	0.47 ± 0.07^{a}	65.42 ± 1.89^{b}
Nd120	16.84 ± 2.06^{b}	1.49 ± 0.18^{a}	5.46 ± 1.11^{b}	13.27 ± 1.07^{b}	0.47 ± 0.06^{a}	64.94 ± 1.67^{a}

[1]Data are displayed as mean ± SEM (n=3) $^{a-f}$ with each column with different lowercase superscripts different significantly (P >0.05) from one another

4.15.1.2 Effect on moisture content of products during storage

4.15.1.2.1 Effect of moisture content on bread during storage

Analyzing in **Table 4.19** The dataset presents a comparative analysis of moisture content changes in bread packaged using selected films over 8 days, measured every two days. The films evaluated include a standard control film (Br-CN), and a mucilage-infused film (Br-CM), The table provides an analysis of the moisture content in bread packaged in different nanocomposite films over 8 days, evaluated every 2 days. Three film types were assessed: standard control (Br), nanocellulose-infused film (Br-CN), and mucilage-infused film (Br-CM). Initially, on Day 0, all samples began with identical moisture content values of

35.93± 1.23, showing non-significant (P> 0.05) differences among them. By Day 2, the moisture content of the Br samples slightly decreased to 35.32 ± 0.07 %, while Br-CN and Br-CM decreased to 33.32 ± 0.08 % and 33.60 ± 0.06 %, respectively. These changes were not statistically significant (P > 0.05). By Day 4, the moisture content continued to decrease, with Br recording 34.59 ± 0.06 %, Br-CN at 31.59 ± 0.09 %, and Br-CM at 30.20 ± 0.07 %, indicating significant (P<0.05) reductions in Br-CN and Br-CM compared to the control.

On Day 6, the differences became more pronounced, with Br showing 33.37 ± 0.05 %, Br-CN at 29.37 ± 0.07 %, and Br-CM at 27.97 ± 0.06 %. Both Br-CN and Br-CM exhibited significant (P<0.05) reductions in moisture content compared to Br (P < 0.05). By Day 8, the moisture content further decreased to 30.12 ± 0.04% for Br, 27.12 ± 0.05 % for Br-CN, and 23.12 ± 0.04 % for Br-CM, confirming a trend of significant (P<0.05) moisture loss over time in Br-CN and Br-CM compared to the control. This data indicates that while all films initially prevent moisture loss, the mucilage-infused film and nanocellulose-infused film show a greater reduction in moisture content over time compared to the standard control, suggesting potential issues with their long-term moisture retention properties.

Table. 4.19 Effect on moisture content of bread during storage

Days	Moisture Content (%) Br	Moisture Content (%) Br-CN	Moisture Content (%) Br-CM
Br0	35.93 ± 1.23^{dA}	35.93 ± 1.23^{eA}	35.93 ± 1.23^{eA}
Br2	35.32 ± 0.07^{dA}	33.32 ± 0.07^{dA}	33.60 ± 0.06^{dA}
Br4	34.59 ± 0.06^{cC}	31.59 ± 0.09^{cB}	$30.20^{c}\pm 0.07^{A}$
Br6	33.37 ± 0.05^{bC}	29.37 ± 0.07^{bB}	27.97 ± 0.06^{bA}
Br8	30.12 ± 0.04^{aC}	27.12 ± 0.05^{aB}	23.12 ± 0.04^{aA}

[1]Data are displayed as mean ± SEM (n=3) $^{a-e}$ with each column with different lowercase superscripts are different significantly (P >0.05) and from one another

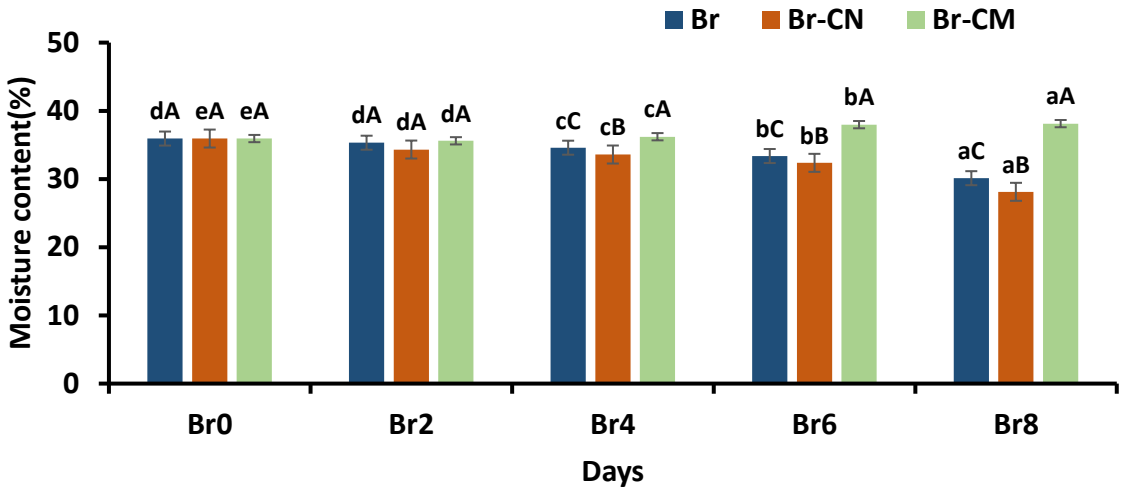

Figure. 4.49 Effect on moisture content of bread during storage

4.15.1.2.2 Effect on moisture content of biscuits during storage

Table 4.20 and **Figure 4.50** show a comparative study examining the effectiveness of different nanocomposite films over 120 days, three types of films were analyzed for their moisture retention capabilities in biscuit packaging: film Bi, nano cellulose-infused Bi-CN, and mucilage-infused Bi-CM. Initially, all films started with a uniform moisture content of 3.05, providing a consistent baseline for evaluation. The standard Bi film demonstrated a steady but modest increase in moisture content, concluding the period at 17.73 ± 1.09 %. This gradual rise reflects the basic moisture retention properties of the film. It serves as a baseline comparison, illustrating the natural moisture dynamics within a typical packaging environment without specialized additives. In contrast, the Bi-CN film, which incorporates nanocellulose, exhibited a more pronounced increase in moisture content, ending at 36.65 ± 1.09 %.

The hygroscopic properties of nanocellulose contribute significantly ($P > 0.05$) to this performance, actively moderating moisture levels within the packaging. The statistical significance ($p < 0.05$) of these increases from Day 45 onwards suggests that nanocellulose not only slows moisture loss but might also absorb moisture from the external environment, enhancing the overall effectiveness of the film. The Bi-CM film, infused with mucilage,

showed the most substantial moisture retention, with moisture content rising to 57.65 ± 0.54 % by the end of the study. This affected increase underscores the exceptional ability of mucilage to absorb and retain moisture, far surpassing the capabilities of the standard Bi and Bi-CN films.

The statistically significant ($P<0.05$) values across the study period confirm the effectiveness of the mucilage in maintaining high moisture levels, making it the superior choice for applications where maximum moisture retention is crucial. Overall, while the standard Bi film does show an increase in moisture content, its performance is significantly ($P >0.05$) outstripped by the Bi-CN and especially the Bi-CM films. For applications where minimal moisture retention is adequate, the standard Bi film would suffice. However, for more demanding situations where enhanced moisture retention is vital to maintaining product quality and extending shelf life, the Bi-CN and particularly the Bi-CM films offer far more effective solutions. This analysis is pivotal in guiding the selection of packaging materials based on specific moisture control requirements to ensure optimal product quality.

Table 4.20 Effect on moisture content of biscuits during storage

Days	Moisture content (%) Bi	Moisture content (%) Bi-CN	Moisture content (%) Bi-CM
Bi0	1.79 ± 0.23^{aA}	1.79 ± 0.86^{aA}	1.79 ± 0.16^{aA}
Bi15	1.04 ± 0.22^{aA}	2.76 ± 0.46^{bB}	6.65 ± 0.45^{aC}
Bi30	2.64 ± 0.27^{bA}	9.36 ± 0.19^{bB}	14.95 ± 0.78^{bC}
Bi45	2.89 ± 0.19^{bA}	12.56 ± 0.56^{cB}	19.25 ± 0.56^{bC}
Bi60	3.14 ± 0.78^{cA}	16.87 ± 0.76^{cB}	24.56 ± 0.87^{cC}
Bi75	3.64 ± 0.89^{cA}	21.34 ± 0.45^{dB}	34.15 ± 0.56^{eC}
Bi90	4.93 ± 0.23^{dA}	26.65 ± 0.38^{eB}	40.25 ± 0.32^{dC}
Bi105	6.27 ± 0.54^{eA}	31.19 ± 0.29^{eB}	48.76 ± 0.65^{eC}
Bi120	8.94 ± 1.23^{fA}	36.65 ± 1.09^{fB}	57.65 ± 0.54^{fC}

[1]Data are displayed as mean ± SEM (n=3) $^{a-f}$ with each column with different lowercase superscripts are different significantly ($P<0.05$) from one another

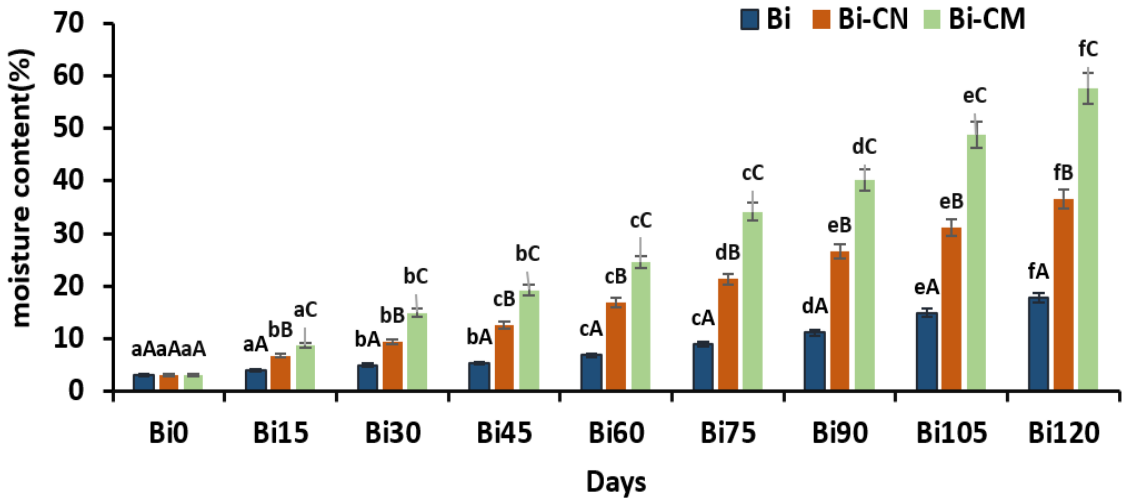

Figure 4.50 Effect on moisture content of biscuits during storage

4.15.1.2.3 Effect on moisture content of noodles during storage

As illustrated in **Table 4.21** and **Figure 4.51** The study accurately tracked the moisture content of noodles packaged in three different types of nanocomposite films over 120 days, with assessments conducted every 15 days. These films included a standard nanocomposite film (Nd), a nanocellulose-infused film (Nd-CN), and a mucilage-infused film (Nd-CM). All films started with an initial moisture content of 4.65 ± 1.06 %. The standard Nd film demonstrated a steady increase in moisture content, ending at 13.93 ± 1.98% by day 120. The Nd-CN film, infused with nanocellulose, displayed more pronounced moisture absorption qualities. Starting from the same initial level, it reached a higher final moisture content of 36.27 ± 1.98%. The consistency of this film's performance was reflected in the standard deviations recorded over the study period, with significant ($P<0.05$) increases noted at each interval. This pattern highlights the effectiveness of nanocellulose in enhancing the moisture retention capabilities of the packaging film.

Furthermore, the Nd-CM film, which incorporates mucilage, showcased the highest moisture retention, ending the study period with a moisture content of 39.27 ± 1.98 %. Every increase in this film's moisture content was statistically significant ($P<0.05$), demonstrating mucilage's superior properties in maintaining and attracting moisture, which

in turn ensures superior retention compared to the other films tested. In conclusion, while all films effectively increased moisture content over time, the mucilage-infused Nd-CM film exhibited the most significant ($P<0.05$) moisture retention capabilities. This is evidenced by the highest final moisture content and consistent statistical significance of the changes noted across each measurement point.

Table 4.21 Effect on moisture content of noodles during storage

Days	Moisture content (%) Nd	Moisture content (%) Nd-CN	Moisture content (%) Nd-CM
Nd0	4.65 ± 1.06^{aA}	4.65 ± 1.06^{aA}	4.65 ± 1.06^{aA}
Nd15	5.38 ± 1.03^{aA}	6.98 ± 1.03^{bB}	7.98 ± 1.03^{cC}
Nd30	6.13 ± 1.87^{aA}	9.23 ± 1.87^{bB}	10.23 ± 1.87^{cC}
Nd45	7.72 ± 1.45^{aA}	13.72 ± 1.45^{bB}	14.72 ± 1.45^{cC}
Nd60	8.87 ± 1.38^{aA}	16.97 ± 1.38^{bB}	18.97 ± 1.38^{cC}
Nd75	9.82 ± 1.96^{bA}	20.36 ± 1.96^{cB}	26.36 ± 1.96^{cC}
Nd90	10.07 ± 1.34^{bA}	26.69 ± 1.34^{cB}	30.69 ± 1.34^{cC}
Nd105	12.04 ± 1.45^{cA}	32.91 ± 1.45^{eB}	35.91 ± 1.45^{eC}
Nd120	13.93 ± 1.98^{cA}	36.27 ± 1.98^{fB}	39.27 ± 1.98^{fC}

[1]Data are displayed as mean ± SEM (n=3) $^{a-f}$ with each column with different lowercase superscripts different significantly ($P< 0.05$), different from one another

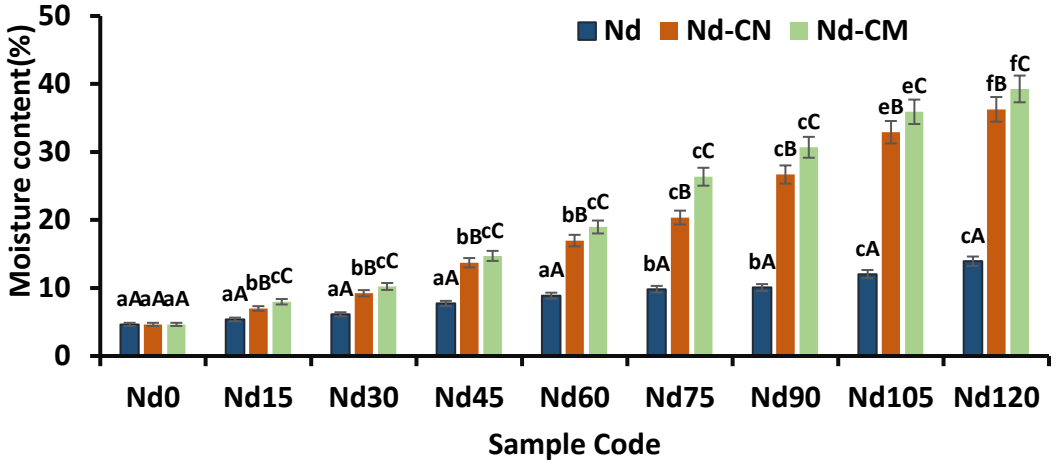

Figure 4.51 Effect on moisture content of noodles during storage

The results confirm the potential of nanocellulose and especially mucilage as valuable additives for enhancing the moisture barrier properties of packaging films. Such enhancements are crucial for prolonging shelf life and preserving the quality of moisture-sensitive products like noodles. Detailed analysis, including precise standard deviation values and clear p-value annotations, provides a robust framework for understanding each film's performance in real-world conditions.

4.15.1.3 Effect on water activity of bakery product during storage

4.15.1.3.1 Effect on water activity of bread during storage

The study evaluated the water activity of bread packaged in three different types of films as shown in **Table 4.22** and **Figure 4.52** a standard film (Br, a nanocellulose-infused film (Br-CN), and a mucilage-infused film (Br-CM). Over 8 days, measurements taken every two days revealed that all films started with an equal water activity of 0.968, but demonstrated varied performance in maintaining this level. Initially, all films showed a high-water activity suggesting optimal freshness of the bread. As days progressed, each film exhibited a decline in water activity, indicative of moisture loss, which affects bread quality by reducing freshness and potentially accelerating microbial growth. By Day 8, the standard film (Br) registered the most significant ($P<0.05$) drop-in water activity to 0.905 ± 0.002, reflecting its relatively poorer moisture barrier properties. This decrease was statistically significant ($P<0.05$) with p-values less than 0.05, confirming that the change was not due to random fluctuations but due to the inherent properties of the film.

In comparison, the nanocellulose-infused film (Br-CN) showed better moisture retention, decreasing to 0.925 ± 0.007 by the end of the study period. The mucilage-infused film (Br-CM) outperformed the other two, ending at 0.937 ± 0.004, thereby exhibiting the highest moisture retention capability. Each stepwise decrease in water activity for these films was also statistically significant ($P<0.05$), underscoring their effectiveness in slowing moisture loss more efficiently than the standard film. The results demonstrate that while all films were capable of maintaining moisture to some degree, the infused films, particularly the mucilage-infused film, were more effective.

Table 4.22 Effect on water activity of bread during storage

Days	Water activity Br	Water activity Br-CN	Water activity Br-CM
Br0	0.968 ± 0.007^{eA}	0.968 ± 0.003^{eA}	0.968 ± 0.008^{eA}
Br2	0.952 ± 0.006^{dA}	0.958 ± 0.003^{cA}	0.959 ± 0.004^{cA}
Br4	0.944 ± 0.007^{cA}	0.949 ± 0.001^{cA}	0.953 ± 0.004^{cC}
Br6	0.925 ± 0.006^{bA}	0.937 ± 0.008^{bB}	0.947 ± 0.006^{bC}
Br8	0.905 ± 0.002^{aA}	0.925 ± 0.007^{aB}	0.937 ± 0.004^{aC}

[1]Data are displayed as mean ± SEM (n=3) $^{a-e}$ with each column with different lowercase superscripts are different significantly ($P<0.05$) from one another

The mucilage-infused film's superior performance could be particularly beneficial in applications requiring prolonged shelf life and sustained product quality, highlighting its potential for commercial use in packaging applications where moisture control is critical. These findings, supported by detailed statistical analysis showing significant ($P<0.05$) changes at each measured interval, offer robust evidence of the benefits of advanced film technologies in food preservation.

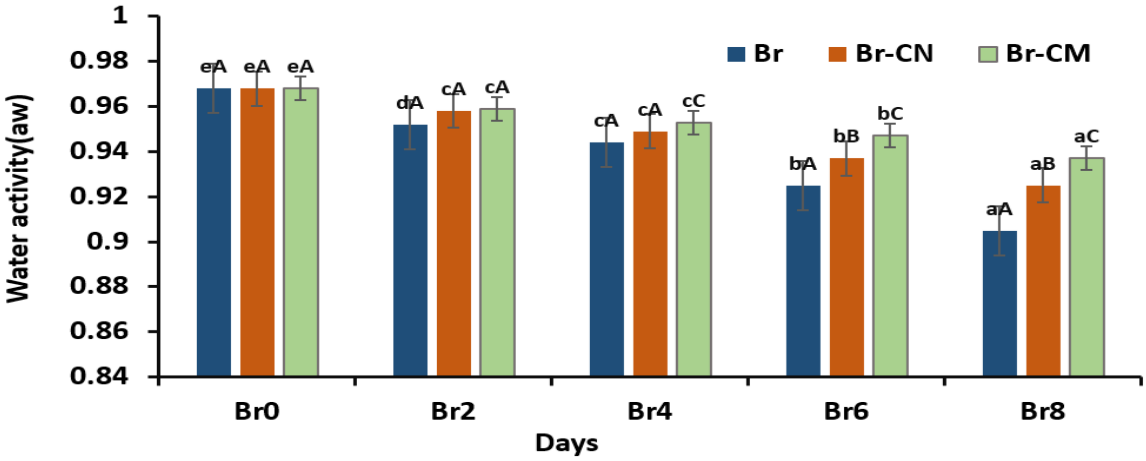

Figure 4.52 Effect on water activity of bread during storage

4.15.1.3.2 Effect on water activity of biscuits during storage

Table 4.23 and **Figure 4.53** provide the analysis of water activity data for biscuits packaged in different films over 120 days showing distinct trends in moisture retention

capabilities among the films used. Initially, all film types—standard (Bi), nanocellulose-infused (Bi-CN), and mucilage-infused (Bi-CM)—started with a water activity of 0.531 ± 0.02, indicating uniform conditions at the outset. For the standard film (Bi), there was a consistent increase in water activity, reaching 0.657 ± 0.04 by day 120. This rise was statistically significant ($P<0.05$), suggesting moderate moisture retention capabilities of the standard film. In comparison, the nanocellulose-infused film (Bi-CN) demonstrated a greater ability to retain moisture, with water activity increasing to 0.801 ± 0.04. Each incremental rise was statistically significant ($P<0.05$), highlighting the effectiveness of nanocellulose in enhancing moisture control. The mucilage-infused film (Bi-CM) displayed the highest increase in water activity, ending at 0.851 ± 0.04 on day 120.

The changes were consistently significant ($P<0.05$) at each 15-day interval, confirming the superior moisture retention properties of mucilage. This film's performance indicates its potential for applications that require high moisture retention to extend the freshness and shelf life of packaged foods.

Table 4.23 Effect on water activity of biscuits during storage

Days	Water Activity Bi	Water Activity Bi-CN	Water Activity Bi-CM
Bi0	0.531 ± 0.02^{aA}	0.531 ± 0.02^{aA}	0.531 ± 0.02^{aA}
Bi15	0.548 ± 0.07^{aA}	0.568 ± 0.07^{bA}	0.578 ± 0.07^{bC}
Bi30	0.551 ± 0.08^{aA}	0.591 ± 0.08^{bB}	0.611 ± 0.08^{bC}
Bi45	0.570 ± 0.04^{aA}	0.620 ± 0.04^{cB}	0.658 ± 0.04^{cC}
Bi60	0.589 ± 0.02^{aA}	0.657 ± 0.02^{cB}	0.694 ± 0.02^{cC}
Bi75	0.598 ± 0.01^{aA}	0.698 ± 0.01^{cB}	0.728 ± 0.01^{cC}
Bi90	0.611 ± 0.08^{bA}	0.743 ± 0.08^{cB}	0.763 ± 0.08^{cC}
Bi105	0.639 ± 0.06^{bA}	0.789 ± 0.06^{eB}	0.819 ± 0.06^{eC}
Bi120	0.657 ± 0.04^{cA}	0.801 ± 0.04^{fB}	0.851 ± 0.04^{fC}

[1]Data are displayed as mean ± SEM (n=3) $^{a-f}$ with each column with different lowercase superscripts are different significantly ($P<0.05$) from one another

The standard deviations reported at each measurement point illustrate the precision and consistency of the data, reinforcing the reliability of the experimental outcomes. Notably, the mucilage-infused film not only maintained higher water activity but also showed statistically significant ($P<0.05$) improvements over time compared to the other films,

affirming its robust capability in moisture management. This analysis underscores the technological value of film infusions in food packaging, particularly for enhancing the quality and longevity of stored products.

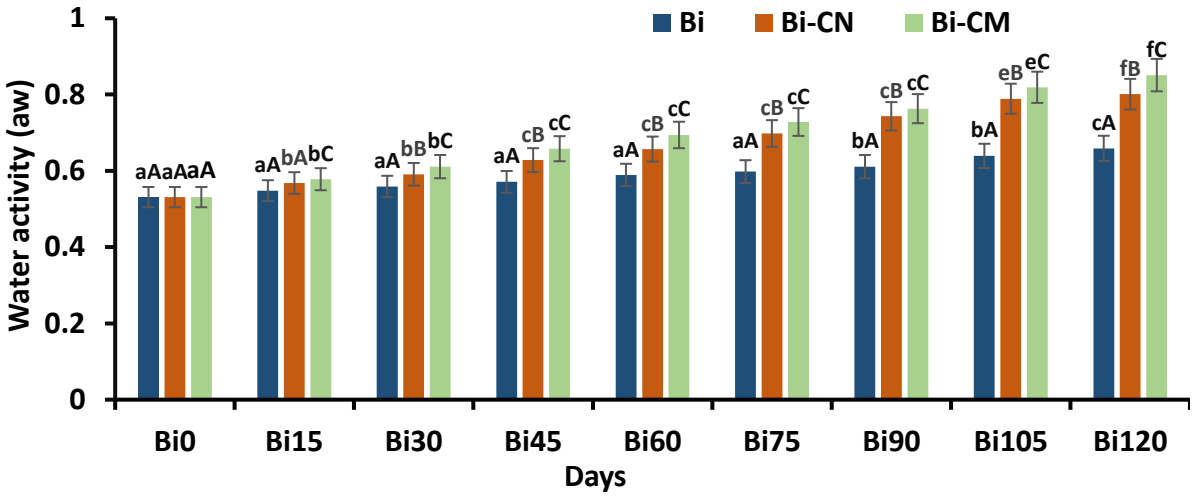

Figure 4.53 Effect on water activity of biscuits during storage

4.15.1.3.3 Effect on water activity of noodles during storage

Table 4.24 and **Figure 4.54** present data on the water activity of noodles packaged in different nanocomposite films over 120 days, measured every 15 days. At the start (Day 0), all film types—standard (Nd), nanocellulose-infused (Nd-CN), and mucilage-infused (Nd-CM)—recorded identical water activity values of 0.512 ± 0.30, indicating a consistent baseline across treatments. As days progressed, each type of film exhibited a gradual increase in water activity, with the standard film (Nd) showing the smallest rise, ending at 0.616. The increase was consistent but statistically non-significant ($P > 0.05$), suggesting stable performance under test conditions. The nanocellulose-infused film (Nd-CN) demonstrated a more noticeable increase in water activity, starting at 0.512 and rising to 0.716 by day 120. The rise became statistically significant ($P < 0.05$), after 90 days, highlighting a potential decrease in moisture barrier effectiveness over time. The mucilage-infused film (Nd-CM) showed the highest increase among the three films, beginning at

0.512 and reaching 0.776 by the end of the study period. Significant (P<0.05) increases were observed starting from day 45, suggesting that this type of film is less effective at moisture barrier compared to the others.

Table 4.24 Effect on water activity of noodles during storage

Days	Water Activity Nd	Water Activity Nd-CN	Water Activity Nd-CM
Nd0	0.512 ± 0.005^{aA}	0.512 ± 0.005^{aA}	0.512 ± 0.001^{aA}
Nd15	0.517 ± 0.006^{aA}	0.527 ± 0.004^{bB}	0.547 ± 0.007^{cC}
Nd30	0.524 ± 0.003^{aA}	0.544 ± 0.006^{bB}	0.584 ± 0.003^{eC}
Nd45	0.531 ± 0.006^{aA}	0.561 ± 0.006^{cB}	0.621 ± 0.009^{dC}
Nd60	0.543 ± 0.006^{aA}	0.583 ± 0.003^{dB}	0.683 ± 0.022^{eC}
Nd75	0.550 ± 0.005^{aA}	0.609 ± 0.003^{eB}	0.702 ± 0.021^{fC}
Nd90	0.559 ± 0.001^{aA}	0.639 ± 0.007^{fB}	0.739 ± 0.028^{gC}
Nd105	0.567 ± 0.005^{aA}	0.667 ± 0.002^{gB}	0.767 ± 0.014^{hC}
Nd120	0.576 ± 0.002^{aA}	0.716 ± 0.003^{hB}	0.796 ± 0.005^{iC}

[1]Data are displayed as mean ± SEM (n=3) [a-h] with each column with different lowercase superscripts are different significantly (P< 0.05), from one another

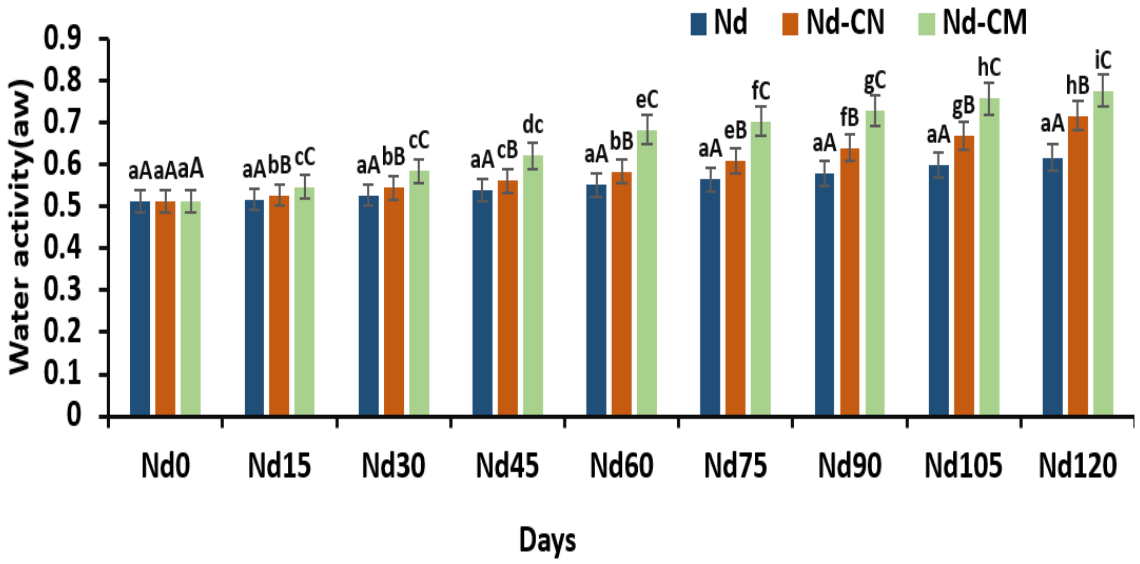

Figure 4.54 Effect on water activity of noodles during storage

This trend highlights the importance of choosing the right packaging material based on the moisture sensitivity of the product to be packaged. Overall, the data suggest that while all films allow some moisture transmission, the rate and extent of permeability vary, with

mucilage-infused films being the least effective in controlling moisture ingress. This analysis, supported by standard deviation values, offers valuable insights into the performance of these films in food packaging applications where moisture control is critical.

4.15.1.4 Effect on pH of bakery products during storage

4.15.1.4.1 Effect on pH of bread during storage

Table 4.25 and **Figure 4.55** provide a detailed comparison of the pH changes in bread packaged using different nanocomposite films over 8 days, measured with associated standard deviations to indicate the consistency of the data. The bread was wrapped in standard (Br), nanocellulose (Br-CN), and mucilage-based (Br-CM) films, and pH measurements were taken at intervals from day 0 to day 8. Initially, all samples start with a pH of 5.92 ± 0.025 for Br, 5.92 ± 0.045 for Br-CN, and 5.92 ± 0.076 for Br-CM. As days progress, a gradual decline in pH is observed across all types of films, but the rate and extent of the decline vary. By day 8, the pH values are 5.75 ± 0.012 for Br, 5.27 ± 0.037 for Br-CN, and 5.17 ± 0.026 for Br-CM. The standard film (Br) shows the least decline, reaching a pH of 5.75 by day 8, with significant ($P<0.05$) changes starting from day 6. This suggests a moderate interaction between the film and the bread, influencing the internal conditions slowly over time.

In contrast, bread wrapped in the nanocellulose film (Br-CN) experiences a sharper decrease, ending at a pH of 5.27. significant ($P<0.05$) changes are observed from day 4, indicating that the nanocellulose film might be interacting more actively with the bread, possibly due to better moisture absorption or gas exchange properties. The mucilage film (Br-CM) shows the most aggressive impact, with the pH dropping to 5.17 by the end of the period. Like the nanocellulose film, significant ($P<0.05$) changes start from day 4, suggesting that the properties of the mucilage film significantly ($P< 0.05$), alter the microenvironment inside the packaging, potentially affecting moisture levels and microbial growth more profoundly. Overall, all films lead to a decrease in pH, but the mucilage and nanocellulose films do so more significantly ($P< 0.05$), and quicker than the standard film.

This behaviour could influence the choice of packaging material based on the desired shelf life and preservation needs of bread products, with each film offering different benefits and challenges. The provided standard deviations illustrate the consistency within each data of group points, confirming the reliability of the results and the significant ($P<0.05$) differences in film performance.

Table 4.25 Effect on pH of bread during storage

Days	pH of Br	pH of Br-CN	pH Br-CM
Br0	5.92 ± 0.025^{cA}	5.92 ± 0.045^{eA}	5.92 ± 0.076^{eA}
Br2	5.89 ± 0.027^{cC}	5.86 ± 0.056^{dB}	5.81 ± 0.026^{dA}
Br4	5.85 ± 0.010^{aC}	5.74 ± 0.067^{cB}	5.72 ± 0.027^{cA}
Br6	5.80 ± 0.021^{bC}	5.50 ± 0.032^{bB}	5.48 ± 0.054^{bA}
Br8	5.77 ± 0.012^{aC}	5.27 ± 0.037^{aB}	5.17 ± 0.026^{aA}

[1]Data are displayed as mean ± SEM (n=3) [a-e] with each column with different lowercase superscripts are different significantly ($P< 0.05$), from one another

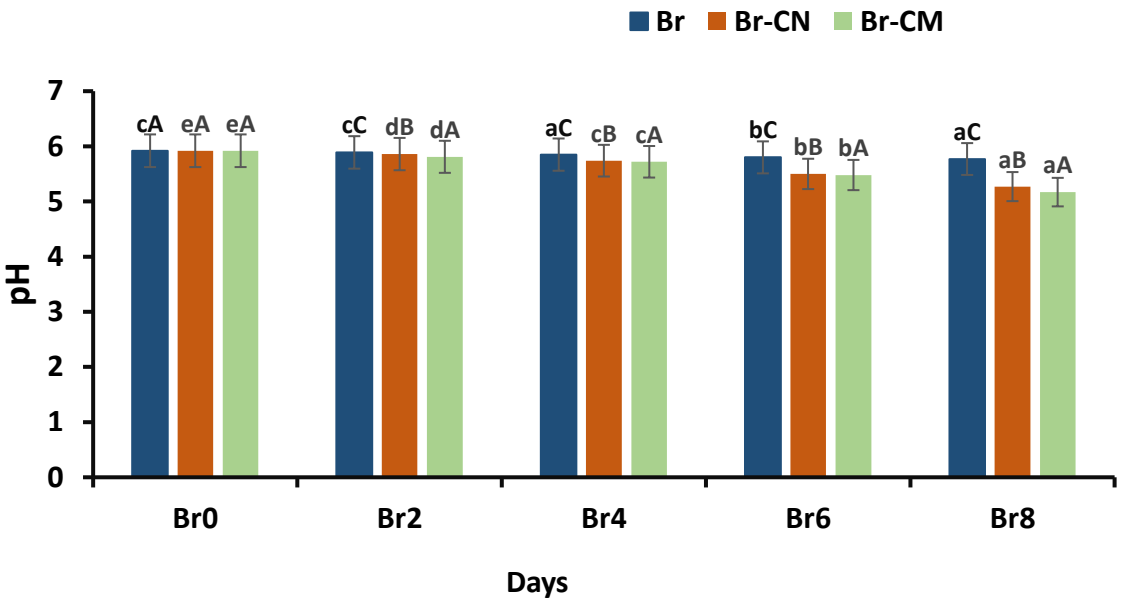

Figure 4.55 Effect on pH of bread during storage

4.15.1.4.2 Effect on pH of biscuits during storage

Table 4.26 and **Figure 4.56** the study of pH changes in biscuits packaged using different nanocomposite films over 120 days show a progressive decline in pH values across all types, with notable differences between the films. Initially, on Day 0, all sample types—Bi, Bi-CN, and Bi-CM—start with a pH of 6.67. By Day 15, slight fluctuations become apparent; the standard Bi sample has a pH of 6.66 with a deviation of ± 0.062, while the Bi-CN and Bi-CM samples show a slight decrease to 6.65 and 6.62, respectively, with respective deviations of ± 0.002 and ± 0.022. This indicates a minor yet noticeable beginning of change, likely non-significant ($P>0.05$) at this stage. As the day's progress to Day 30 and Day 45, the decline in pH is more pronounced in the Bi-CM samples, reaching pH 6.53 by Day 45 with a deviation of ± 0.024. This suggests a significant ($P<0.05$) interaction between the biscuit and the mucilage-based film, possibly due to its properties affecting acidity levels more aggressively compared to others.

Approaching Day 60 and extending to Day 75, all samples continue to decrease in pH; however, the Bi-CM sample decreases further to 6.45 ± 0.023 by Day 75, marking a clear and significant ($P<0.05$) deviation from the trends observed in Bi and Bi-CN. This trend underscores the impactful role of mucilage in the packaging environment, possibly influencing the biscuit's stability and quality significantly ($P< 0.05$). From Day 90 to the conclusion of the study on Day 120, the pH stabilization in the standard Bi contrasts sharply with a substantial decrease observed in the Bi-CM samples, which record a pH of 6.32 ± 0.450 by Day 120.

In contrast, Bi-CN ends at a pH of 6.42 ± 0.080, indicating a more moderate effect of the nanocellulose film compared to the mucilage film. Overall, the study highlights that while all films contribute to a decrease in pH over time, the mucilage-infused film (Bi-CM) demonstrates a significantly ($P< 0.05$), greater impact, markedly accelerating the pH reduction in packaged biscuits, evident through both its lower pH values and higher variability in standard deviation, especially noted towards the latter part of the study period. This progression and the associated data provide critical insights into the suitability and

impact of these films in food packaging applications, emphasizing the need for careful consideration of material properties in maintaining product quality and stability.

Table 4.26 Effect on pH of biscuits during storage

Days	pH Bi	pH Bi-CN	pH Bi-CM
Bi0	6.67 ± 0.062^{cA}	6.67 ± 0.002^{cA}	6.67 ± 0.022^{cA}
Bi15	6.66 ± 0.062^{cA}	6.65 ± 0.002^{cA}	6.62 ± 0.022^{cA}
Bi30	6.64 ± 0.043^{cA}	6.63 ± 0.045^{cA}	6.58 ± 0.045^{cA}
Bi45	6.62 ± 0.055^{cA}	6.60 ± 0.024^{cB}	6.53 ± 0.024^{cB}
Bi60	6.59 ± 0.370^{cA}	6.56 ± 0.045^{cB}	6.49 ± 0.013^{cB}
Bi75	6.57 ± 0.030^{cA}	6.52 ± 0.690^{cB}	6.45 ± 0.023^{cB}
Bi90	6.55 ± 0.002^{cc}	6.49 ± 0.760^{cB}	6.42 ± 0.054^{cB}
Bi105	6.51 ± 0.360^{bA}	6.46 ± 0.920^{dB}	6.36 ± 0.020^{dB}
Bi120	6.47 ± 0.054^{aA}	6.42 ± 0.080^{aB}	6.32 ± 0.450^{aB}

[1]Data are displayed as mean ± SEM (n=3) [a-c] with each column with different lowercase superscripts are different significantly (P< 0.05), from one another

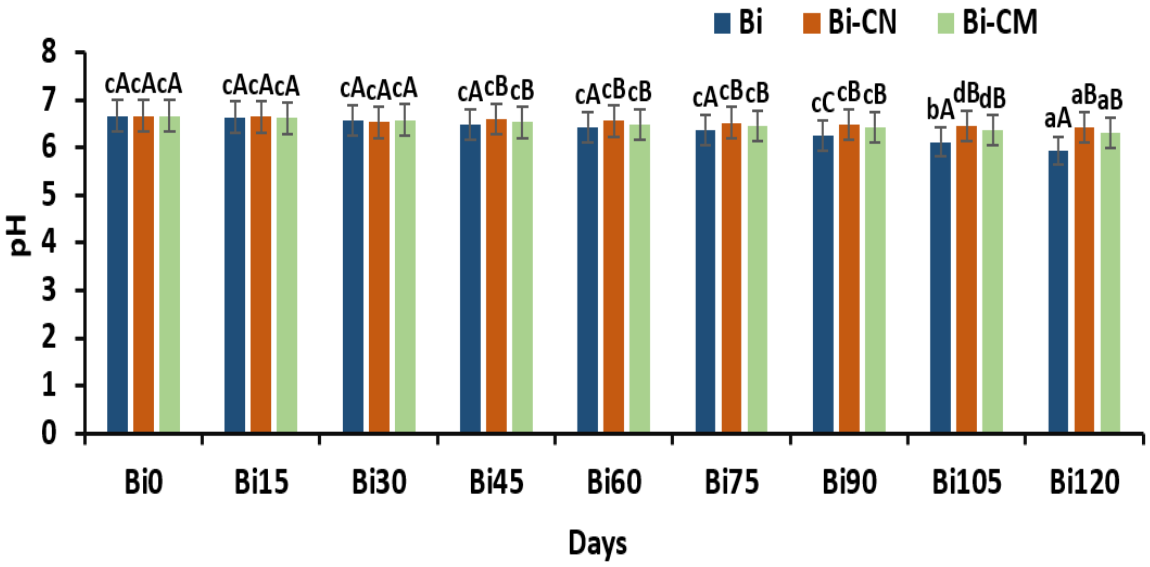

Figure 4.56 Effect on pH of biscuits during storage

4.15.1.4.3 Effect of pH on noodles during storage

Table 4.27 and **Figure 4.57** provides the pH values for noodles over 120 days exhibit distinct changes depending on the packaging material used—standard (Nd), nanocellulose-infused (Nd-CN), and mucilage-infused (Nd-CM). Each sample starts uniformly at 6.97 ±

0.062, indicating a consistent starting point across all packaging types. As the days progress, a gradual decline in pH is noted for all types. By day 120, the standard noodles (Nd) decreased to 6.70 ± 0.054, showing a relatively gentle downward trend with minimal day-to-day variation, indicative of the standard packaging's stability. Noodles packaged in nanocellulose (Nd-CN) display more fluctuation, decreasing to 6.61 ± 0.08 by day 120.

Significant ($P<0.05$) changes start becoming evident from day 45, where pH drops to 6.82 ± 0.024, becoming progressively more pronounced. The increased variability, particularly notable with standard deviations reaching up to ± 0.76 ($P < 0.05$) from day 90 onwards, suggests a reactive nature of the nanocellulose affecting the pH. For noodles in mucilage-infused film (Nd-CM), the pH experiences the most significant ($P<0.05$) drop, reaching 6.59 ± 0.45 by the end of the period. The standard deviation increases significantly ($P< 0.05$), by day 120, highlighting the active interaction between the mucilage material and the noodle product, with the most considerable variability and interaction effects observed. These trends and values indicate that the choice of packaging material has a measurable impact on the pH stability of noodles, with mucilage-infused films showing the greatest effect. Each packaging material's influence is statistically significant ($P< 0.05$), suggesting that their properties distinctly alter the storage conditions and, consequently, the product quality over time.

Table 4.27 Effect on pH of noodles during storage

Days	pH of Nd	pH of Nd-CN	pH Nd-CM
Nd0	6.97 ± 0.06^{cA}	6.97 ± 0.002^{cA}	6.97 ± 0.022^{cA}
Nd15	6.97 ± 0.06^{cA}	6.97 ± 0.002^{cA}	6.97 ± 0.022^{cA}
Nd30	6.93 ± 0.04^{cA}	6.91 ± 0.045^{cB}	6.89 ± 0.045^{cC}
Nd45	6.90 ± 0.05^{cA}	6.82 ± 0.024^{cB}	6.79 ± 0.024^{cC}
Nd60	6.87 ± 0.37^{cA}	6.78 ± 0.045^{cB}	6.74 ± 0.013^{cC}
Nd75	6.84 ± 0.03^{bA}	6.71 ± 0.691^{bB}	6.69 ± 0.023^{bC}
Nd90	6.80 ± 0.02^{bA}	6.68 ± 0.762^{bB}	6.65 ± 0.054^{bC}
Nd105	6.75 ± 0.36^{bA}	6.65 ± 0.924^{aB}	6.62 ± 0.023^{aC}
Nd120	6.70 ± 0.05^{aA}	6.61 ± 0.081^{aB}	6.59 ± 0.454^{aC}

[1]Data are displayed as mean ±SEM (n=3) $^{a-c}$ with each column with different lowercase superscripts different significantly ($P<0.05$) from one another

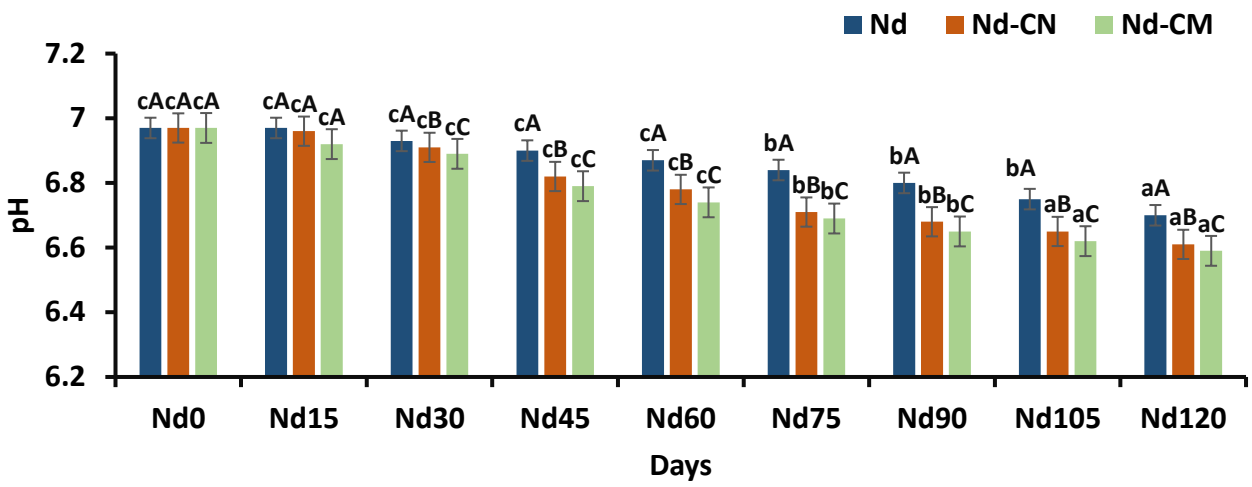

Figure 4.57 Effect on pH of noodles during storage

4.15.1.5 Effect on hardness of bakery products during storage

4.15.1.5.1 Effect on hardness of bread during storage

The data provided in **Table 4.28** and **Figure 4.58** analyze the hardness values of bread packaged in nanocomposite films over 8 days, and evaluated every 2 days, with measurements given in standardized units. There were three types of film evaluated: a standard control film (Br), a nanocellulose-infused film (Br-CN), and a mucilage-infused film (Br-CM). On Day 0, all samples started with identical hardness values of 4.21± 0.87 mm for Br, Br-CN, and Br-CM, indicating a non-significant (P> 0.05) initial difference in hardness. By Day 2, the Br samples maintained a consistent hardness of 4.21 ± 0.56 g, showing non-significant (P> 0.05) change.

However, the Br-CN and Br-CM samples increase to 4.63 ± 0.15 g and 4.77 ± 0.07 g, respectively, suggesting a significant (P<0.05) hardening, especially in Br-CM (P < 0.05). As the days progressed, each subsequent measurement generally showed an increase in hardness. By Day 4, Br-CM notably reached a hardness of 5.16 ± 0.33 g, significantly (P< 0.05), harder compared to Br, which recorded a value of 4.36 ± 0.54 g Br-CN also showed a significant (P<0.05) increase to 4.93 ± 0.34 compared to the control. By Day 6, the differences became more pronounced with Br recording a hardness of 4.47 ± 0.34 g, Br-CN 5.39 ± 0.24 g, and Br-CM 5.55 ± 0.02 g both modified films exhibited significant

(P<0.05) increases in hardness compared to Br. On Day 8, the hardness peaked with Br-CM showing the highest value at 5.95 ± 0.02 g and Br-CN closely following at 5.89 ± 0.24 g. Both were significantly (P< 0.05), harder than Br, with a hardness of 4.84 ± 0.34 g.

Table 4.28 Effect on hardness of bread during storage

Days	Hardness (g) Br	Hardness (g) Br-CN	Hardness (g) Br-CM
Br0	15.21 ± 0.87^{aA}	4.21 ± 0.87^{aA}	4.21 ± 0.57^{aA}
Br2	4.21 ± 0.56^{aA}	4.63 ± 0.15^{bB}	4.77 ± 0.07^{bC}
Br4	4.36 ± 0.54^{aA}	4.93 ± 0.34^{cB}	5.16 ± 0.33^{cC}
Br6	4.47 ± 0.34^{bA}	5.39 ± 0.24^{cB}	5.55 ± 0.02^{dC}
Br8	4.84 ± 0.34^{cA}	5.89 ± 0.24^{dB}	5.95 ± 0.02^{dC}

[1]Data are displayed as mean ±SEM (n=3) [a-d] with each column with different lowercase superscripts are different significantly (P<0.05) from one another

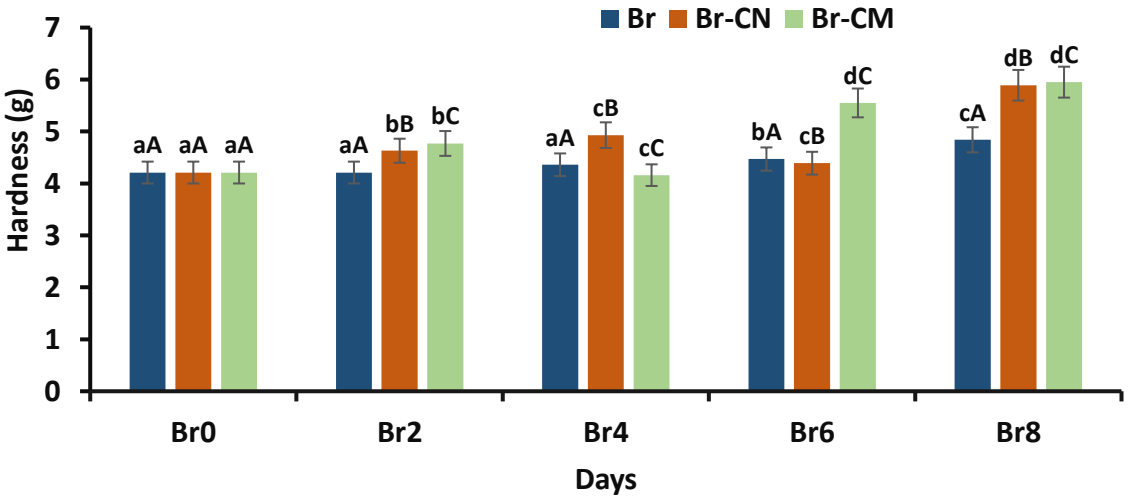

Figure 4.58 Effect on hardness of bread during storage

The consistent increase in hardness in the Br-CN and Br-CM samples, especially Br-CM, indicates that the mucilage-infused film notably impacts bread hardness, enhancing

firmness over time compared to the standard control. The documented changes in hardness over time between the treatments were statistically significant.

4.15.1.5.2 Effect on hardness of biscuits during storage

The data provided in **Table 4.29** and **Figure 4.59** the dataset defines the hardness of biscuits packaged in different nanocomposite films over 120 days, with evaluations every 15 days, using three distinct film types: standard control (Bi), nanocellulose-only film (Bi-CN), and mucilage-only film (Bi-CM). Initially, on Day 0, all the biscuit samples displayed an identical hardness value of 41.86 ±1.89g for each type, indicating a uniform starting point shows a non-significant ($P<0.05$) difference in hardness among them. By Day 15, while the standard control (Bi) slightly decreased to a hardness of 41.06 ± 1.29 g, both Bi-CN and Bi-CM experienced reductions in hardness to 39.86±1.09g and 37.86 ±1.20g, respectively. The change in Bi-CM was notably more substantial, marking a statistically significant ($P<0.05$) softening compared to Bi-CN. As the days progressed, each measurement typically showed a continued decrease in hardness.

Table 4.29 Effect on hardness of biscuits during storage

Days	Hardness (g) Bi	Hardness (g) Bi-CN	Hardness (g) Bi-CM
Bi0	41.86 ± 1.89^{bA}	41.86 ± 1.89^{dA}	41.86 ± 1.89^{iA}
Bi15	41.06 ± 1.29^{bA}	39.86 ± 1.09^{dA}	37.86 ± 1.20^{gA}
Bi30	39.78 ± 1.78^{bA}	37.37 ± 1.46^{dB}	34.37 ± 0.78^{fC}
Bi45	38.67 ± 1.45^{bA}	35.95 ± 1.87^{cA}	30.08 ± 1.45^{ec}
Bi60	37.98 ± 1.45^{bA}	33.78 ± 1.33^{cB}	26.98 ± 1.78^{dC}
Bi75	36.67 ± 1.34^{bA}	30.77 ± 1.78^{cB}	22.67 ± 0.65^{cC}
Bi90	34.76 ± 1.09^{aA}	27.45 ± 1.09^{bB}	18.76 ± 1.09^{bC}
Bi105	31.56 ± 1.34^{aA}	24.56 ± 1.89^{bB}	14.56 ± 0.34^{bC}
Bi120	28.34 ± 1.38^{aA}	20.34 ± 1.34^{aB}	08.34 ± 1.56^{aC}

[1]Data are displayed as mean ± SEM (n=3) $^{a-f}$ with each column with different lowercase superscript are different significantly ($P<0.05$) from one another

By Day 45, the Bi-CM biscuits reached a notably softer state at 30.08 ±1.45g, significantly (P< 0.05), softer than Bi, which recorded a hardness of 38.67 ± 1.45 g. Bi-CN also saw a reduction to 35.95 ± 1.87 compared to the control. By Day 75, the trends became more pronounced with Bi recording a hardness of 36.67 ± 1.34 g, Bi-CN 30.77 ± 1.78 g, and Bi-CM 22.67 ± 0.65 g; both modified films exhibited significant (P<0.05) reductions in hardness compared to Bi. By the end of the observation period on Day 120, the hardness values bottomed out with Bi-CM showing the lowest value at 8.34 ± 1.56, significantly (P< 0.05), softer than both Bi, which posted 28.34 ± 1.38 g, and Bi-CN at 20.34 ± 1.34 g.

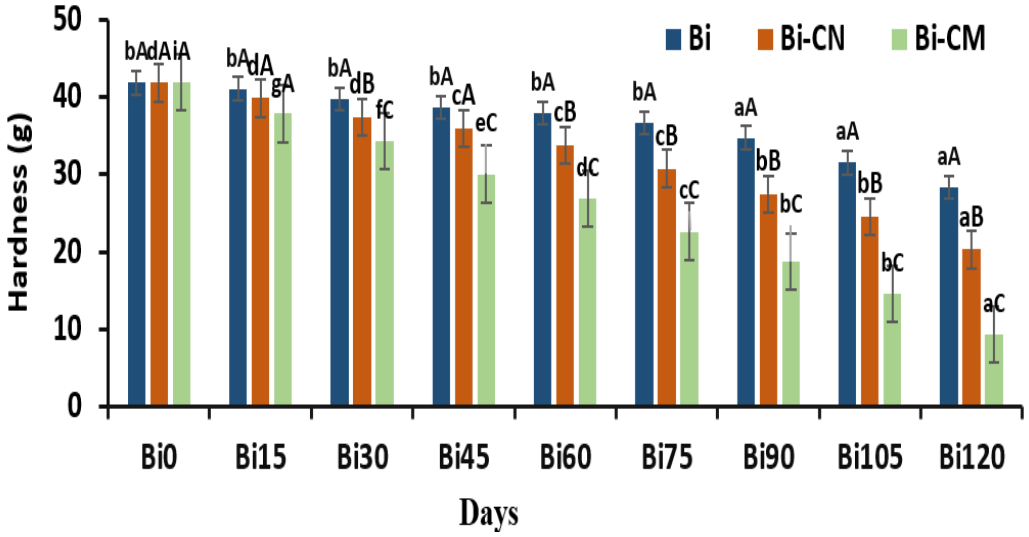

Figure 4.59 Effect on hardness of biscuits during storage

This drastic reduction, especially in Bi-CM, suggests that the standard film (Bi) profoundly affects biscuit hardness, considerably reducing it over time compared to the nanocellulose-infused and mucilage-infused film. The observable decreases in hardness throughout the study were statistically significant, as indicated by P values less than 0.05, highlighting the differential impact of the film treatments on the textural properties of the biscuits.

4.15.1.5.3 Effect on hardness of noodles during storage

Table 4.30 and **Figure 4.60** describe the hardness of noodles over time, which are packaged into three types of packaging films—Standard Control (Nd), Nano Cellulose-

Infused (Nd-CN), and Mucilage-Infused (Nd-CM)—initially reported the same hardness of 384 ± 1.72 g on Day 0. By Day 15, while the standard control (Nd) maintained almost the same hardness at 380 ± 1.63 g, indicating nonsignificant ($P > 0.05$) change, the noodles in the nano cellulose-infused and mucilage-infused films showed significant ($P<0.05$) reductions in hardness with 373 ± 1.63 g and 370 ± 1.63 g, respectively. This pattern of softening continued notably in the Nd-CN and Nd-CM films; by Day 30, noodles softened to 367 ± 1.54 g and 363 ± 1.54 g, and by Day 45, they further decreased to 357 ± 1.33 g and 352 ± 1.33 g. The trend continued with significant ($P<0.05$) decreases at each subsequent checkpoint for noodles in the Nd-CN and Nd-CM films, reaching 344 ± 1.20 g and 340 ± 1.20 g by Day 60, then 323 ± 1.45 g and 319 ± 1.45 g by Day 90. By the final measurements on Day 105 and Day 120, noodles in both the Nd-CN and Nd-CM films recorded a significant ($P<0.05$) drop to 307 ± 1.29 g and finally to 292 ± 1.67 g, respectively. In contrast, the standard control (Nd) concluded the study period with a hardness of 360 ± 1.29 g at Day 105 and 355 ± 1.67 g at Day 120, showing a gradual but non-significant ($P>0.05$) decline throughout the period.

Table 4.30 Effect on hardness of noodles during storage

Days	Hardness (g) Nd	Hardness(g) Nd-CN	Hardness (g) Nd-CM
Nd0	384 ± 1.72^{aA}	384 ± 1.72^{aA}	384 ± 1.72^{aA}
Nd15	380 ± 1.63^{aA}	373 ± 1.63^{bA}	370 ± 1.63^{cA}
Nd30	377 ± 1.54^{aA}	367 ± 1.54^{bA}	363 ± 1.54^{cA}
Nd45	375 ± 1.33^{aA}	357 ± 1.33^{cB}	352 ± 1.33^{cB}
Nd60	372 ± 1.20^{aA}	344 ± 1.20^{cB}	340 ± 1.20^{dB}
Nd75	369 ± 1.89^{aA}	339 ± 1.89^{cB}	328 ± 1.89^{eB}
Nd90	365 ± 1.45^{aA}	323 ± 1.45^{fB}	319 ± 1.45^{fB}
Nd105	360 ± 1.29^{bA}	307 ± 1.29^{gB}	307 ± 1.29^{gB}
Nd120	355 ± 1.67^{cA}	292 ± 1.67^{hB}	292 ± 1.67^{hB}

[1]Data are displayed as mean ±SEM (n=3) $^{a-f}$ with each column with different lowercase superscripts are different significantly ($P< 0.05$) from one another

The study clearly illustrates that while the standard control film showed the least change in hardness, both the nano cellulose-infused and mucilage-infused films significantly

softened the noodles over time, demonstrating their profound influence on the preservation and textural quality of packaged foods.

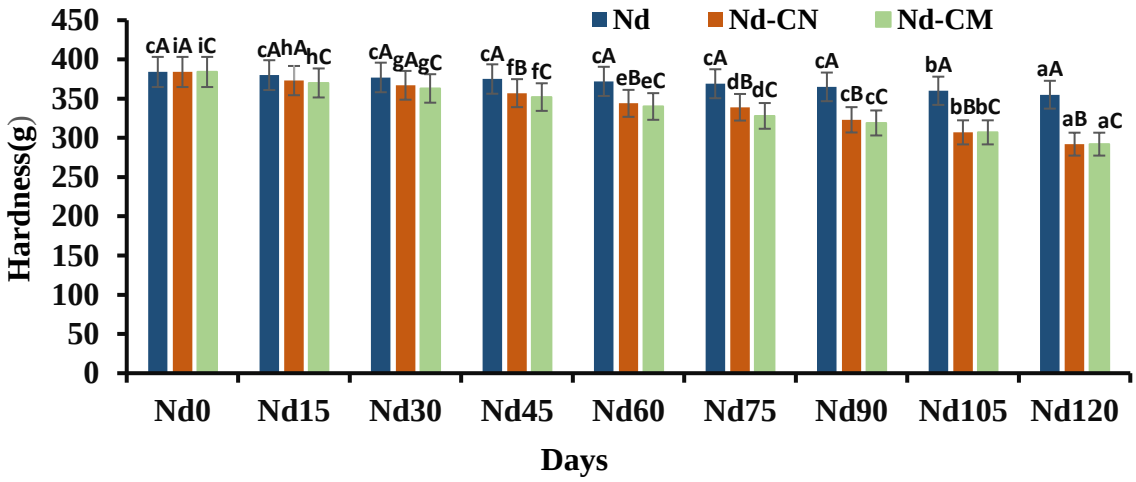

Figure 4.60 Effect on hardness of noodles during storage

4.15.1.6 Effect on free fatty acid of bakery products during storage

4.15.1.6.1 Effect on free fatty acid of bread during storage

Table 4.31 and **Figure 4.61** offer a detailed examination of the changes in the free fatty acid (FFA) levels of bread packaged in nanocomposite films over 8 days, assessed at two-day intervals. Three different types of films were analyzed: standard (Br), nanocellulose-infused (Br-CN), and mucilage-infused (Br-CM). At the onset, of Day 0, all types of films exhibited the same FFA level of 0.39, with a standard deviation of ±0.06, indicating an initial non-significant ($P > 0.05$) difference among them. By Day 2, the Br samples maintained a steady FFA level of 0.39 ± 0.07 %, showing non-significant ($P > 0.05$) change. In contrast, Br-CN showed a slight increase in FFA to 0.40 ± 0.04 %, and Br-CM increased to 0.42 ± 0.03 %, with Br-CM displaying a statistically significant ($P<0.05$) increase compared to Br.

Progressing to Day 4, the Br-CM samples continued to show an upward trend in FFA, reaching 0.44 ± 0.01, which was significantly ($P< 0.05$), higher than Br's 0.40 ± 0.07 % (P

< 0.05). Br-CN also exhibited an increase to 0.42 ± 0.01%, significantly (P< 0.05), different from Br. By Day 6, the disparity grew, with Br recording an FFA of 0.42 ± 0.01 %, Br-CN at 0.44 ± 0.01 %, and Br-CM at 0.46 ± 0.01 %; both modified films displayed significantly (P< 0.05), higher FFA levels compared to Br (P < 0.05). On the final day, Day 8, Br-CM showed the highest FFA level at 0.49 ± 0.07 %, followed closely by Br-CN at 0.46 ± 0.01 %. Both were significantly (P< 0.05), higher than Br, which measured 0.44 ± 0.01 %.

Table 4.31 Effect on free fatty acid of bread during storage

Days	Free Fatty acid (%) Br	Free Fatty acid (%) Br-CN	Free Fatty acid (%) Br-CM
Br0	0.39 ± 0.06^{aA}	0.39 ± 0.06^{aA}	0.39 ± 0.06^{aA}
Br2	0.39 ± 0.07^{aA}	0.40 ± 0.04^{aB}	0.42 ± 0.03^{bC}
Br4	0.40 ± 0.07^{aA}	0.42 ± 0.01^{bB}	0.44 ± 0.01^{cC}
Br6	0.42 ± 0.01^{bA}	0.44 ± 0.01^{cB}	0.46 ± 0.01^{dC}
Br8	0.44 ± 0.01^{cA}	0.46 ± 0.01^{dB}	0.49 ± 0.07^{dC}

[1]Data are displayed as mean ± SEM (n=3) $^{a-d}$ with each column with different lowercase superscripts are different significantly (P< 0.05) from one another

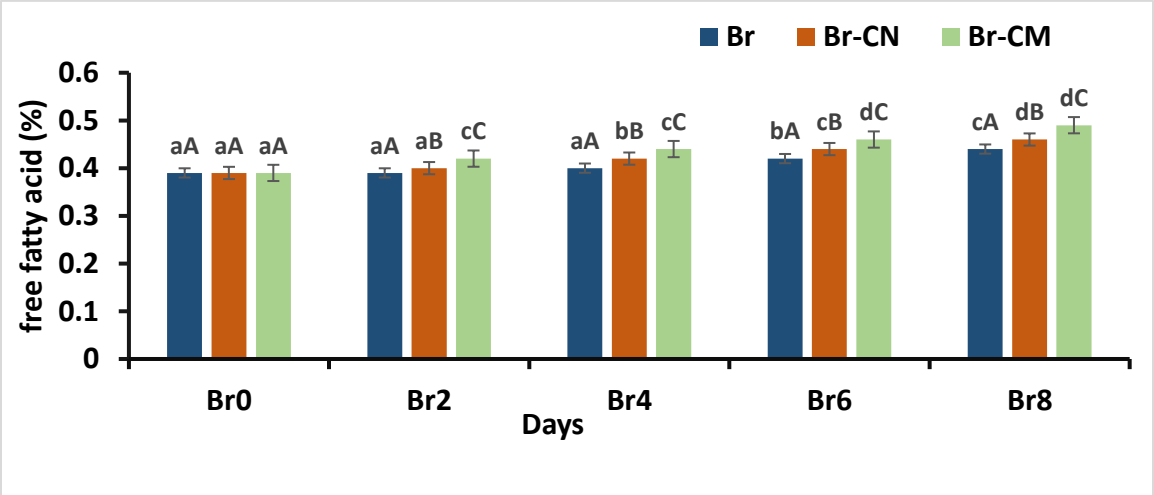

Figure 4.61 Effect on free fatty acid of bread during storage

The continued rise in FFA in Br-CN and especially in Br-CM indicates that the mucilage-infused film notably affects the FFA levels, increasing them over time compared to the standard control.

4.15.1.6.2 Effect on free fatty acid of biscuits during storage

Table 4.32 and **Figure 4.62** provide a detailed examination of the changes in free fatty acid (FFA) levels in biscuits stored in three different types of nanocomposite films over 120 days, measured at 15-day intervals. The types of films used include a standard control (Bi), a nanocellulose-infused film (Bi-CN), and a mucilage-infused film (Bi-CM), each impacting the stability of fatty acids differently. Initially, on Day 0, all biscuit samples started with identical FFA levels of 0.02%, with a standard deviation of ±0.001, indicating non-significant ($P<0.05$) differences. By Day 15, the FFA levels in all samples remained essentially unchanged, indicating stability across all types of films. However, as time progressed, distinct patterns began to emerge. By Day 30, while the Bi sample maintained an FFA level of 0.02 ± 0.009%, the Bi-CN and Bi-CM samples experienced slight increases to 0.03 ± 0.002 % and ±0.009, respectively), marking the beginning of significant ($P<0.05$) differences ($P < 0.05$ for Bi-CM). These differences became more pronounced over time. By Day 45, the Bi-CM sample's FFA level increased to 0.04% (±0.003), significantly ($P< 0.05$), higher than that of the Bi sample at 0.03 ±0.003 %, indicating the impact of the mucilage-infused film on accelerating fat degradation. The trend of increasing FFA levels continued, with the Bi-CM sample showing the most rapid increase.

By Day 60, the FFA level in Bi-CM was 0.05 ± 0.005 %, compared to 0.04 ± 0.002 % in Bi-CN and 0.03 ± 0.001 in Bi. This trend indicates a significantly ($P< 0.05$), faster degradation of fats in the Bi-CM samples, attributed to the possible interactions between the mucilage components and the fats, which may enhance the rate of lipid oxidation or hydrolysis. By Day 120, the FFA levels in the Bi-CM samples had more than quadrupled to 0.12 ± 0.001 %, a significant ($P<0.05$) increase compared to 0.06 ± 0.001% in Bi and 0.08 ± 0.001% in Bi-CN ($P < 0.05$). This suggests that the mucilage-infused film significantly ($P< 0.05$) impacts the stability of fats in the biscuits, accelerating the increase in FFA levels over time compared to the other films. Throughout the study, the observed increases in FFA levels in the Bi-CM samples were consistently higher than those in the Bi and Bi-CN samples, with statistically significant ($P<0.05$) differences. This indicates the profound effect of the mucilage-infused film on the acceleration of fat degradation in

biscuits highlighting the importance of selecting appropriate packaging materials to enhance shelf life and maintain quality in food products.

Table 4.32 Effect on free fatty acid of biscuits during storage

Days	Free fatty acid (%) Bi	Free Fatty acid (%) Bi-CN	Free Fatty acid (%) Bi-CM
Bi0	0.02 ± 0.001^{aA}	0.02 ± 0.001^{aA}	0.02 ± 0.001^{aA}
Bi15	0.02 ± 0.008^{aA}	0.02 ± 0.001^{aA}	0.02 ± 0.001^{aA}
Bi30	0.02 ± 0.009^{aA}	0.03 ± 0.002^{bA}	0.03 ± 0.009^{bA}
Bi45	0.03 ± 0.003^{aA}	0.03 ± 0.005^{bA}	0.04 ± 0.003^{cA}
Bi60	0.03 ± 0.001^{aA}	0.04 ± 0.002^{bB}	0.05 ± 0.005^{cB}
Bi75	0.04 ± 0.002^{bA}	0.05 ± 0.003^{cB}	0.06 ± 0.004^{cB}
Bi90	0.04 ± 0.004^{cA}	0.06 ± 0.007^{eB}	0.08 ± 0.001^{fB}
Bi105	0.05 ± 0.001^{cA}	0.07 ± 0.001^{eB}	0.10 ± 0.004^{fC}
Bi120	0.06 ± 0.001^{cA}	0.08 ± 0.001^{fB}	0.12 ± 0.001^{fC}

[1]Data are displayed as mean ±SEM (n=3) [a-f] with each column with different lowercase superscripts different significantly (P< 0.05) from one another

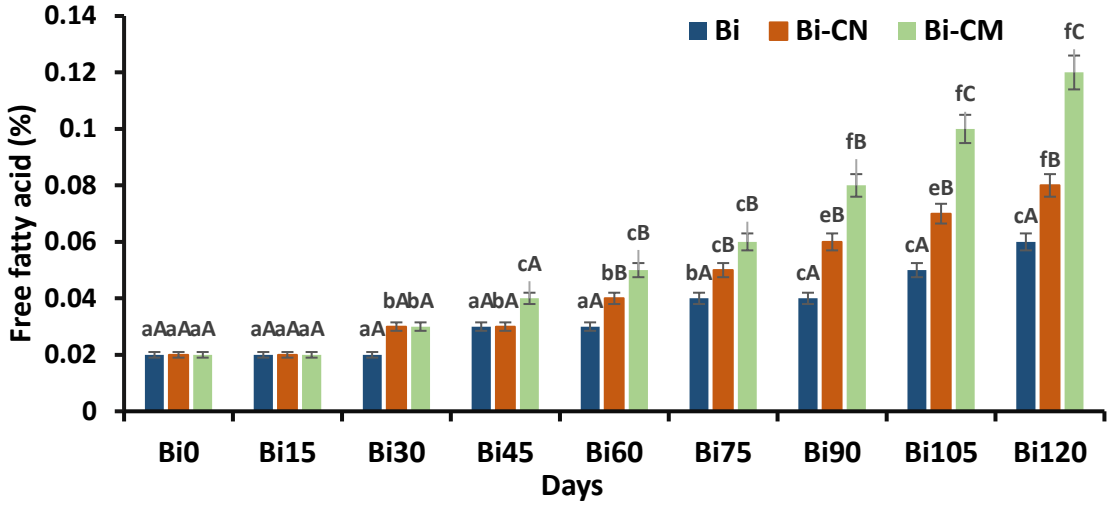

Figure 4.62 Effect on free fatty acid of biscuit during storage

4.15.1.6.3 Effect on free fatty acid of noodles during Storage

Tables 4.33 and **Figure 4.63** offer a comprehensive evaluation of the free fatty acid levels in noodles packaged in various nanocomposite films over 120 days, recorded at 15-day intervals. Three distinct types of films were used: standard control (Nd), a film infused

with nanocellulose (Nd-CN), and a film infused with mucilage (Nd-CM). Initially, on Day 0, all types of noodles began with identical free fatty acid levels of 0.32 ±0.001 %, indicating uniformity across the samples and non-significant (P> 0.05) initial difference. By Day 15, there was a slight increase in the free fatty acids in the Nd-CN and Nd-CM samples to 0.36 ± 0.008 % and 0.38 ±0.006 %, respectively, suggesting a beginning of differentiation in the film's effects, especially noticeable in the Nd-CM (P < 0.05 for Nd-CM compared to Nd-CN).

As the study continued, each subsequent measure generally indicated an increase in free fatty acid levels. By Day 45, Nd-CM samples had reached a level of 0.47 ± 0.001%, significantly (P< 0.05) higher compared to Nd, which showed a level of 0.38 ± 0.03%. Nd-CN also demonstrated a noticeable increase to 0.42 ± 0.005 % compared to the control. By Day 75, the increments became even more distinct with Nd registering a level of 0.43 ± 0.09 %, Nd-CN at 0.48 ± 0.005 %, and Nd-CM advancing to 0.57 ± 0.004 %; both modified films showed significant (P<0.05) increases in free fatty acid levels compared to Nd. Towards the end of the period on Day 120, the free fatty acid levels peaked with Nd-CM showing the highest value at 0.76 ± 0.004 % and Nd-CN following at 0.62 ± 0.002 %. Both were significantly (P< 0.05), higher than Nd, which recorded a level of 0.55 ±0.02 %.

Table 4.33 Effect on free fatty acid of noodles during storage

Days	Free fatty acid (%) Nd	Free fatty acid (%) Nd-CN	Free fatty acid (%) Nd-CM
Nd0	0.32 ± 0.01^{aA}	0.34 ± 0.003^{aA}	0.35 ± 0.003^{aA}
Nd15	0.34 ± 0.08^{aA}	0.36 ± 0.008^{bA}	0.38 ± 0.006^{cA}
Nd30	0.36 ± 0.08^{aA}	0.39 ± 0.005^{bA}	0.42 ± 0.008^{dA}
Nd45	0.38 ± 0.03^{aA}	0.42 ± 0.005^{cA}	0.47 ± 0.001^{cA}
Nd60	0.40 ± 0.05^{bA}	0.45 ± 0.005^{cB}	0.52 ± 0.003^{dC}
Nd75	0.43 ± 0.09^{bA}	0.48 ± 0.005^{cB}	0.57 ± 0.004^{eC}
Nd90	0.46 ± 0.04^{cA}	0.53 ± 0.006^{dB}	0.63 ± 0.002^{fC}
Nd105	0.50 ± 0.06^{cA}	0.57 ± 0.007^{eB}	0.69 ± 0.008^{fC}
Nd120	0.55 ± 0.02^{cA}	0.62 ± 0.002^{fB}	0.76 ± 0.004^{fC}

[1]Data are displayed as mean ± SEM (n=3) $^{a\text{-}f}$ with each column with different lowercase superscripts are different significantly (P< 0.05) from one another

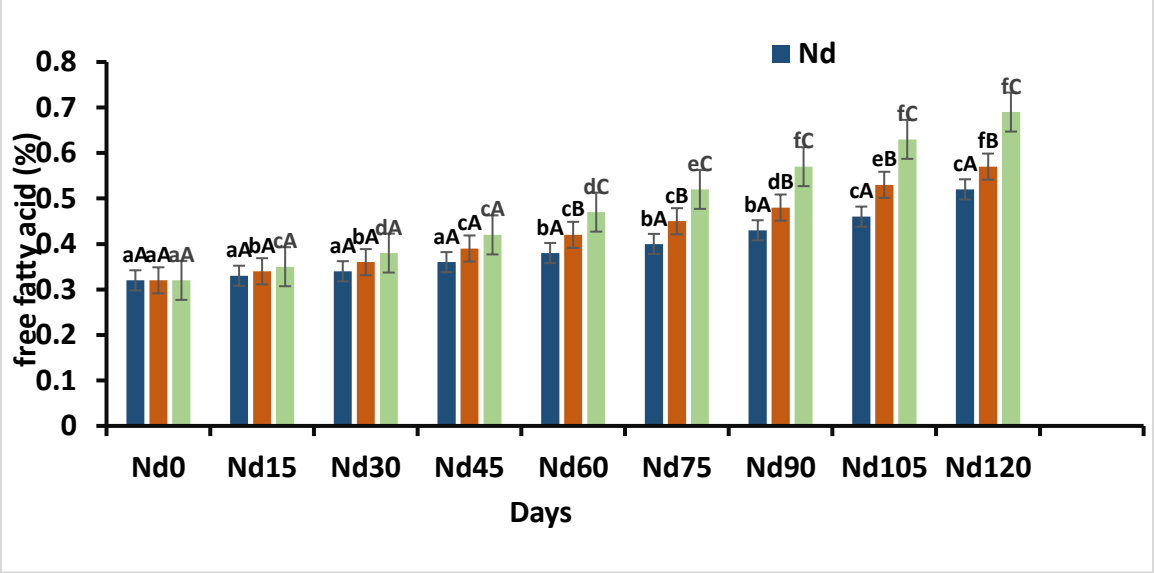

Figure 4.63 Effect on free fatty acid of noodles during storage

This consistent increase in free fatty acids in the Nd-CN and particularly in the Nd-CM samples indicates that the mucilage-infused film significantly ($P < 0.05$), impacts the preservation or degradation processes within the packaged noodles, likely influencing lipid oxidation or hydrolysis, enhancing the increased in free fatty acids over time compared to the standard control. The changes observed over the period were statistically significant, as denoted by P values less than 0.05, highlighting the distinct influence of each film treatment on the chemical stability of the noodles.

4.15.1.7 Effect on TBA of bakery products during storage

4.15.1.7.1 Effect on TBA of bread during storage

Table 4.34 and **Figure 4.64** provide data outlining the thiobarbituric acid reactive substances (TBA) values for bread packaged in various nanocomposite films over 8 days, evaluated every two days. The films assessed include a standard control (Br), a nanocellulose-infused film (Br-CN), and a mucilage-infused film (Br-CM). Initially, on Day 0, all bread samples started with identical TBA values of 6.88, with a standard deviation of ±0.04 across all types, indicating a non-significant ($P > 0.05$) initial difference in lipid oxidation levels. By Day 2, a notable differentiation began to arise; while the Br

samples showed a modest increase to 7.08 ± 0.05 mg MDA/ kg, Br-CN and Br-CM samples demonstrated more significant (P<0.05) increases to 7.67 ± 0.08 mg MDA/ kg and 8.17 ± 0.01 mg MDA/ kg, respectively, indicating a statistically significant (P<0.05) increase in lipid oxidation in the modified films, especially in Br-CM. Progressing to Day 4 and beyond, the TBA values continued to escalate, suggesting a sustained and pronounced lipid oxidation. Br-CM consistently showed the highest TBA values, reaching 10.78 ± 0.05 mg MDA/ kg by Day 4, compared to Br-CN's 9.86 ± 0.06 mg MDA/ kg and Br's 8.86 ± 0.03 mg MDA/ kg. The significant (P<0.05) difference between Br-CM and the other films indicates that the mucilage-infused film accelerates lipid oxidation more effectively than the nanocellulose-infused film. By Day 6, this trend intensified, with Br-CM achieving a TBA value of 13.89 ± 0.03 mg MDA/ kg, significantly (P< 0.05), higher than Br-CN's 11.89 ± 0.07 mg MDA/ kg and Br's 10.12 ± 0.03 mg MDA/ kg.

The elevated TBA values in Br-CM suggest a higher rate of lipid oxidation, possibly due to interactions between the mucilage components and the lipids in the bread-enhancing oxidation processes. On Day 8, the peak of the measurements, Br-CM's TBA value reached 15.34 ± 0.01 mg MDA/ kg, which was significantly (P< 0.05), higher than both Br-CN at 13.67 ± 0.08 mg MDA/ kg and Br at 12.67 ± 0.07 mg MDA/ kg. These observations highlight the progressive and significant (P<0.05) increase in lipid oxidation in the bread samples packaged with Br-CM compared to those with Br and Br-CN, confirming the pronounced impact of mucilage-infused films on accelerating lipid oxidation in bread stored over multiple days.

Table 4.34 Effect on TBA of bread during storage

Days	TBA (mg MDA/ kg) Br	TBA (mg MDA/ kg) Br-CN	TBA (mg MDA/ kg) Br-CM
Br0	6.88 ± 0.04^{aA}	6.88 ± 0.04^{aA}	6.88 ± 0.04^{aA}
Br2	7.08 ± 0.05^{aA}	7.67 ± 0.08^{aB}	8.17 ± 0.01^{bc}
Br4	8.86 ± 0.03^{bA}	9.86 ± 0.06^{bB}	10.78 ± 0.05^{cc}
Br6	10.12 ± 0.03^{cA}	11.89 ± 0.07^{bB}	13.89 ± 0.03^{dc}
Br8	12.67 ± 0.07^{cA}	13.67 ± 0.08^{cB}	15.34 ± 0.01^{ec}

[1]Data are displayed as mean ± SEM (n=3) $^{a-f}$ with each column with different lowercase superscripts are different significantly (P< 0.05) from one another

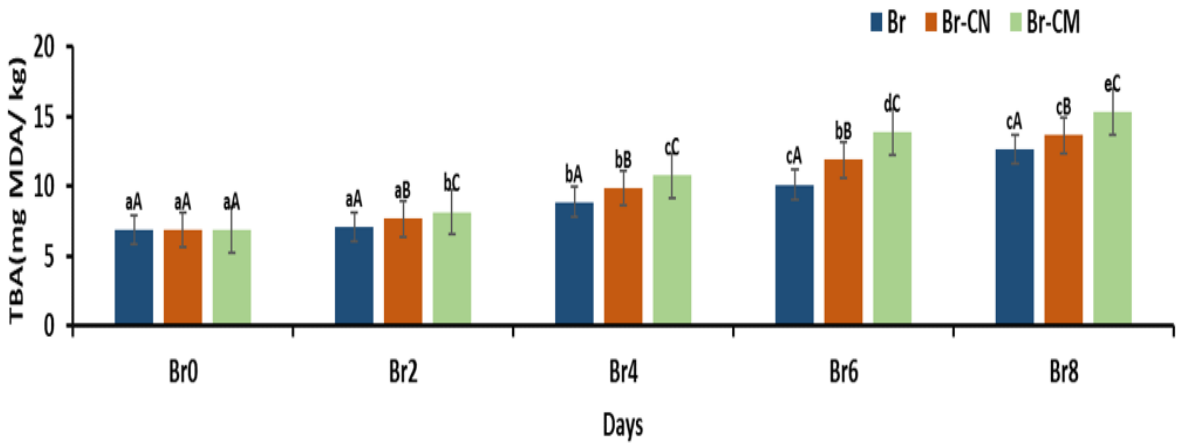

Figure 4.64 Effect on TBA of bread during storage

Each increase in TBA values across the different packaging films was statistically significant ($P<0.05$) as indicated by P values less than 0.05, demonstrating the varying impacts of these nanocomposite films on the lipid stability and quality of the bread over time. The observed trends suggest that while nanocellulose and mucilage-infused films alter the lipid oxidation trajectory, the mucilage-infused films markedly increase the rate of lipid oxidation, impacting the shelf life and sensory qualities of the bread.

4.15.1.7.2 Effect on TBA of biscuit during storage

The data provided in **Table 4.35** and **Figure 4.65** shows an analysis of the thiobarbituric acid reactive substances (TBA) values for biscuits packaged in different nanocomposite films over 120 days, evaluated every 15 days. The types of films assessed were a standard control film (Bi), a nanocellulose-infused film (Bi-CN), and a mucilage-infused film (Bi-CM). Initially, on Day 0, all biscuit samples displayed identical TBA values of 0.38 ± 0.08, suggesting a uniform start with non-significant ($P> 0.05$) oxidative changes among them ($P > 0.05$). This uniformity continued into Day 15 with negligible change across all film types, maintaining the TBA values within a similar range. As the days advanced, each subsequent measurement indicated a gradual increase in TBA values, signifying a progression in lipid oxidation. By Day 45, Bi-CM biscuits showed a TBA value of $0.41 \pm$

0.02 mg MDA/ kg, which was statistically higher compared to Bi, which recorded 0.39 ± 0.02 mg MDA/ kg ($P < 0.05$). Bi-CN also saw a modest increase to 0.39 ± 0.02 mg MDA/ kg, slightly less pronounced than Bi-CM. By Day 75, the differences became more pronounced with Bi recording a TBA value of 0.39 ± 0.03 mg MDA/ kg, while Bi-CN increased to 0.41 ± 0.03 mg MDA/ kg, and Bi-CM further elevated to 0.45 ± 0.03 mg MDA/ kg. Both modified films demonstrated significant ($P<0.05$) increases compared to the standard control, indicating more pronounced lipid oxidation.

By the conclusion of the study on Day 120, the TBA values reached their peak with Bi-CM showing the highest increase at 0.50 ± 0.17 mg MDA/ kg. This was significantly ($P< 0.05$), higher than Bi-CN at 0.44 ± 0.17 mg MDA/ kg and markedly higher than Bi, which posted 0.42 ± 0.17 mg MDA/ kg. This consistent rise in Bi-CM and to a lesser degree in Bi-CN suggests that the mucilage-infused film substantially affects the oxidation stability of lipids in biscuits, increasing their susceptibility to degradation over time compared to the standard and nanocellulose-infused films. The documented changes in TBA values over time among the treatments were statistically significant, as indicated by P values less than 0.05, highlighting the impact of the film treatments on the oxidative stability of the biscuits.

Table. 4.35 Effect on TBA of biscuit during storage

Days	TBA (mg MDA/ kg) Bi	TBA (mg MDA/ kg) Bi-CN	TBA (mg MDA/ kg) Bi-CM
Bi0	0.38 ± 0.08^{aA}	0.38 ± 0.08^{aA}	0.38 ± 0.08^{aA}
Bi15	0.38 ± 0.07^{aA}	0.38 ± 0.07^{aA}	0.39 ± 0.07^{bB}
Bi30	0.38 ± 0.06^{aA}	0.39 ± 0.06^{bA}	0.40 ± 0.06^{cB}
Bi45	0.39 ± 0.02^{aA}	0.39 ± 0.02^{aA}	0.41 ± 0.02^{cB}
Bi60	0.39 ± 0.03^{aA}	0.40 ± 0.03^{bB}	0.43 ± 0.03^{cC}
Bi75	0.39 ± 0.03^{aA}	0.41 ± 0.03^{cB}	0.45 ± 0.03^{cC}
Bi90	0.40 ± 0.02^{aA}	0.42 ± 0.02^{bB}	0.47 ± 0.02^{cC}
Bi105	0.41 ± 0.05^{aA}	0.43 ± 0.05^{bB}	0.49 ± 0.05^{cC}
Bi120	0.42 ± 0.17^{bA}	0.44 ± 0.17^{cB}	0.50 ± 0.17^{cC}

[1]Data are displayed as mean ± SEM (n=3) $^{a-c}$ with each column with different lowercase superscript are different significantly ($P< 0.05$) from one another

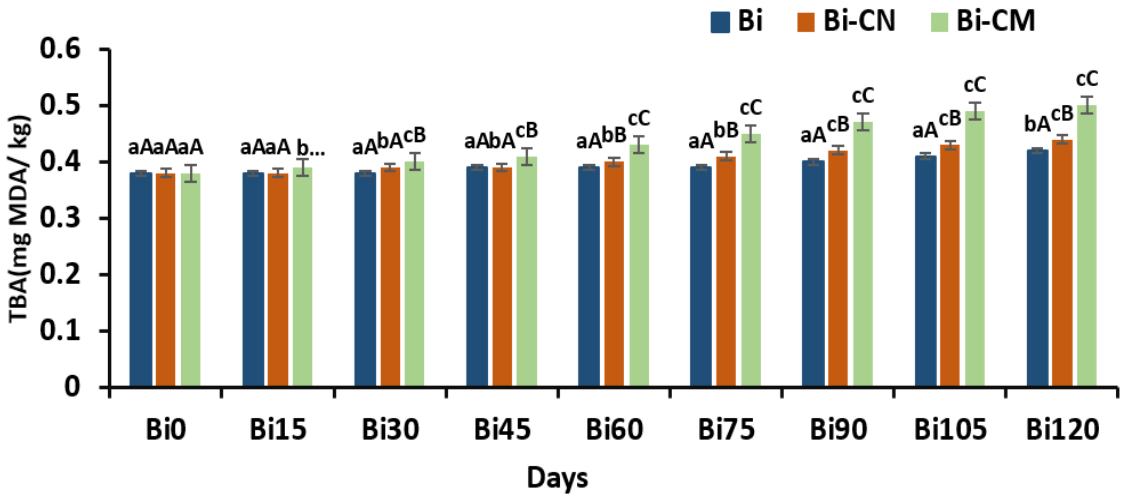

Figure 4.65 Effect on TBA of biscuit during storage

4.15.1.7.3 Effect on TBA of Noodles during storage

The data provided in **Table 4.36** and **Figure 4.66** provide a comprehensive analysis of Thiobarbituric Acid (TBA) values for noodles packaged in different nanocomposite films over a span of 120 days, measured at 15-day intervals. The films were used as a standard control (Nd), a nanocellulose-infused film (Nd-CN), and a mucilage-infused film (Nd-CM). At the outset, on Day 0, all noodle groups exhibited identical TBA values at 0.11 ± 0.06 mg MDA/ kg for Nd and Nd-CN, and slightly lower at 0.11 ± 0.04 mg MDA/ kg for Nd-CM, indicating non-significant ($P>0.05$) oxidative differences initially. This similarity suggests comparable protective qualities among the films at the beginning of the storage period. By Day 15, the TBA values for the Nd-CN and Nd-CM groups began to differentiate slightly from the Nd group, though changes remained statistically non-significant ($P>0.05$). Nd-CN recorded a TBA value of 0.14 ± 0.07 mg MDA/ kg, and Nd-CM was at 0.14 ± 0.05 mg MDA/ kg, compared to 0.13 ± 0.08 mg MDA/ kg for Nd.

Progressing to Day 30, TBA values continued to rise incrementally for all groups, with Nd-CM showing a TBA of 0.17 ± 0.08, now statistically different from Nd's 0.15 ± 0.09 mg MDA/ kg ($P < 0.05$), indicating faster lipid oxidation in the mucilage-infused films. By Day 45, the separation in TBA values became more pronounced; Nd-CM recorded 0.21 ± 0.04 mg MDA/ kg, significantly ($P< 0.05$), higher than Nd's 0.17 ± 0.01 mg MDA/ kg. Nd-

CN's value of 0.19 ± 0.02 mg MDA/ kg remained closer to Nd, though it was starting to show a trend towards higher oxidation. This trend continued, and by Day 75, Nd-CM's TBA value of 0.32 ± 0.04 mg MDA/ kg was significantly ($P< 0.05$), higher than both Nd's 0.22 ± 0.01 mg MDA/ kg and Nd-CN's 0.29 ± 0.09 mg MDA/ kg, illustrating a less effective barrier against oxidation provided by the mucilage-infused film over time.

By the end of the study period on Day 120, Nd-CM reached the highest TBA value of 0.56 ± 0.02 mg MDA/ kg, significantly ($P< 0.05$), higher than Nd-CN's 0.41 ± 0.02 mg MDA/ kg and Nd's 0.34 ± 0.07 mg MDA/ kg ($P < 0.05$). This stark increase emphasizes the progressive decline in oxidative stability under the mucilage-infused film, suggesting it may not be the best choice for long-term storage of noodles compared to the other two film types. Each significant ($P<0.05$) change, marks an important consideration in the selection and use of these films for packaging, particularly with the desired shelf-life and quality retention of packaged foods.

Table 4.36 Effect of TBA on noodles during storage

Days	TBA (mg MDA/ kg) Nd	TBA (mg MDA/ kg) Nd-CN	TBA (mg MDA/ kg) Nd-CM
Nd0	0.11 ± 0.06^{aA}	0.11 ± 0.06^{aA}	0.11 ± 0.04^{aA}
Nd15	0.13 ± 0.08^{aA}	0.14 ± 0.07^{aA}	0.14 ± 0.05^{aA}
Nd30	0.15 ± 0.09^{aA}	0.16 ± 0.01^{bA}	0.17 ± 0.08^{bA}
Nd45	0.17 ± 0.01^{aA}	0.19 ± 0.02^{bA}	0.21 ± 0.04^{cB}
Nd60	0.19 ± 0.03^{aA}	0.25 ± 0.08^{bB}	0.26 ± 0.07^{cB}
Nd75	0.22 ± 0.01^{aA}	0.29 ± 0.09^{cB}	0.32 ± 0.04^{cC}
Nd90	0.25 ± 0.08^{bA}	0.34 ± 0.03^{cB}	0.39 ± 0.04^{dC}
Nd105	0.29 ± 0.06^{cA}	0.38 ± 0.01^{dB}	0.46 ± 0.05^{eC}
Nd120	0.34 ± 0.07^{cA}	0.41 ± 0.02^{eB}	0.56 ± 0.02^{fC}

[1]Data are displayed as mean ± SEM (n=3) $^{a-f}$ with each column with different lowercase superscript are different significantly ($P< 0.05$) from one another

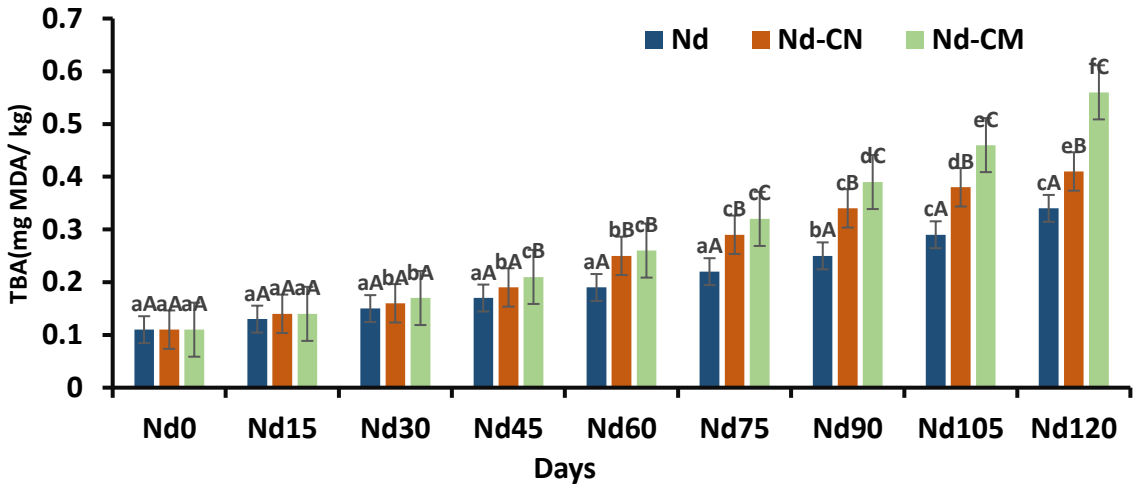

Figure 4.66 Effect o TBA of noodles during storage

4.15.1.8 Effect on peroxide value of bakery products during storage

4.15.1.8.1 Effect on peroxide value of bread during storage

In this study, **Table 4.37** and **Figure 4.67** outline the peroxide values for bread packed in a nanocellulose + mucilage-based film, measured over the initial eight days. Peroxide value is an important indicator of lipid peroxidation, reflecting the primary oxidation products that contribute to food spoilage, particularly in fat-containing products like bread. The data observed the peroxide values (PV) in bread wrapped in three different nanocomposite films: standard (Br), nanocellulose-infused (Br-CN), and mucilage-infused (Br-CM). Initially, all samples started uniformly with a PV of 1.88 ± 0.45 meq O2/ kg, showing non-significant ($P > 0.05$) initial variation. By the second day, Br-CM exhibited a considerable increase to 2.67 ± 0.04 meq O2/ kg, a change indicating significant ($P<0.05$) oxidative activity compared to Br and Br-CN.

This trend of increasing PV was consistently observed particularly in Br-CM, which reached a peak PV of 4.62 ± 1.05 meq O2/ kg by day eight, significantly ($P< 0.05$), higher than the other films. This progression not only underscores the differences in oxidative stability provided by each film type but also suggests that mucilage-infused films may not inhibit peroxide formation as effectively as other films, leading to faster oxidation rates in packaged bread. The consistently higher PV in Br-CM across the days indicates its lesser

effectiveness at maintaining oxidative stability, highlighting the critical impact of film choice on food preservation quality.

Table. 4.37 Effect on peroxide value of bread during storage

Days	Peroxide Value (meq O2/ kg) Br	Peroxide Value (meq O2/ kg) Br-CN	Peroxide Value (meq O2/ kg) Br -CM
Br0	1.88 ± 0.45^{aA}	1.88 ± 0.45^{aA}	1.88 ± 0.45^{aA}
Br2	1.95 ± 0.78^{aA}	2.07 ± 1.02^{aB}	2.67 ± 0.04^{bB}
Br4	2.23 ± 0.72^{aA}	2.83 ± 0.98^{bB}	3.23 ± 0.23^{cB}
Br6	2.49 ± 0.056^{aA}	3.27 ± 0.067^{bB}	3.89 ± 0.002^{cB}
Br8	3.78 ± 1.05^{bA}	3.93 ± 0.87^{cB}	4.62 ± 1.05^{dC}

[1]Data are displayed as mean ±SEM (n=3) [a-c] with each column with different lowercase superscripts are different significantly (P< 0.05) from one another

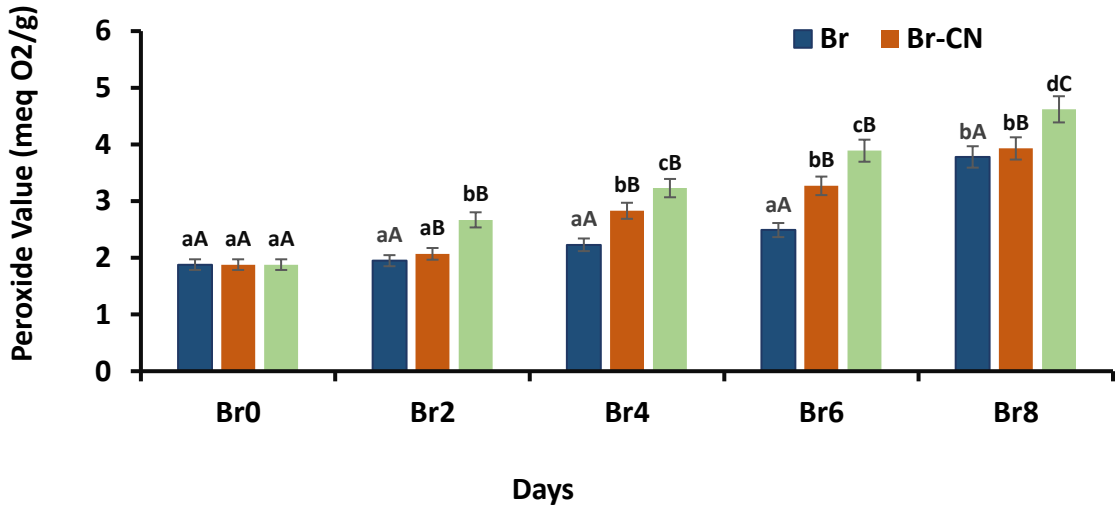

Figure 4.67 Effect on peroxide of bread during storage

4.15.1.8.2 Effect on peroxide value of biscuits during storage

The data presented in **Table 4.38** and **Figure 4.68** detail the analysis of peroxide values for biscuits packaged in various nanocomposite films over 120 days, measured every 15 days. Three types of films were evaluated: a standard film (Bi), a nanocellulose-infused film (Bi-CN), and a mucilage-infused film (Bi-CM). Initially, all films started with a peroxide value of 0.47, indicating a non-significant (P> 0.05) difference at the onset. Over

time, peroxide values gradually increased across all types, with the Bi-CM showing the most significant ($P<0.05$) increase, especially noticeable from Day 105 onwards, suggesting a faster rate of lipid oxidation in the mucilage-infused film. By Day 120, the peroxide values were 0.79 for Bi, 0.80 for Bi-CN, and 0.93 for Bi-CM, with the differences between the films becoming statistically significant ($P< 0.05$), particularly between Bi-CM and the other two types. This trend indicates that the Bi-CM film may interact differently with the biscuit's constituents, potentially enhancing lipid oxidation processes.

Table 4.38 Effect on peroxide value of biscuits during storage

Days	Peroxide Value (meq O2/ kg) Bi	Peroxide Value (meq O2/ kg) Bi-CN	Peroxide Value (meq O2/ kg) Bi -CM
Bi0	0.47 ± 0.006^{aA}	0.47 ± 0.008^{aA}	0.47 ± 0.008^{aA}
Bi15	0.49 ± 0.003^{aA}	0.51 ± 0.003^{aA}	0.53 ± 0.003^{bB}
Bi30	0.51 ± 0.001^{aA}	0.55 ± 0.002^{aB}	0.57 ± 0.005^{cB}
Bi45	0.53 ± 0.001^{aA}	0.58 ± 0.005^{bB}	0.62 ± 0.004^{cC}
Bi60	0.56 ± 0.003^{aA}	0.62 ± 0.006^{bB}	0.68 ± 0.006^{cC}
Bi75	0.60 ± 0.001^{aA}	0.66 ± 0.007^{bB}	0.70 ± 0.001^{cC}
Bi90	0.67 ± 0.002^{aA}	0.71 ± 0.008^{bB}	0.77 ± 0.005^{cC}
Bi105	0.74 ± 0.005^{bA}	0.75 ± 0.002^{bB}	0.85 ± 0.003^{cC}
Bi120	0.79 ± 0.008^{cA}	0.80 ± 0.004^{cB}	0.93 ± 0.002^{dC}

[1]Data are displayed as mean ± SEM (n=3) $^{a-d}$ with each column with different lowercase superscript are different significantly ($P< 0.05$) from one another

The data provides an analysis of the peroxide values for biscuits packaged in different nanocomposite films over 120 days. Measurements were taken every 15 days for three types of films: standard (Bi), nanocellulose-infused (Bi-CN), and mucilage-infused (Bi-CM). At the start, all types recorded a peroxide value of 0.47 ± 0.008 meq O2/ kg, with non-significant ($P> 0.05$) differences. Over time, peroxide values increased with all types of films, with Bi-CM showing the most notable increase. By Day 120, the values reached 0.79 ± 0.008 meq O2/ kg for Bi, 0.80 ± 0.004 meq O2/ kg for Bi-CN, and 0.93 ± 0.002 meq O2/ kg for Bi-CM. The increases from Bi-CM were statistically significant ($P<0.05$) compared to the others, particularly from Day 105 onward, indicating enhanced lipid oxidation potentially due to the interaction of the mucilage content with the biscuits. This

trend suggests that the Bi-CM film may accelerate lipid oxidation, impacting the shelf life and quality of the packaged biscuits.

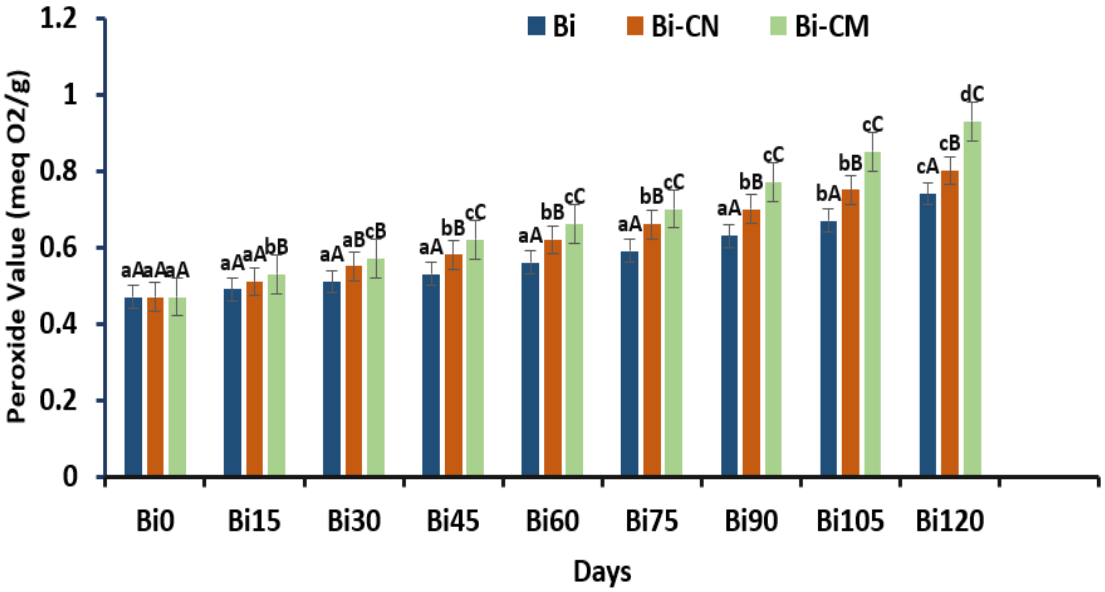

Figure 4.68 Effect on peroxide of biscuit during storage

4.15.1.8.3 Effect on peroxide value of noodles during storage

The data explored in **Table 4.39** and **Figure 4.69** displays the peroxide values of noodles packaged in different nanocomposite films over 120 days, measured every 15 days. Initially, all types—Nd, Nd-CN, and Nd-CM—started with a peroxide value of 0.68 ± 0.003, indicating non-significant ($P>0.05$) initial oxidative differences. As time progressed, gradual increases in peroxide values were observed across all films, with Nd-CM consistently showing the highest values, reflecting a faster rate of oxidation. By Day 120, the differences became more pronounced where the Nd reached 1.13 ± 0.001 meq O2/ kg, Nd-CN at 1.45 ± 0.002 meq O2/ kg, and Nd-CM peaked at 1.64 ± 0.003 meq O2/ kg, demonstrating significant ($P<0.05$) increments at each 15-day interval, especially for Nd-CM which consistently exhibited the most significant ($P<0.05$) increases.

This trend suggests that while all films gradually allow oxidation, the mucilage-infused Nd-CM accelerates it, highlighting its comparative ineffectiveness at inhibiting oxidation over time. These findings underscore the importance of selecting appropriate packaging

materials based on the desired oxidative stability and shelf life of the product. Moreover, the films evaluated include a standard control (Nd), a nanocellulose-infused film (Nd-CN), and a mucilage-infused film (Nd-CM). Initially, all samples started uniformly with peroxide values at 0.68. Throughout the 120 days, peroxide values increased for all types, but the standard film (Nd) showed the least increase, peaking at 1.13, compared to 1.45 for Nd-CN and 1.64 for Nd-CM.

This indicates that Nd is the best film in terms of maintaining lower peroxide values, suggesting its superior capability in preserving the quality of noodles against oxidation ($P < 0.05$). This lesser increase in peroxide values highlights Nd's effectiveness in inhibiting peroxide formation, possibly due to better barrier properties against oxygen, making it the most suitable choice for extending the shelf life of noodles.

Table 4.39 Effect on peroxide value of noodles during storage

Days	Peroxide Value (meq O2/ kg) Nd	Peroxide Value (meq O2/ kg) Nd-CN	Peroxide Value (meq O2/ kg) Nd - CM
Nd0	0.68 ± 0.003^{aA}	0.68 ± 0.003^{aA}	0.68 ± 0.003^{aA}
Nd15	0.69 ± 0.002^{aA}	0.72 ± 0.005^{bB}	0.77 ± 0.006^{bC}
Nd30	0.71 ± 0.005^{aA}	0.78 ± 0.007^{bB}	0.89 ± 0.003^{cC}
Nd45	0.73 ± 0.002^{aA}	0.87 ± 0.002^{bB}	0.99 ± 0.002^{cC}
Nd60	0.76 ± 0.001^{aA}	0.98 ± 0.008^{bB}	1.11 ± 0.003^{cC}
Nd75	0.82 ± 0.006^{aA}	1.09 ± 0.001^{bB}	1.24 ± 0.002^{cC}
Nd90	0.89 ± 0.001^{aA}	1.19 ± 0.003^{bB}	1.36 ± 0.001^{cC}
Nd105	0.97 ± 0.003^{bA}	1.31 ± 0.003^{cB}	1.49 ± 0.005^{dC}
Nd120	1.13 ± 0.001^{cA}	1.45 ± 0.002^{dB}	1.64 ± 0.003^{eC}

[1]Data are displayed as mean ± SD $(n=3)^{a-e}$ with each column with different lowercase superscripts different significantly ($P< 0.05$), from one another

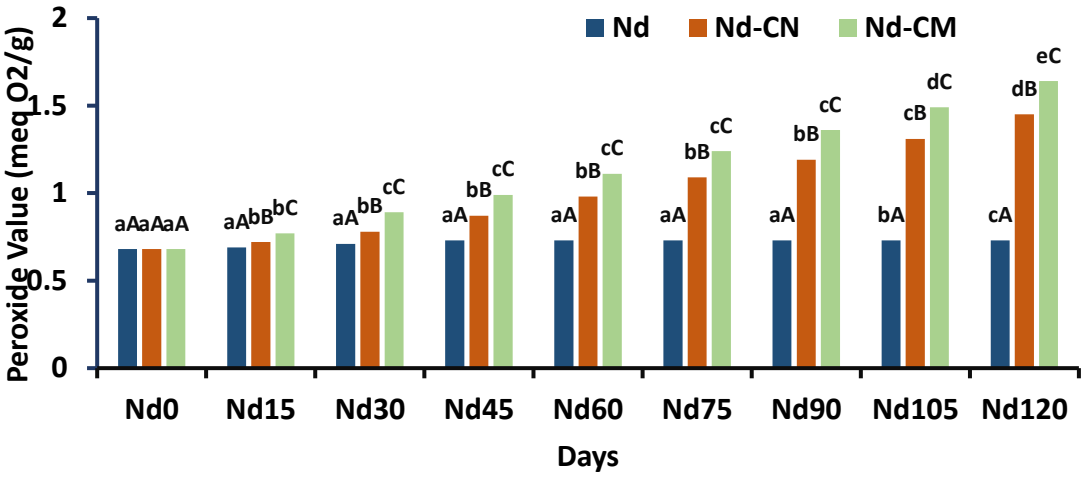

Figure 4.69 Effect on peroxide of noodles during storage

4.15.1.9 Effect on total plate count. of bakery products

4.15.1.9.1 Effect on total plate count. of bread during storage

The data presented in **Table 4.40** and **Figure 4.70** display the data examine the total plate count for bread wrapped in three types of nanocomposite films over eight days, measured at two-day intervals. Initially, all samples registered no detectable microbes (ND), indicating an effective start with no initial contamination. By the second day, microbial levels were low and uniform across all samples at 0.47 ± 0.05 meq O2/ kg, with non-significant (P> 0.05) differences in microbial growth. By day four, microbial counts escalated to 0.87 ± 0.09 meq O2/ kg for the standard film (Br), 1.09 ± 0.09 meq O2/ kg for the nanocellulose-infused film (Br-CN), and 1.33 ± 0.09 meq O2/ kg for the mucilage-infused film (Br-CM). This day marked the beginning of statistically significant (P<0.05) differences, particularly for Br-CM, which showed higher microbial proliferation than Br, suggesting reduced antimicrobial efficacy of the mucilage film. On day 6, counts increased further, recording at 1.12 ± 0.07 meq O2/ kg for Br, 1.29 ± 0.07 meq O2/ kg for Br-CN, and significantly (P< 0.05), higher at 2.33 ± 0.07 meq O2/ kg for Br-CM. The higher microbial count in Br-CM continued to be statistically significant (P<0.05) compared to the other films, indicating ongoing microbial growth in the mucilage-infused film.

The trend continued into day eight, where Br showed a count of 1.98 ± 0.54 meq O2/ kg, Br-CN 2.87 ± 0.54 meq O2/ kg, and Br-CM significantly (P< 0.05), higher at 3.98 ± 0.54. The growth in Br-CM was significantly (P< 0.05), more noticeable than in the other films, confirming a persistent trend of higher microbial proliferation in the mucilage-infused film, suggesting it might require enhancements to its antimicrobial properties to be effective for longer-term usage. The increasing counts in all films, however, indicate that while the mucilage film had the least effective antimicrobial properties, the overall trend suggests a need for improved preservation capabilities across all film types.

Table 4.40 Effect on total plate count of bread during storage

Days	TPC (cfu/g) Br	TPC (cfu/g) Br-CN	TPC (cfu/g) Br-CM
Br0	ND	ND	ND
Br2	0.47 ± 0.05^{aA}	0.47 ± 0.05^{aA}	0.47 ± 0.05^{aA}
Br4	0.87 ± 0.09^{bA}	1.09 ± 0.04^{aB}	1.33 ± 0.22^{bC}
Br6	1.12 ± 0.07^{cA}	1.29 ± 0.08^{bB}	2.33 ± 0.01^{cC}
Br8	1.98 ± 0.54^{cA}	2.87 ± 0.12^{cB}	3.98 ± 0.19^{dC}

[1]Data are displayed as mean± SD (n=3) $^{a-d}$ with each column with different lowercase superscript are different significantly (P< 0.05) from one another

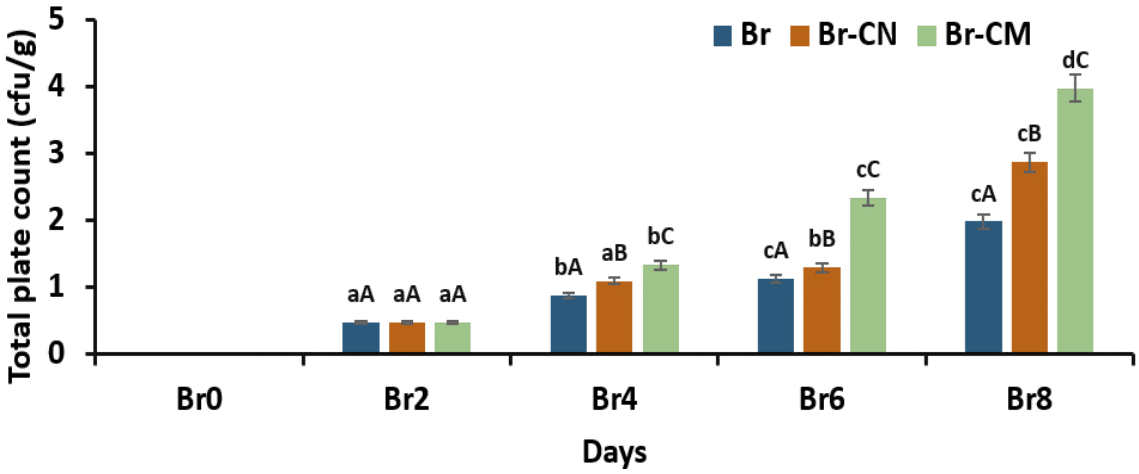

Figure 4.70 Effect on total plate count of bread during storage

4.15.1.9.2 Effect on total plate count of biscuit during storage

Table 4.41 illustrating the total plate count of biscuits encapsulates a study aimed at evaluating the microbial stability of biscuits packaged in nanocellulose + mucilage-based film over a span of 100 days. The provided table outlines the microbial growth, measured as colony-forming units, on biscuits wrapped in various nanocomposite films over a span of 120 days. Measurements were taken every 15 days. The types of films evaluated were a standard film (Bi), a nanocellulose-infused film (Bi-CN), and a mucilage-infused film (Bi-CM). From the onset until day 75, no microbial growth (ND - Not Detected) was observed in any of the samples, indicating effective microbial inhibition likely due to the protective properties of the films. However, significant ($P<0.05$) changes were observed from day 90 onward, particularly in the mucilage-infused samples (Bi-CM). On day 90, the Bi-CN film showed minimal growth at 0.49 ± 0.05 cfu/g, while a drastic increase to 89 ± 0.09 cfu/g was observed in the Bi-CM film, indicating a significant ($P<0.05$) difference between the two.

Table 4.41 Effect on total plate count on biscuits during storage

Days	Total plate count (cfu/g) Bi	Total plate count (cfu/g) Bi-CN	Total plate count (cfu/g) Bi-CM
Bi0	ND	ND	ND
Bi15	ND	ND	ND
Bi30	ND	ND	ND
Bi45	ND	ND	ND
Bi60	ND	ND	ND
Bi75	ND	ND	ND
Bi90	ND	0.49 ± 0.05^{aA}	89 ± 0.09^{aB}
Bi105	ND	1.16 ± 0.09^{bA}	1.89 ± 0.07^{bB}
Bi120	ND	1.32 ± 0.07^{cA}	2.65 ± 0.54^{cB}

[1]Data are displayed as mean ± SD (n=3) $^{a-c}$ with each column with different lowercase superscripts are different significantly ($P< 0.05$) from one another

This trend continued, with microbial counts rising to 1.16 ± 0.09 cfu/g in Bi-CN and 1.89 ± 0.07 cfu/g in Bi-CM by day 105, and further to 1.32 ± 0.07 cfu/g in Bi-CN and 2.65 ± 0.54 cfu/g in Bi-CM by day 120. These results illustrate a marked increase in microbial

counts over time, with Bi-CM showing significantly ($P< 0.05$), higher values compared to Bi-CN. The data suggest that while all films initially prevent microbial growth, the mucilage-infused films (Bi-CM) may become less effective over time, potentially due to degradation or other factors affecting their antimicrobial properties. This underscores the importance of considering long-term stability and efficacy in choosing or designing nanocomposite films for food packaging.

4.15.1.9.3 Effect on total plate count of noodles during storage

Table 4.42 presents the total plate count results for noodles packaged in different nanocomposite films over 120 days, measured at intervals of 15 days. The films assessed include a standard control (Nd), a nanocellulose-infused film (Nd-CN), and a mucilage-infused film (Nd-CM). From days 0 to 75, there were no detectable changes (ND) in the total plate count across all film types, indicating effective microbial control during this period. At day 90, the nanocellulose film (Nd-CN) showed a minimal significant ($P<0.05$) increase in plate count 0.56 ± 0.05 cfu/g while the mucilage-infused film (Nd-CM) showed a significant ($P<0.05$) increase. A value of 97 ± 0.09 cfu/g, suggests a sudden significant ($P<0.05$) decrease in microbial control efficiency, particularly for the mucilage film.

By day 105, the significant ($P< 0.05$), increase in total plate count became more pronounced, with Nd-CN recording 1.37 ± 0.09 cfu/g and Nd-CM showing a significant ($P <0.05$) higher count of 1.92 ± 0.07 cfu/g. By day 120, the total plate count. was further significant ($P< 0.05$), increased to 1.168 ± 0.07 cfu/g for Nd-CN and 2.96 ± 0.54 cfu/g for Nd-CM, confirming a trend of increasing microbial activity over time, particularly in the mucilage-infused film which showed significantly ($P< 0.05$), higher values compared to the control and nanocellulose films. This suggests that while all films initially prevent microbial growth, the effectiveness of the mucilage-infused film diminishes more rapidly, indicating potential issues with long-term microbial resistance or film integrity.

Table 4.42 Effect on total plate count of noodles during storage

Days	Total plate count (cfu/g) Nd	Total plate count (cfu/g) Nd-CN	Total plate count (cfu/g) Nd-CM
Nd0	ND	ND	ND
Nd15	ND	ND	ND
Nd30	ND	ND	ND
Nd45	ND	ND	ND
Nd60	ND	ND	ND
Nd75	ND	ND	ND
Nd90	ND	0.56 ± 0.05^{aA}	97 ± 0.09^{aB}
Nd105	ND	1.37 ± 0.09^{bA}	1.92 ± 0.07^{bB}
Nd120	ND	1.68 ± 0.07^{cA}	2.96 ± 0.54^{cB}

[1]Data are displayed as mean ± SD (n=3) $^{a-C}$ with each column with different lowercase superscript are different significantly ($P< 0.05$), from one another.

4.16 Comparative analysis of Different types of Packaging material

4.16.1 Surface morphology of different types of packaging material

The provided SEM images in **Figure 4.71** offer a comprehensive look at three different types of packaging materials, each magnified 1,000 times to highlight their unique surface morphologies, which play a critical role in their application in the packaging industry.

Where Image A shows a nanocomposite film enriched with mucilage. This film displays a highly textured, layered, and porous structure. The incorporation of natural polymers like mucilage contributes to this unique morphology, enhancing the film's barrier properties and biodegradability. Such features are beneficial for applications requiring active ingredient release or moisture control, making it suitable for innovative and sustainable packaging material.

This trend continued, with microbial counts rising to 1.16 ± 0.09 cfu/g in Bi-CN and 1.89 ± 0.07 cfu/g in Bi-CM by day 105, and further to 1.32 ± 0.07 cfu/g in Bi-CN and 2.65 ± 0.54 cfu/g in Bi-CM by day 120. These results illustrate a marked increase in microbial counts over time, with Bi-CM showing significantly ($P< 0.05$), higher values compared to Bi-CN. The data suggest that while all films initially prevent microbial growth, the mucilage-infused films (Bi-CM) may become less effective over time, potentially due to degradation or other factors affecting their antimicrobial properties. This underscores the

importance of considering long-term stability and efficacy in choosing or designing nanocomposite films for food packaging.

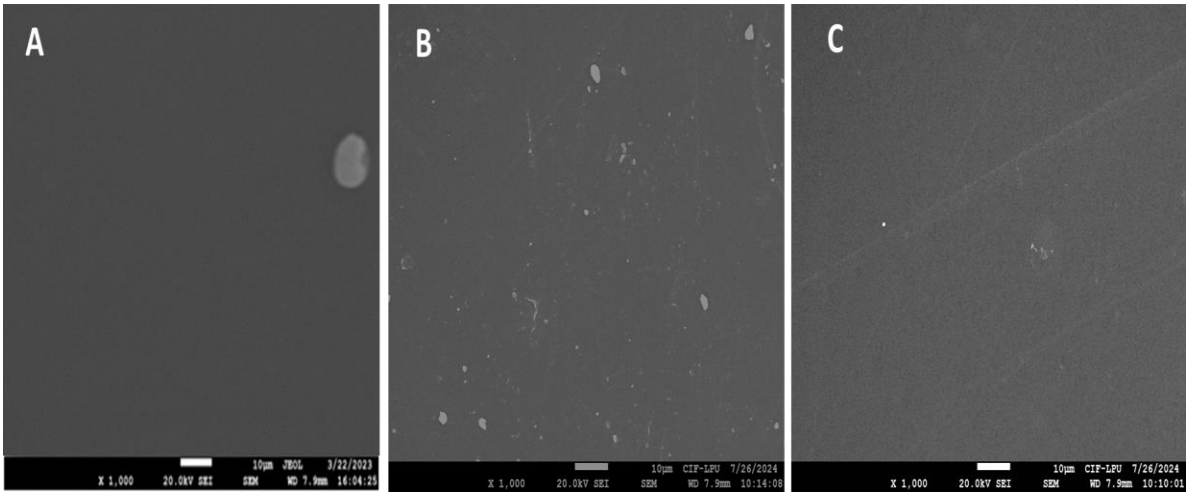

Figure 4.71 Comparative analysis of surface morphology of different types of packaging material (A) Nanocomposite film (B) Cellophane film (C) Polypropylene film.

Where, Image B features a cellophane film, which is noticeably smoother compared to the nanocomposite film but still presents minor white spots, likely imperfections or dust. Cellophane, made from regenerated cellulose, is valued for its high transparency and effective barrier against oils and greases, though it only provides moderate moisture resistance. Its smooth and clear appearance makes it ideal for packaging where product visibility is crucial, such as in food packaging. Image C illustrates a polypropylene film, characterized by its extremely smooth and even surface, showing almost no imperfections. Polypropylene is a widely used thermoplastic polymer noted for its excellent chemical resistance and mechanical properties, including superior moisture barrier capabilities. This makes it an excellent choice for packaging applications that require robust protection against environmental factors, suitable for a wide range of products from dry goods to electronic components.

In summary, each film has its unique advantages required for different packaging materials, each material has its unique advantages based on its inherent properties to meet diverse packaging requirements. The choice of the best film depends on balancing factors such as

environmental impact, barrier requirements, product visibility, and the specific physical properties required by the packaged goods. When evaluating packaging materials based on biodegradability and environmental sustainability, the nanocomposite film incorporating mucilage as depicted in Image A emerges as the most favorable option. This structure of the film, characterized by its porous and layered morphology, indicates the inclusion of natural polymers which are often more biodegradable than synthetic alternatives.

4.16.2 Confirmation of functional group of different types of packaging material

The provided FTIR images in **Figure 4.72** offer a comprehensive look at three different types of packaging materials. The Fourier Transform Infrared Spectroscopy (FTIR) spectra for the nanocomposite film (A), cellophane film (B), and polypropylene film (C) reveal distinct functional groups characteristic of each material, highlighting differences in their chemical compositions. The nanocomposite film exhibits a broad peak around 3400 cm^-1, indicative of -OH groups, suggesting the presence of hydroxyl functional groups from natural polymers like mucilage. Additional peaks around 2925 and 2850 cm^-1 reflect C-H stretching typical of organic compounds, while a range of signals between 1500 and 1000 cm^-1 likely represent various C-O stretches associated with esters, ethers, or alcohols.

The cellophane film, derived from regenerated cellulose, shows a sharp peak around 3340 cm^-1 for O-H stretching and around 2900 cm^-1 for C-H stretching. The region between 1500 and 900 cm^-1 contains multiple peaks indicative of glycosidic linkages in cellulose, reflecting its semi-crystalline structure. In contrast, the polypropylene film displays a simpler spectral pattern with a prominent peak around 2950 cm^-1 for C-H stretching and additional peaks between 1450 and 1375 cm^-1 associated with CH_3 bending modes. This pattern is characteristic of the synthetic, saturated hydrocarbon structure of polypropylene.

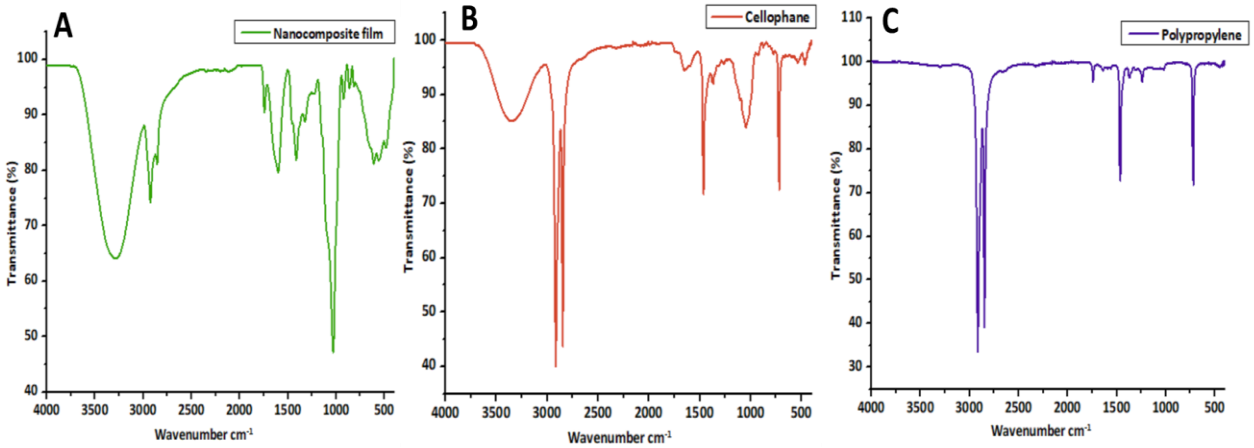

Figure 4.72 Comparative analysis of the functional group of different types of packaging material (A) Nanocomposite film (B) Cellophane film (C) Polypropylene film

Comparatively, the nanocomposite film shows a more complex range of functional groups than the simpler, more uniform patterns observed in the synthetic polypropylene. This complexity in the nanocomposite film may offer advantages such as enhanced biodegradability and environmental interaction due to the presence of natural polymers. On the other hand, cellophane and polypropylene films exhibit characteristics aligned with their respective natural and synthetic origins, influencing their applications in packaging. The presence of broad O-H peaks in both the nanocomposite and cellophane suggest higher hydrophilicity compared to the predominantly hydrophobic polypropylene, which impacts their suitability for different packaging needs based on moisture barrier requirements.

This comprehensive study evaluated the impact of various nanocomposite films on the preservation and quality of bakery products bread, biscuits, and noodles over specified periods. Key findings and observations from the study are summarized below. The proximate analysis of Parmal and Basmati rice straw powders revealed significant differences in their composition. Parmal rice straw powder exhibited higher moisture and protein content, while Basmati had higher crude fat and fiber content. These compositional differences influence the suitability of each rice straw variety for specific applications such as packaging, absorbent materials, and energy storage. Functional property analyses highlighted the importance of factors such as density, porosity, water-holding capacity, and oil-holding capacity in determining the suitability of rice straw for various applications.

- The study on cellulose extraction from rice straw, specifically Basmati and Parmal varieties, focused on optimizing pretreatment and delignification processes using NaOH and calcium chlorite. Optimal conditions identified were 4.83 % NaOH concentration, 116.66 min reaction time, and 107.79 °C temperature, and 4. 68 % NaOH concentration, 90 min reaction time, and 91.23 °C temperature and 4.68 %. These conditions yielded 89.37 % cellulose for Basmati and 89.23 % for Parmal respectively. The findings underscore the importance of precise control over extraction variables to maximize cellulose yield, highlighting significant industrial applications.

- Nanocellulose, synthesized using citric acid and ferric chloride, demonstrated significant potential in enhancing the properties of biodegradable films.

- FTIR, SEM, and other analyses confirmed the successful modification and structural integration of nanocellulose into the films.

- Formulations incorporating varying concentrations of nanocellulose, mucilage, glycerol, and sodium alginate were optimized for specific properties. The formulation F8, with a balance of 5% nanocellulose and 4% mucilage, was identified as optimal for achieving superior mechanical strength, moisture content, and other critical properties.

- The study provided a comprehensive analysis of moisture content in bread, biscuits, and noodles packaged with various nanocomposite films over designated periods. Bread samples packaged in standard control, nanocellulose-infused, and mucilage-infused films showed significant moisture loss over 8 days, with mucilage-infused films exhibiting the most substantial decrease.

- Biscuits showed significant moisture increases over 120 days, with mucilage-infused films again demonstrating the highest retention, significantly affecting the shelf life of the products. Similarly, noodles packaged in mucilage-infused films exhibited the highest moisture content over 120 days than standard films, demonstrating

- These findings highlight significantly better performance than mucilage-infused films and nanocellulose-infused films. The superior moisture retention capabilities of mucilage, suggest its potential for enhancing packaging film properties to maintain product quality and extend shelf life. In the context of pH stability, both biscuits and noodles showed a progressive decline in pH over 120 days, with mucilage-infused films exhibiting the most significant impact. This suggests a strong interaction between the mucilage film and the food products, potentially affecting their quality. The study also analyzed the hardness and textural properties of bread and biscuits, finding that mucilage-infused films led to significant changes in hardness, indicating an impact on the texture of these products. For bread, the mucilage-infused films led to a significant increase in hardness, while biscuits showed a notable softening over time.

- The study also highlighted the impact of different nanocomposite films on lipid oxidation in bread, biscuits, and noodles. Free Fatty Acid (FFA) levels, Thiobarbituric Acid Reactive Substances (TBA) values, and peroxide values were measured to assess lipid oxidation. Mucilage-infused films consistently led to the highest increases in FFA levels across all food types, indicating a significant effect on lipid degradation. Similarly, TBA and peroxide values were highest in products

packaged with mucilage-infused films, suggesting accelerated lipid oxidation compared to nanocellulose-infused and standard films. These findings highlight the need for careful selection of packaging materials to manage lipid oxidation and maintain product quality.

- Furthermore, the total plate count analysis for bread, biscuits, and noodles packaged in different nanocomposite films over various periods demonstrated significant differences in microbial growth. For bread over 8 days, the mucilage-infused film consistently showed higher microbial counts compared to the standard and nanocellulose-infused films, indicating reduced antimicrobial efficacy of the mucilage film.

- For biscuits and noodles over 120 days, similar trends were observed, with mucilage-infused films exhibiting higher microbial growth from day 90 onwards, suggesting diminishing effectiveness in preventing microbial proliferation compared to the other films. Overall, while all films initially provided effective microbial inhibition, the mucilage-infused films demonstrated a trend of reduced long-term effectiveness, highlighting the need for improved antimicrobial properties for extended food preservation. In conclusion, this study demonstrates the significant influence of nanocomposite films on the quality and preservation of various food products.

- Mucilage-infused films, while superior in moisture retention, showed higher rates of lipid oxidation and microbial growth, indicating potential trade-offs. Nanocellulose-infused films offered a balance between structural integrity and oxidative stability but were less effective in long-term microbial control.

The findings of this study underscore the critical role that packaging materials play in preserving the quality and extending the shelf life of food products. The selection of suitable packaging materials must be tailored to the specific preservation needs of each food product, considering factors such as moisture sensitivity, susceptibility to microbial spoilage, and oxygen permeability requirements. While this study highlights the potential

of mucilage-infused films as a sustainable packaging option, there are several avenues for future research to further optimize and expand their applicability in food packaging:

Future research should focus on enhancing the antimicrobial properties of mucilage-infused films and conducting broader evaluations of different film compositions to optimize their applications in food packaging. Given the increasing emphasis on sustainability, future studies should also examine mucilage-based films' biodegradability and environmental impact. Understanding their degradation rate and impact on soil or water systems will provide critical insights into their viability as eco-friendly alternatives to conventional plastic packaging. Research should focus on optimizing extraction methods for mucilage to reduce costs, improve yield, and enhance consistency. Additionally, studies should analyze the cost-effectiveness of producing these films at industrial levels compared to conventional packaging options. Consumer acceptance of mucilage-infused films as a food packaging material is another important aspect for future research. Studies involving sensory evaluation and market trials can help understand consumer perceptions of these films. Furthermore, ensuring that the films comply with food safety regulations and packaging standards in various regions will be essential. By addressing these research directions, mucilage-infused films can evolve into a versatile and sustainable packaging solution, catering to the food industry's diverse needs while reducing reliance on non-biodegradable materials.

1. Abaku, E. A., and A. C. Odimarha. 2024. “Sustainable Supply Chain Management in the Medical Industry: A Theoretical and Practical Examination.” *International Medical Science Research Journal* 4 (3): 319–40.

2. Aminah, S., J. Hermanianto, N. E. Suyatma, and E. S. Iriani. 2024. “Producing Nanocellulose from Kenaf (Hibiscus Cannabinus L) as a Nanoreinforcing Agent for Polyvinyl Alcohol (PVA) Film.” *International Journal of Nano and Biomaterials* 10 (3): 189–203.

3. Ariga, Katsuhiko. 2024. “Materials Nanoarchitectonics at Dynamic Interfaces: Structure Formation and Functional Manipulation.” *Materials* 17 (1). https://doi.org/10.3390/ma17010271.

4. Badr-Eddine, Ayoub El, Younes Idrissi, and Mohamed Essamlali. 2024. “Nanocellulose: Structure, Modification, Biodegradation and Applications in Agriculture as Slow/Controlled Release Fertilizer, Superabsorbent, and Crop Protection: A Review.” *Journal of Environmental Management* 352.

5. Barik, M., G. V. S. Bhagyaraj, K. K. Dash, and R. Shams. 2024. “A Thorough Evaluation of Chitosan-Based Packaging Film and Coating for Food Product Shelf-Life Extension.” *Journal of Agriculture and Food Research*.

6. Berglund, Jennie, Deirdre Mikkelsen, Bernadine M. Flanagan, Sushil Dhital, Stefan Gaunitz, Gunnar Henriksson, Mikael E. Lindström, Gleb E. Yakubov, Michael J. Gidley, and Francisco Vilaplana. 2020. “Wood Hemicelluloses Exert Distinct Biomechanical Contributions to Cellulose Fibrillar Networks.” *Nature Communications* 11 (1): 4692.

7. Cabrera-Villamizar, Laura Andrea, Mahrokh Ebrahimi, Antonio Martínez-Abad, David Talens-Perales, Amparo López-Rubio, and María José Fabra. 2024. “Order Matters: Methods for Extracting Cellulose from Rice Straw by Coupling Alkaline, Ozone and Enzymatic Treatments.” *Carbohydrate Polymers* 328 (March): 121746.

8. Cheng, Juan, Rui Gao, Yong Zhu, and Qinbao Lin. 2024. “Applications of Biodegradable Materials in Food Packaging: A Review.” *Alexandria Engineering Journal* 91 (March): 70–83.

9. Danapriatna, N., I. Ismarani, R. Luthifadi, and M. Dede. 2023. “Effect of Straw Compost (Oryza Sativa L).” *Oryza Sativa L.) on Crop Production*.

10. Eversole, L. M., R. Adjorlolo, J. F. Renaud, and M. Bhowmick. 2024. “Optical Limiting from CdSe-Based Multiphase Polymer Nanocomposite Films.” *Coatings* 14 (5).

11. Ghosh, Tabli, Swarup Roy, Ajahar Khan, Kona Mondal, Parya Ezati, and Jong-Whan Rhim. 2024. “Agricultural Waste-Derived Cellulose Nanocrystals for Sustainable Active Food Packaging Applications.” *Food Hydrocolloids* 154 (110141): 110141.

12. Gupta, R. K., P. Guha, and P. P. Srivastav. 2024. “Packaging Requirements of Processed Citrus Juice and Products.” In *Citrus Fruits and Juice: Processing and Quality Profiling*, 365–89. Singapore; Singapore: Springer Nature.

13. Han, H., Z. Zeeshan, B. A. Talpur, T. Sadiq, U. A. Bhatti, E. M. Awwad, and Ghadi. 2024. “Studying Long Term Relationship between Carbon Emissions, Soil, and Climate Change: Insights from a Global Earth Modeling Framework.” *International Journal of Applied Earth Observation and Geoinformation* 130.

14. Hawanis, H. S. N., R. A. Ilyas, R. Jalil, R. Ibrahim, R. A. Majid, and N. H. Hamid. 2024. *Insights into Lignocellulosic Fiber Feedstock and Its Impact on Pulp and Paper Manufacturing: A Comprehensive Review. Sustainable Materials and Technologies*.

15. Jaouahar, Mohamed, El-Houssaine Ablouh, Zouhair Hanani, Blaž Jaklič, Matjaz Spreitzer, Fatima-Zahra Semlali, Anass Ait Benhamou, Youssef Samih, Mounir El

Achaby, and Houssine Sehaqui. 2024. “Preparation and Characterization of Sulfated Nanocellulose: From Hydrogels to Highly Transparent Films.” *International Journal of Biological Macromolecules* 260 (Pt 1): 129464.

16. Kaur, Ajit, and Rajwinder Singh. 2024. “Rice Straw: Status, Management and Strategies for Sustainable Development with Special Emphasis on the Northern India and Government-Supported Initiatives.” *Clean Technologies and Environmental Policy*, February. https://doi.org/10.1007/s10098-024-02749-7.

17. Lengowski, Elaine C., Talita Szlapak Franco, Livia Cassia Viana, Eraldo A. Bonfatti Júnior, and Graciela I. B. de Muñiz. 2023. “Micro and Nanoengineered Structures and Compounds: Nanocellulose.” *Cellulose (London, England)* 30 (17): 10595–632.

18. Li, Xiaoning, Liping Wang, Bin Tan, and Ren Li. 2024. “Effect of Structural Characteristics on the Physicochemical Properties and Functional Activities of Dietary Fiber: A Review of Structure-Activity Relationship.” *International Journal of Biological Macromolecules* 269 (Pt 2): 132214.

19. Mahato, Richa Prasad, and Saurabh Kumar. 2024. “A Review on Green Approach toward Carbohydrate-Based Nanocomposite Synthesis from Agro-Food Waste to Zero Waste Environment.” *Nanotechnology for Environmental Engineering*, March. https://doi.org/10.1007/s41204-024-00361-0.

20. Onwuka, O. U., and A. Adu. 2024. “Eco-Efficient Well Planning: Engineering Solutions for Reduced Environmental Impact in Hydrocarbon Extraction.” *International Journal of Scholarly Research in Multidisciplinary Studies* 4 (01): 33–043.

21. Parihar, D. S., M. K. Narang, B. Dogra, A. Prakash, and A. Mahadik. 2023. “Rice Residue Burning in Northern India: An Assessment of Environmental Concerns

and Potential Solutions-a Review." *Environmental Research Communications*, no. 5.

22. Parra-Palma, C., C. Valdes, M. Muñoz-Vera, L. Morales-Quintana, and R. I. Castro. 2024. "Assessing the Modifications and Degradation of Cell Wall Polymers during the Ripening Process of Rubus Ulmifolius Schott Fruit." *The Journal of Horticultural Science and Biotechnology*, 1–9.

23. Ponnalagar, Dineshkumar, Da-Ren Hang, Chi-Te Liang, and Mitch M. C. Chou. 2024. "Recent Advances and Future Prospects of Low-Dimensional Mo2C MXene-Based Electrode for Flexible Electrochemical Energy Storage Devices." *Progress in Materials Science* 145 (101308): 101308.

24. Rajasekar, M., V. Kavyashree, E. Sangamithra, P. Baskaran, M. F. Maria, and J. Mary. 2024. "Review on Biomaterial Applications of Photoresponsive Based Chromophore Hydrogels: Recent Developments and Future Perspectives." In *Chemistry 101462*.

25. Rajasekar, M., V. Kavyashree, E. Sangamithra, P. Baskaran, M. F. Maria, J. Mary, and Selvam. 2024. "Review on Biomaterial Applications of Photoresponsive Based Chromophore Hydrogels: Recent Developments and Future Perspectives." *Results in Chemistry* 101462.

26. Röder, Mirjam, Patricia Thornley, and Craig Jamieson. 2024. "The Greenhouse Gas Performance and Climate Change Mitigation Potential from Rice Straw Biogas as a Pathway to the UN Sustainable Development Goals." *Biomass & Bioenergy* 182 (107072): 107072.

27. Selvaraj, S., A. Chauhan, V. Dutta, R. Verma, S. K. Rao, A. Radhakrishnan, and S. Ghotekar. 2024. "A State-of-the-Art Review on Plant-Derived Cellulose-Based Green Hydrogels and Their Multifunctional Role in Advanced Biomedical Applications." *International Journal of Biological Macromolecules*.

28. Shakeel, Usama, Yu Zhang, Evangelos Topakas, Wen Wang, Cuiyi Liang, and Wei Qi. 2024. “Unraveling Interplay between Lignocellulosic Structures Caused by Chemical Pretreatments in Enhancing Enzymatic Hydrolysis.” *Carbohydrate Polymers* 334 (122037): 122037.

29. Siddiqui, S. A., X. Yang, R. K. Deshmukh, K. K. Gaikwad, N. A. Bahmid, and R. Castro-Muñoz. 2024. “Recent Advances in Reinforced Bioplastics for Food Packaging-A Critical Review.” *International Journal of Biological Macromolecules*.

30. Singh, Ashwani Kumar, Raman Bedi, and Akhil Khajuria. 2024. “A Review of Composite Materials Based on Rice Straw and Future Trends for Sustainable Composites.” *Journal of Cleaner Production*, no. 142417 (May): 142417.

31. Suleiman, Gasim Sebit Ahmed, Xu Zeng, Rupesh Chakma, Ibrahim Y. Wakai, and Yakai Feng. 2024. “Recent Advances and Challenges in Thermal Stability of PVA-based Film: A Review.” *Polymers for Advanced Technologies* 35 (2). https://doi.org/10.1002/pat.6327.

32. Sun, Jinsheng, Liyao Dai, Kaihe Lv, Zhibo Wen, Yecheng Li, Dongqing Yang, Hao Yan, Xinyue Liu, Chaozheng Liu, and Mei-Chun Li. 2024. “Recent Advances in Nanomaterial-Stabilized Pickering Foam: Mechanism, Classification, Properties, and Applications.” *Advances in Colloid and Interface Science* 328 (May): 103177.

33. Taher, M. A., K. F. Hasan, and J. Zhu. 2024. “Novel Transparent Lignin/Epoxy Resin Nanocomposite Film Development with Enhanced UV Resistance Performance.” *Journal of Applied Polymer Science* 141 (18).

34. Thivya, P., P. N. Gururaj, N. Bhanu Prakash Reddy, and R. Rajam. 2024. “Recent Advances in Protein-Polysaccharide Based Biocomposites and Their Potential Applications in Food Packaging: A Review.” *International Journal of Biological Macromolecules* 268 (Pt 2): 131757.

35. Verma, M., P. Singh, and M. Dhanorkar. 2024. “Sustainability in Residue Management: A Review with Special Reference to Indian Agriculture.” *Paddy and Water Environment* 22 (1): 1–15.

36. Wang, X., X. Chang, L. Ma, J. Bai, M. Liang, and S. Yan. 2023. “Global and Regional Trends in Greenhouse Gas Emissions from Rice Production, Trade, and Consumption.” *Environmental Impact Assessment Review* 101.

37. Abdallah, Areej Fathelrahman, Mohammad Jawaid, Ainun Zuriyati Mohamed, Paridah Md Tahir, Fathelrahman Abdalla Osman, and Ummi Hani Abdullah. 2023. “A Review on Alkaline Sulfite Anthraquinone Methanol as an Alternative Pulping Process for Non-Woody Biomass.” *Biomass Conversion and Biorefinery*, November. https://doi.org/10.1007/s13399-023-05006-x.

38. Agrawal, Ruchi, Amit Verma, Reeta Rani Singhania, Sunita Varjani, Cheng Di Dong, and Anil Kumar Patel. 2021. “Current Understanding of the Inhibition Factors and Their Mechanism of Action for the Lignocellulosic Biomass Hydrolysis.” *Bioresource Technology* 332 (125042): 125042.

39. Ahmad, A., A. Qurashi, and D. Sheehan. 2023. “Nano Packaging-Progress and Future Perspectives for Food Safety, and Sustainability. Food Packaging and Shelf Life” 35.

40. Amoakwah, E., J. Sangho, J. H. Shim, S. H. Kim, Y. H. Lee, S. I. Kwon, and S. J. Park. 2024. “Temporal Variations in Carbon Stocks and Soil Fertility in Inceptisols after 12 Years of Paddy Rice Cultivation.” *Plant and Soil* 497 (1): 339–57.

41. Anand, Shubham, and Harleen Kaur. 2024. “Challenges and Opportunities in Sustainable Stubble Management in Punjab: A Review.” *International Journal of Environment and Climate Change* 14 (3): 274–97.

42. Andersen, J., A. Mancini, M. Bosetti, P. Solovyev, T. Nardin, R. Larcher, and E. Franciosi. 2022. “Enrichment of Model-Cheeses with Blackcurrant or Cornelian Cherry Increases the Total Amount of Polyphenols.” In *36th EFFoST International Conference: Shaping the Production of Sustainable, Healthy Foods for the Future*. Dublin, Ireland.

43. Anusiya, Ganesan, and Rengarajan Jaiganesh. 2022. “A Review on Fabrication Methods of Nanofibers and a Special Focus on Application of Cellulose Nanofibers.” *Carbohydrate Polymer Technologies and Applications* 4 (100262): 100262.

44. Arnold, Nathanael D., Wolfram M. Brück, Daniel Garbe, and Thomas B. Brück. 2020. “Enzymatic Modification of Native Chitin and Conversion to Specialty Chemical Products.” *Marine Drugs* 18 (2): 93.

45. Babaei-Ghazvini, Amin, Bahareh Vafakish, Ravi Patel, Kehinde James Falua, Matthew J. Dunlop, and Bishnu Acharya. 2024. “Cellulose Nanocrystals in the Development of Biodegradable Materials: A Review on CNC Resources, Modification, and Their Hybridization.” *International Journal of Biological Macromolecules* 258 (Pt 1): 128834.

46. Bandara, K. M. N. T. K., and G. A. G. Kavindi. 2023. “Insights of Circular Economics Practices in Rice Cultivation and Processing-A.” *Journal of Agriculture and Value Addition* 6 (2): 1–36.

47. Bangar, Sneh Punia, William Scott Whiteside, Priyanka Kajla, and Milad Tavassoli. 2023. “Value Addition of Rice Straw Cellulose Fibers as a Reinforcer in Packaging Applications.” *International Journal of Biological Macromolecules* 243 (125320): 125320.

48. Bar, Mahadev, R. Alagirusamy, and Apurba Das. 2019. “Influence of Friction Spun Yarn and Thermally Bonded Roving Structures on the Mechanical Properties of

Flax/Polypropylene Composites." *Industrial Crops and Products* 135 (September): 81–90.

49. Basha, Zaid Ali. 2023. "The Agrarian Question in Yemen: The National Imperative of Reclaiming and Revalorizing Indigenous Agroecological Food Production." *The Journal of Peasant Studies* 50 (3): 879–930.

50. Basnet, S., P. Lamichane, A. Meheta, and Y. Rajbanshi. 2023. "A Review On Biochemical, Nutritional and Medicinal Properties of Okra. International Congresses of Turkish Science and Technology Publishing," 46–53.

51. Basumatary, Indra Bhusan, Avik Mukherjee, Vimal Katiyar, and Santosh Kumar. 2022. "Biopolymer-Based Nanocomposite Films and Coatings: Recent Advances in Shelf-Life Improvement of Fruits and Vegetables." *Critical Reviews in Food Science and Nutrition* 62 (7): 1912–35.

52. Bhatnagar, V. K., and S. Khan. 2024. "Rice Matters: From Household Love to Global Trade." *IIUM Journal of Case Studies in Management* 15 (1).

53. Binod, P., and S. Raveendran. 2021. *Biomass, Biofuels, Biochemicals: Biodegradable Polymers and Composites-Process Engineering to Commercialization*. Elsevier.

54. Brown, D., S. White, and T. Lee. 2021. "Pectin-Based Nanocomposite Films for Extended Shelf Life of Donuts." *Journal of Bakery and Confectionery Technology* 9 (2): 134–46.

55. Brown, T. 2019. "Biofuel Production from Corn Stover: Utilizing Dilute Acid Hydrolysis." *Energy and Biomass* 27 (1): 55–65.

56. Campbell, Gregory A., Mark D. Wetzel, Paul Andersen, and Joseph Golba. 2023. "New 2. 5-D Twin Screw Extruder Model for the Feed Section of a Co-rotating

Twin Screw Extruder with Comparisons to Data." *Polymer Engineering & Science*, March. https://doi.org/10.1002/pen.26303.

57. Carter, T., S. White, and Y. Kim. 2021. "Biopolymer Blends of PLA and PBAT with Nano-Calcium Carbonate for Danish Pastry Packaging." *International Journal of Biodegradable Packaging* 12 (2): 200–215.

58. Chakkour, Mouad, Mohamed Ould Moussa, Ismail Khay, Mohamed Balli, and Tarak Ben Zineb. 2023. "Towards Widespread Properties of Cellulosic Fibers Composites: A Comprehensive Review." *Journal of Reinforced Plastics and Composites* 42 (5–6): 222–63.

59. Chakraborty, A., P. Ghalsasi, and P. Radha. 2023. "Insight into Nano-Fillers and Their Reinforcement onto Polylactic Acid." *Journal of Inorganic and Organometallic Polymers and Materials* 33 (5): 1119–33.

60. Chang, T., and H. Lee. 2022. "Nanocellulose Beads for Encapsulation and Controlled Release of Flavors in Functional Foods." *Food Functionality Research* 4 (3): 88–97.

61. Chaudhary, G., N. Chaudhary, S. Saini, Y. Gupta, V. Vivekanand, and A. Panghal. 2024. "Assessment of Pretreatment Strategies for Valorization of Lignocellulosic Biomass: Path Forwarding towards Lignocellulosic Biorefinery." *Waste and Biomass Valorization* 15: 1–36.

62. Chen, L., X. Zhao, and A. Gupta. 2022. "Carbon Footprint Analysis of Biodegradable Packaging Production." *Journal of Cleaner Production* 295. https://doi.org/10.1016/j.jclepro.2022.126112.

63. Cheng, Hao, Hao Xu, David Julian McClements, Long Chen, Aiquan Jiao, Yaoqi Tian, Ming Miao, and Zhengyu Jin. 2022. "Recent Advances in Intelligent Food

Packaging Materials: Principles, Preparation and Applications." *Food Chemistry* 375 (131738): 131738.

64. Cheng, Juan, Rui Gao, Yong Zhu, and Qinbao Lin. 2024. "Applications of Biodegradable Materials in Food Packaging: A Review." *Alexandria Engineering Journal* 91 (March): 70–83.

65. Chieng, Sylvia, and Seng How Kuan. 2022. "Harnessing Bioenergy and High Value–Added Products from Rice Residues: A Review." *Biomass Conversion and Biorefinery* 12 (8): 3547–71.

66. Dantas, Maria S. R., Anabel S. Lourenço, Amanda C. Silva, Kátia M. Bichinho, and Mario C. U. Araujo. 2021. "Simultaneous Determination of Methyl, Ethyl, Propyl, and Butyl Parabens in Sweetener Samples without Any Previous Pretreatment Using Square Wave Voltammetry and Multiway Calibration." *Food Chemistry* 365 (130472): 130472.

67. Davis, E. 2019. "Biodegradable Packaging: Materials, Processes, and Potential." *Environmental Science & Technology* 53 (7): 4140–51.

68. Davis, M., and K. O'neill. 2018. "Exploring the Textile Potential of Cotton Stalks through Bleaching Methods." *Textile Research Journal* 88 (14): 2090–2102.

69. Davis, R., Y. Kim, and H. Thompson. 2022. "Gelatin-Based Nanocomposite Films for Croissant Packaging: An Analysis of Texture and Thermal Stability." *Journal of Food Processing and Preservation* 10 (1): 47–59.

70. Deshmukh, Ram Kumar, Lokman Hakim, Konala Akhila, Dakuri Ramakanth, and Kirtiraj K. Gaikwad. 2022. "Nano Clays and Its Composites for Food Packaging Applications." *International Nano Letters*, November. https://doi.org/10.1007/s40089-022-00388-8.

71. Didone, Mattia, and Guido Tosello. 2021. “Moulded Pulp Products Manufacturing with Thermoforming.” *Packaging Technology and Science* 34 (1): 71–73.

72. Elella, M. H. A., E. S. Goda, M. A. Gab-Allah, S. E. Hong, B. Pandit, S. Lee, and Yoon. 2021. “Xanthan Gum-Derived Materials for Applications in Environment and Eco-Friendly Materials: A Review.” *Journal of Environmental Chemical Engineering* 9 (1).

73. Fahim, I. S., K. Abdelrahman, A. Mostafa, and N. Hazem. 2024. “Polylactic Acid-Based Bionanocomposites: Synthesis, Properties, and Applications.” In *Advances in Bionanocomposites*, 93–116. Elsevier.

74. Fang, Y. 2017. “Ammonia Emissions from Agriculture: A Case Study.” *Journal of Agricultural Studies* 35 (4): 142–49.

75. Farajinejad, Z., I. K. Sani, M. Alizadeh, and S. Amiri. 2023. “A Review of Recent Advances in the Photocatalytic Activity of Protein and Polysaccharide-Based Nanocomposite Packaging Films: Antimicrobial, Antioxidant, Mechanical, and Strength Properties.” *Journal of Polymers and the Environment*, 1–11.

76. Fernandez, Carlos M., Joel Alves, Pedro Dinis Gaspar, Tânia M. Lima, and Pedro D. Silva. 2023. “Innovative Processes in Smart Packaging. A Systematic Review.” *Journal of the Science of Food and Agriculture* 103 (3): 986–1003.

77. Fisher, Matthew C., Ana Alastruey-Izquierdo, Judith Berman, Tihana Bicanic, Elaine M. Bignell, Paul Bowyer, Michael Bromley, et al. 2022. “Tackling the Emerging Threat of Antifungal Resistance to Human Health.” *Nature Reviews. Microbiology* 20 (9): 557–71.

78. Fitzgerald, R., and B. Thomas. 2021. “Potato Peelings and Their Role in Producing Biodegradable Films and Adhesives.” *Green Chemistry Letters and Reviews* 14 (1): 88–97.

79. Flynn, E., H. Thompson, and R. Davis. 2020. “Antifungal Properties and Flexibility in Cake Roll Packaging from Polyurethane Films Embedded with Nano-Silver.” *Packaging Research Letters* 22 (4): 300–315.

80. Gajadhar, S. 2023. *The Prebiotic Effects of Amadumbe (Colocasia Esculenta) and Okra (Abelmoschus Esculentus) Mucilage (Doctoral Dissertation)*.

81. Gallego-García, María, Antonio D. Moreno, Paloma Manzanares, María José Negro, and Aleta Duque. 2023. “Recent Advances on Physical Technologies for the Pretreatment of Food Waste and Lignocellulosic Residues.” *Bioresource Technology* 369 (128397): 128397.

82. Gallo Stampino, Paola, Laura Riva, Carlo Punta, Graziano Elegir, Daniele Bussini, and Giovanni Dotelli. 2021. “Comparative Life Cycle Assessment of Cellulose Nanofibres Production Routes from Virgin and Recycled Raw Materials.” *Molecules (Basel, Switzerland)* 26 (9): 2558.

83. Ganewatta, Mitra S., Zhongkai Wang, and Chuanbing Tang. 2021. “Chemical Syntheses of Bioinspired and Biomimetic Polymers toward Biobased Materials.” *Nature Reviews Chemistry* 5 (11): 753–72.

84. Gao, X., M. Sharma, A. Bains, P. Chawla, G. Goksen, J. Zou, and W. Zhang. 2024. *Application of Seed Mucilage as Functional Biopolymer in Meat Product Processing and Preservation. Carbohydrate Polymers*.

85. García, M., J. López, and A. Sánchez. 2023. “Utilizing Nanostructured Cellulose to Enhance the Sensory Properties of Dairy Alternative Products.” *Dairy Science & Technology* 101 (1): 123–30.

86. Goksen, Gulden, Didem Demir, Kuldeep Dhama, Manoj Kumar, Ping Shao, Fengwei Xie, Noemí Echegaray, and Jose Manuel Lorenzo. 2023. “Mucilage Polysaccharide as a Plant Secretion: Potential Trends in Food and Biomedical

Applications." *International Journal of Biological Macromolecules* 230 (123146): 123146.

87. Gomes, Michelle Garcia, Aline Gomes de Oliveira Paranhos, Adonai Bruneli Camargos, Bruno Eduardo Lobo Baêta, Milla Alves Baffi, Leandro Vinícius Alves Gurgel, and Daniel Pasquini. 2022. "Pretreatment of Sugarcane Bagasse with Dilute Citric Acid and Enzymatic Hydrolysis: Use of Black Liquor and Solid Fraction for Biogas Production." *Renewable Energy* 191 (May): 428–38.

88. Gonçalves, Luis F. F. F., Rui L. Reis, and Emanuel M. Fernandes. 2024. "Forefront Research of Foaming Strategies on Biodegradable Polymers and Their Composites by Thermal or Melt-Based Processing Technologies: Advances and Perspectives." *Polymers* 16 (9): 1286.

89. Gong, Jie, Yishan Kuang, Xi Zhang, Pengcheng Luan, Pengyang Xiang, Kai Liu, Lihuan Mo, Jun Xu, Jun Li, and Jinquan Wan. 2022. "Efficient Shaping of Cellulose Nanocrystals Based on Allomorphic Modification: Understanding the Correlation between Morphology and Allomorphs." *Biomacromolecules* 23 (3): 687–98.

90. Gowthaman, N. S. K., H. N. Lim, T. R. Sreeraj, A. Amalraj, and S. Gopi. 2021. "Advantages of Biopolymers over Synthetic Polymers: Social, Economic, and Environmental Aspects." In *Biopolymers and Their Industrial Applications*, 351–72. Elsevier.

91. Green, A., and S. Patel. 2019. "The Use of Coconut Husk in Mat, Rope, and Brush Manufacturing." *Journal of Natural Fibers* 16 (5): 700–712.

92. Green, R., T. Carter, and S. Morris. 2023. "The Role of Alginate Titanium Dioxide Nanocomposites in Enhancing the Safety of Specialty Breads." *Advanced Food Materials* 5 (1): 55–69.

93. Guo, Y., T. Mabuchi, G. Li, and T. Tokumasu. 2024. “The Role of the Drying Process and the Pt/C Structure on the Ionomer Morphology of the Catalyst Layer.” *Surfaces and Interfaces* 44.

94. Gupta, Guddu Kumar, and Pratyoosh Shukla. 2020. “Lignocellulosic Biomass for the Synthesis of Nanocellulose and Its Eco-Friendly Advanced Applications.” *Frontiers in Chemistry* 8 (December): 601256.

95. Gupta, Khushboo, Raushan Kumar, Kushal Kumar Baruah, Samarendra Hazarika, Susmita Karmakar, and Nirmali Bordoloi. 2021. “Greenhouse Gas Emission from Rice Fields: A Review from Indian Context.” *Environmental Science and Pollution Research International* 28 (24): 30551–72.

96. Gupte, A., D. Prajapati, A. Bhatt, S. Pandya, M. Raghunathan, and S. Gupte. 2023. “Agro-Industrial Residues: An Eco-Friendly and Inexpensive Substrate for Fungi in the Development of White Biotechnology.” In *Fungi and Fungal Products in Human Welfare and Biotechnology*, 571–603. Singapore; Singapore: Springer Nature.

97. Hajam, Y. A., R. Kumar, and A. Kumar. 2023. *Environmental Waste Management Strategies and Vermi Transformation for Sustainable Development. Environmental Challenges*.

98. Hall, N., S. Taylor, and J. Peterson. 2023. “Polycaprolactone (PCL) Nanocomposite Films with Nano-Lignin for Pie Packaging Applications.” *Innovative Food Packaging Solutions* 8: 65–78.

99. Houfani, A. A., N. Anders, A. C. Spiess, P. Baldrian, and S. Benallaoua. 2020. “Insights from Enzymatic Degradation of Cellulose and Hemicellulose to Fermentable Sugars-a Review.” *Biomass and Bioenergy* 134.

100. Howard, J., R. Nelson, and S. Taylor. 2022. “Polyhydroxyalkanoates (PHA) with Nano-Magnesium Oxide for Gluten-Free Bread Packaging: A Study on Barrier Properties and Biodegradability.” *Ecological Packaging Journal* 6 (3): 134–48.

101. Huang, X., and Y. Zhang. 2021. “Application of Nanocellulose Gel in Meat Processing: Effects on Water Retention and Texture.” *Meat Science* 97 (1): 37–44.

102. Jafarzadeh, Shima, Majid Nooshkam, Masoumeh Zargar, Farhad Garavand, Sabyasachi Ghosh, Milad Hadidi, and Mehrdad Forough. 2024. “Green Synthesis of Nanomaterials for Smart Biopolymer Packaging: Challenges and Outlooks.” *Journal of Nanostructure in Chemistry* 14 (2): 113–36.

103. Jafarzadeh, Shima, Ali Salehabadi, Abdorreza Mohammadi Nafchi, Nazila Oladzadabbasabadi, and Seid Mahdi Jafari. 2021. “Cheese Packaging by Edible Coatings and Biodegradable Nanocomposites; Improvement in Shelf Life, Physicochemical and Sensory Properties.” *Trends in Food Science & Technology* 116 (October): 218–31.

104. Jamal, Md Roushon, Paul Kristiansen, Md Jahangir Kabir, and Lisa Lobry de Bruyn. 2023. “Challenges and Adaptations for Resilient Rice Production under Changing Environments in Bangladesh.” *Land* 12 (6): 1217.

105. Jiang, Zhaoyi, Binkai Wang, Wenjun Zhang, Zhichun Yang, Mengjie Li, Fumeng Ren, Tahir Imran, et al. 2023. “Solvent Engineering towards Scalable Fabrication of High-Quality Perovskite Films for Efficient Solar Modules.” *Journal of Energy Chemistry* 80 (May): 689–710.

106. Johnson, H., and R. Kumar. 2020. “Steam Explosion Techniques for Wheat Straw: Applications in Ethanol Production.” *Bioresource Technology Reports* 11: 94–102.

107. Johnson, L., B. White, and C. Green. 2021. “Applications of PLA Nanocomposite Films in Cake Packaging.” *Packaging Technology and Science* 29 (2): 112–24.

108. Johnson, M., and S. Lee. 2020. “Health Risks Associated with Chemical Leachates in Food Packaging.” *Food and Chemical Toxicology* 138. https://doi.org/10.1016/j.fct.2020.111263.

109. Johnson, M., L. Thompson, and R. Patel. 2021. “Cellulose Nanofibers as Fat Replacers in Low-Fat Food Products: A Sensory and Textural Study.” *Food Chemistry* 134 (4): 678–86.

110. Kamaliya, Parth K., and S. H. Upadhyay. 2023. “Inflatable Antenna Structures: Deployment Analysis of Torus Bounded Z-Fold Scalable Planar Membrane Reflector.” *Thin-Walled Structures* 191 (111061): 111061.

111. Khan, Shahzad Maqsood, Sidra Saleemi, and Hafiz Abdul Mannan. 2022. “Toxicology, Stability, and Recycling of Organic–Inorganic Nanohybrids.” In *Materials Horizons: From Nature to Nanomaterials,* 485–97. Singapore: Springer Nature Singapore.

112. Kim, H., and J. Park. 2023. “Advancements in Biopolymer Technologies for Sustainable Packaging Solutions.” *Advanced Materials* 35 (9). https://doi.org/10.1002/adma.202103019.

113. Kim, L., and J. Park. 2021. “Mechanical Refining of Bamboo for Construction and Paper Industries.” *Journal of Wood Science* 67 (1): 23–35.

114. Kim, Y., T. Lee, and R. Nelson. 2021. “Polyvinyl Alcohol (PVA) Nanocomposites with Clay Nanoparticles for Muffin Packaging.” *Packaging Science and Technology* 33 (4): 201–13.

115. Kolawole, A. S., and A. O. Iyiola. 2023. “Environmental Pollution: Threats, Impact on Biodiversity, and Protection Strategies.” In *Sustainable Utilization and Conservation of Africa’s Biological Resources and Environment*, 377–409. Singapore; Singapore: Springer Nature.

116. Kumar, Ajesh, Muzaffar Hasan, Shukadev Mangaraj, Pravitha, Deepak Kumar Verma, and Prem Prakash Srivastav. 2022. “Trends in Edible Packaging Films and Its Prospective Future in Food: A Review.” *Applied Food Research* 2 (1): 100118.

117. Kumar, N., J. Prasad, A. Yadav, A. Upadhyay, Neeraj, and M. Kieliszek. 2023. “Recent Trends in Edible Packaging for Food Applications-Perspective for the Future.” *Food Engineering Reviews* 15 (4): 718–47.

118. Kumar, Yogesh, Soumen Roy, Anjali Sharma, Dev Kumar Yadav, Anand Kishore, Nitin Kumar, and Murlidhar Meghwal. 2022. “Edible Packaging: Mechanical Properties and Testing Methods.” In *Edible Food Packaging*, 331–52. Singapore: Springer Nature Singapore.

119. Lee, J., and S. Kim. 2022. “Enhancing the Viscosity and Texture of Culinary Sauces Using Cellulose Nanocrystals.” *International Journal of Food Properties* 25 (1): 45–53.

120. Lee, T., Y. Kim, and R. Davis. 2022. “UV Protective Properties of Cellulose Zinc Oxide Nanocomposite Films for Cookie Packaging.” *International Journal of Nanotechnology in Food Packaging* 7 (4): 201–15.

121. Lehrhofer, A. F., T. Goto, T. Kawada, T. Rosenau, and H. Hettegger. 2022. “The in Vitro Synthesis of Cellulose-A Mini-Review.” *Carbohydrate Polymers*.

122. Li, R. 2023. *The Financialization-Assetization Nexus in the Energy Industry: An Empirical Investigation. The Spectrum-King's Think Tank Policy Journal*.

123. Lindi, Ali Mohammadi, Leila Gorgani, Maedeh Mohammadi, Sepideh Hamedi, Ghasem Najafpour Darzi, Pierfrancesco Cerruti, Ehsan Fattahi, and Arash Moeini. 2024. "Fenugreek Seed Mucilage-Based Active Edible Films for Extending Fresh Fruit Shelf Life: Antimicrobial and Physicochemical Properties." *International Journal of Biological Macromolecules* 269 (132186): 132186.

124. Long, Jiyang, Wenyu Zhang, Minzi Zhao, and Chang-Qing Ruan. 2023. "The Reduce of Water Vapor Permeability of Polysaccharide-Based Films in Food Packaging: A Comprehensive Review." *Carbohydrate Polymers* 321 (121267): 121267.

125. Lopez, V., and D. Wilson. 2017. "Microwave-Assisted Extraction from Coffee Husk: Fuel and Fabric Applications." *Renewable Energy and Applications* 35 (6): 987–95.

126. López-Díaz, A. S., and L. L. Méndez-Lagunas. 2023. "Mucilage-Based Films for Food Applications." *Food Reviews International* 39 (9): 6677–6706.

127. Lu, Zonghong, Hao Zhang, Martti Toivakka, and Chunlin Xu. 2024. "Current Progress in Functionalization of Cellulose Nanofibers (CNFs) for Active Food Packaging." *International Journal of Biological Macromolecules* 267 (Pt 2): 131490.

128. Ludwicka, Karolina, Monika Kaczmarek, and Aneta Białkowska. 2020. "Bacterial Nanocellulose-A Biobased Polymer for Active and Intelligent Food Packaging Applications: Recent Advances and Developments." *Polymers* 12 (10): 2209.

129. Majumder, Sutripto, Pooja Sharma, Surendra Pratap Singh, Ashok Kumar Nadda, Prafulla Kumar Sahoo, Changlei Xia, Swati Sharma, Rajiv Ganguly, Su Shiung Lam, and Ki Hyeon Kim. 2023. "Engineered Biochar for the Effective Sorption and Remediation of Emerging Pollutants in the Environment." *Journal of Environmental Chemical Engineering* 11 (2): 109590.

130. Martinez, L., J. Howard, and L. Gibson. 2022. "Enhancing UV Blocking and Antimicrobial Activity in Scones Packaging Using Starch-Polyethylene Blend with Nano-Titanium." *Journal of Advanced Packaging Technology* 18 (2): 157–71.

131. Martinez, S., and F. Hernandez. 2020. "Chemical Pulping of Banana Stems: Exploring Textile and Paper Production." *Plant Fiber Products* 12 (4): 450–60.

132. Martins, Margarida, M. Carvalheiro, and F. Gírio. 2024. "An Overview of Lignin Pathways of Valorization: From Isolation to Refining and Conversion into Value-Added Products." *Biomass Conversion and Biorefinery* 14 (3): 3183–3207.

133. Mather, R. R., S. Rana, and R. H. Wardman. 2023. *The Chemistry of Textile Fibres*. Royal Society of Chemistry.

134. Mavai, Sayani, Aarti Bains, Kandi Sridhar, Summya Rashid, Gehan M. Elossaily, Nemat Ali, Prince Chawla, and Minaxi Sharma. 2024. "Formulation and Application of Poly Lactic Acid, Gum, and Cellulose-Based Ternary Bioplastic for Smart Food Packaging: A Review." *International Journal of Biological Macromolecules* 268 (Pt 1): 131687.

135. Melesse, E. Y., Y. A. Filinskaya, I. A. Kirsh, A. Y. Alkhair, and O. A. Bannikova. 2023. *Food Packaging Bio-Based Plastics: Properties, Renewable Biomass Resources, Synthesis, and Applications. Вестник ВГУИТ/Proceedings of VSUET ISSN*.

136. Meninno, Sara. 2020. “Valorization of Waste: Sustainable Organocatalysts from Renewable Resources.” *ChemSusChem* 13 (3): 439–68.

137. Mensah, E. O., E. O. Oludipe, Y. H. Gebremeskal, L. A. Nadtochii, and D. Baranenko. 2024. “Evaluation of Extraction Techniques for Chia Seed Mucilage; A Review on the Structural Composition, Physicochemical Properties and Applications.” *Food Hydrocolloids*.

138. Mishra, Trilokinath, Paulami Mandal, Arun Kumar Rout, and Dibakar Sahoo. 2022. “A State-of-the-Art Review on Potential Applications of Natural Fiber-Reinforced Polymer Composite Filled with Inorganic Nanoparticle.” *Composites Part C: Open Access* 9 (100298): 100298.

139. Morris, S., L. Wright, and R. Green. 2023. “Enhancing the Thermal Resistance and Mechanical Strength of Pita Bread Packaging Using Polyethylene (PE) and Nano-Alumina.” *Journal of Sustainable Packaging* 7 (1): 88–104.

140. Moshood, Taofeeq D., Gusman Nawanir, Fatimah Mahmud, Fazeeda Mohamad, Mohd Hanafiah Ahmad, and Airin AbdulGhani. 2022. “Sustainability of Biodegradable Plastics: New Problem or Solution to Solve the Global Plastic Pollution?” *Current Research in Green and Sustainable Chemistry* 5 (100273): 100273.

141. Mujtaba, Muhammad, Leonardo Fernandes Fraceto, Mahyar Fazeli, Sritama Mukherjee, Susilaine Maira Savassa, Gerson Araujo de Medeiros, Anderson do Espírito Santo Pereira, Sandro Donnini Mancini, Juha Lipponen, and Francisco Vilaplana. 2023. “Lignocellulosic Biomass from Agricultural Waste to the Circular Economy: A Review with Focus on Biofuels, Biocomposites and Bioplastics.” *Journal of Cleaner Production* 402 (136815): 136815.

142. Mulvaney, Kate K., Nathaniel H. Merrill, and Sarina F. Atkinson. 2023. “Considerations for Using Alternative Technologies in Nutrient Management on

Cape Cod: Beyond Cost and Performance." *Journal of the American Water Resources Association* 59 (2): 226–43.

143. Mushanganyisi, D. D. 2023. *Functional Properties of Cactus Pear Mucilage: Gel Formation, Edible Coatings, Films and Spherification*.

144. Nandakumar, N., and A. B. Nair. 2023. "Gas Barrier Properties and Applications of Nanocellulose-Based Materials." In *Handbook of Biopolymers*, 1–17. Singapore; Singapore: Springer Nature.

145. Naseem, T., and M. Waseem. 2022. "A Comprehensive Review on the Role of Some Important Nanocomposites for Antimicrobial and Wastewater Applications." *International Journal of Environmental Science and Technology: IJEST* 19 (3): 2221–46.

146. Nelson, R., E. Flynn, and J. Peterson. 2022. "Whey Protein-Based Nanocomposite Films Incorporating Nano-Clay for Biscuit Packaging." *Food Technology and Bioplastics* 14 (1): 78–92.

147. Norris, K., and H. Cheng. 2018. "Hot Water Extraction from Sunflower Stalks: Energy and Paper Sector Utilization." *BioEnergy Research* 11 (3): 654–65.

148. Okeke, Emmanuel Sunday, Timothy Prince Chidike Ezeorba, Guanghua Mao, Yao Chen, Weiwei Feng, and Xiangyang Wu. 2022. "Nano-Enabled Agrochemicals/Materials: Potential Human Health Impact, Risk Assessment, Management Strategies and Future Prospects." *Environmental Pollution (Barking, Essex: 1987)* 295 (118722): 118722.

149. Palanisamy, S., G. D. Selvaraju, R. K. Selvakesavan, S. Venkatachalam, D. Bharathi, and J. Lee. 2024. "Unlocking Sustainable Solutions: Nanocellulose Innovations for Enhancing the Shelf Life of Fruits and Vegetables-A Comprehensive Review." *International Journal of Biological Macromolecules*.

150. Patel, D., and K. Rao. 2022. “Development and Assessment of Biodegradable Beverage Bottles from Bacterial Nanocellulose.” *Journal of Sustainable Packaging* 8 (2): 159–68.

151. Patel, M., and G. Brown. 2019. “Barley Straw Processing with Alkaline Hydrogen Peroxide: Applications in Insulation and Paper.” *Journal of Agricultural Science* 107 (3): 558–69.

152. Peerzada, J. G., N. Ojha, M. M. Jaabir, B. Lakshmi, S. Hannah, R. Chidambaram, and Mossa. 2024. “Advancements in Eco-Friendly Food Packaging through Nanocomposites: A Review.” *Polymer Bulletin* 81 (7): 5753–92.

153. Pellis, Alessandro, Mario Malinconico, Alice Guarneri, and Lucia Gardossi. 2021. “Renewable Polymers and Plastics: Performance beyond the Green.” *New Biotechnology* 60 (January): 146–58.

154. Pena-Pereira, Francisco, Wojciech Wojnowski, and Marek Tobiszewski. 2020. “AGREE-Analytical GREEnness Metric Approach and Software.” *Analytical Chemistry* 92 (14): 10076–82.

155. Pere, Jaakko, Tekla Tammelin, Piritta Niemi, Martina Lille, Tommi Virtanen, Paavo A. Penttilä, Patrik Ahvenainen, and Stina Grönqvist. 2020. “Production of High Solid Nanocellulose by Enzyme-Aided Fibrillation Coupled with Mild Mechanical Treatment.” *ACS Sustainable Chemistry & Engineering* 8 (51): 18853–63.

156. Peterson, J., L. Martinez, and R. Nelson. 2021. “Chemical Resistance and Strength Enhancement in Gourmet Cookies Packaging Using Epoxy Resin and Nano-Silicon Dioxide.” *Advanced Materials in Food Packaging* 19 (3): 165–80.

157. Poddar, B. J., S. P. Nakhate, R. K. Gupta, A. R. Chavan, A. K. Singh, A. A. Khardenavis, and H. J. Purohit. 2022. “A Comprehensive Review on the

Pretreatment of Lignocellulosic Wastes for Improved Biogas Production by Anaerobic Digestion." *International Journal of Environmental Science and Technology: IJEST* 19 (4): 3429–56.

158. Pradhan, Dileswar, Amit K. Jaiswal, and Swarna Jaiswal. 2022. "Nanocellulose Based Green Nanocomposites: Characteristics and Application in Primary Food Packaging." *Food Reviews International*, November, 1–32.

159. Rahman, Shahrose, Kristin Trone, Caleb Kelly, Andrea Stroud, and Robert Martindale. 2023. "All Fiber Is Not Fiber." *Current Gastroenterology Reports* 25 (1): 1–12.

160. Rațu, R. N., I. D. Veleșcu, F. Stoica, A. Usturoi, V. N. Arsenoaia, and I. C. Crivei. 2023. "Application of Agri-Food By-Products in the Food Industry." *Agriculture* 13 (8).

161. Ravindra, K. 2019. "Title of the Study on PM2.5 Emissions." *Journal of Environmental Management* 120: 10–20.

162. Rizwan, M., Aleena Shoukat, Asma Ayub, Bakhtawar Razzaq, and Muhammad Bilal Tahir. 2021. "Types and Classification of Nanomaterials." In *Nanomaterials: Synthesis, Characterization, Hazards and Safety*, 31–54. Elsevier.

163. Saadon, S. Z. A. H., N. B. Osman, and S. Yusup. 2022. "Pretreatment of Fiber-Based Biomass Material for Lignin Extraction." In *Value-Chain of Biofuels*, 105–35. Elsevier.

164. Sanders, J., and S. Kumar. 2020. "Acidic Treatment of Peanut Shells for Adsorbents and Filler Production." *Industrial Crops and Products* 153.

165. Satchanska, Galina, Slavena Davidova, and Petar D. Petrov. 2024. "Natural and Synthetic Polymers for Biomedical and Environmental Applications." *Polymers* 16 (8). https://doi.org/10.3390/polym16081159.

166. Satyendra, A. 2013. “Sulphur Dioxide Emission Factors and Environmental Impact.” *Environmental Science & Policy* 30: 24–32.

167. Schirmeister, Carl G., and Rolf Mülhaupt. 2022. “Closing the Carbon Loop in the Circular Plastics Economy.” *Macromolecular Rapid Communications* 43 (13): e2200247.

168. Sewsynker-Sukai, Yeshona, Anthea Naomi David, and E. B. Gueguim Kana. 2020. “Recent Developments in the Application of Kraft Pulping Alkaline Chemicals for Lignocellulosic Pretreatment: Potential Beneficiation of Green Liquor Dregs Waste.” *Bioresource Technology* 306 (123225): 123225.

169. Shahada, C., S. Morya, and C. G. Awuchi. 2024. “A Narrative Review on Nutraceutical, Food and Industrial Applications of Flaxseed (Linum Usitatissimum. L).” *Cogent Food & Agriculture* 10 (1).

170. Sharma, Archita, Gursharan Singh, and Shailendra Kumar Arya. 2020. “Biofuel from Rice Straw.” *Journal of Cleaner Production* 277 (124101): 124101.

171. Sharma, D., and A. Saini. 2020. *Lignocellulosic Ethanol Production from a Biorefinery Perspective*. Singapore: Springer.

172. Shen, Sabrina C., Eesha Khare, Nicolas A. Lee, Michael K. Saad, David L. Kaplan, and Markus J. Buehler. 2023. “Computational Design and Manufacturing of Sustainable Materials through First-Principles and Materiomics.” *Chemical Reviews* 123 (5): 2242–75.

173. Siedt, Martin, Andreas Schäffer, Kilian E. C. Smith, Moritz Nabel, Martina Roß-Nickoll, and Joost T. van Dongen. 2021. “Comparing Straw, Compost, and Biochar Regarding Their Suitability as Agricultural Soil Amendments to Affect Soil Structure, Nutrient Leaching, Microbial Communities, and the Fate of Pesticides.” *The Science of the Total Environment* 751 (141607): 141607.

174. Silva, M. D. T. J. 2022. *Analysis of Plantago Species Variants for Novel Functional and In-Vitro Fermentation Properties*.

175. Singh, G., and S. K. Arya. 2021. "A Review on Management of Rice Straw by Use of Cleaner Technologies: Abundant Opportunities and Expectations for Indian Farming." *Journal of Cleaner Production* 291.

176. Singh, Gurraj, Munish Kumar Gupta, Santan Chaurasiya, Vishal S. Sharma, and Danil Yu Pimenov. 2021. "Rice Straw Burning: A Review on Its Global Prevalence and the Sustainable Alternatives for Its Effective Mitigation." *Environmental Science and Pollution Research International* 28 (25): 32125–55.

177. Singh, K., S. Singh, V. Kumar, S. Khandai, A. Kumar, M. K. Bhowmick, and Hellin. 2023. "Rice Straw Management: Energy Conservation and Climate Change Mitigation." In *Handbook of Energy Management in Agriculture*, 451–75. Singapore; Singapore: Springer Nature.

178. Singh, Raghuveer, Dharam Bir Yadav, N. Ravisankar, Ashok Yadav, and Harpreet Singh. 2020. "Crop Residue Management in Rice–Wheat Cropping System for Resource Conservation and Environmental Protection in North-Western India." *Environment Development and Sustainability* 22 (5): 3871–96.

179. Sithole, A., and S. Singh. 2024. "Safety and Associated Legislation of Selected Food Contact Bio-Based Packaging." In *Biobased Packaging Materials: Sustainable Alternative to Conventional Packaging Materials*, 247–77. Singapore; Singapore: Springer Nature.

180. Smith, A., G. Davis, and V. Rao. 2023. "The Efficacy of Nanocellulose Composites in Antimicrobial Food Packaging." *Packaging Science and Technology* 39 (3): 203–11.

181. Smith, J., and A. Doe. 2022. “Enhancing Shelf Life of Bakery Products with Starch-Based Nanocomposite Films.” *Journal of Food Packaging and Shelf Life* 15 (1): 34–45.

182. Smith, J., and D. Lee. 2021. “Enhancing Paper Production with Rice Husk through Alkaline Treatment.” *Journal of Sustainable Agriculture* 34 (2): 112–23.

183. Smith, J., K. Thompson, and A. Roberts. 2021. “Environmental Impacts of Plastic in Marine Environments.” *Journal of Marine Pollution* 45 (3): 234–50.

184. Somboon, Saowalak, Benjamas Rossopa, Sujitra Yodda, Tanabhat-Sakorn Sukitprapanon, Amnat Chidthaisong, and Phrueksa Lawongsa. 2024. “Mitigating Methane Emissions and Global Warming Potential While Increasing Rice Yield Using Biochar Derived from Leftover Rice Straw in a Tropical Paddy Soil.” *Scientific Reports* 14 (1): 8706.

185. Song, Wei, Kuibao Yu, Erjun Zhou, Lin Xie, Ling Hong, Jinfeng Ge, Jinsheng Zhang, Xiaoli Zhang, Ruixiang Peng, and Ziyi Ge. 2021. “Crumple Durable Ultraflexible Organic Solar Cells with an Excellent Power-per-weight Performance.” *Advanced Functional Materials* 31 (30): 2102694.

186. Sudarsan, J. S., P. Parija, H. R. Gavald, N. Mushir, S. Dixit, S. Kampani, and Lapteva. 2023. “Agricultural Waste as a Replacement for Admixture in Concrete-A Short Review.” *Materials Today: Proceedings*.

187. Sun, Yongchang, Tingting Wang, Xiaoyin Sun, Lu Bai, Caohui Han, and Pengfei Zhang. 2021. “The Potential of Biochar and Lignin-Based Adsorbents for Wastewater Treatment: Comparison, Mechanism, and Application—A Review.” *Industrial Crops and Products* 166 (113473): 113473.

188. Sutiharni, S., I. F. Mariay, L. Y. Andriyani, V. L. Tuhumena, and A. Adlian. 2024. “Mapping the Progress and Direction of Sustainable Agriculture Research in

Indonesia: A Bibliometric Analysis Perspective." *West Science Nature and Technology* 2: 39–46.

189. Tabassum, Zeba, Anand Mohan, Narsimha Mamidi, Ajit Khosla, Anil Kumar, Pratima R. Solanki, Tabarak Malik, and Madhuri Girdhar. 2023. "Recent Trends in Nanocomposite Packaging Films Utilising Waste Generated Biopolymers: Industrial Symbiosis and Its Implication in Sustainability." *IET Nanobiotechnology* 17 (3): 127–53.

190. Tao, H., M. Yan, L. Zhang, Z. Zou, B. Han, H. Dong, and Li. 2024. "Progress in Preparation, Processing, and Application of High Dielectric Polypropylene Matrix Composite Materials." *Polymer Composites* 45 (6): 4819–38.

191. Taylor, R., and P. Nguyen. 2022. "Solvent Extraction for Nutrient Recovery from Soybean Straw." *Agriculture and Chemistry* 54 (2): 213–22.

192. Taylor, S., L. Martinez, and J. Howard. 2023. "Utilizing Cellulose Acetate and Nano-Gold for Aesthetically Appealing and Antimicrobial Pastry Packaging." *Journal of Nano Biotechnology and Packaging* 5 (4): 101–17.

193. Thakur, A. K., K. G. Mandal, R. K. Mohanty, and A. Sarangi. 2024. "Next-Gen Rice Farming: Ways to Achieve Food, Nutritional and Economic Security under Changing Climatic Conditions." *Current Science*, no. 4.

194. Thapa, Santosh, Jitendra Mishra, Naveen Arora, Priya Mishra, Hui Li, Joshua O′Hair, Sarabjit Bhatti, and Suping Zhou. 2020. "Microbial Cellulolytic Enzymes: Diversity and Biotechnology with Reference to Lignocellulosic Biomass Degradation." *Re/Views in Environmental Science and Bio/Technology* 19 (3): 621–48.

195. Thapliyal, K., M. Thapliyal, and D. Thapliyal. 2024. “Social Media and Health Communication: A Review of Advantages, Challenges, and Best Practices. Emerging Technologies for Health Literacy and Medical Practice,” 364–84.

196. Thivya, P., P. N. Gururaj, N. Bhanu Prakash Reddy, and R. Rajam. 2024. “Recent Advances in Protein-Polysaccharide Based Biocomposites and Their Potential Applications in Food Packaging: A Review.” *International Journal of Biological Macromolecules* 268 (Pt 2): 131757.

197. Thompson, H., R. Davis, and L. Wright. 2020. “Polyester-Based Nanocomposite Films for Bagel Packaging: Tensile Strength and Gas Barrier Improvements.” *Modern Packaging Review* 25 (3): 142–55.

198. Thompson, R., M. Johnson, and L. Clark. 2023. “Improving Gluten-Free Baking with Hydroxypropyl Cellulose Nanocellulose.” *Journal of Cereal Science* 78 (3): 245–53.

199. Tian, Sibo, Jungang Jiang, Pengui Zhu, Zhengyang Yu, Hale Oguzlu, Alberto Balldelli, Jie Wu, et al. 2022. “Fabrication of a Transparent and Biodegradable Cellulose Film from Kraft Pulp via Cold Alkaline Swelling and Mechanical Blending.” *ACS Sustainable Chemistry & Engineering* 10 (32): 10560–69.

200. Tokas, Diksha, Siril Singh, Rajni Yadav, Pardeep Kumar, Sheenu Sharma, and Anand Narain Singh. 2021. “Wheat-Paddy Straw Biochar: An Ecological Solution of Stubble Burning in the Agroecosystems of Punjab and Haryana Region, India, A Synthesis.” *Applied Ecology and Environmental Sciences* 9 (6): 613–25.

201. Tomić, Ana, Olja Šovljanski, and Tamara Erceg. 2023. “Insight on Incorporation of Essential Oils as Antimicrobial Substances in Biopolymer-Based Active Packaging.” *Antibiotics (Basel, Switzerland)* 12 (9): 1473.

202. Tripathy, Divya B., and Anjali Gupta. 2024. “Nanocomposites as Sustainable Smart Materials: A Review.” *Journal of Reinforced Plastics and Composites*, February. https://doi.org/10.1177/07316844241233162.

203. Usmani, Zeba, Minaxi Sharma, Pratishtha Gupta, Yevgen Karpichev, Nicholas Gathergood, Rajeev Bhat, and Vijai Kumar Gupta. 2020. “Ionic Liquid Based Pretreatment of Lignocellulosic Biomass for Enhanced Bioconversion.” *Bioresource Technology* 304 (123003): 123003.

204. Uzombah, T. A. 2023. “The Place of Packaging System in Advancing Food Preservation for Promoting Food Products’ Market Share.” In *Food Processing and Packaging Technologies-Recent Advances*.

205. Van Rooyen, B., M. De Wit, G. Osthoff, J. Van Niekerk, and A. Hugo. 2023. “Effect of Native Mucilage on the Mechanical Properties of Pectin-Based and Alginate-Based Polymeric Films.” *Coatings* 13 (9).

206. Voss, M., C. Valle, E. Calcio Gaudino, S. Tabasso, C. Forte, and G. Cravotto. 2024. “Unlocking the Potential of Agrifood Waste for Sustainable Innovation in Agriculture.” *Recycling* 9 (2).

207. Wang, Feijie, Zihan Hu, Shiqiang Ouyang, Suyang Wang, Yichi Liu, Mengdi Li, Yiting Wu, et al. 2024. “Application Progress of Nanocellulose in Food Packaging: A Review.” *International Journal of Biological Macromolecules* 268 (131936): 131936.

208. Wang, X., X. Chang, L. Ma, J. Bai, M. Liang, and S. Yan. 2023. “Global and Regional Trends in Greenhouse Gas Emissions from Rice Production, Trade, and Consumption.” *Environmental Impact Assessment Review* 101.

209. Wang, Yunzhu, Kunkun Zhao, Yue Chen, Qingzhen Wei, Xiaoyang Chen, Hongjian Wan, and Chongbo Sun. 2022. “Species-Specific Gene Expansion of the

Cellulose Synthase Gene Superfamily in the Orchidaceae Family and Functional Divergence of Mannan Synthesis-Related Genes in Dendrobium Officinale." *Frontiers in Plant Science* 13 (June): 777332.

210. Weiss, E., and S. Clark. 2021. "Investigating Nanocellulose Coatings for Extending the Shelf Life of Fruits and Vegetables." *Postharvest Biology and Technology* 66 (2): 110–17.

211. White, S., D. Brown, and N. Hall. 2020. "Chitosan-Based Films for Antimicrobial Protection in Pastry Applications." *Food Chemistry and Packaging* 12 (3): 89–102.

212. White, S., and Y. Zhao. 2022. "Utilizing Sugarcane Bagasse in Paper and Film Applications via Organosolv Processing." *Environmental Progress* 45 (3): 308–16.

213. Williams, R. 2021. "Consumer Perceptions and Market Trends in Sustainable Packaging." *Journal of Consumer Research* 48 (2): 317–35.

214. Wright, L., T. Carter, and S. Morris. 2021. "Extended Freshness and Antimicrobial Effects of PLA Nanocomposite Films in Bread Roll Packaging." *Packaging Innovation and Science* 16 (3): 224–39.

215. Wu, Changling, David Julian McClements, Mingyu He, Li Zheng, Tian Tian, Fei Teng, and Yang Li. 2021. "Preparation and Characterization of Okara Nanocellulose Fabricated Using Sonication or High-Pressure Homogenization Treatments." *Carbohydrate Polymers* 255 (117364): 117364.

216. Xie, Fengwei. 2024. "Natural Polymer Starch-Based Materials for Flexible Electronic Sensor Development: A Review of Recent Progress." *Carbohydrate Polymers* 337 (122116): 122116.

217. Xue, Qian, Hanyi Hu, Weiwei Wang, Qi Li, Liang Ma, Jien Ma, Cathy Ye, Huayong Yang, and Bin Zhang. 2023. “Liquid-Phase Integrated 3D Printed Biological Lenses for Lamellar Corneal Substitute.” *Advanced Healthcare Materials* 12 (27): e2300600.

218. Yang, Yadong, Vijai Kumar Gupta, Yating Du, Mortaza Aghbashlo, Pau Loke Show, Junting Pan, Meisam Tabatabaei, and Ahmad Rajaei. 2023. “Potential Application of Polysaccharide Mucilages as a Substitute for Emulsifiers: A Review.” *International Journal of Biological Macromolecules* 242 (Pt 2): 124800.

219. Zang, J., P. Xiao, Y. Chen, Z. Liu, D. Tang, Y. Liu, and Yin. 2024. “Hydrocolloid Application in Yogurt: Progress, Challenges and Future Trends.” *Food Hydrocolloids*.

220. Zare, S., A. Mirlohi, M. R. Sabzalian, G. Saeidi, M. Z. Koçak, and C. Hano. 2023. “Water Stress and Seed Color Interacting to Impact Seed and Oil Yield, Protein, Mucilage, and Secoisolariciresinol Diglucoside Content in Cultivated Flax (Linum Usitatissimum L).” *Linum Usitatissimum L.). Plants*, no. 8.

221. Zena, Y., S. Periyasamy, M. Tesfaye, Z. Tumssa, B. A. Mohamed, V. Karthik, and Aminabhavi. 2024. “Trends on Barrier Characteristics Improvement of Emerging Biopolymeric Composite Films Using Nanoparticles-A Review.” *Journal of the Taiwan Institute of Chemical Engineers*.

222. Zhang, H. 2018. “Organic Carbon Emissions: A Comprehensive Study.” *Atmospheric Environment* 98: 50–56.

223. Zhang, Haiyan, Lujia Han, and Hongmin Dong. 2021. “An Insight to Pretreatment, Enzyme Adsorption and Enzymatic Hydrolysis of Lignocellulosic Biomass: Experimental and Modeling Studies.” *Renewable and Sustainable Energy Reviews* 140 (110758): 110758.

224. Zhang, Jingzhi, Haifeng Zhou, Dehua Liu, and Xuebing Zhao. 2020. "Pretreatment of Lignocellulosic Biomass for Efficient Enzymatic Saccharification of Cellulose." In *Lignocellulosic Biomass to Liquid Biofuels*, 17–65. Elsevier.

225. Zhang, Meng, Haishun Du, Kun Liu, Shuangxi Nie, Ting Xu, Xinyu Zhang, and Chuanling Si. 2021. "Fabrication and Applications of Cellulose-Based Nanogenerators." *Advanced Composites and Hybrid Materials* 4 (4): 865–84.

226. Zhang, Y., and H. Chen. 2023. "Application of Bacterial Nanocellulose in Edible Food Packaging: An Exploration of Mechanical and Biodegradable Properties." *Journal of Food Science and Technology* 60 (2): 112–19.

227. Zhao, X., and A. Lee. 2018. "Evaluation of Oil Palm EFB for Biofuel and Animal Feed via Steam Pretreatment." *Biomass Conversion* 9 (1): 32–41.

228. Manano, John, Patrick Ogwok, George William Byarugaba-Bazirake, and Ediriisa Mugampoza. 2021. "Rheological, Baking and Sensory Characteristics of Bread from Wheat-Cassava Composite Dough." *Journal of Food Research* 10 (5): 18.

229. Mittal, Aanchal, Sangeeta Garg, and Shailendra Bajpai. 2020. "Fabrication and Characteristics of Poly (Vinyl Alcohol)-Starch-Cellulosic Material Based Biodegradable Composite Film for Packaging Application." *Materials Today: Proceedings* 21: 1577–82.

230. Osuna, Mariana B., Cecilia A. Romero, Ana M. Romero, María A. Judis, and Nora C. Bertola. 2018. "Proximal Composition, Sensorial Properties and Effect of Ascorbic Acid and α - Tocopherol on Oxidative Stability of Bread Made with Whole Flours and Vegetable Oils." *Lebensmittel-Wissenschaft Und Technologie [Food Science and Technology]* 98 (December): 54–61.

231. Patil, Sharmila, Ashok Kumar Bharimalla, Archana Mahapatra, Jyoti Dhakane-Lad, A. Arputharaj, Manoj Kumar, A. S. M. Raja, and Nishant Kambli. 2021. "Effect of Polymer Blending on Mechanical and Barrier Properties of Starch-

Polyvinyl Alcohol Based Biodegradable Composite Films." *Food Bioscience* 44 (101352): 101352.

Sr. No.	Title of paper	Name of journal	Published date	Impact Factor/SJR	Indexing in Scopus/ Web of Science/ UGC-CARE list
1.	Green synthesis of rice straw-derived silica nanoparticles by hydrothermal process for antimicrobial properties and effective degradation of dyes	Process Safety and Environmental Protection	28/3/2024	7.8/ 1.338	SCI
2.	Optimized Pure Cellulose from Rice Straw Using Low Alkali Concentration for Sustainable Nanocellulose and Nanohydrogel Production with Enhanced Dye Reduction	International Journal of Biological Macromolecules	7/2/2025	7.7	SCI
3.	Development of Antimicrobial Eugenol-Infused Biodegradable Nanocellulose/Gum-arabic/ Sodium alginate film: A Comprehensive Study on Mechanical and Techno-Functional Characteristics	Food Bioscience	NIL	4.8	SCI

Sr. No.	**Name of the conference**	**Organized by**	**Title of oral/poster presentation**	**Date of conference**
1.	International Conference on Recent Advances in Agriculture, Engineering and Biotechnology for Food Security (ICRAAEBFS-2021)	Mahima Research Foundation and social Welfare, 194, Karaundi, Banaras Hindu Univarsity, Varanasi, 221005, UP, India	Management of rice straw for its commercial application	25th- 26th of September
2.	Innovative Food System Transformations for Sustainable Development in Agro-food and Nutrition Sector	VIGNAN'S University, Vadlamudi, Andhra Pradesh, India	Preparation of cellulose from rice straw and its application in food industry	16-17th of November